Annual Report

Investigation of the Interaction of Elastic Waves with Buried Mines

Submitted by

Waymond R. Scott, Jr.[a], Peter H. Rogers[b], and James S. Martin[b]

[a]School of Electrical and Computer Engineering
[b]School of Mechanical Engineering
Georgia Institute of Technology
Atlanta, GA 30332

waymond.scott@ece.gatech.edu
404-894-3048

July 12, 2000

20000719 035

DTIC QUALITY INSPECTED 4

Project Overview

Seismic/elastic techniques show considerable promise for the reliable detection of all types of buried mines, even low-metal anti-personnel mines. The reason for this is that mines have mechanical properties that are significantly different from soils and typical forms of clutter. For example, the shear wave velocity is more than 20 times higher in the explosive and the plastics used in typical mines than in the surrounding soil. In addition, mines are complex mechanical structures with a flexible case, a trigger assembly, air pockets etc. The complex structure gives rise to structural resonances, non-linear interactions, and other phenomenology that is atypical for both naturally occurring and man made forms of clutter. Thus, this phenomenology can potentially be used to distinguish a mine from clutter.

Seismic detection techniques have fallen into disfavor because of practical system implementation issues. Both the detection and generation of seismic waves has previously been conducted with ground contacting transducers (thumpers and geophones) which are impractical in the vicinity of land mines because of the threat these pose to both the system and the operator. Mines are generally very small in comparison with the wavelengths used in seismic exploration. Their target strengths are, therefore, fairly small and it has been nearly impossible to pick them out from the background.

A system has recently been developed at Georgia Tech that exploits the advantages of seismic techniques while overcoming the implementation issues. The technique uses an interrogation sensor that detects the elastic waves in the earth without contacting the earth. A radar is currently being used as the interrogation sensor. The system employs an elastic wave source that launches a surface (Rayleigh) wave that travels over the minefield. This technique uses wavelengths comparable to the size of a mine; thus, the target strength of the mine is much stronger than that of traditional seismic techniques. In addition, it can detect the localized interactions of the mine and the elastic waves since this technique safely interrogates the earth directly above the mine.

The objective of this research is to support ongoing development of the seismic mine detection technique. Specifically this involves the creation of a reliable three-dimensional theoretical (numerical) model for the propagation of elastic waves in the earth. The model will be used to investigate the interaction of elastic waves with buried objects, thus providing both a predictive capability for system performance and a technique for the design of future field experiments. As a part of this modeling, an experimental effort to measure the relevant physical properties of soils and mines has also been undertaken.

The activities undertaken on this project over the last year are outlined below. Additional technical details pertaining to these activities may be found in the manuscripts that are included in the appendices to this report.

I. Three-Dimensional FDTD Model

a) A linear three-dimensional FDTD model has been developed to model wave propagation in soil and the interactions of elastic waves with buried objects. The model has been written to run efficiently on a massively parallel computer. Stratification of the soil and the structure of the target are accounted for in the FDTD code. The model is presented in the attached papers [P1-P4].

b) The linear 3-D FDTD model has been validated by comparison to experimental data taken in a sandbox at Georgia Tech [P1-P4].

c) The linear 3-D FDTD model has been used to study the interactions with a variety of buried mines and clutter objects [P1,P3,P4].

d) The effects of trenching have been modeled numerically [P2]. The numerical trenching model has been validated experimentally.

e) Initial investigations have been performed on techniques for including the non-linearity and the loss of the sand in the model. This is described in Appendix I.

f) Because of the computational requirements for the model, a Beowulf cluster consisting of 50 500MHz Pentium III processors and 6 GB of memory has been assembled as part of this project. The three-dimensional FDTD model has been implemented to run efficiently on the Beowulf cluster.

II Soil Property Measurements

a) Physical properties of wet compacted sand and local soil samples have been measured through seismic propagation experiments involving surface coupled accelerometers.

b) The depth dependence of shear wave velocity in the experimental model has been studied using an inversion technique involving surface measurements and the three dimensional model [P1]. The technique presumes the depth dependance of the velocity to be the dominant source of surface wave dispersion. The vertical profile is then derived by matching measured time domain waveforms to model predictions.

c) Experiments have been performed to investigate the non-linear properties of the sand in the experimental model as a function of frequency and range [P5]. These experiments have shown that the transfer function of the measurement system has strong nonlinearities above 1,000 Hz in the range of normal drive levels. Increasing the source drive signal by a factor of 10 produces significant nonlinearity over the entire operating bandwidth (100-2,000 Hz). The dominant source of the measured nonlinearities was found to be source to surface coupling and near source effects. Evidence of nonlinear dispersion in the propagation path was also observed.

III Collaboration with NPGS

a) In December 1999, a three-man team from Georgia Tech toured facilities at NPGS and met with Tom Muir to discuss plans for field tests.

b) A series of pilot field tests will be performed form July 16 to August 16, 2000 to test the propagation characteristics and ambient noise field at the NPGS test site. These tests are also intended to resolve logistical issues, which will be encountered in full system tests.

Plans for Future Work

- Develop a method for modeling the non-linear nature of the sand and incorporate it into the three-dimensional FDTD model.

- Include the fine structural details of mines in the numerical model.

- Measure the depth dependence of the shear waves speed explicitly both at the NPGS field site and in the laboratory model.

- Use the numerical model to study the interactions of a variety of mines and burial scenarios.

- Use the numerical model to study alternate configurations of the system including alternative source and sensor concepts and signal processing schemes.

List of Manuscripts Submitted/Published under ONR Support

P1 Schroeder, C.T. and Scott, W.R., Jr., "Three-Dimensional Finite-Difference Time-Domain Model for Interaction of Elastic Waves with Buried Land Mines," *Proceedings of the SPIE: 2000 Annual International Symposium on Aerospace/Defense Sensing, Simulation, and Controls*, Orlando, FL, Vol. 4038, April 2000.

P2 Scott, W.R., Jr., Schroeder, C.T., Martin, J.S., and Larson, G.D., "Investigation of a Technique that Uses Both Elastic and Electromagnetic Waves to Detect Buried Land Mines," *Proceedings of the AP2000 – Millennium Conference an Antennas and Propagation*, Davos, Switzerland, April 2000.

P3 Schroeder, C.T., Kim, K., and Scott, W.R., Jr., "A Three-Dimensional Model for Elastic Waves in the Ground," *Proceedings of the 139th Meeting of the Acoustical Society of America*, Atlanta, Georgia, June 2000.

P4 Schroeder, C., and Scott, W.R., Jr., "Three-Dimensional FDTD model to Study the Elastic –Wave Interaction with Buried Land Mines," *Proceedings of the 2000 International Geoscience and Remote Sensing Symposium*, Honolulu, Hawaii, July 2000.

P5 Albert, B.C., "Characterization of Nonlinearities in the Propagation of High Frequency Seismic Waves," Thesis, School of Mechanical Engineering, Georgia Institute of Technology, April 2000.

Scientific Personnel

Faculty: Waymond Scott, Peter Rogers, Gregg Larson, James Martin, George McCall

Students: Chistoph Schroeder, Kong-Wook Kim, Blace Albert.

Appendix I

Model for Nonlinearities and Loss

It is common to assume linear elasticity or linear viscoelasticity in numerical models because of the associated conceptual and computational simplicity. [R20] However, soil is generally an unconsolidated material and even a relatively small excitation can cause nonlinearities. In addition, linear elasticity does not include an attenuation mechanism, which every real material has. For these reasons it is inadequate to model unconsolidated soils with a linear elastic model in many applications.

Initial investigations have been performed on techniques for including the non-linearity and the loss of the soil in the model. Several approaches for including the non-linearities and the loss into the model have been presented in the literature. These fall into three categories: viscoelastic models [R1-R7], simple nonlinear elastic models [R8-R10], and nonlinear endochronic models [R11-R20]. From our initial investigations, these models do not seem to be adequate to model the propagation in the soil. The elastic limit and yield limit of unconsolidated materials, unlike consolidated materials, are widely separated having very small strains for the elastic limit and large strains for the yield limit. This causes the nonlinear propagation zone of the unconsolidated material to be of considerable width even for a small excitation on surface. [R8] In this nonlinear zone, the materials show cusped hysteresis loops, amplitude dependent wave speed, harmonic generation, redistribution of spectral energy, and amplitude-dependent attenuation. [R8 – R10, R16, R20]

For the model to be able to accurately predict wave propagation in unconsolidated soil, it must be able to model the hysteresis loops in the stress-strain relationship with reasonable accuracy. This is very important for two reasons. First, the nonlinear nature of the stress-strain relationship will generate harmonics and, second, the hysteresis will generate loss. These must be properly balanced or the model will be incorrect. Without the loss, the nonlinearities will generate more and more harmonics. This will result in an ever-increasing frequency content of the modeled signal, and eventually cause the FDTD model to fail. In the real physical system, the loss due to the hysteresis limits the frequency content of the signal.

Unlike linear elasticity, linear viscoelasticity has attenuation mechanisms. These attenuation mechanisms are realized by introducing relaxation times and memory variables in the FDTD code. [R4-R7] With this formulation, it is not possible to model the nonlinearities, and it will be difficult, if not impossible, to properly model the loss seen in the soils. This is because the loss is closely tied to the nonlinear mechanisms and can not be properly modeled with a linear model.

The simple nonlinear elastic models include nonlinearities and hysteresis, but they do not do a very good job of modeling the hysteresis loops in the stress-strain relationship. Thus, they are not suitable because they underestimate the loss at the high frequencies and fail due to the above-mentioned mechanism.

The endochronic models also include nonlinearities and hysteresis. The endochronic theory was first introduced by Valanis [R11,R12] and was developed from the concepts of irreversible thermodynamics of internal variables. It is a phenomenological model

[R13]. In endochronic theory, the kernel needs to be singular, and the weakly singular kernel function can be approximated by the finite sum of exponential functions [R13-R16]. The medium response is determined by the kernel function. The endochronic model does a better job of modeling hysteresis loops than does the previously mentioned models, but the kernels that have been developed do not accurately model the experimental observations that we have made. It is not clear that it is possible to modify the kernel so that it will fit our experimental observations. In addition, endochronic theory is very complex and greatly increases the computational burden for the FDTD code.

It may be possible to extend the endochronic model so that it will correctly model soils, but we have been developing another approach that we believe will perform better and be simpler to implement. This approach is essentially an extension to the simple nonlinear approach in which the hysteresis loops are modeled more accurately.

References

R1   S. M. Day and J. B. Minster, "Numerical simulation of attenuated wavefields using a Pade approximant method," *Geophys. J. R. astr. Soc.*, vol. 78. pp. 105-118, 1984.

R2   J. O. Blanch, J. O. A. Robertsson, and W. W. Symes, "Modeling of a constant Q: Methodology and algorithm for an efficient and optimally inexpensive viscoelastic technique," *Geophysics*, vol. 60, no. 1, pp. 176-184, Jan. 1995.

R3   J. O. Blanch, J. O. A. Robertsson, and W. W. Symes, "Viscoelastic finite-difference modeling," *Geophysics*, vol. 59, no. 9, pp. 1444-1456, Sep. 1994.

R4   J. M. Carcione, D. Kosloff, and R. Kosloff, "Wave propagation simulation in a linear viscoelastic medium," *Geophysical Journal*, vol. 95, pp. 597-611, 1988.

R5   T. Xu and G. A. McMechan, "Efficient 3-D viscoelastic modeling with application to near-surface land seismic data," Geophysics, vol. 63, no. 2, pp. 601-612, Mar. 1998.

R6   S. Hestholm, "Three-dimensional finite difference viscoelastic wave modeling including surface topography," *Geophys. J. Int.*, vol. 139, pp. 852-878, 1999.

R7   J. O. A. Robertsson, "A numerical free-surface condition for elastic/viscoelastic finite-difference modeling in the presence of topography," *Geophysics*, vol. 61, no. 6, pp. 1921-1934, Nov. 1996.

R8   D. W. Kosik, "Propagation of a nonlinear seismic pulse in an anelastic homogeneous medium," *Geophysics*, vol. 58, no. 7, pp. 949-963, July 1993.

R9   N. Cheng, "Nonlinear wave propagation in sandstone: a numerical study," *Geophysics*, vol. 61, no. 6, pp. 1935-1938, Nov. 1996.

R10 G. Yu, J. G. Anderson, and R. Siddharthan, "On the characteristics of nonlinear soil response," *Bulletin of the Seismological Society of America*, vol. 83, no. 1, pp. 218-244, Feb. 1992.

R11 K.C. Valanis, "A theory of viscoplasticity without a yield surface; part I. General theory," *Archives of Mechanics*, vol. 23, no. 4, pp. 517-533, 1971.

R12 K.C. Valanis, "A theory of viscoplasticity without a yield surface; part II. Application to mechanical behavior of metals," *Archives of Mechanics*, vol. 23, no. 4, pp. 535-551, 1971.

R13 H. Murakami and H. E. Read, "A second-order numerical scheme for integrating the endochronic plasticity equations," *Computers and Structures*, vol. 31, no. 5, pp. 663-672, 1989.

R14 K.C. Valanis and C. Lee, "Some recent developments of the endochronic theory with applications," *Nuclear Engineering and Design*, vol. 69, pp. 327-344, 1982.

R15 W. Pan, W. Chiang, and C. Wang, "Endochronic analysis for rate-dependent elasto-plastic deformation," International Journal of Solids and Structures, vol.36, pp. 3215-3237, 1999.

R16 H. Xu, S. M. Day, and J. H. Minster, "Hysteresis and two-dimensional nonlinear wave propagation in Berea Sandstone," Journal of Geophysical Research, vol. 105, no. B3, pp. 6163-6175, Mar. 10, 2000.

R17 H. Xu, S. M. Day, and J. H. Minster, "Model for nonlinear wave propagation derived from rock hysteresis measurements," Journal of Geophysical Research, vol. 103, no. B12, pp. 29915-29929, Dec. 10, 1998.

R18 S. Xu, Q. Zhang, M.G. Britton, "An endochronic constitutive model for grain en masse," J. agric. Engng Res., vol. 63, pp. 121-128, 1996.

R19 C.S Liu, T. W. Yang, and W. H. Wu, "The viscoelastic model on endochronic theory," Journal of Strain Analysis, vol. 32, no. 4, pp. 267-271, 1997.

R20 H. Xu, S. M. Day, and J. H. Minster, "Two-Dimensional linear and nonlinear wave propagation in a half-space," Bulletin of the Seismological Society of America, vol. 89, no. 4, pp. 903-917, Aug. 1999.

Appendix II

Schroeder, C.T. and Scott, W.R., Jr., "Three-Dimensional Finite-Difference Time-Domain Model for Interaction of Elastic Waves with Buried Land Mines," *Proceedings of the SPIE: 2000 Annual International Symposium on Aerospace/Defense Sensing, Simulation, and Controls*, Orlando, FL, Vol. 4038, April 2000.

Three-Dimensional FDTD Model to Study the Elastic-Wave Interaction with Buried Land Mines

Christoph T. Schröder and Waymond R. Scott, Jr.

School of Electrical and Computer Engineering
Georgia Institute of Technology
Atlanta, GA 30332-0250
USA

ABSTRACT

A three-dimensional finite-difference model for elastic waves in the ground has been developed and implemented. The model is used to investigate the interaction of elastic waves with buried land mines. When elastic waves interact with a buried mine, a strong resonance occurs at the mine location. The resonance can be used to enhance the mine's signature and to distinguish the mine from clutter. Results are presented for a single mine buried in the ground and several mines in the presence of clutter. The predictions of the numerical model are in fairly good agreement with experimental results.

Keywords: land mine detection, elastic, acoustic, FDTD, finite-difference

1. INTRODUCTION

A new technique is being investigated at the Georgia Institute of Technology, in which buried land mines are located by using both elastic (acoustic) and electromagnetic waves in a synergistic manner.[1-3] Here, elastic waves interact with a buried land mine and cause the mine and the surface above the mine to vibrate. An electromagnetic radar records the vibrations and, thus, detects the mine. During the process of developing the elastic/electromagnetic sensor, a major part has been the implementation of a numerical model which simulates the interaction of the elastic waves with the buried land mines.[4]

The numerical model is based on the finite-difference time-domain (FDTD) method. The equation of motion and the stress-strain relation, together with a constitutive relation, form a set of first-order partial differential equations that completely describes the elastic wave motion in a medium. Introducing finite differences, this set of equations can be discretized and adapted to the finite-difference time-domain modeling scheme. Assuming that the field is known at one initial time t_0, this numerical scheme is used to determine the field values at later times $t > t_0$.

The finite-difference model has been implemented in two and three dimensions. The solution space is discretized and a staggered finite-difference grid is introduced. The grid is surrounded by a perfectly matched layer, that absorbs the outward traveling waves and, thus, models the infinite extend of the solution space. The finite-difference model has been implemented in a fully parallel fashion. The computations for this paper's results have been performed both on a Cray T3E parallel supercomputer located at the ERDC Massively Shared Resource Center in Vicksburg, Mississsppi, and on a Beowulf PC cluster located at the Georgia Institute of Technology. The Beowulf cluster has been developed and built especially for the model described in this paper.

The numerical model has been very helpful for explaining and understanding the experimental results. The numerical model bears several advantages over the experimental model. With the numerical model, it is possible to visualize the elastic wave motion within the ground, whereas with the experimental model only the wave fields on the surface can be observed. Furthermore, no noise is present in the numerical model, and material parameters can be adjusted easily.

Electronic Mail and Telephone: christoph.schroeder@ee.gatech.edu, 404-894-3123, waymond.scott@ee.gatech.edu, 404-894-3048

Results obtained with the three-dimensional model are presented in this paper. In Sec. 3.1, the propagation of a Rayleigh surface wave is shown as measured experimentally and computed numerically. The surface wave is seen to disperse as it propagates along the surface. The same effect can be also modeled numerically. In Sec. 3.2, the interaction of elastic waves with a buried anti-personnel mine is shown. In both experiment and numerical model, a strong resonance is observed at the mine location. Finally, in Sec. 3.3, the interaction of elastic waves with several buried mines in the presence of clutter is described.

2. THREE-DIMENSIONAL NUMERICAL MODEL

In a realistic setting, one or several mines are buried in the ground, surrounded and covered by various kinds of clutter. To approximate these conditions, experiments have been performed with mines buried in a large sand box.[1] In these experiments, elastic waves are launched by an electrodynamic transducer placed on the surface of the ground. The waves propagate along the surface and interact with the buried land mines. To study these mine-wave interactions, a three-dimensional finite-difference model has been developed.

2.1. Finite-Difference Model

Figure 1 shows the three-dimensional finite-difference model. To reasonably simplify the model, the ground is assumed to be linear, isotropic and lossless. The surface of the ground is modeled as a free-surface, a *Perfectly Matched Layer* terminates the solution space at the remaining grid edges and absorbs the outward traveling waves. The solution space is discretized using a staggered finite-difference grid.[5]
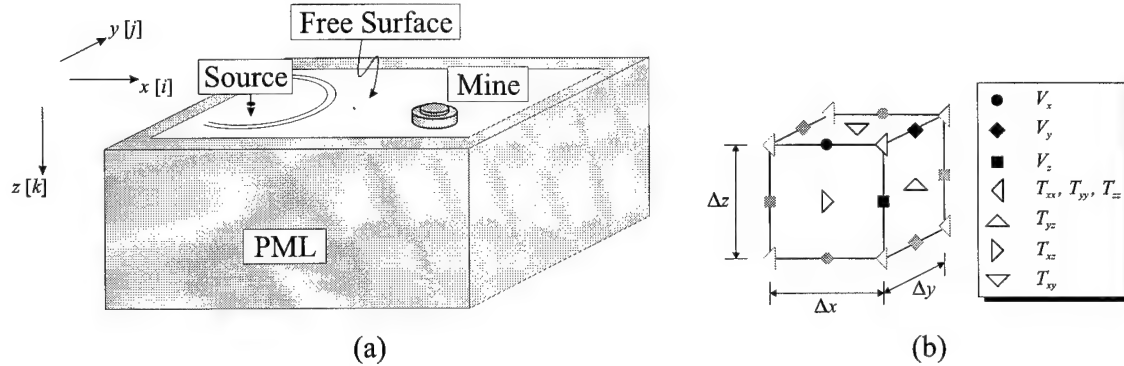

Figure 1. Three-dimensional finite-difference model; (a) lay-out, (b) finite-difference cell.

The elastic wave motion in solids is described by a set of fundamental partial-differential equations: the equation of motion relating the particle velocity vector and the mechanic stress tensor, the strain-velocity relation and the elastic constitutive relation. Combining these equations, a first-order system of equations is obtained describing the elastic wave fields entirely in terms of the particle velocity and the mechanic stress. In three dimensions, three unknown velocity components and six unknown stress tensor components arise.

For the numerical finite-difference model, the derivatives of the partial differential equations are approximated by finite-differences. The finite-difference algorithm shall be explained by deriving the update equations for the x-component of the particle velocity, v_x, (from the first component of the equation of motion) and for the longitudinal stress component, τ_{xx} (from the combined strain-velocity and constitutive relation). Update equations for the other field components can be derived in a similar manner.

The first-order system of equations consists of nine linear independent equations for the three unknown velocity vector components v_x, v_y and v_z, and the six stress tensor components τ_{xx}, τ_{yy}, τ_{zz}, τ_{yz}, τ_{xz} and τ_{xy}. The equations can be written out as

$$\rho \frac{\partial v_x}{\partial t} = \frac{\partial \tau_{xx}}{\partial x} + \frac{\partial \tau_{xy}}{\partial y} + \frac{\partial \tau_{xz}}{\partial z} \tag{1}$$

$$\rho \frac{\partial v_y}{\partial t} = \frac{\partial \tau_{xy}}{\partial x} + \frac{\partial \tau_{yy}}{\partial y} + \frac{\partial \tau_{yz}}{\partial z} \tag{2}$$

$$\rho \frac{\partial v_z}{\partial t} = \frac{\partial \tau_{xz}}{\partial x} + \frac{\partial \tau_{xz}}{\partial y} + \frac{\partial \tau_{zz}}{\partial z} \tag{3}$$

$$\frac{\partial \tau_{xx}}{\partial t} = (\lambda + 2\mu)\frac{\partial v_x}{\partial x} + \lambda\frac{\partial v_y}{\partial y} + \lambda\frac{\partial v_z}{\partial z} \tag{4}$$

$$\frac{\partial \tau_{yy}}{\partial t} = \lambda\frac{\partial v_x}{\partial x} + (\lambda + 2\mu)\frac{\partial v_y}{\partial y} + \lambda\frac{\partial v_z}{\partial z} \tag{5}$$

$$\frac{\partial \tau_{zz}}{\partial t} = \lambda\frac{\partial v_x}{\partial x} + \lambda\frac{\partial v_y}{\partial y} + (\lambda + 2\mu)\frac{\partial v_z}{\partial z} \tag{6}$$

$$\frac{\partial \tau_{yz}}{\partial t} = \mu(\frac{\partial v_y}{\partial z} + \frac{\partial v_z}{\partial y}) \tag{7}$$

$$\frac{\partial \tau_{xz}}{\partial t} = \mu(\frac{\partial v_x}{\partial z} + \frac{\partial v_z}{\partial x}) \tag{8}$$

$$\frac{\partial \tau_{xy}}{\partial t} = \mu(\frac{\partial v_x}{\partial y} + \frac{\partial v_y}{\partial x}), \tag{9}$$

where λ and μ are *Lame's constants* and describe the isotropic solid, and ρ is the material density of the medium.

Taking Eq. (1) and Eq. (4), the update equations for the particle velocity v_x and the longitudinal stress τ_{xx} are derived. Introducing finite-differences in space and time, the partial-differential equations are discretized:

$$\rho \frac{V_x^{l+0.5}(i, j - 0.5, k - 0.5) - V_x^{l-0.5}(i, j - 0.5, k - 0.5)}{\Delta t} =$$

$$\frac{T_{xx}^l(i + 0.5, j - 0.5, k - 0.5) - T_{xx}^l(i - 0.5, j - 0.5, k - 0.5)}{\Delta x} + \frac{T_{xy}^l(i, j, k - 0.5) - T_{xx}^l(i, j - 1, k - 0.5)}{\Delta y}$$

$$+ \frac{T_{xz}^l(i, j - 0.5, k) - T_{xz}^l(i, j - 0.5, k - 1)}{\Delta z}, \tag{10}$$

$$\frac{T_{xx}^{l+1}(i + 0.5, j - 0.5, k - 0.5) - T_{xx}^l(i + 0.5, j - 0.5, k - 0.5)}{\Delta t} =$$

$$(\lambda + 2\mu)\frac{V_x^{l+0.5}(i + 1, j - 0.5, k - 0.5) - V_x^{l+0.5}(i, j - 0.5, k - 0.5)}{\Delta x}$$

$$+ \lambda\frac{V_y^{l+0.5}(i + 0.5, j, k - 0.5) - V_y^{l+0.5}(i + 0.5, j - 1, k - 0.5)}{\Delta y}$$

$$+ \lambda\frac{V_z^{l+0.5}(i + 0.5, j - 0.5, k) - V_z^{l+0.5}(i + 0.5, j - 0.5, k - 1)}{\Delta z}. \tag{11}$$

Here, the capital letters mark the numerical value of the correspondent field component at a discrete location in space and time. For example, $V_x^{l+0.5}(i, j - 0.5, k - 0.5)$ stands for the numerical value of the particle velocity v_x at $(x, y, z) = (i\Delta x, (j - 0.5)\Delta y, (k - 0.5)\Delta z)$ at time $t = (l + 0.5)\Delta t$. Knowing $V_x^{l-0.5}$, T_{xx}^l, T_{xy}^l and T_{xz}^l, Eq. (10) can be solved for $V_x^{l+0.5}$, i.e. for the particle velocity at the incremented time $t = (l + 0.5)\Delta t$:

$$V_x^{l+0.5}(i, j - 0.5, k - 0.5) = V_x^{l-0.5}(i, j - 0.5, k - 0.5) +$$

$$+ \frac{\Delta t}{\rho}\left[\frac{T_{xx}^l(i + 0.5, j - 0.5, k - 0.5) - T_{xx}^l(i - 0.5, j - 0.5, k - 0.5)}{\Delta x} + \frac{T_{xy}^l(i, j, k - 0.5) - T_{xx}^l(i, j - 1, k - 0.5)}{\Delta y} \right.$$

$$+ \left. \frac{T_{xz}^l(i, j - 0.5, k) - T_{xz}^l(i, j - 0.5, k - 1)}{\Delta z}\right]. \tag{12}$$

Similarly, T_{xx}^{l+1} is obtained from Eq. (11):

$$T_{xx}^{l+1}(i + 0.5, j - 0.5, k - 0.5) = T_{xx}^l(i + 0.5, j - 0.5, k - 0.5) +$$

$$+ \Delta t\left[(\lambda + 2\mu)\frac{V_x^{l+0.5}(i + 1, j - 0.5, k - 0.5) - V_x^{l+0.5}(i, j - 0.5, k - 0.5)}{\Delta x} \right.$$

$$+ \lambda\frac{V_y^{l+0.5}(i + 0.5, j, k - 0.5) - V_y^{l+0.5}(i + 0.5, j - 1, k - 0.5)}{\Delta y}$$

$$+ \lambda \frac{V_z^{l+0.5}(i+0.5, j-0.5, k) - V_z^{l+0.5}(i+0.5, j-0.5, k-1)}{\Delta z} \right].$$ (13)

In the same manner, discrete update equations can be obtained for all field components.[6]

The discretization leads to the characteristic finite-difference grid. In this grid, the field components are staggered in space and time. The finite-difference grid can be thought of as being comprised of basis cells. The three-dimensional basis cell for the elastodynamic case resembles strongly the three-dimensional basis cell for electromagnetic finite-difference modeling, the so-called *Yee*-cell.[7] However, due to the stress being a tensor, more field components are present in the elastodynamic case. Figure 1 (b) shows the three-dimensional finite-difference basis cell. The position of the cell in space is labeled with i in the x-direction, with j in the y-direction and with k in the z-direction. Only the field components in black are assigned to the (i, j, k)-th cell. The other field components belong to adjacent cells and are gray in Fig. 1 (b). Note that the field components are not known at the same points in space and time. The grid is laid out such that each field component is surrounded by the field components it is dependent on. The finite-difference algorithm then works as follows. Knowing the field components at one initial time t_0 throughout the entire grid, the field values for later times can be determined. First, the velocity components on the grid are calculated at the incremented time $t_0 + 0.5\Delta t$ using Eq. (10) for v_x and equivalent equations for v_y and v_z. The stress components at $t_0 + \Delta t$ are determined from the velocity components using Eq. (11) and its equivalences. Then, the velocity components are updated using the stress values, the stress components are computed from the velocity components and so on. In this way, the field values can be determined up to any desired time.

When implementing the finite-difference scheme, boundary conditions have to be treated in a special manner. Three different kinds of boundaries arise: the source, internal boundaries (i.e. boundaries within the medium marked by a change in material properties), and external boundaries (i.e. the grid edges).

In the experimental model, an electrodynamic transducer placed on the surface launches the elastic waves. The transducer foot has the shape of a bar. In the numerical model, the transducer is approximated by exciting the particle velocity component normal to the surface, v_z, on an area equivalent to the area of the foot. The motion of the transducer foot has been measured using accelerometers and resembles closely the shape of a differentiated Gaussian pulse. In the numerical model, a differentiated Gaussian pulse is used as excitation, because the excitation must have a smooth shape to avoid numerical dispersion artifacts. To compare the experimental and numerical results, the transfer function of the numerical model at each point in space is determined and convolved with the excitation of the transducer. In this way, the elastic wave fields due to excitation with the real transducer foot motion are obtained.

The conditions at internal boundaries, i.e. at the interfaces between different media, are usually satisfied implicitly. However, to ensure numerical stability, the material properties have to be averaged for components on the boundary. While the material density ρ, appearing in the equation of motion, is averaged directly, the inverse of Lame's constants, λ and μ from the stress-strain relation, must be averaged.

Four external boundaries arise at the four outer grid edges. At its upper edge, the half-space is bounded by a free surface. Due to the continuity of normal stress, the normal stress components vanish at a free surface. In order to satisfy this condition, an extra row must be inserted into the finite-difference grid one step beyond the free-surface boundary.

In order to model the infinite half-space, all waves that are reaching the three remaining outer grid edges must be perfectly transmitted and absorbed. The boundary condition that does this most accurately is the *Perfectly Matched Layer* (PML) boundary condition, first introduced by Berenger[8] and adapted to elastodynamics by Chew and Liu.[9] Here, a non-physical splitting of the wave fields allows the introduction of a lossy boundary layer that is perfectly matched to the solution space. In continuous space, it has been shown that an arbitrarily polarized wave incident on this PML medium is perfectly transmitted. The wave experiences the exact same phase velocity and wave impedance as in the solution space, while rapidly decaying along the axis normal to the PML-medium interface. In discrete space, however, the PML will not be matched perfectly to the solution space. To keep reflections at the interface small, a tapered loss profile is chosen for the PML.[3]

2.2. Parallelization

The finite-difference model has been implemented in a fully parallel fashion. When implemented on a parallel computer, the three-dimensional finite-difference grid is divided into several sub-grids, and each sub-grid is assigned

to one processor of the parallel machine. The processors compute the wave fields on their sub-grids and share only the field values on the interfaces with their neighbors. The finite-difference model has been implemented to run both on a Cray T3E supercomputer with 544 processors (located at the ERDC Massively Shared Resource Center in Vicksburg, Miss.) and on a PC computer cluster located at the Georgia Institute of Technology. The PC cluster contains 50 Pentium III processors and has been especially built for this project.

3. INTERACTION OF ELASTIC WAVES WITH BURIED ANTIPERSONNEL MINES

The interaction of elastic waves with anti-personnel mines, buried in sand, is to be investigated. First, the propagation of a Rayleigh surface waves along the surface is compared as measured experimentally and as computed numerically. Then, the interaction of elastic waves with a single anti-personnel mine is described. Finally, three anti-personnel mines are buried in the ground together with some rocks and a wooden stick.

In the experiment, the mines are buried in a large sand-filled box. The properties of sand, together with the properties of plastic, air, rocks, and wood, are depicted in Table 1. Note that the shear wave speed in sand is assumed to be depth-dependent. Note also that wood is usually anisotropic, but is assumed to be isotropic to simplify the numerical model. This assumption is justified by considering the small dimensions of the wooden stick used here.

Table 1. Parameters used for finite-difference simulation.

Sand	Shear wave velocity	$c_{s,\text{sand}}$	(depth-dependent)
	Pressure wave velocity	$c_{p,\text{sand}}$	250 m/s
	Material density	ρ_{sand}	1400 kg/m^3
Plastic	Shear wave velocity	$c_{s,\text{plastic}}$	1100 m/s
	Pressure wave velocity	$c_{p,\text{plastic}}$	2700 m/s
	Material density	ρ_{plastic}	1200 kg/m^3
Air	Shear wave velocity	$c_{s,\text{air}}$	0 m/s
	Pressure wave velocity	$c_{p,\text{air}}$	330 m/s
	Material density	ρ_{air}	1.3 kg/m^3
Granite	Shear wave velocity	$c_{s,\text{granite}}$	3500 m/s
	Pressure wave velocity	$c_{p,\text{granite}}$	5500 m/s
	Material density	ρ_{granite}	4100 kg/m^3
Wood	Shear wave velocity	$c_{s,\text{wood}}$	100 m/s
	Pressure wave velocity	$c_{p,\text{wood}}$	300 m/s
	Material density	ρ_{wood}	650 kg/m^3

The space step for the numerical model is chosen to be $\Delta x = \Delta y = \Delta z = 0.5$ cm; the time step is $\Delta t = 11.54$ μs and, thus, fulfills the Courant condition (the necessary condition for stability of the finite-difference algorithm). The excitation has the shape of a Gaussian pulse. To be able to compare the numerical and experimental results, the transfer function of the system is determined in a post-processing step for each point in space and convolved with the transducer motion as measured in the experiment.

3.1. Surface Wave Dispersion

A Rayleigh surface wave is seen to disperse as it propagates along the surface of the ground. This effect has been observed experimentally[1,2] and is believed to be mainly due to the shear wave speed in sand increasing with depth. The pressure within the sand grows with depth, thus enhancing the cohesion between the grains of the sand. The

increased cohesion causes the medium to be stiffer and the shear wave speed to become larger. The shear wave speed as a function of depth is empirically found to be

$$c_s = 150 \left(1 - \frac{3}{10z^{0.3} + 5} \right) \text{ m/s}, \tag{14}$$

where z is the depths in meters. The depth profile is graphed in Fig. 2.
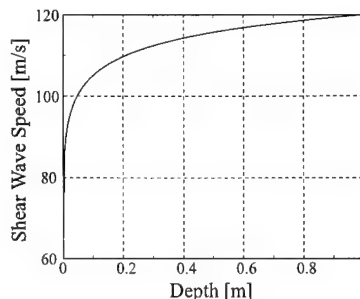

Figure 2. Shear-wave-speed depth profile.

Figure 3 shows waterfall graphs of the vertical particle displacement at the surface as measured experimentally (Fig. 3 (a)) and as determined numerically (Fig. 3 (b)). In these graphs, the displacement at a number of points along a straight line on the surface is plotted as a function of time and offset by the distance from the source. The slope of the traveling waves in the graph indicates the wave speed. Thus, by determining the slope, the different wave types can be distinguished.

Both in the experiment and in the numerical model, a pressure wave (P) and a Rayleigh surface wave (R) are seen to propagate. The pressure wave is faster than the Rayleigh wave and, thus, its slope is larger. The pressure wave is seen to decay quickly, due to the pressure wave being a volume wave rather than a surface wave. As the surface wave propagates, the pulse disperses and changes its shape. Dispersion arises, if wave components with different frequencies travel with different speeds. Due to the shear-wave speed increasing with depth, high-frequency components, which are more confined to the surface, will experience a lower shear-wave speed than low-frequency components, which reach deep into the ground. The agreement of experiment and numerical simulation is fairly good. The differences are mostly due to non-linear effects occurring in the sand. The non-linearities dampen the high-frequency components and, in this way, cause the pulse to broaden and to change in shape. By decreasing the amplitude of the excitation in the experiment, the agreement of experiment and numerical simulation can be improved. However, the signal-to-noise ratio of the radar output in the experiment will also decrease and, thus, the noise contents of the data will increase. Thus far, the non-linear effects are not incorporated into the numerical model.

Figure 4 shows the the vertical particle displacement on the surface and on a cross section through the ground at two times, T_1 and T_2, corresponding to the vertical lines in Fig. 3 (b). The wave fields have been computed numerically and are plotted on a logarithmic scale, in which black corresponds to the largest magnitude (0 dB) and white to the smallest (-60 dB). At T_1, a Rayleigh surface wave (R), a shear wave (S) and a pressure wave (P) are seen to propagate. The shear wave and the pressure wave are visisble only on the cross section through ground. The pressure wave induces head waves (H) as it propagates along the surface. Head waves are downwardly directed plane shear waves generated by the passage of bulk waves along the free surface. They usually decay rather quickly. Both the head waves and the surface wave are visible on the cross section and on the surface. At T_2, the waves have propagated farther. The pressure wave has left the range of the plot. The surface wave (R) and the shear wave (S) have separated. The head waves (H) have decayed and are not visible any more on the surface.

3.2. Interaction with a Buried Anti-Personnel Mine

To investigate the interactions with a buried land mine, a simple model for an anti-personnel mine is inserted into the numerical model. Figure 5 shows the simple model, together with a simplified cross-sectional drawing and a picture of a real TS-50 anti-personnel mine. The simple mine model consists of a main chamber containing plastic
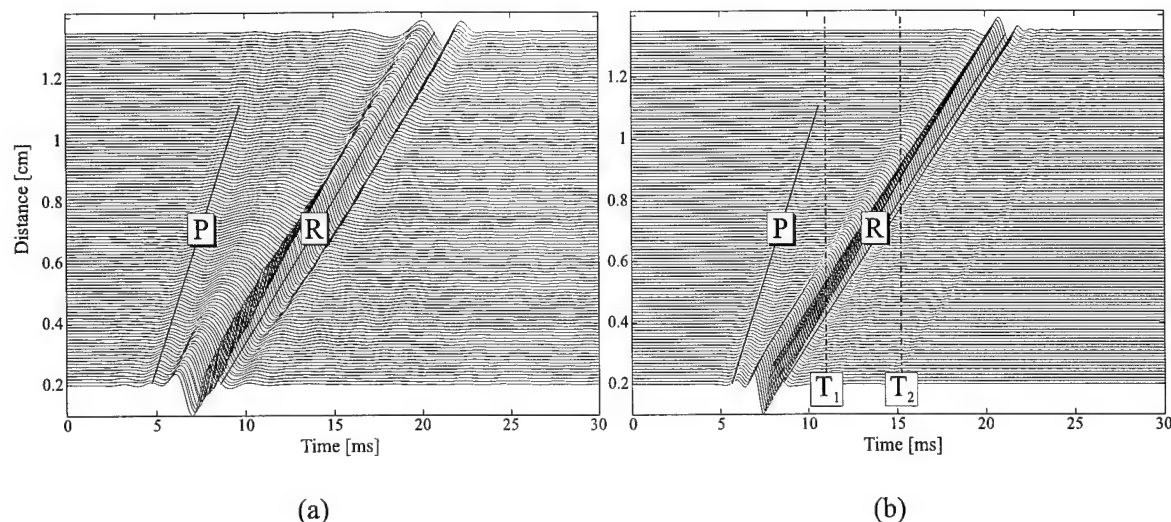
Figure 3. Waterfall graphs of the vertical particle displacement on the surface according to (a) experiment and (b) numerical simulation.
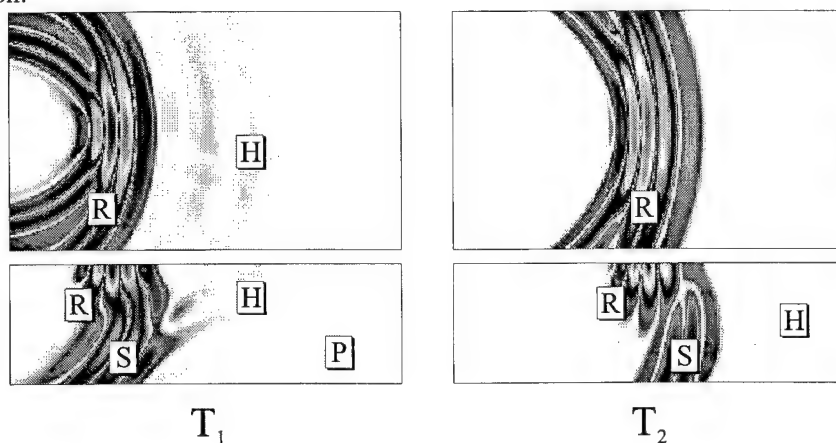

Figure 4. Normal particle displacement on the surface (top) and on a cross section through the ground (bottom). T_1 and T_2 correspond to the vertical lines in Fig. 3 (b).

explosives, and a smaller chamber on top of the mine's main chamber filled with air. In the cubic finite-difference grid, the round shape of the mine is approximated by cubes, leading to the stair-case form evident in Fig. 5. The air-filled chamber is inserted into the model to approximate the structure of a real TS-50 mine. A real TS-50 mine contains plastic explosives, a trigger mechanism, several chambers and is enclosed in a plastic case (see Fig. 5).

Figure 6 shows waterfall graphs of the mine-wave interaction for both experiment and numerical simulation. The mine is buried 2 cm beneath the surface, at a distance of 70 cm from the source. A pressure wave (P) and a Rayleigh surface wave (R) arise. The waves hit the mine and are reflected (rR) and transmitted. While the interaction of the mine with the pressure wave is weak, the surface wave strongly interacts with the mine. In both experiment and numerical simulation, resonant oscillations occur at the mine location and remain even after the waves have passed the mine. For the numerical model, it can be shown that the incident waves couple into flexural waves which arise in the thin soil layer above the mine.[4] These flexural waves are confined to the thin layer and form a standing wave pattern, giving rise to the resonant oscillations. While this explains the resonance in the numerical model, it gives only one possible cause for the resonance in the experiment. A real TS-50 mine has several chambers, it has a flexible case that can support both flexural and longitudinal waves, and it contains springs that can also give rise to resonances. The authors are currently working on refining the numerical model to incorporate more details of the mine.
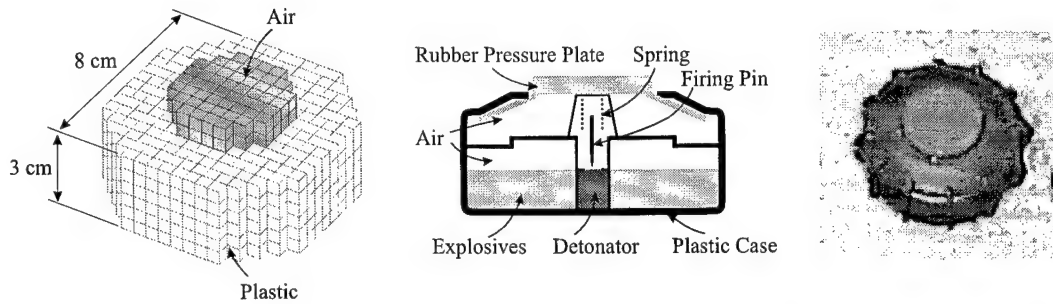
Figure 5. Simple model for the TS-50 anti-personnel mine; cross-sectional drawing and photograph of a real TS-50 mine.
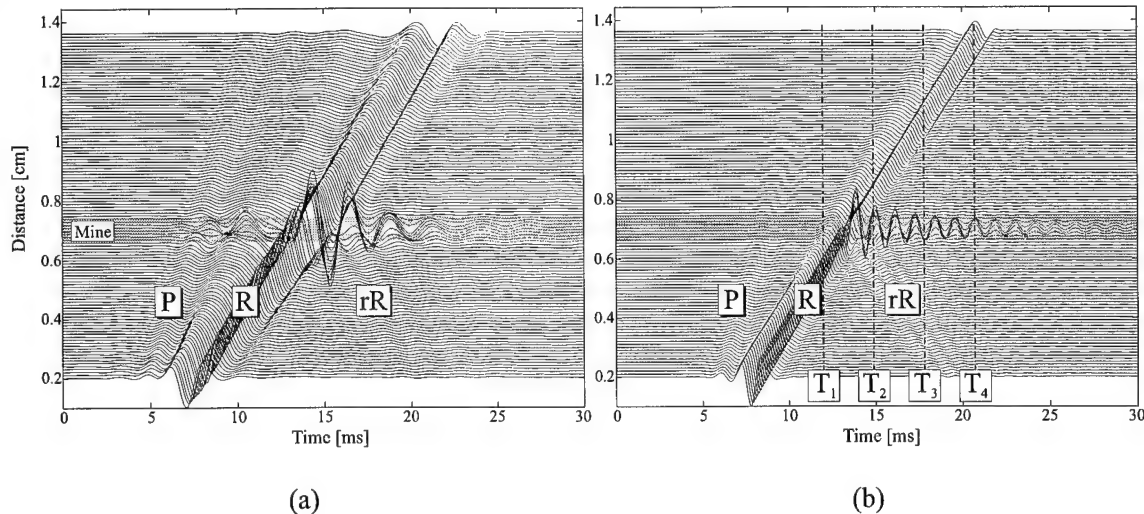

(a)

(b)

Figure 6. Interaction of elastic waves with a buried anti-personnel mine; waterfall graphs of the vertical particle displacement on the surface according to (a) experiment and (b) numerical simulation.

In Fig. 7, the vertical particle displacement on the surface and on a cross section through the ground is plotted. The fields are determined using the numerical model. The dynamic range of the plots is 50 dB. The wave fields are shown at four different instances in time, corresponding to the vertical lines marked with T_1, T_2, T_3 and T_4 in Fig. 6 (b). In the first plot, the surface wave is seen to just hit the mine. While only the surface wave (R) is visible on the surface, both the surface wave (R) and the shear wave (S) appear on the cross section. In the second plot, the surface wave has just passed the mine. The interaction of the surface wave with the mine gives rise to reflected surface waves (rR) and reflected shear waves (rS), which are clearly visible on the cross section. Pressure waves are also induced by the surface wave, but they are weak and not visible. In the third and fourth plot, the surface wave has passed the mine. Some energy, however, remains at the mine and causes the mine to vibrate and to radiate.

3.3. Mine-Wave Interaction in the Presence of Clutter

Next, it is investigated how the presence of clutter affects the mine-wave interaction. For this, three mines are buried in the ground together with a wooden stick and four rocks of various sizes and shapes. The material properties of the rocks (granite) and wood can be found in Table 1. Figure 8 shows how the mines, the rocks and the stick are arranged in the ground. The mine closest to the source is smaller (6 cm in diameter) than the other two mines (8 cm). The mines are buried 2 cm beneath the surface. The first mine lies at a distance of 50 cm from the source, the second at 70 cm and the third at 80 cm. The rocks and the wooden stick are located at different depth and have different shapes. The rock closest to the source is a tilted cuboid, the second rock is a sphere, and the other two consist of rectangular plates of random size. The wooden stick is modeled as a cylinder with a bent axis.

Figure 9 shows the vertical particle displacement on the surface in two series of pseudo color plots as obtained with the numerical model. The first series, Fig. 9 (a), has a dynamic range of 40 dB, whereas the second series,
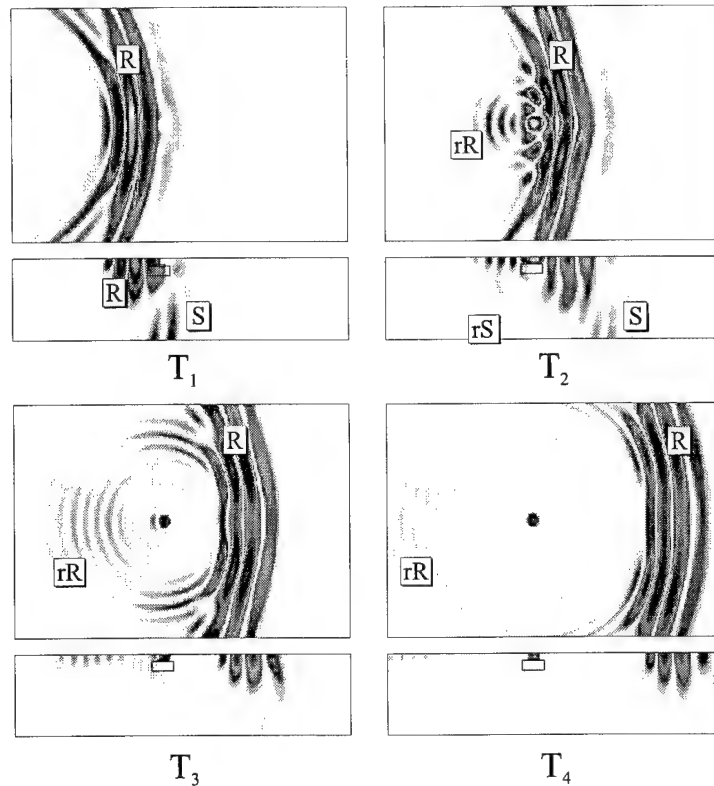
Figure 7. Interaction of elastic waves with a buried anti-personnel mine; pseudo color plots of the normal particle displacement on the surface (top) and on a cross section through the ground (bottom) at four instances in time, corresponding to the vertical lines in Fig. 6 (b).
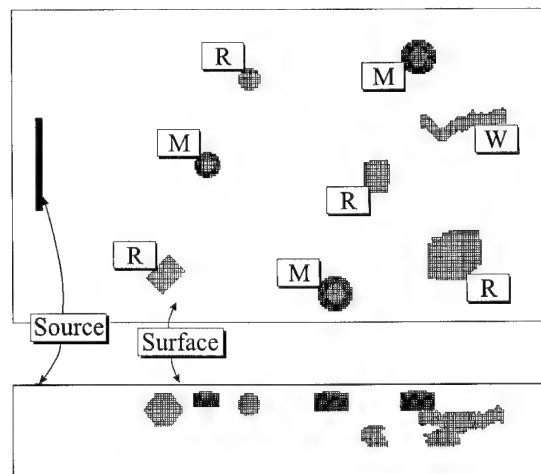

Figure 8. Three mines (M), 4 rocks (R) and a wooden stick (W) buried in the ground; top view and side view.

Fig. 9 (b), has a range of 70 dB. The dynamic range of the first series (40 dB) corresponds to the dynamic range of the experimental measurements. In the 70 dB range, however, more details of the wave-interaction with mines and clutter will be visible. In all plots, black represents the highest magnitude (0 dB) and white the lowest (-40 and -70 dB, respectively). The wave fields are shown at four instances in time.

At the first instance, i.e. the first row in Fig. 9, the surface wave just hits the mine closest to the source. In front

of the surface wave, head waves are propagating. The head waves decay quickly and, therefore, appear only at the earliest instance. On the 40 dB scale, only one faint head wave is visible. However, on the 70 dB scale, three head wave fronts are evident. These head waves have already reached the other two mines. At the second instance, the surface wave has passed the first and second mine and has just reached the third mine. A similar resonance to the one described in Sec. 3.2 is observed at the location of the first mine. Energy is trapped at the mine, and the mine radiates continuously. At the third and fourth time, the surface wave has passed all mines and all three are excited to resonant oscillations. The mines are clearly visible on the surface, whereas the rocks and the stick cannot be seen. The interaction with all rocks is rather weak. Very similar results have been observed also experimentally using real anti-personnel mines. Strong resonances could be seen at the mine locations, making it easily possible to distinguish the mines from the clutter.

4. CONCLUSIONS

A three-dimensional finite-difference model for elastic waves in the ground has been developed and implemented in a fully parallel fashion. Results are obtained and compared to experimental results. Experimentally, a Rayleigh surface wave is seen to disperse as it travels along the surface of the ground. This dispersion effect can be modeled also numerically by assuming a depth-dependent shear-wave speed profile. When an anti-personnel mine interacts with elastic waves, a strong resonance occurs at the mine location. This resonance has been observed in both experiment and numerical simulation. When clutter is present, this resonance can be used to distinguish mines from objects like rocks and wooden sticks, making it easy to locate the mines in the ground.

ACKNOWLEDGMENTS

REFERENCES

1. W. R. Scott, Jr., C. T. Schröder, and J. S. Martin, "An acousto-electromagnetic sensor for locating land mines," in *Detection and Remediation Technologies for Mines and Minelike Targets III, Proc. SPIE*, vol. 3392, pp. 176–186, 1998.
2. W. R. Scott, Jr. and J. S. Martin, "Experimental investigation of the acousto-electromagnetic sensor for locating land mines," in *Detection and Remediation Technologies for Mines and Minelike Targets IV, Proc. SPIE*, 1999.
3. C. T. Schröder and W. R. Scott, Jr., "Finite-difference time-domain model for elastic waves in the ground," in *Detection and Remediation Technologies for Mines and Minelike Targets IV, Proc. SPIE*, 1999.
4. C. T. Schröder and W. R. Scott, Jr., "A finite-difference model to study the elastic-wave interactions with buried land mines," *IEEE Trans. on Geophysics and Remote Sensing*, to be published.
5. C. T. Schröder, *A Finite-Difference Model for Elastic Waves in the Ground*, Diploma Thesis, Technische Universität Braunschweig, 1999.
6. J. Virieux, "P-SV wave propagation in heterogenous media: Velocity-stress finite-difference method," *Geophysics* **51**, pp. 889–901, April 1986.
7. A. Tavlove, *Computational Electromagnetics: The Finite-Difference Time-Domain Method*, Artech House, 1995.
8. J.-P. Berenger, "A perfectly matched layer for the absorption of electromagnetic waves," *J. Comput. Physics* **114**, pp. 185–200, 1994.
9. W. C. Chew and Q. H. Liu, "Perfectly matched layer for elastodynamics; a new absorbing boundary condition," *J. Comput. Acoustics* **4**, pp. 341–359, 1996.
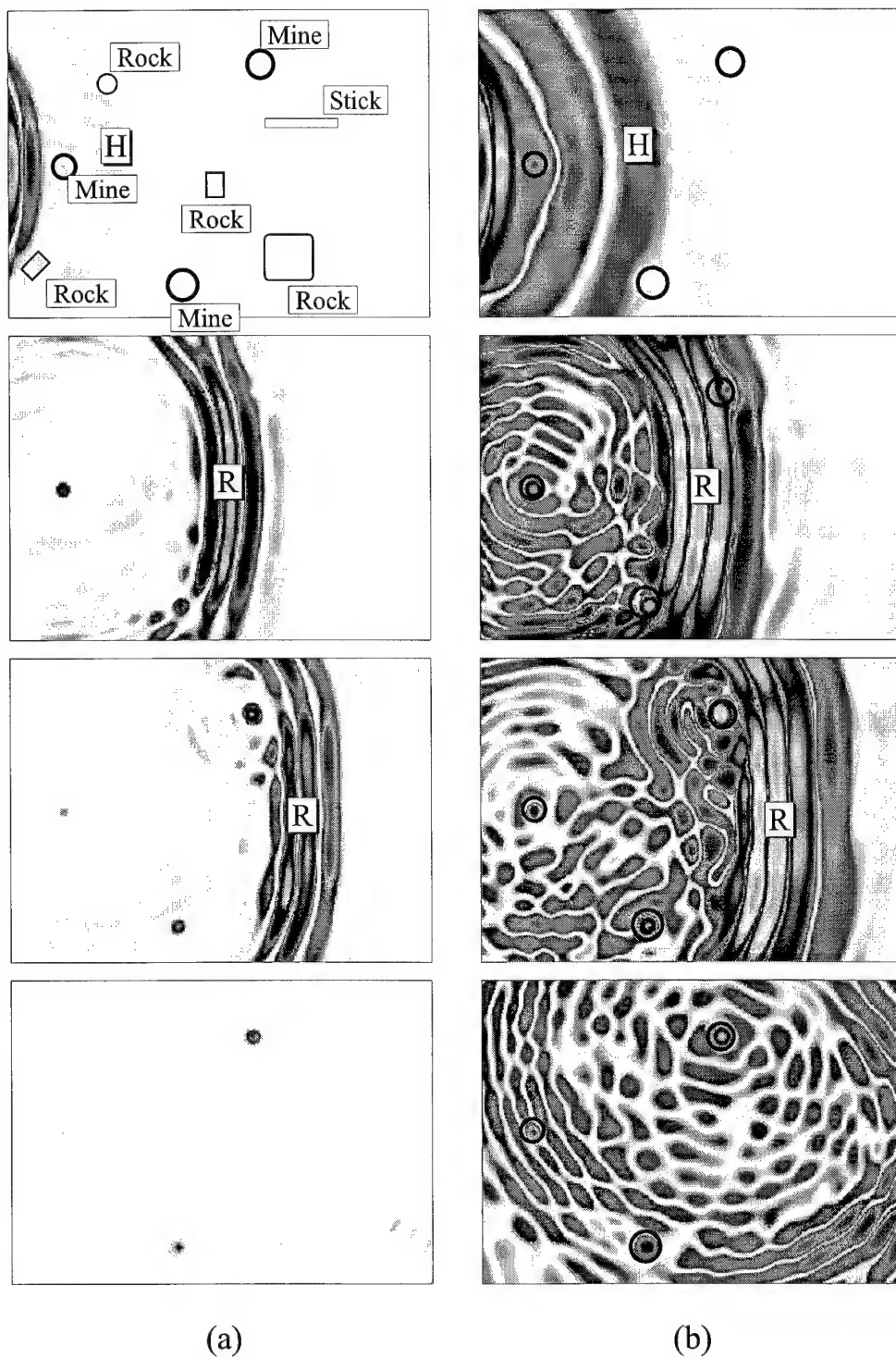
Figure 9. Three mines, 4 rocks and a wooden stick buried in the ground; pseudo color plots of the normal particle displacement on the surface with a dynamic range of (a) 40dB and (b) 70 dB.

Appendix III

Scott, W.R., Jr., Schroeder, C.T., Martin, J.S., and Larson, G.D., "Investigation of a Technique that Uses Both Elastic and Electromagnetic Waves to Detect Buried Land Mines," *Proceedings of the AP2000 – Millennium Conference an Antennas and Propagation*, Davos, Switzerland, April 2000.

INVESTIGATION OF A TECHNIQUE THAT USES BOTH ELASTIC AND ELECTROMAGNETIC WAVES TO DETECT BURIED LAND MINES

Waymond R. Scott, Jr[(1)]**, Christoph T. Schroeder**[(1)]**,
James S. Martin**[(2)]**, and Gregg D. Larson**[(2)]

[(1)]School of Electrical and Computer Engineering
[(2)]School of Mechanical Engineering
Georgia Institute of Technology
Atlanta, GA 30332-0250

INTRODUCTION

A system is being investigated that uses elastic waves as the primary detection mechanism to detect buried land mines [1]. The system is shown in Fig. 1. In the system, a stationary transducer, located on the surface of the soil adjacent to the search region, generates an elastic wave in the earth. The elastic wave propagates through the search region and interacts with the buried mine. This causes both the mine and the earth to be displaced. The displacement of the mine is different than that of the earth, because the mechanical properties of the mine are different than those of the earth. The radar is used to detect these displacements and, thus, the mine. The interaction of elastic waves with buried land mines is being investigated using both numerical and experimental models.
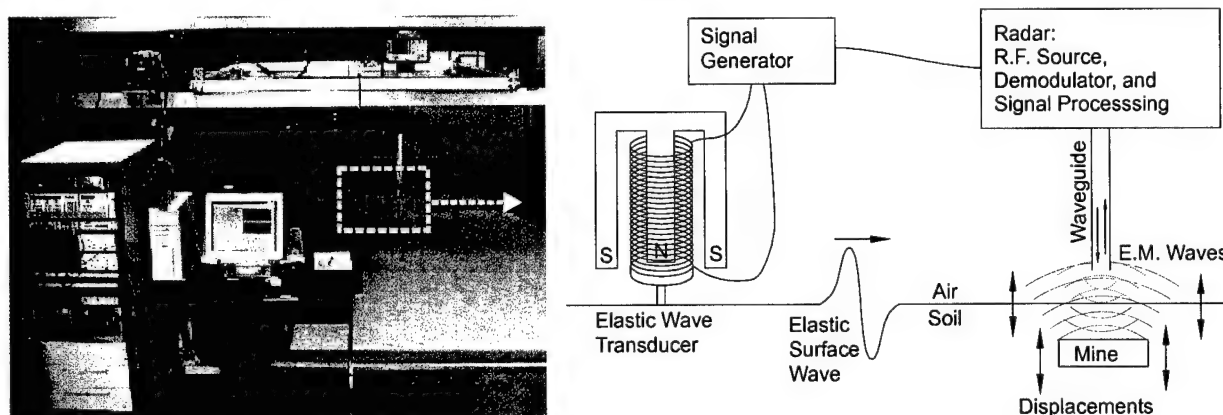

Figure 1. Photograph and schematic diagram of the experimental model.

EXPERIMENTAL AND NUMERICAL MODELS

Numerical and experimental models for the system have been constructed. The numerical model is a three-dimensional, finite-difference time-domain (FDTD) model for elastic waves traveling in the earth. The model is linear and is based on the first-order elastodynamic equations that are differenced in space and time. Pressure, shear, and Rayleigh (surface) waves are all modeled by the algorithm. A perfectly matched layer is used to absorb the waves at the edges of the model, and a free surface boundary condition is used to model the boundary between the earth and the air.

The experimental model uses an electrodynamic transducer to induce the elastic waves, a sand filled tank, a simulated mine, and a radar to measure the surface displacements. The transducer is a 20 LB moving coil shaker coupled to the sand through a narrow foot to preferentially excite surface waves. The tank is approximately 4.5 m wide, 1.5 m deep and 4.5 m long; and is filled with 50 tons of packed damp sand to simulate the earth. The radar is an 8 GHz continuous wave homodyne system specially designed for measuring the surface displacements. The radar is automatically scanned over the surface of the sand to measure the surface displacement field.

RESULTS

The models have been used to study the interaction of the elastic waves with a variety of different mines, simulated and inert. The results in this paper are for a simulated mine that consists of an air-filled plastic cylindrical container. The container is 9 cm in diameter and 2.2 cm in height and has thin flexible walls. This simulated mine was chosen because it is a simple structure that can be easily modeled using the current numerical code by neglecting the effects of the walls. The walls of the container are not expected to contribute significantly to the response of the mine because they are more compliant than the overlaying layer of sand. For the experiment, the simulated mine is buried in the sand and the sand is carefully re-compacted around the mine. The mine is placed 80 cm from the shaker in the center of the scan region.

A series of waterfall graphs of the displacement of the sand surface is presented in Fig. 2 for both the experimental and numerical results using two different burial depths for the simulated mine. In these graphs, the displacement is plotted as a function of time for 101 measurement points spaced in 1 cm increments away from the source in the direction of the mine. Each of the 101 time traces is shifted vertically from the previous one. The bottom trace represents the measurement point closest to the source. The region in which the mine is located is indicated in gray. Many of the discrepancies between the experimental and numerical results can be attributed to non-uniform motion of the shaker foot. The foot exhibits several sand-loaded resonances in the frequency range of interest. In addition, the depth dependence of the mechanical properties of the sand produced by the static pressure gradient is very coarsely approximated in the numerical model.

The incident pressure wave is seen to propagate toward and across the mine. The pressure wave is more apparent in the experimental data than in the model. The incident Rayleigh wave is also seen to travel toward and across the mine. Larger displacements are observed above the mine in all the data sets. These are due to a resonance of the buried mine. This resonance makes it much easier to detect the mine. In spite of the resonance, travelling waves reflected from the mine are seen to be relatively small. This indicates the difficulty that would be encountered in detecting this mine using a classical pulse-echo technique. The diameter of the mine is smaller than the wavelength of the Rayleigh wave at frequencies below 900 Hz. The resonance is spring mass like and occurs between 200 and 300 Hz. Thus, the resonance makes the mine detectable with a lower frequency seismic incident signal than would otherwise be expected. Since low frequencies attenuate more slowly in the earth, the resonance effect extends the possible search range outward from the source.

The effects of a mine resonance are not always repeatable in the experiments. This is probably due to variability in the coupling between the mine and the surrounding sand introduced when it is dug up and re-buried. Care is taken to uniformly compact the sand. However, there seems to be a long time scale cohesion of the sand that cannot be reproduced by simple wetting and compaction. Plots A and B are for burial depths of 2 and 4 cm. In both these cases, the sand in the entire scan region was tilled and repacked to make the sand more homogenous when the mine was buried. The surface displacement associated with the resonance is more pronounced for 2 cm burial depth. Plots B and C of Fig. 2 depict different results for the same mine at a 4 cm depth. The sand for case C was disturbed only above and immediately around the mine and then repacked. This approximates an actual mine burial. Case C was modeled numerically by defining a cylindrical region of earth around the mine with 20% lower wave speeds than the bulk of the medium. It can be seen from the plots that this model predicts most of the qualitative features of the data and reinforces the observation that recently disturbed volumes of soil can be more easily detected than mines. Several authors have noted this trenching effect. Interestingly, both the model and the experiment predict that the trenching effect enhances the resonant response of the mine.

Fig. 3 shows pseudo-color graphs of the displacement over the entire scan region in both the experimental and the numerical model for two different time instants. At time 1, the incident waves have not yet reached the mine. The wave fronts of the pressure and surface waves are seen to have separated in time. Small surface manifestations of head waves are discernable between these wave fronts. At time 2, both the pressure and surface incident waves have propagated beyond the mine. The circular wave fronts of scattered waves can be seen surrounding the mine location and a substantial amount of resonant motion can still be observed over the mine. Unlike the experimental data, the numerical model is able to reproduce displacements below the earth's surface. This can be seen in the cross-sectional graphs at the bottom of the figure. Here it is apparent that the surface manifestations of pressure waves have associated shear head waves propagating into the medium. It can also be seen that the dominant effect of the mine resonance is confined to the soil layer between the mine and the surface. Mode conversions can be seen to occur as both the incident pressure wave and surface wave are scattered from the mine. There is good agreement between the model and experiment at both times depicted.
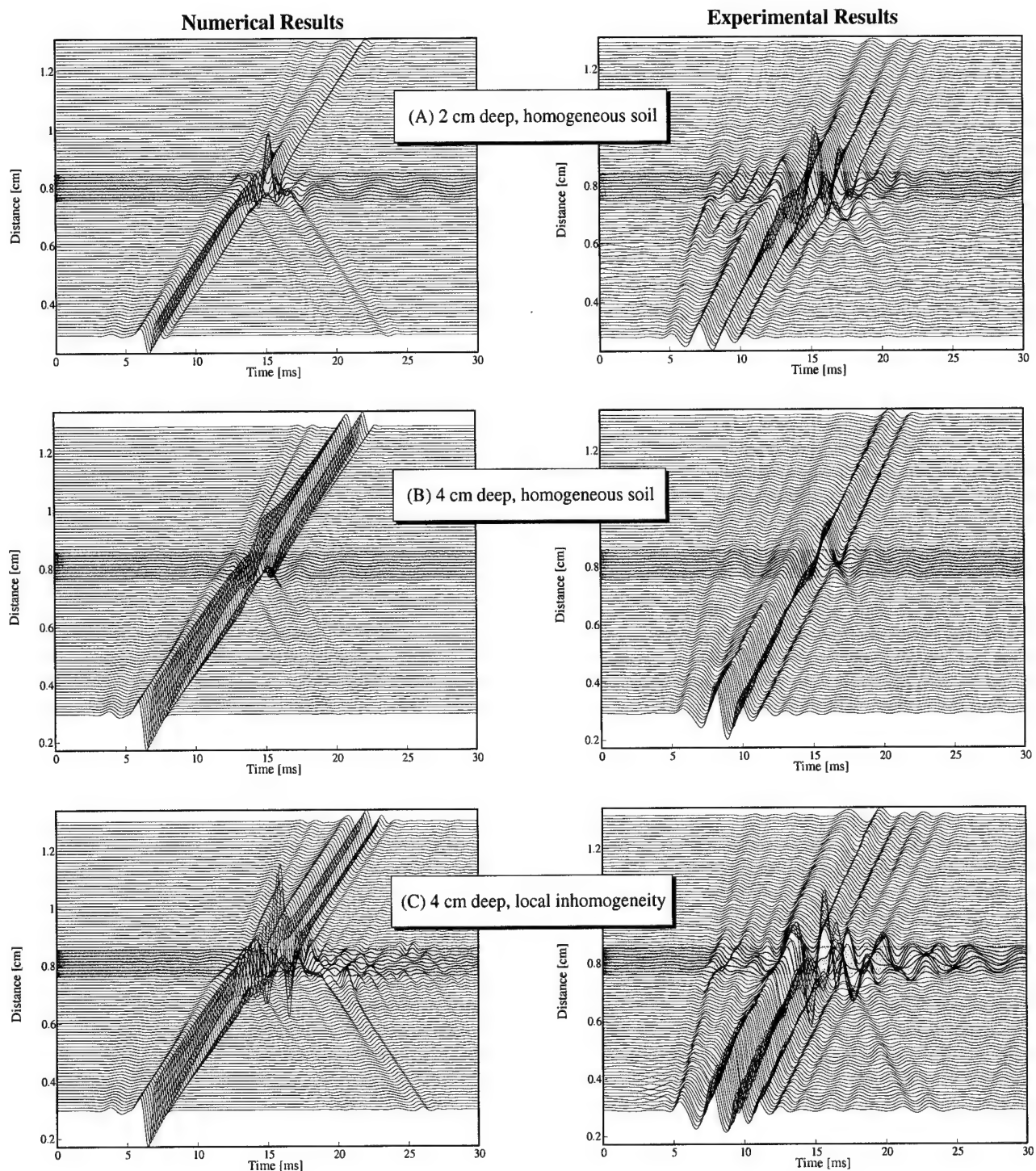
Numerical Results   **Experimental Results**

Figure 2. Waterfall graphs of the surface displacement.

CONCLUSIONS

Good agreement has been shown between experimental and numerical models for the seismic mine detection system. This agreement could be improved by eliminating resonances of the source used in the experiments and by determining the actual depth dependence of the properties of the wet compacted sand. The measured source response and depth dependence can then be incorporated into the numerical model

REFERENCES

[1] W.R. Scott, Jr. and J.S. Martin, "Experimental Investigation of the Acousto-Electromagnetic Sensor for Locating Land Mines," *Proceedings of the SPIE: 1999 Annual International Symposium on Aerospace/Defense Sensing, Simulation, and Controls*, Orlando, FL, Vol. 3710, pg. 204-14, April 1999.

[2] C.T. Schroeder and W.R. Scott, Jr., "Finite-Difference Time-Domain Model for Elastic Waves in the Ground," *Proceedings of the SPIE: 1999 Annual International Symposium on Aerospace/Defense Sensing, Simulation, and Controls*, Orlando, FL, Vol. 3710, pg. 1361-72, April 1999.
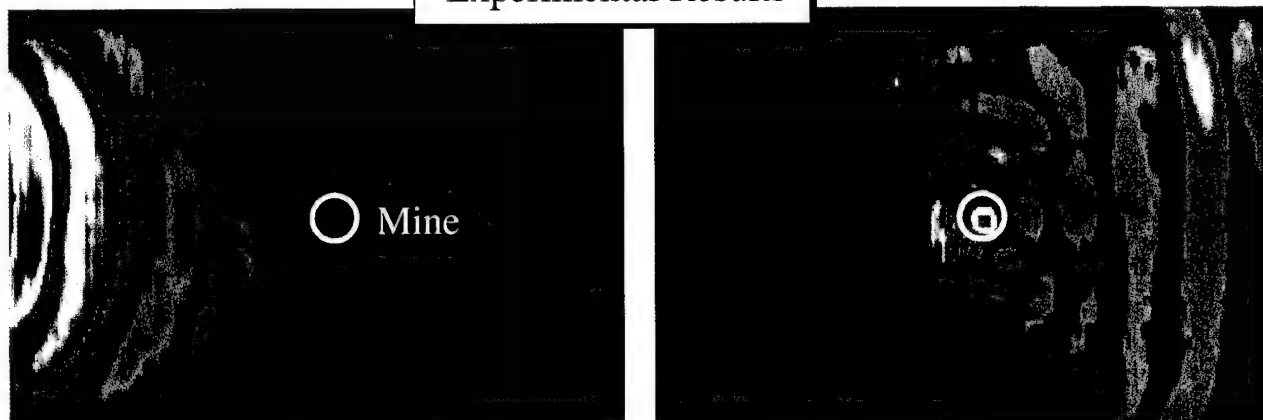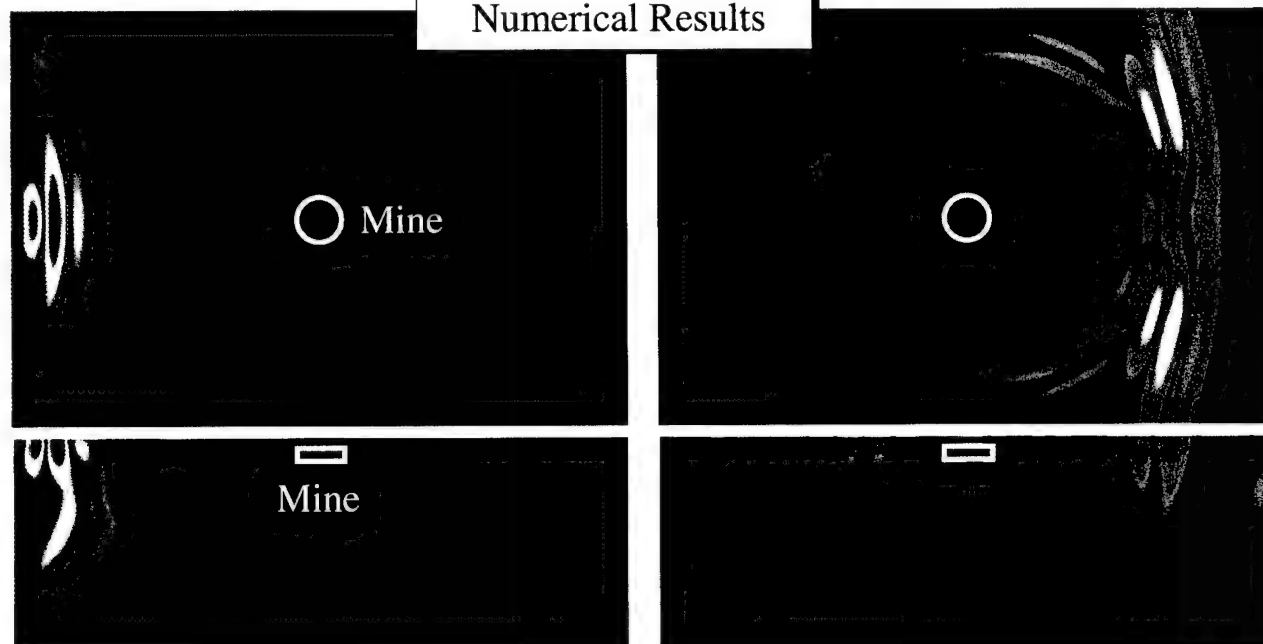
Figure 3. Pseudo-color graphs of the displacement over the entire scan region in both the experimental and the numerical model for two different time instants.

Appendix IV

Schroeder, C.T., Kim, K., and Scott, W.R., Jr., "A Three-Dimensional Model for Elastic Waves in the Ground," *Proceedings of the 139th Meeting of the Acoustical Society of America*, Atlanta, Georgia, June 2000.

4pPA5. A three-dimensional model for elastic waves in the ground.

Session: Friday Afternoon, Jun 02

Time: 2:30

Author: Christoph T. Schroeder
Location: School of Elec. and Computer Eng., Georgia Inst. of Technol., 777 Atlantic Dr., Atlanta, GA 30332, christoph.schroeder@ee.gatech.edu
Author: Kangwook Kim
Location: School of Elec. and Computer Eng., Georgia Inst. of Technol., 777 AtlanticSchool of Elec. and Computer Eng., Georgia Inst. of Technol., 777 Atlantic Dr., Atlanta, GA 30332, christoph.schroeder@ee.gatech.edu
Author: Waymond R. Scott, Jr.
Location: School of Elec. and Computer Eng., Georgia Inst. of Technol., 777 AtlanticSchool of Elec. and Computer Eng., Georgia Inst. of Technol., 777 Atlantic Dr., Atlanta, GA 30332, christoph.schroeder@ee.gatech.edu

Abstract:

A three-dimensional finite-difference time-domain model for elastic waves in the ground has been developed and implemented on a massively parallel computer. The model is based on the three-dimensional equation of motion and the stress--strain relation, from which a first-order stress-velocity formulation is obtained. The boundary between the soil and the air is modeled as a free surface. A perfectly matched layer is implemented at the remaining grid edges to absorb the outward traveling waves. The numerical model has been developed as part of a project in which elastic and electromagnetic waves are used synergistically to detect buried landmines. The numerical model is being used to study the interaction of the elastic waves with the buried mines. To verify that the model accurately predicts the mine--wave interaction, the eigenfrequencies of various solid bars and plates are determined numerically and compared to analytical solutions. Currently, the model is being refined to incorporate loss within the bulk medium. Results will be shown for various landmines buried in both loss-free and lossy ground. [Work supported by ARO and ONR.]

Appendix V

Schroeder, C., and Scott, W.R., Jr., "Three-Dimensional FDTD model to Study the Elastic –Wave Interaction with Buried Land Mines," *Proceedings of the 2000 International Geoscience and Remote Sensing Symposium*, Honolulu, Hawaii, July 2000.

Three-Dimensional FDTD Model to Study the Elastic-Wave Interaction with Buried Land Mines

Christoph T. Schröder[a] and Waymond R. Scott, Jr.[b]
School of Electrical and Computer Engineering
Georgia Institute of Technology
Atlanta, GA 30332-0250, USA
(a) christoph.schroeder@ee.gatech.edu, 404-894-3123
(b) waymond.scott@ee.gatech.edu, 404-894-3048

ABSTRACT

A three-dimensional finite-difference model for elastic waves in the ground has been developed and implemented. The model is used to investigate the interaction of elastic waves with buried land mines. When elastic waves interact with a buried mine, a strong resonance occurs at the mine location. The resonance can be used to enhance the mine's signature and to distinguish the mine from clutter. Results are presented for a single mine buried in the ground. The predictions of the numerical model are in fairly good agreement with experimental results.

INTRODUCTION

A new technique is being investigated at the Georgia Institute of Technology, in which buried land mines are located by using both elastic (acoustic) and electromagnetic waves in a synergistic manner [1]–[4]. Here, elastic waves interact with a buried land mine and cause the mine and the surface above the mine to vibrate. An electromagnetic radar records the vibrations and, thus, detects the mine. During the process of developing the elastic/electromagnetic sensor, a major part has been the implementation of a numerical model which simulates the interaction of the elastic waves with the buried land mines.

The numerical model is based on the finite-difference time-domain (FDTD) method. The equation of motion and the stress-strain relation, together with a constitutive relation, form a set of first-order partial differential equations that completely describes the elastic wave motion in a medium. Introducing finite differences, this set of equations can be discretized and adapted to the finite-difference time-domain modeling scheme.

The finite-difference model has been implemented in two and three dimensions. The numerical model is used to investigate the mine-wave interactions and has been very helpful for explaining and understanding the experimental results. In this paper, results obtained with the three-dimensional model are presented. The interaction of elastic waves with a buried antipersonnel mine is shown.

THREE-DIMENSIONAL NUMERICAL MODEL

In a realistic setting, one or several mines are buried in the ground, surrounded and covered by various kinds of clutter. To approximate these conditions, experiments have been performed with mines buried in a large sand box [1], [2]. In these experiments, elastic waves are launched by an electrodynamic transducer placed on the surface of the ground. The waves propagate along the surface and interact with the buried land mines. To study these mine-wave interactions, a three-dimensional finite-difference model has been developed.

Finite-Difference Model

Fig. 1 shows the three-dimensional finite-difference model. To reasonably simplify the model, the ground is assumed to be linear, isotropic and lossless. The surface of the ground is modeled as a free-surface, and a *Perfectly Matched Layer* terminates the solution space at the remaining grid edges and absorbs the outward traveling waves [5]. The solution space is discretized using a staggered finite-difference grid.
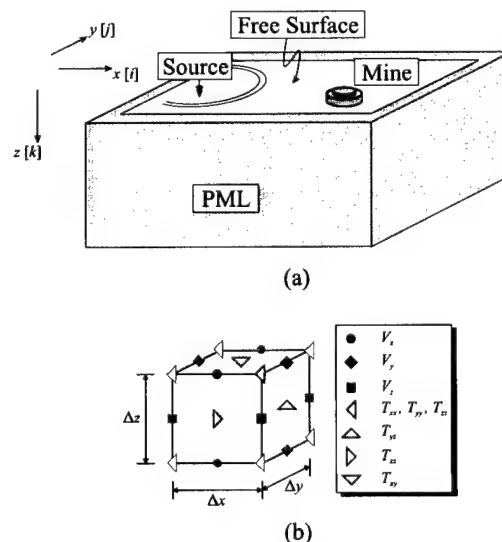

(a)

(b)

Fig. 1. Three-dimensional finite-difference model; (a) layout, (b) finite-difference cell.

The elastic wave motion in solids is described by a set of fundamental partial-differential equations: the equation of motion relating the particle velocity vector and the mechanical stress tensor, the strain-velocity relation and the elastic constitutive relation. Combining these equations, a first-order system of equations is obtained describing the elastic wave fields entirely in terms of the particle velocity and the mechanical stress. In three dimensions, nine equations for three unknown velocity components and six unknown stress tensor components arise.

The equations are discretized by introducing finite-differences. The discretization leads to the characteristic finite-difference grid. In this grid, the field components are staggered in space and time. The finite-difference grid can be thought of as being comprised of basis cells. The three-dimensional basis cell for the elastodynamic case resembles strongly the three-dimensional basis cell for electromagnetic finite-difference modeling, the so-called *Yee*-cell. However, due to the stress being a tensor, more field components are present in the elastodynamic case. Fig. 1 (b) shows the three-dimensional finite-difference basis cell. Note that the field components are not known at the same points in space and time. The grid is laid out such that each field component is surrounded by the field components it is dependent on.

The finite-difference model has been implemented in a fully parallel fashion. The computations for this paper's results have been performed both on a Cray T3E parallel supercomputer located at the ERDC Massively Shared Resource Center in Vicksburg, Mississippi, and on a Beowulf PC cluster located at the Georgia Institute of Technology. The Beowulf cluster has been developed and built especially for the model described in this paper.

INTERACTION OF ELASTIC WAVES WITH BURIED ANTIPERSONNEL MINES

The interaction of elastic waves with antipersonnel mines, buried in sand, is to be investigated. In the experiment, the mines are buried in a large sand-filled box. If the sand is assumed to be linear, isotropic and lossless, its properties can be described by three parameters: the material density, $\rho = 1400$ kg/m^3, the pressure wave speed, $c_p = 250$ m/s, and the shear wave speed. The shear wave speed is not constant and increases with depth.

The space step for the numerical model is chosen to be $\Delta x = \Delta y = \Delta z = 0.5$ cm; the time step is $\Delta t = 11.54$ μs and, thus, fulfills the Courant condition (the necessary condition for stability of the finite-difference algorithm). The excitation has the shape of a Gaussian pulse. To be able to compare the numerical and experimental results, the transfer function of the system is determined in a postprocessing step for each point in space and convolved with the transducer motion as measured in the experiment.

To investigate the interactions with a buried land mine, a simple model for an antipersonnel mine is inserted into the numerical model. Fig. 2 shows the simple model, together with a simplified cross-sectional drawing of a real TS-50 antipersonnel mine. The simple mine model con-

sists of a main chamber containing plastic explosives, and a smaller chamber on top of the mine's main chamber filled with air. The air-filled chamber is inserted into the model to coarsely approximate the structure of a real TS-50 mine (see Fig. 2 (a)).
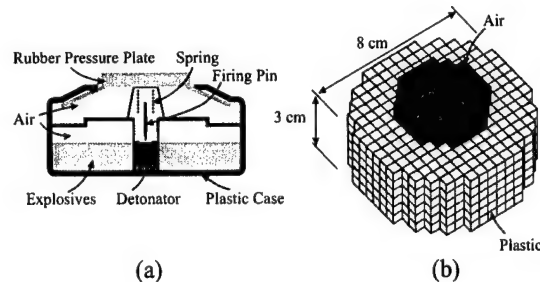

Fig. 2. (a) Cross-sectional drawing of a real TS-50 mine; (b) simple model.

Fig. 3 shows waterfall graphs of the mine-wave interaction for both experiment and numerical simulation. In these graphs, the vertical particle displacement at a number of points along a line on the surface is plotted as a function of time and offset by the distance from the source. The slope of the traveling waves in the graph indicates the wave speed. Thus, by determining the slope, the different wave types can be distinguished. The mine is buried 2 cm beneath the surface, at a distance of 70 cm from the source. A pressure wave (P) and a Rayleigh surface wave (R) arise. The waves hit the mine and are reflected (rR) and transmitted. While the interaction of the mine with the pressure wave is weak, the surface wave strongly interacts with the mine. In both experiment and numerical simulation, resonant oscillations occur at the mine location and remain even after the waves have passed the mine. For the numerical model, it can be shown that the incident waves couple into flexural waves which arise in the thin soil layer above the mine [4]. These flexural waves are confined to the thin layer and form a standing wave pattern, giving rise to the resonant oscillations. While this explains the resonance in the numerical model, it gives only one possible cause for the resonance in the experiment. A real TS-50 mine has several chambers, it has a flexible case that can support both flexural and longitudinal waves, and it contains springs that can also give rise to resonances. The authors are currently working on refining the numerical model to incorporate more details of the mine.

In Fig. 4, the vertical particle displacement on the surface and on a cross section through the ground is shown in some pseudo-color plots as obtained with the numerical model. The upper plots show the wave fields on the surface, the lower plots correspond to a cross section through the ground. The surface plane has dimensions of 120 cm by 80 cm and the cross section has a size of 120 cm by 30 cm. The source is located on the surface, off the left edge of the plots. The dynamic range of the plots is 60 dB. The wave fields are shown at four different instances in time, corresponding to the vertical lines indicated by T$_1$, T$_2$, T$_3$ and T$_4$ in Fig. 3 (b). In the first plot, the surface wave is
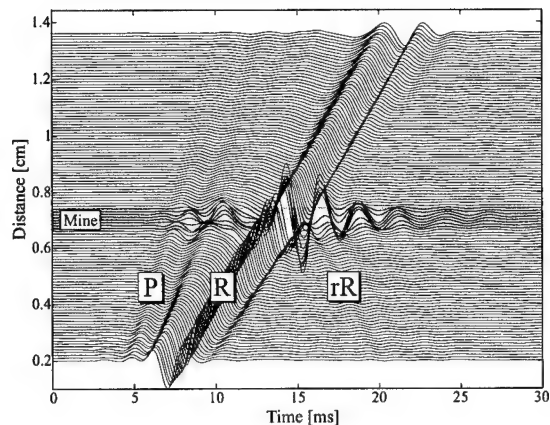
(a)
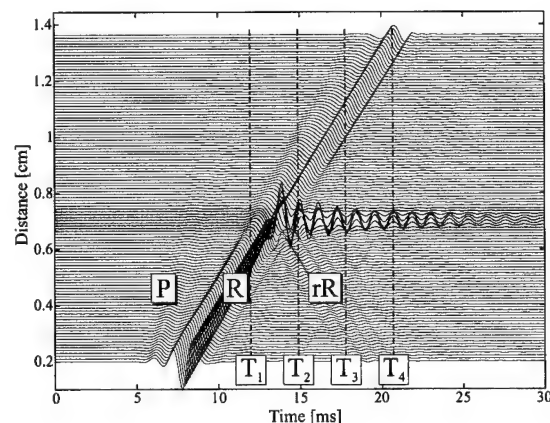
(b)

Fig. 3. Interaction of elastic waves with a buried antipersonnel mine; waterfall graphs of the vertical particle displacement on the surface according to (a) experiment and (b) numerical simulation.

seen to just hit the mine. While only the surface wave (R) is visible on the surface, both the surface wave (R) and the shear wave (S) appear on the cross section. In the second plot, the surface wave has just passed the mine. The interaction of the surface wave with the mine gives rise to reflected surface waves (rR) and reflected shear waves (rS), which are clearly visible on the cross section. Pressure waves are also induced by the surface wave, but they are weak and not visible. In the third and fourth plot, the surface wave has passed the mine. Some energy, however, remains at the mine and causes the mine to vibrate and to radiate.

CONCLUSIONS

A three-dimensional finite-difference model for elastic waves in the ground has been developed and implemented in a fully parallel fashion. Results are obtained and compared to experimental results. When an antipersonnel mine interacts with elastic waves, a strong resonance oc-
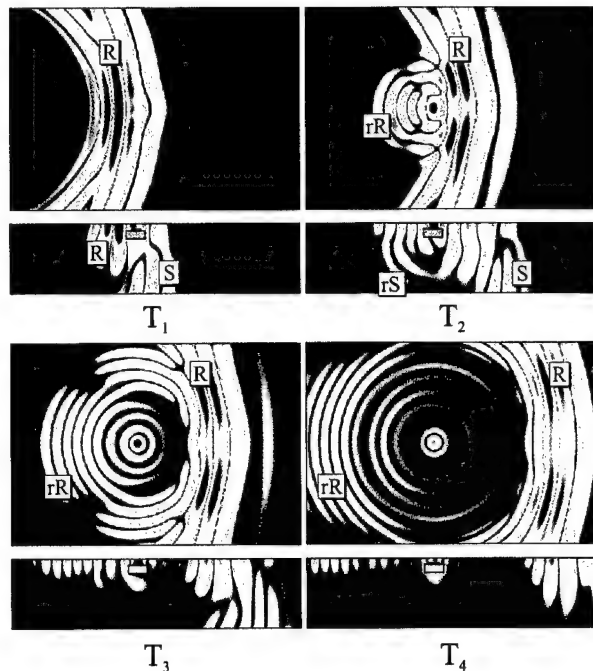

Fig. 4. Interaction of elastic waves with a buried antipersonnel mine; pseudo color plots of the normal particle displacement on the surface (top) and on a cross section through the ground (bottom) at four instances in time, corresponding to the vertical lines in Fig. 3 (b).

curs at the mine location. This resonance has been observed in both experiment and numerical simulation.

REFERENCES

[1] W. R. Scott, Jr., C. T. Schröder, and J. S. Martin, "An acousto-electromagnetic sensor for locating land mines," in Detection and Remediation Technologies for Mines and Minelike Targets III, Proc. SPIE, 1998, vol. 3392, pp. 176–186.

[2] W. R. Scott, Jr. and J. S. Martin, "Experimental investigation of the acousto-electromagnetic sensor for locating land mines," in Detection and Remediation Technologies for Mines and Minelike Targets IV, Proc. SPIE, 1999.

[3] C. T. Schröder and W. R. Scott, Jr., "Three-dimensional FDTD model to study the elastic-wave interaction with buried land mines," in Detection and Remediation Technologies for Mines and Minelike Targets V, Proc. SPIE, 2000.

[4] C. T. Schröder and W. R. Scott, Jr., "A finite-difference model to study the elastic-wave interactions with buried land mines," IEEE Trans. on Geophysics and Remote Sensing, to be published.

[5] W. C. Chew and Q. H. Liu, "Perfectly matched layer for elastodynamics; a new absorbing boundary condition," J. Comput. Acoustics, vol. 4, pp. 341–359, 1996.

Appendix VI

Albert, B.C., "Characterization of Nonlinearities in the Propagation of High Frequency Seismic Waves," Thesis, School of Mechanical Engineering, Georgia Institute of Technology, April 2000.

CHARACTERIZATION OF NONLINEARITIES IN THE PROPAGATION OF HIGH FREQUENCY SEISMIC WAVES

A Thesis
Presented to
The Academic Faculty

by

Blace C. Albert
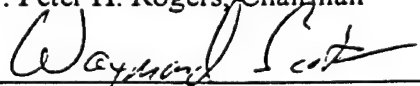
In Partial Fulfillment
of the Requirements for the Degree
Master of Science in Mechanical Engineering

Georgia Institute of Technology
April 2000

CHARACTERIZATION OF NONLINEARITIES IN THE
PROPAGATION OF HIGH FREQUENCY SEISMIC WAVES

Approved:

Dr. Peter H. Rogers, Chairman

Dr. Waymond R. Scott

Dr. Gary W. Caille

Date Approved 17 Apr 00

ii

DEDICATION

To the Sappers of the

82nd Airborne Division and 101st Airborne Division (AASLT),

and to all U.S. ground soldiers, who for lack of better technology

are prepared to locate mines with their bayonets...carefully.

ACKNOWLEDGEMENT

TABLE OF CONTENTS

LIST OF TABLES

LIST OF FIGURES

LIST OF SYMBOLS AND ABREVIATIONS

* - any file name (followed by .file type)

> - greater than

< - less than

% - percent

AC – alternating current

amp – amplifier or amplitude or ampere

c – sound speed

cm – centimeter

cm^2 – square centimeters

cw – continuous wave

DAC – data acquisition card

dB – decibel

dBm – decibels measured

DC – direct current

deg – degree

e – scientific notation ($1e5 = 10^5$)

FFT – fast Fourier transform

ft – feet

g – gravity ($9.8\ m/s^2$)

G – shear modulus

GPR – ground penetrating radar

Hz – Hertz

IFFT – inverse fast Fourier transform

lb – pound

m – meter

MHz – megahertz

MS – megasamples

ms – millisecond

mV – millivolt

nm – nanometer

P-wave – pressure wave

pts – points

r – radius

s – second

S-wave – shear wave

SASW – spectral analysis of surface waves

sec – second

t – time

u – displacement in x direction

U.S. – United States

V – volt

W – watt

ε - cubic dilatation

λ - Lame''s constant

∇^2 – Laplacian operator $((\partial^2/\partial x^2)+ (\partial^2/\partial y^2)+ (\partial^2/\partial z^2))$

ρ - mass density

σ - normal stress

∂ - partial derivative

Φ - potential function

Ψ - potential function

τ - shear stress

SUMMARY

An acousto-electromagnetic land mine detection technique is being investigated. A two-dimensional finite-difference model for elastic waves has also been developed, but it is a purely linear model. Strong nonlinearities are typical of the soils in which mines are buried. The purpose of this thesis is to characterize these nonlinearities for the propagation of high frequency seismic waves (30 – 2000 Hz) in moist, compacted sand so that the parameters used in acousto-electromagnetic land mine detection may be improved and the nonlinearities may be incorporated in the computer model.

The frequency response of the soil model was recorded as a function of drive amplitude and propagation distance. The amplitude response of the soil model was recorded as a function of frequency and propagation distance. The fundamental and first five harmonics were saved for each. Three elastic wave transducers (shakers) were characterized so that source nonlinearities could be compared to propagation path nonlinearities. Characterization of the shakers included foot motion under unloaded and sand-loaded conditions.

The source and propagation path produced nonlinearities as shown by harmonic generation in accelerometers mounted to the shaker foot and radar measurements of the soil surface displacement. Frequencies in the 100 – 600 Hz band propagated best while frequencies above 600 Hz attenuated rapidly. Once the shaker foot to sand coupling was changed results did not repeat with the same precision as when it was left alone.

CHAPTER I

INTRODUCTION

Responsible for approximately 26,000 injuries or deaths per year, an estimated 100 million land mines lay in countries throughout the world [1]. Modern land mines are constructed primarily of plastic, making detection with conventional metal detectors unreliable. This has motivated many researchers to examine new techniques of mine detection. One such technique interrogates for the presence of mines using high frequency (30-2000 Hz) seismic waves. Radar is used as a non-contact measure of the mine's seismic signature. This eliminates the signal to noise and signal to reverberation problems that have been encountered in attempts to employ conventional pulse-echo techniques to the seismic detection of mines. The technique requires relatively high frequency seismic excitations in order to interrogate the shallow burial depths and the small dimensions typical for landmines (<12 inches) [2].

Mine detection operations commonly occur in unconsolidated soils. Typically there are strong nonlinearities found in these conditions. The purpose of this research was to experimentally characterize these features using moist, compacted sand as a soil model. Propagation responses were measured as a function of frequency, amplitude, and propagation distance over the ranges of interest for mine detection. Analysis of the generated data yielded conclusions about the following subjects: (a) frequency threshold dependency on the amplitude of excitation and propagation distance, (b) saturation

threshold dependency on the frequency of excitation and propagation distance, (c) source and near source nonlinearities versus propagation path nonlinearities, (d) differences between various acoustic transducer arrangements (transducer type, frequency response, motion behavior, sources of nonlinearities, etc.) and (e) possible exploitation of nonlinearities to enhance characteristics of the incident signal (level, bandwidth, directivity, duration, etc.).

CHAPTER II

BACKGROUND

General

Finding new and better ways of detecting land mines has become increasingly important in recent years due primarily to the large numbers actively employed throughout the world and the shift towards mines manufactured with plastic casings. Mine warfare has also gained public attention through recent attempts at an international ban on landmines, changes in U.S. landmine usage policy, and U.S. deployments to densely mine-laden countries such as Bosnia.

Current technology relies heavily upon electromagnetic detection techniques. The most prevalent is common metal detection, and for good reason. This technique is very reliable and easy to employ due to the significant differences in the electromagnetic properties of the metal mine and the ground. Even with newer mines encased in plastic, there is still a detectable albeit fainter, electromagnetic signature that may be found with this equipment. Ground Penetrating Radar (GPR) also exploits the mine-ground electromagnetic properties successfully. One of the problems with these techniques however is that they will also detect every soda can, coin, bolt, and any other piece of elctromagnetically significant trash in the ground. This yields a large percentage of false alarms when attempting to clear an area of mines.

As researchers attempt to improve mine detection capabilities by finding a way to augment electromagnetic exploitation techniques, many have turned to the development of acoustic detection techniques. The biggest advantage of acoustic detection is the large contrast between the acoustic properties of the ground and those of the mine, regardless of metal or plastic casing. Buried clutter such as rocks, sticks, or man-made objects also exhibit significantly different acoustical properties than landmines. An example of how different the ground and mine acoustic properties are is the shear wave velocity, which is approximately 20 times greater through the mine's explosives than it is through the surrounding soil [2].

A mine is also a complex structure that includes a flexible, smooth plastic, wooden, or metal casing; a quantity of explosive materials; a firing mechanism (trigger, firing pin, and volatile initiating charge); and air pockets (usually surrounding the firing mechanism). Each of these components may vibrate under the action of forces inherent in the mine without an externally applied force. The frequency at which this vibration occurs is called the natural frequency. If a frequency of excitation coincides with any of the natural frequencies of the mine, resonance occurs. At resonance, the amplitudes of motion may become very large [3]. Because the mine structure is so complex the probability of achieving resonance is higher than it would be for a simple, homogeneous material or structure. The exaggerated displacement amplitudes associated with achieving resonance can be used to detect the location of the mine when buried.

Much of the current research involves pulse-echo techniques such as the use of echo location (direct excitation and reception of seismic waves) [4], or detection by

4

spectral analysis of surface waves (SASW) [5]. Some of the problems that these techniques have encountered are practical implementation issues, low signal to noise ratios, inability to differentiate between mines and debris of similar acoustic reflectivity [6], and significant residue hiding the object reflection when incident-reflected signal subtraction is used [7]. Also, in the case of SASW, incident surface waves arrive at the receivers almost simultaneously with the reflected waves from a shallowly buried object such as a mine.

A new mine detection technique that has shown potential for minimizing the previously mentioned pulse-echo problems utilizes an elastic wave and an electromagnetic sensor [2]. An elastic wave transducer (shaker) has been used to generate waves in the ground. An electromagnetic radar is used to measure the surface displacement as these elastic waves travel through the ground. Because the mine has very different mechanical properties, as previously mentioned, the unique resonances of the mine and the reflection and scattering of the waves cause the ground above it to vibrate differently from the surrounding ground. The radar identifies where the ground particle displacements are different, thus identifying where the mine is buried.

This technique has resolved several practical implementation issues and has shown results with excellent signal to noise ratios. Experiments have also been performed with various types of buried clutter such as rocks and sticks. In all cases the clutter has not been detected which indicates that this method would greatly reduce the number of false alarms in a de-mining operation. The technique has detected mines buried 12 inches deep and has also been able to detect mines underneath a groundcover

(pine straw). In addition to this procedure showing promise for use on its own, another advantage would be its use in conjunction with other detection systems. Because the acousto-electromagnetic detection technique senses different phenomena, it may be employed with conventional detection techniques such as metal detection, ground-penetrating radar, or infrared detection in order to synergistically improve the chances of successful mine detection.

The tests of this system are being done in a large "sandbox". Sand was chosen as the soil medium for its workability when burying and digging up mines, and its relevance. Moist sand is the most common soil encountered by Marines when conducting amphibious landings so it was also of practical interest. Figure 2.1 is a picture of the experimental setup showing this sandbox.

Within the sandbox there is a 120 cm by 80 cm area referred to as the scan region. The scan region is the entire area used to take surface displacement measurements when looking for mines. The lead edge of the scan region is approximately 30 cm from the shaker foot. The radar is mounted on a three-dimensional positioner that moves it around the scan region. The x axis of the scan region is defined as perpendicular to the length of the rectangular shaker foot and the y axis is defined as parallel to the length of the rectangular shaker foot. Surface displacement measurements are taken every cm in the x-direction and every two cm's in the y-direction for a total of 4,961 measurements. This two-dimensional scan may be processed in time in order to create a time progression, or movie, of the wave propagating. Different colors represent the magnitude of surface
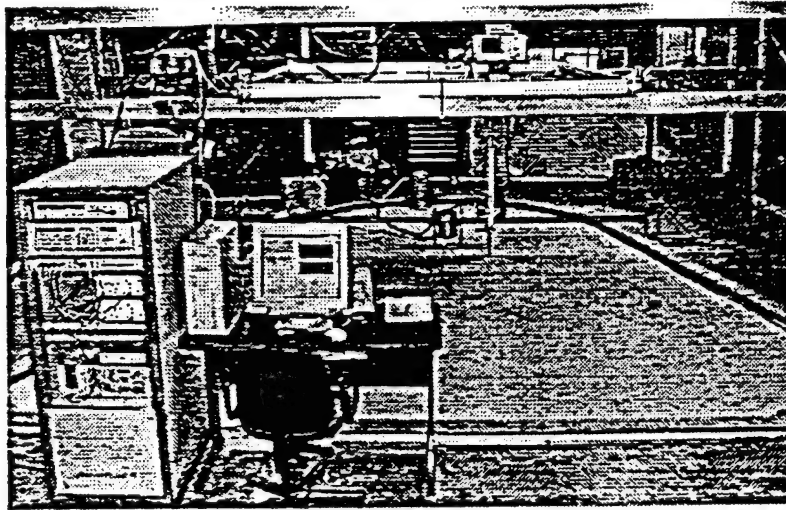
Figure 2.1 Photograph of the Experimental Setup
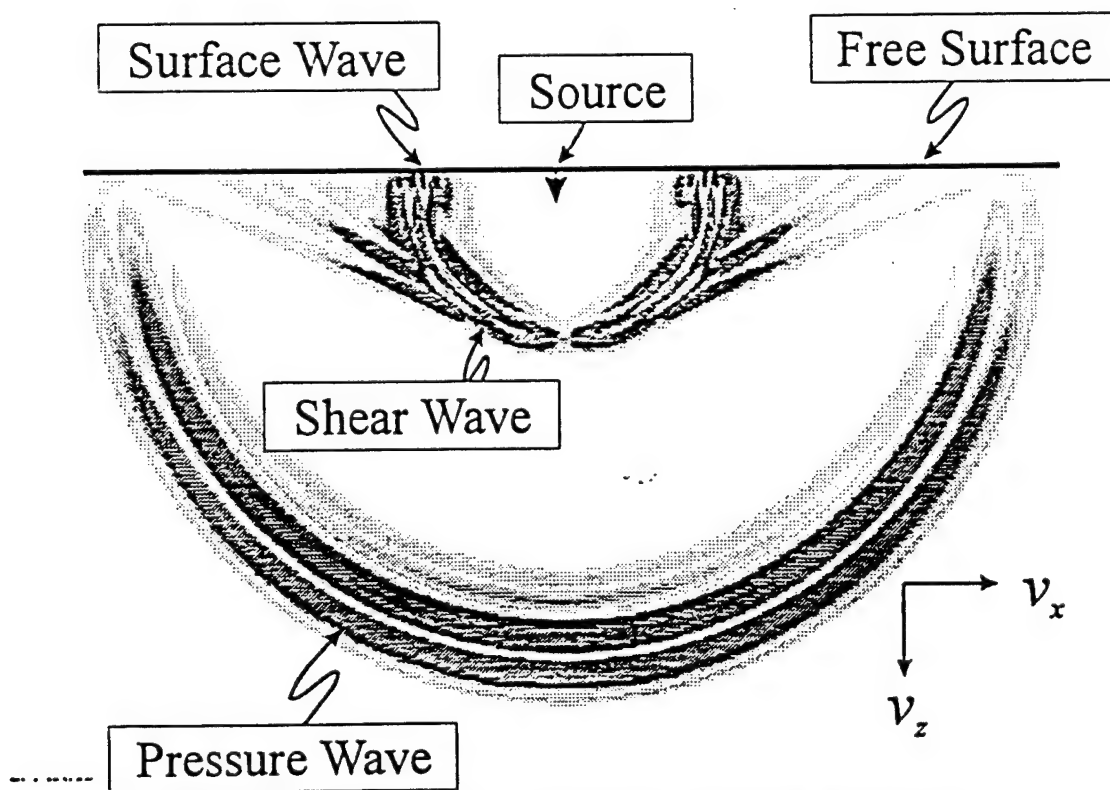
Figure 2.2 Cross-section of Waves Propagating in Half Space

displacements thereby showing how the wave propagates and identifying where the mine is located.

The shaker generates the elastic waves utilizing a 30 Hz – 2000 Hz chirp of 3.6 second duration and a rectangular shaker foot that sits parallel to the lead edge of the scan region. These relatively high frequencies are necessary in order to interrogate the soil for smaller anti-personnel mines, which can be as small as two inches in diameter. The shaker produces compressional, shear, and surface waves within the sandbox.

Figure 2.2 illustrates the different types of waves produced. The picture comes from a computer simulation of the waves [8]. It is a cross-sectional view of an elastic half space with a point source. The lower half represents the sand containing the waves propagating in three dimensions (x,z,t). The half space is bounded on top by a free surface which separates the sand from the air. The boundary condition at this surface is pressure = 0. This causes an impedance mismatch at the boundary creating a pressure release surface ($\rho c_{sand} \gg \rho c_{air}$).

The various waves are defined by their particle motion. The compressional wave propagates by means of pure translational particle motion (particle volume changes but is irrotational). This wave travels the fastest (250 m/s for the model in Figure 2.2) and has the lowest surface normal displacement. The shear wave propagates by means of pure rotational particle motion (particles remain equivoluminal). It travels slower than the compressional wave but slightly faster than the surface wave (87 m/s for the model in Figure 2.2). The particle motion of the surface wave is elliptical in that it contains both translational and rotational components of motion. It travels at a speed very close to, but

8

slightly less than, the shear wave and is confined to approximately one wavelength from the free surface. It propagates cylindrically while the compressional and shear waves propagate spherically [9]. The shear and surface waves cannot be separated within the sandbox because the dimensions are such that the waves do not propagate far enough for the waves traveling at almost identical speeds to separate.

Another way to view the surface displacements is by using a waterfall plot, which is also called a seismogram. Waterfall plots are generated by reading the surface displacements with a one-dimensional scan. The radar reads the surface displacement at a point in front of the shaker and records the information in the time-domain. A fast Fourier transform (FFT) algorithm then takes the measurement into the frequency-domain. During post-processing, this is convolved with the FFT of a differentiated Gaussian pulse and then taken back to the time-domain with an inverse fast Fourier transform (IFFT) algorithm. The result is a pulse that represents the waveform in the time-domain. The radar then moves to the next position along the axis of interest and the process is repeated. Once all of the pulses are recorded, they are plotted one above the other so that the bottom line is the data taken at the closest position and the top line is the data taken at the furthest position. The y axis of the waterfall plot represents the distance from the shaker.

Figure 2.3 shows six different waterfall plots side by side [2]. For all of the waterfall plots, 121 measurements were taken along the x-axis (perpendicular to the shaker foot) at one cm intervals. The first plot was done with no mine present which is also referred to as a clean scan. The other plots have mines present in the vicinity of the

9
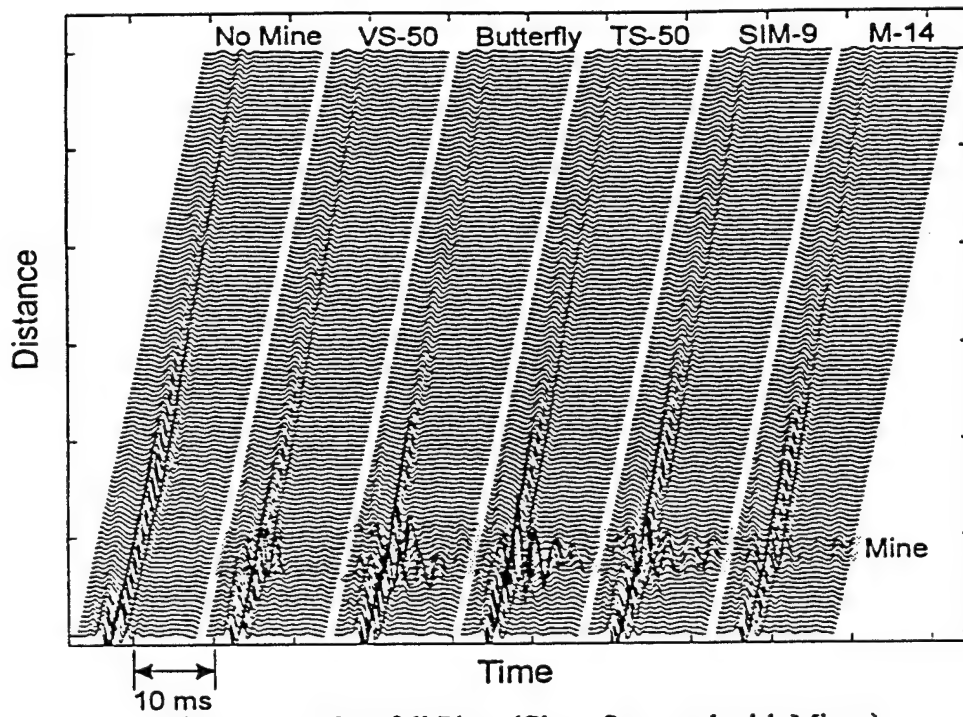
Figure 2.3 Waterfall Plots (Clean Scan and with Mines)
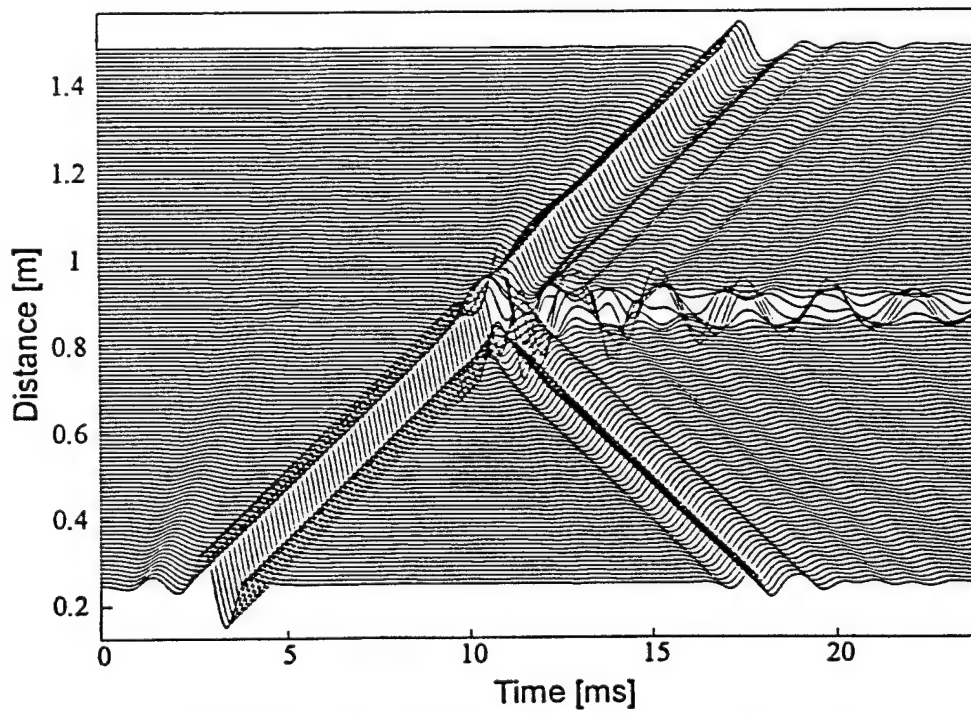
Figure 2.4 Computer Simulation Detecting Buried Mine

10

shaded area. The pulse amplitude is larger in these regions due to the greater surface displacements caused by the mine resonances. These figures illustrate the value of one-dimensional scans and also show what the waveform looks like as it propagates, attenuates, and disperses through the sand when there is no mine present and how the waveform is affected in the presence of a mine.

Efforts to model these waves and their interaction with mines are also underway. In order to do this a two-dimensional finite-difference model for elastic waves has been developed. The model develops a first order stress-velocity formulation from the equation of motion and the stress-strain relations. The system's equations are then discretized using centered finite-differences. The outward traveling waves are absorbed by a perfectly matched layer surrounding the discretized solution space [8]. The results of this modeling have proven to be fairly accurate.

Figure 2.4 is a waterfall plot, for a mine buried at $x = 90$ cm, generated by this computer model [8]. Although the two-dimensional finite-difference model yields reasonably accurate results, it does not take into consideration nonlinearities present in the system. This figure shows the mine resonance and a reflected wave. The results of the computer model are much smoother than an actual one-dimensional scan however. The same levels of dispersion are not present and the reflected pulse is much more noticeable in the computer model. The model's accuracy could be improved if nonlinearities were taken into consideration.

Literature Review

Current literature on wave propagation in unconsolidated soil is incomplete for the mine detection system discussed. There are two main reasons for this. The first is inadequate information about the frequency range of interest. Seismology research is concerned primarily with very low frequencies. The acousto-electromagnetic form of detection however, utilizes a bandwidth of 30-2000 Hz which is regarded as noise by many seismologists. The reason for this bandwidth is twofold. One, frequencies less than 100 Hz are extremely susceptible to dispersion and experience much greater attenuation between 5 and 10 meters [4]. The wavelengths associated with the surface wave for frequencies lower than 100 Hz are also not suitable for detecting smaller mines. Frequencies higher than this do not propagate far enough to be useful. Two, the purpose of the launched ground wave is to excite the resonances of the mine. The greater the bandwidth of the incident signal, the more modes of vibration in the mine that are excited.

The second reason that the current literature is incomplete is the depth at which the mine is buried. Seismological research has not been concerned with shallow depths (< 12 inches). Underground obstacle or cavity detection has focussed much deeper. Some current methods of detection encounter problems when applied this close to the surface as was the case with the SASW method.

Although current seismological research is insufficient to support this method of mine detection, it does yield valuable insight into the particle behavior observed in the sandbox. The equations of motion that apply to homogeneous, isotropic, elastic media

12

can be written in terms of stresses as shown in Equation 2.1 which applies to the x
direction only:

$$\rho(\partial^2 u/\partial t^2) = (\partial \sigma_x/\partial x) + (\partial \tau_{xy}/\partial y) + (\partial \tau_{xz}/\partial z) \quad \text{Eqn. 2.1 [9]}$$

In order to express the right-hand side of this equation in terms of displacements,
relationships for the stresses in terms of Lame''s constant, the shear modulus, cubical
dilatation, and shear strain are used. Combining these with relationships for strain and
rotation in terms of displacement yield Equation 2.2:

$$\rho(\partial^2 u/\partial t^2) = (\lambda \div G)(\partial \epsilon/\partial x) + G\nabla^2 u \quad \text{Eqn. 2.2 [9]}$$

There are two solutions for this equation of motion. The first applies to the
propagation of a dilatational wave (compressional wave or P-wave). The second applies
to a distortional wave (shear wave or S-wave). Because the experiments in the sandbox
are in an elastic half-space, a third type of wave is also present. This wave is the
Rayleigh or surface wave. A surface wave is confined to the surface of the elastic half-
space and contains both x and z direction displacements. If potential functions Φ and Ψ
are chosen to correspond to dilatation and rotation of the wave respectively, then
Equation 2.3 is the equation of motion for the surface wave derived from Equation 2.2.

$$\rho(\partial/\partial x)(\partial^2 \Phi/\partial t^2) + \rho(\partial/\partial z)(\partial^2 \Psi/\partial t^2) = (\lambda + 2G)(\partial/\partial x)(\nabla^2 \Phi) + G(\partial/\partial z)(\nabla^2 \Psi) \quad \text{Eqn. 2.3 [9]}$$

The compressional wave has the highest velocity. The shear waves and surface
waves are slower and their velocities are very similar. The surface wave travels
approximately 94 % as fast as the shear wave. The particle motion of the compressional
wave is in the x direction and the shear wave particle motion is in the z direction. If the x
and z components of the surface wave are added the particle motion is in a

13

counterclockwise direction as the wave propagates to the right. The percent of total energy carried by each of these three waves was measured for a circular footing and found to be distributed as such: surface wave 67%, shear wave 26%, and compressional wave 7% [9]. As the waves propagate, the compressional and shear wave amplitudes decrease as r^{-1} due to spherical spreading. The surface wave amplitude decreases as $r^{-0.5}$ due to cylindrical spreading.

Biot developed stress-strain relationships for wave propagation in porous saturated solids. He discovered that there is only one type of shear wave that propagates through the elastic structure because there is no structural coupling between the elastic structure and the fluid. This is because there is no shearing stiffness in the fluid. There are two compressional waves however. One propagates through the elastic medium and the other through the fluid. They are coupled by the stiffnesses and motions of the elastic medium and fluid. The compressional wave propagating in the fluid is the fastest. It is faster than if it were traveling in fluid alone due to a pushing effect by the elastic medium. The next fastest is the compressional wave in the elastic medium. This is slower than if the medium were dry because of the drag caused by the water in the pores [9].

The horizontal water table affects wave propagation also. If the water table is close enough to the surface, then reflected and refracted waves from this boundary can become a factor. It can also influence the wave velocities depending on whether the measurements are taken below or above the water table. The amount of air in the pores of the half-space makes a large impact on the wave velocity. Richart gives an example in

14

which a 0.1% increase in air bubbles slows wave speed from 4800 ft/sec to 1204 ft/sec. This is important to note because the sand being used for the mine detection experiments is not saturated completely by water. The water table is a couple feet below the surface while the sand at the surface and through the depths pertaining to mine detection is damp. There is plenty of air in the pores of the sand because after it is watered the sand has room to drain to the lower water table.

Some relevant material was found done by Sabatier [10, 11] in the area of acoustic-seismic coupling. Within this research are conclusions about the frequency and depth dependence of attenuation. In general, Sabatier found that higher frequencies in the ground attenuate faster than lower frequencies. For example, 200 Hz attenuates at a rate of 0.06 – 0.1 dB/cm but 1200 Hz attenuates at a rate of 0.16 – 0.22 dB/cm [10]. Sabatier also did tests with a speaker source in the air and a buried microphone to determine the effects of frequency and depth on the wave attenuation. He found that at 5 cm below the surface waves at 1 Hz were attenuating at approximately 2 dB/cm while waves of 1000 Hz at the same point were attenuating at approximately 14 dB/cm. The same test was done 10 cm below the surface. This time waves of 1 Hz were attenuating at approximately 3 dB/cm and waves of 1000 Hz were attenuating at 30 dB/cm [11]. These results showed that wave attenuation is dependent on both frequency and depth and that the effects of frequency and depth are related. Waves attenuate at a more rapid rate the deeper they travel and this rate of attenuation is greater for higher frequencies than for lower frequencies.

Sabatier has also employed acoustic techniques to the detection of buried objects [12]. The system used in this study included a sound source that was above the ground. Acousto-seismo coupling was relied upon to transmit a wave through the ground. The receiver was a microphone that recorded the reflected signal. This signal contained the reflection from the surface and a reflection of smaller amplitude from a buried object. The tests proved effective for objects buried less than five cm deep. Some results that could be a problem when applying this to mine detection were also found. The type of porous media made a difference as to how pronounced the reflected signal from a buried object was, a significant signal is reflected from a hole (false alarms), and smearing of the surface reflection and buried object reflection occurred.

Objective

The objective of this thesis was to characterize the nonlinearites of the propagation path so that the results may then be used to refine the experimental procedure for acousto-electromagnetic mine detection and be applied to the finite-difference time-domain computer model. An example of an observed nonlinearity that prompted this research was a graph of displacement versus input voltage in which the curve rose linearly, as expected, until it began to saturate. When the voltage continued to increase, the curve eventually began to rise again until it reached a second point of saturation. When this same test was done at a different point in the box, the voltage where the saturation effects were seen was different. This indicated that the phenomenon was a result of nonlinearities in the propagation path and not the source.

Another indicator of nonlinearities in the system included several harmonics being produced in the frequency response of the surface displacements. How much the propagation path contributed to these nonlinearities versus how much the source or source to sand coupling contributed was unknown. The goal was to characterize the nonlinearities of the propagation path but this could not be done without considering the entire system. Nonlinearities may occur in the power amplifier, impedance mismatches between the power amplifier and the shaker resulting in oscillating transfer functions, the motion of the shaker foot, the shaker foot to sand coupling, along the propagation path, or at the receiver. These sources of nonlinearities must be isolated to determine which are routinely encountered, the relative impact of these nonlinear effects, how these effects may be reduced or eliminated, and which of these effects should be considered in the computer model.

The data collected fell into two major categories: 1) frequency response as a function of drive amplitude and distance between the source and receiver and 2) surface displacement as a function of drive frequency and distance between the source and receiver. The frequency response data would show how the drive amplitude of the incident wave and the propagation path affect the surface displacement as a function of frequency for a fixed distance. The surface displacement data would show how the frequency and the propagation path affect the surface displacement as a function of the drive amplitude for a fixed distance. In both cases, the fundamental driving frequency and its harmonics were evaluated.

CHAPTER III

INSTRUMENTATION AND EQUIPMENT

Figure 3.1 shows the general configuration of the experimental arrangement for Experiment Two. The only difference in Experiment One was that accelerometers were not used. Table 3.1 lists the major components of the experimental setup, the manufacturers of the equipment, and the equipment models. This configuration is the same one used when scans are performed for the acousto-electromagnetic detection of mines.

The sandbox is approximately 4.5 m long, 4.5 m wide, and 1.5 m deep. It is wedge shaped as seen in Figure 2.1. The end where the shaker sits is approximately five feet deep. This depth extends across half of the sandbox and then slopes up to the top of the far end. It contains about 50 tons of packed sand with a water table that averages two feet below the surface. The dimensions are such that measurements in the scan region do not record reflections from the sides.

The elastic wave transducers are 20 pound and 100 pound shakers. They make contact with the sand through the use of a shaker "foot" which can be different sizes and shapes. The radar is a homodyne type mounted on an XYZ positioner. The data acquisition and positioning is automated using LabVIEW code to control the generated signal, the position of the radar, the various circuitry, and the collection and processing of data. The major component details are listed below.
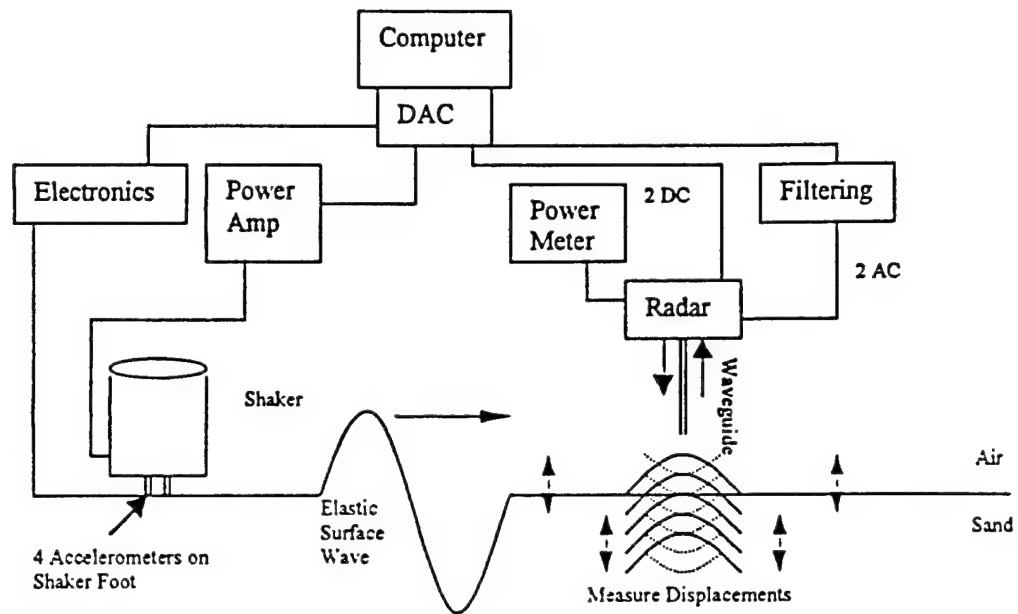
Figure 3.1 Experimental Setup

NAME	MANUFACTURER	MODEL	REMARKS
Data Acquisition Card	National Instruments	PCI-MIO-16E-1	1.25 MS/s (single channel)
Multi-channel filter	Krohn-Hite	3944	Filters out < 30 Hz
Low-noise pre-amp	Stanford Research System	SR560	
Low-noise pre-amp	Stanford Research System	SR560	
Power supply	Topward	3303D	Accelerometers
Power supply	Topward	3303D	Radar
Amplifier	Crown	CE2000	Modified
Shaker	Vibration Test Systems	VG 100-6	100 lb
Power meter	Hewlett-Packard	437B	
Radar	Home-made		Homodyne
Accelerometers	Kistler		Sensitivity: 3.4-3.6mV/g
Accelerometers	PCB Piezotronics	352C67	Sensitivity: 109.5mV/g
Accelerometers	PCB Piezotronecs	352B22	Sensitivity: 9.3-10.6mV/g

Table 3.1 Experimental Component Details

19

Software

The collection of data and operation of the instrumentation was coded in LabVIEW. The LabVIEW codes are contained in Chapter XIII – Appendix E. The data processing and analysis was done with MATLAB. The various MATLAB codes are found in Chapter XII – Appendix D.

Data Acquisition Card

The data was collected with the use of a National Instruments Data Acquisition Card (DAC). The PCI-MIO-16E-1 model card used had the following analog input characteristics: 16 single-ended or 8 differential channels, 12 bit resolution, and a maximum single channel sampling rate of 1.25 MS/s. It had a 1.6 MHz bandwidth for small (-3dB) signals and a 1 MHz bandwidth for large (1% total harmonic distortion) signals. The DAC had the following analog output characteristics: 2 voltage channels, 12 bit resolution, and a maximum single channel update rate of 1MS/s. Digital input/output had 8 input/output channels.

Radar

The homodyne type radar measured surface displacements by executing a phase comparison. It operated with a power of 1 W and had a sensitivity of 1 nm. The spot size was approximately 2 cm in diameter. This spot size would limit the accuracy of measurements above 3000 Hz due to the small wavelengths. A power meter was mounted above the radar to monitor whether or not the radar was operating within its 5 dBm to 15 dBm optimal range (-5 dBm to 5 dBm as read on the power meter).

Positioner

The positioner is mounted approximately 1.5 m above the surface of the sand. It is capable of moving in the x, y, or z directions at various rates and ranges. With the experimental arrangement currently employed, the positioner is limited to 190 cm in the x direction. It can easily range 120 cm in the y direction and 30 cm in the z direction which in no way limits current data collection processes. All data for Experiments One and Two were taken along the x axis with the waveguide positioned 1.3 to 1.8 cm above the sand surface.

Shaker

The signal that drives the shaker is produced in LabVIEW and sent through the break-out box to a Crown CE2000 amplifier. The signal is then sent to a shaker that makes contact with the sand through the use of a shaker foot. All measurements for Experiment One were made with a 20 pound shaker using a rectangular foot measuring 21.6 cm in length by 1.3 cm in width (surface area = 28.1 cm^2). During Experiment Two, three shaker-foot combinations were utilized. The first was the same shaker and foot used in Experiment One. The second was the 20 pound shaker and a round foot with a diameter of 10.2 cm (surface area = 81.7 cm^2). The third was a VG 100-6 shaker, capable of producing a force of 100 pounds, and a rectangular foot measuring 30.2 cm in length and 3.2 cm in width (surface area = 96.6 cm^2). A blower cools the shaker throughout its operation. Figure 3.2 is a picture of the different shakers and feet. Figure 3.3 is a picture of the accelerometer placement for Experiment Two.
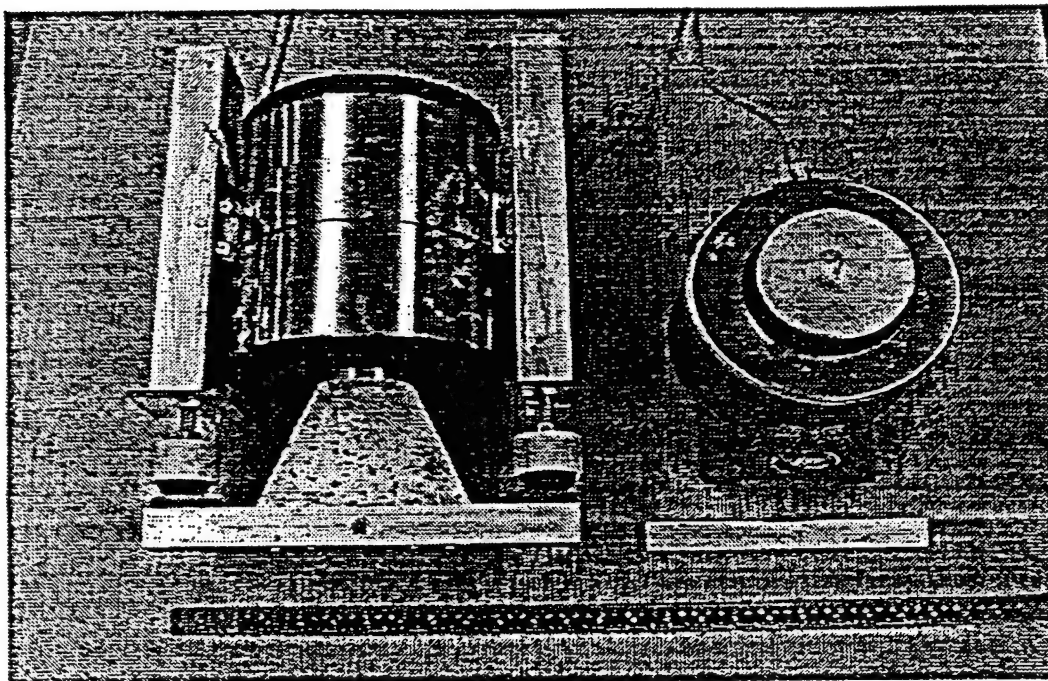
Figure 3.2 100lb Shaker with Rectangular Foot Mounted (left - view from side), 20lb Shaker with Circular Foot Mounted (right top - view from bottom), Small Rectangular Foot for 20lb Shaker (right bottom - view from side)
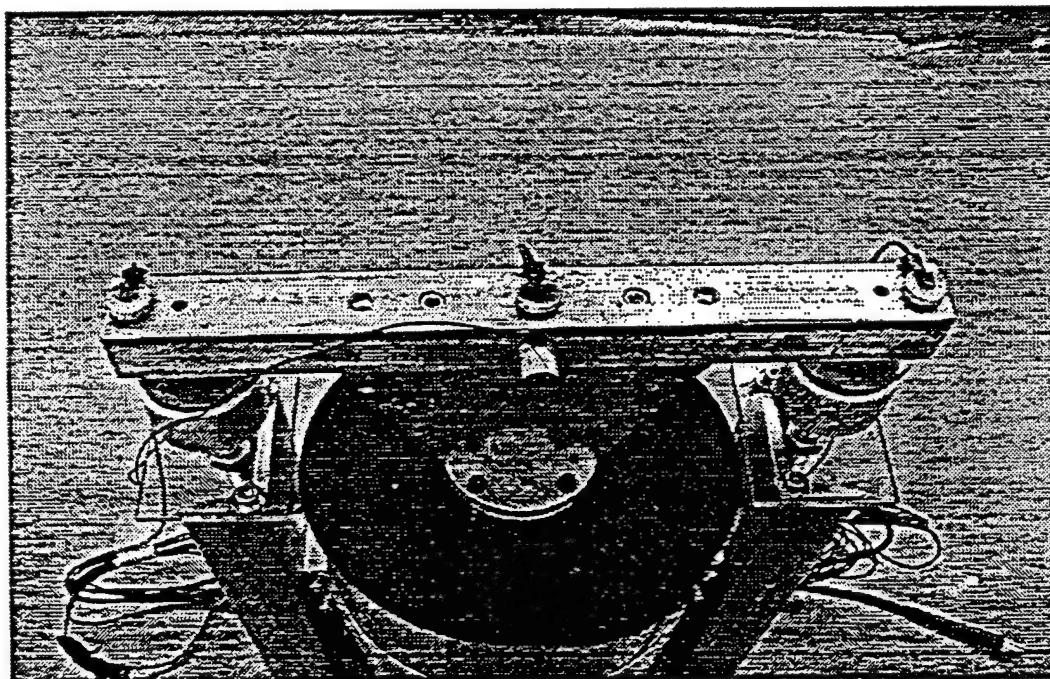
Figure 3.3 Accelerometer Placement on the 100lb Shaker with Rectangular Foot (Bottom View) - 3 PCB 352B22 accelerometers to record vertical acceleration and 1 PCB 352C67 accelerometer to record horizontal acceleration

CHAPTER IV

EXPERIMENT ONE

The objective of this experiment was to measure the surface displacements of the sandbox as a function of drive amplitude, drive frequency, and propagation distance. The resulting data would be used to determine both the frequency responses and amplitude responses for the fundamental frequency and harmonics. There were also two secondary objectives. First, data would be collected in order to separate the compressional and surface waves. Second, data would be taken with a different shaker foot to try to alter the relative content of pressure wave and surface wave. As a result of collecting and processing this data, many ways to improve the data collection were found. This lead to Experiment Two which is discussed in Chapter VI.

Data was taken the following way in order to determine the frequency and amplitude response of the sand. Continuous wave (CW) signals from 33 Hz to 2002 Hz, at 11 Hz increments, were used at a given amplitude and position. It was already known, from the mine detection experiments, that the waves propagated through the box in less than 0.07 second. Therefore a frequency increment of 14 Hz (1/0.07) provided ample resolution to document the wave propagation. It was also known that 60 Hz and its harmonics were very large in the noise floor. By choosing 11 Hz as the frequency increment however, of the 180 frequencies, only three coincided with a multiple of 60 Hz and the first would not occur until 660 Hz. This reduced the impact of the 60 Hz noise.

Once the frequencies had been swept through, the amplitude increased linearly and the frequencies swept through again. A total of 24 amplitudes were used ranging from 0.06 volts to 0.96 volts (input to power amplifier) at a given setting on the power amplifier. All voltages are peak unless otherwise specified. Once the frequencies had swept through the given range for each of the 24 amplitudes, the radar was moved to a different location and the procedure was repeated. This process was done at the following locations in the sandbox: x = 40 cm, x = 80 cm, and x = 120 cm, all along the x axis (origin located 26 cm from shaker foot). The idea behind collecting the data like this was that both the frequencies and amplitudes used were dense enough to generate both the frequency response and the amplitude response from the same data. The details of this experiment, including the experimental design, data collection procedure, and results, may be found in Chapter IX – Appendix A.

Several lessons were learned when this data was processed. First, the voltages ranging from 0.06 to 0.96 were only meaningful for producing total system transfer functions for a given power amplifier setting. They could also be normalized by the data for 0.06 V in order to study relative effects. It would have been much more useful however to know what force the shaker foot applied to the sand. That way frequency response as a function of the shaker force would be known. This involved measuring the current input to the shaker (could be used to calculate power amplifier transfer function) and using the shaker specifications to realize what force was applied given the input voltage from LabVIEW. This was done in Chapter VI – Experiment Two.

The second lesson learned was that the method for processing the data produced a significant leakage of the fundamental and harmonics into the surrounding frequencies. This was evidenced by the noise level rising with the increasing amplitude of the incident signal. A three and a half second incident signal was used so that any ring-up or ring-down transients could be cut out of the data. Only two seconds from the middle of the signal was saved but this was not being cut out at an integer number of periods for each frequency. When this piece of the signal was taken into the frequency-domain, the additional amount past the integer number of cycles contained frequency components different than the continuous wave. These components showed up in the noise floor. Figure 4.1 shows this rising noise level for two different amplitudes. This problem was corrected for Experiment Two as described in Chapter VI.

The third lesson learned was that the amplitudes increased to a point where dynamic fluidization occurred. This happened around amplitudes in the vicinity of 0.82 V. Once the shaker foot would bury itself in the sand, it would be removed, the sand would be repacked, and the shaker would be placed back on the ground. Although this was not an anticipated problem, once the shaker was moved the results were not repeatable. The shaker foot to sand contact was different every time the shaker was placed in the sandbox and therefore measurements needed to be taken without moving the shaker until the data collection was complete. This precluded the use of the high amplitudes that caused dynamic fluidization or a different shaker foot was needed.

The problem of burying the shaker foot was best seen in the amplitude response measurements such as the one shown in Figure 4.2. The curve begins relatively

Position = 80 cm
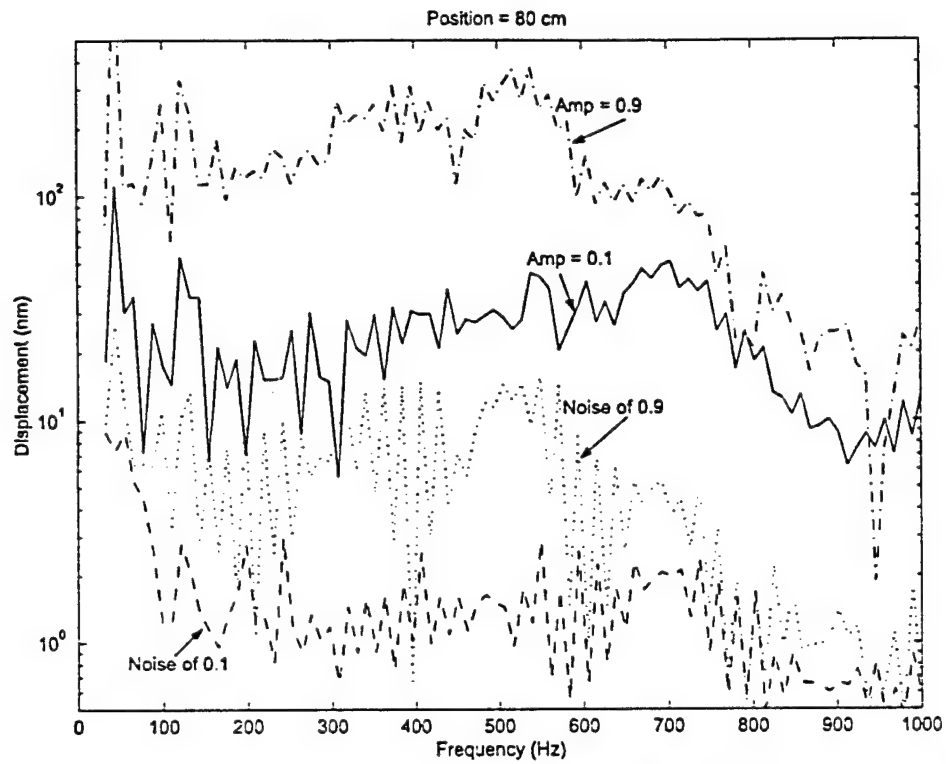
Figure 4.1 Comparison of the Noise Floor for Two Different Amplitudes

Frequency = 88 Hz, Position = 40 cm
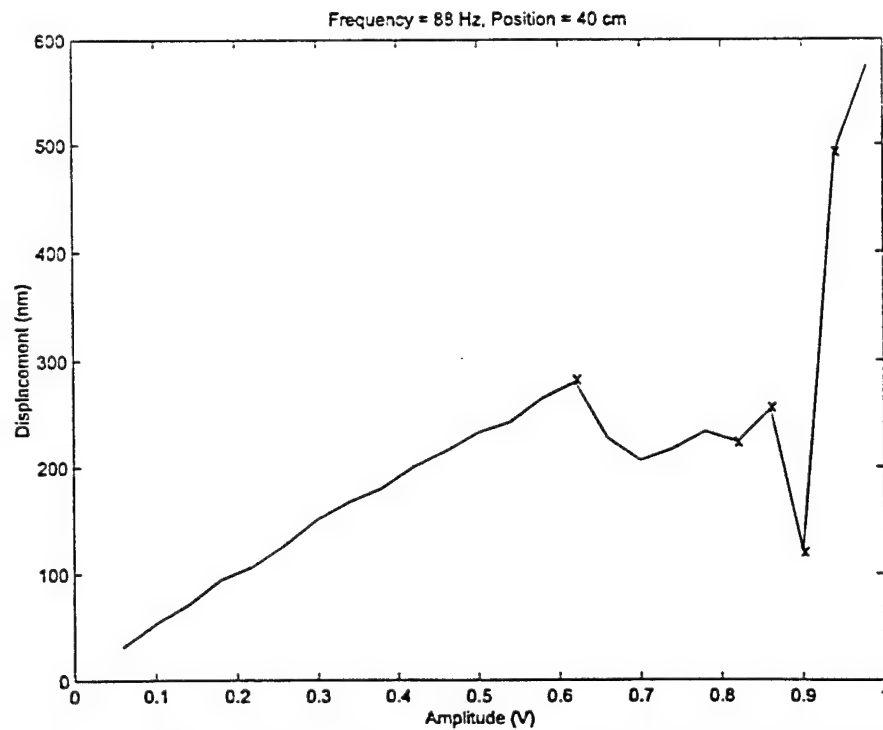
Figure 4.2 Amplitude Response Showing Where Shaker Was Moved

smoothly. Everywhere there is an x on the curve is where the shaker had been picked up in order to repack the sand under it. These places yielded very large jumps in the curve because the new shaker foot to sand contact and the sand particle matrix under the foot was significantly different. The method of collecting the data for Experiment Two corrected this problem as described in Chapter VI.

The fourth lesson learned involved the range of amplitudes being used. The lower end of the amplitudes was not low enough to ensure that the data collection was beginning in a linear region prior to becoming nonlinear. There were also not enough data points to generate a smooth amplitude response. On the other hand, there were many more amplitudes than required to generate the frequency response for increasing amplitudes. This also changed the way data was collected for Experiment Two as described in Chapter VI.

The next phase of Experiment One was to collect data in order to separate the compressional wave from the surface wave. Data was taken in the same format as described above but it was taken on the x axis for x = 190 cm. The intent was to let the waves propagate far enough that they would separate into distinguishable pressure and surface waves in the time domain. From here the waves would be zeroed out one at a time while the other was taken back into the frequency domain. The same frequency responses and amplitude responses would be produced for each individual component to measure the relative contribution of each.

Two problems arose during this procedure. The first was a linear assumption used when taking the data into the time domain. The frequency response for 33 Hz to

2002 Hz was convolved with the FFT of a differentiated Gaussian pulse as described for the mine detection data processing in Chapter II – Background. This was then taken into the time-domain with an IFFT algorithm. This processing method did not take into account that any given frequency may have been producing harmonics that would show up in another frequency bin. Because of the significant nonlinearities in the system this assumption was not going to be reasonable.

The second problem came in trying to determine at what point the surface wave ended and the pressure wave began. Although the waves had propagated through a considerable distance, significant dispersion seemed to occur. This caused the lagging compressional wave fronts to remain close to the leading surface wave fronts. In addition to this the compressional wave had attenuated to a point where it was difficult to see. This was a result of having taken data at $x = 190$ cm instead of doing a one dimensional scan out to 190 cm and then using a waterfall plot to trace the progress of the compressional wave. The results of this phase of Experiment One led to the conclusion that the compressional and surface waves could not be separated to determine their relative contribution to the frequency response of the sand.

Experiment One ended at this point. The problems encountered prompted a significant redesign of the data collection and processing procedure. The new experimental procedure needed to make use of the lessons learned in Experiment One to fix the leakage during data acquisition, increase the dynamic range of amplitudes used to generate the amplitude response, and prevent the shaker from causing dynamic fluidization or having to be moved during the data collection. A study of various shakers

and shaker feet was performed to try to fix this last problem. The results of this study are found in Chapter V – Acoustic Transducers. The lessons learned from Experiment One and the study of shakers were incorporated into Experiment Two in order to correct the above mentioned problems. The way this was done is addressed in Chapter VI – Experiment Two.

CHAPTER V

ACOUSTIC TRANSDUCERS

One of the biggest problems with Experiment One was the fact that the shaker foot was experiencing dynamic fluidization at the moderately high amplitudes. It would also bury in a very short amount of time at frequencies less than 100 Hz. This was due mainly to the small surface area of the foot as opposed to the duration of the experiments. It was also assumed that a significant amount of the nonlinearites in the system were being produced either by the shaker foot or due to the shaker foot to sand contact. The objective of the experiments was to determine characteristics of nonlinearities in the sand however. In order to do this, nonlinearities produced at the shaker foot needed to be quantified and minimized.

The above mentioned problems prompted a study of the acoustic transducers. The purpose of the study was to characterize the motion of different shaker feet, determine propagation characteristics for each of their radiated waves, and select the one with the fewest nonlinearities to conduct Experiment Two. Three shaker – shaker foot combinations were examined in detail. The first was the arrangement used in Experiment One consisting of the 20 pound shaker with the small rectangular foot (surface area = 28.1 cm^2). The second was the 20 pound shaker with a circular foot (surface area = 81.7 cm^2). The third was a 100 pound shaker with a large rectangular foot (surface area = 96.6 cm^2). This last combination was the one chosen to conduct Experiment Two.

In order to characterize the behavior of the different shaker feet, data was taken in a three-step process. The first step was to look for resonance of the foot. The frequency response and amplitude response of the foot under no load (shaker turned upside down so that foot is in air) was measured. This was done utilizing four accelerometers three of which were PCB 352B22's and one of which was a PCB 352C67. During the tests conducted under no load the power amplifier was put on one gain setting lower than that of the tests done loaded. This prevented the foot from bottoming out the suspension of the shaker. The second step was to look for sand loaded resonances. The same measurements were taken under loaded conditions (shaker foot placed on sand as it was during the experiments). All four accelerometers were left in position from step one to step two. The third step was to measure the shaker – shaker foot combination's propagation behavior by taking a sample amplitude response using the radar for a given frequency at two different positions in the sandbox ($x = 10$ cm and $x = 40$ cm).

For each of the frequency response data sets, frequencies between 33 and 2002 Hz were measured at 33 Hz increments. This was done for 0.5 V, 1.0 V, 2.0 V, 4.0 V, and 8.0 V. For each of the amplitude response measurements, amplitudes were swept logarithmically from 0.03 to 8.3 volts and then back down through the same amplitudes for a total of 120 measurements. This was done for 99 Hz, 198 Hz, 396 Hz, 792 Hz, and 1584 Hz. On these graphs the upward sweep was plotted with a solid line and the downward sweep was plotted with a dotted line in order to check for any hysteresis effect. The shaker used in Experiment Two was selected based on these tests. At that

31

time the input voltage was related to the shaker foot force as described in Chapter VI –

Experiment Two.

20lb Shaker (Rectangular Foot)

The four accelerometers were arranged in the following fashion for the test of this

foot. The three PCB 352B22 accelerometers were placed on the bottom of the foot at the

left edge, center, and right edge. This placement looked just like Figure 3.3 for the 100 lb

shaker and large rectangular foot. Their sensitivities were 10.6 mV/g, 9.3 mV/g, and 10.1

mV/g respectively. The PCB 352C67 accelerometer was placed on the side of the foot,

in the center, to capture any horizontal motion. Its sensitivity is approximately 11 times

(109.5 mV/g) that of the PCB 352B22 accelerometers.

Figure 5.1 shows the unloaded response of the 20 lb shaker with rectangular foot.

For the unloaded test in air the motion of the center of the foot increased linearly with

increasing amplitude. As (a) shows however, the amplitude was substantially reduced at

1584 Hz. This was indicative of a null in the frequency response located around 1575 Hz

as shown in (b). This figure also shows a resonance centered at 1785 Hz for the motion

in the center of the foot. The harmonics remain in the noise floor (over 40 dB less than

the fundamental) for the entire range of amplitudes, which indicates a linear behavior

when the foot is unloaded. The ends of the foot are not experiencing the same null at

1575 Hz however. This is indicated in Figure (c) as the left edge normalized by the

center is 30 to 45 times greater for 1584 Hz than it is for the other frequencies. The foot

is functioning as a dynamic vibration absorber when it resonates in this mode. A

comparison of the left and right edges normalized by the center is shown in (d). There is

32
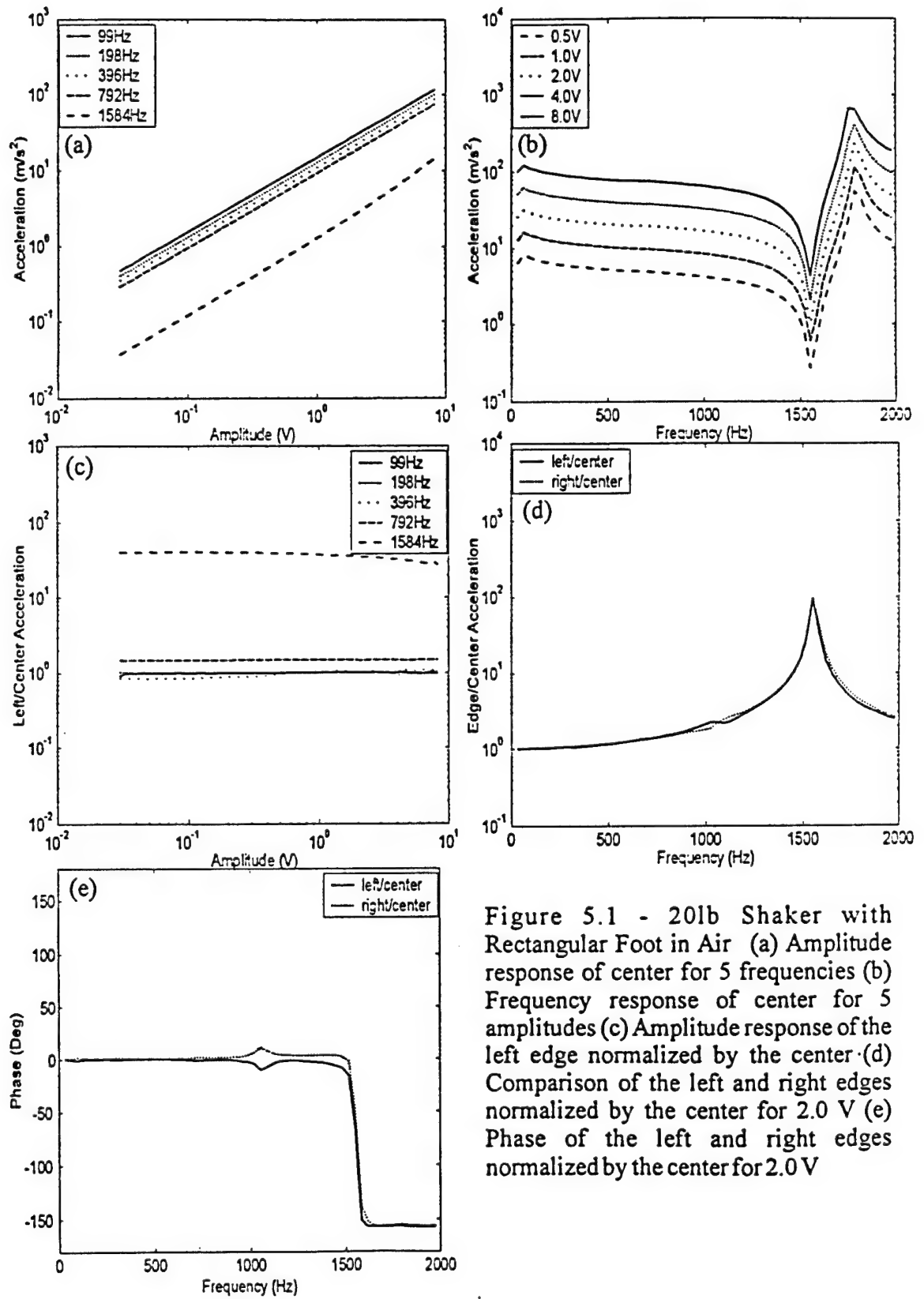
Figure 5.1 - 20lb Shaker with Rectangular Foot in Air (a) Amplitude response of center for 5 frequencies (b) Frequency response of center for 5 amplitudes (c) Amplitude response of the left edge normalized by the center (d) Comparison of the left and right edges normalized by the center for 2.0 V (e) Phase of the left and right edges normalized by the center for 2.0 V

a symmetric, relative resonance at 1575 Hz with an associated phase shift shown in (e). The horizontal accelerometer did not register anything within 20 dB of the values of the vertical motion.

Figure 5.2 shows what happened when the sand loaded resonances were examined. As expected, the loaded response of the shaker in sand was much different. The frequency response for the motion in the center of the foot changed as shown in (a). It was no longer simply related to the drive level due to several new resonances. The fundamental and two harmonics for the center accelerometer and left edge accelerometer are shown in (b) and (c) respectively. The motion became nonlinear as indicated by the number of harmonics that were produced in the loaded situation. Just how complicated this foot motion became when the shaker was placed on the sand is shown in (d). Not only did the shaker exhibit several new resonances in the frequency response, but the left edge could vibrate more or less than the center depending on which frequency is examined. To complicate matters further, (e) shows that the flapping of the ends is not symmetrical across the foot. Vertical displacements, bending about the center (in phase end displacements), and rocking about the center (out of phase end displacements) were mode shapes that all appeared to be present.

Finally, the amplitude response data was taken with the radar. These measurements were taken along the x axis at x = 10 cm and x = 40 cm on the positioner (origin 26 cm from shaker foot). This data, shown in Figure 5.3, begins at amplitudes that are down in the noise floor. They rise above the floor once the input voltage reaches approximately 0.1 V. The curves appear to rise linearly although there is more deviance

34
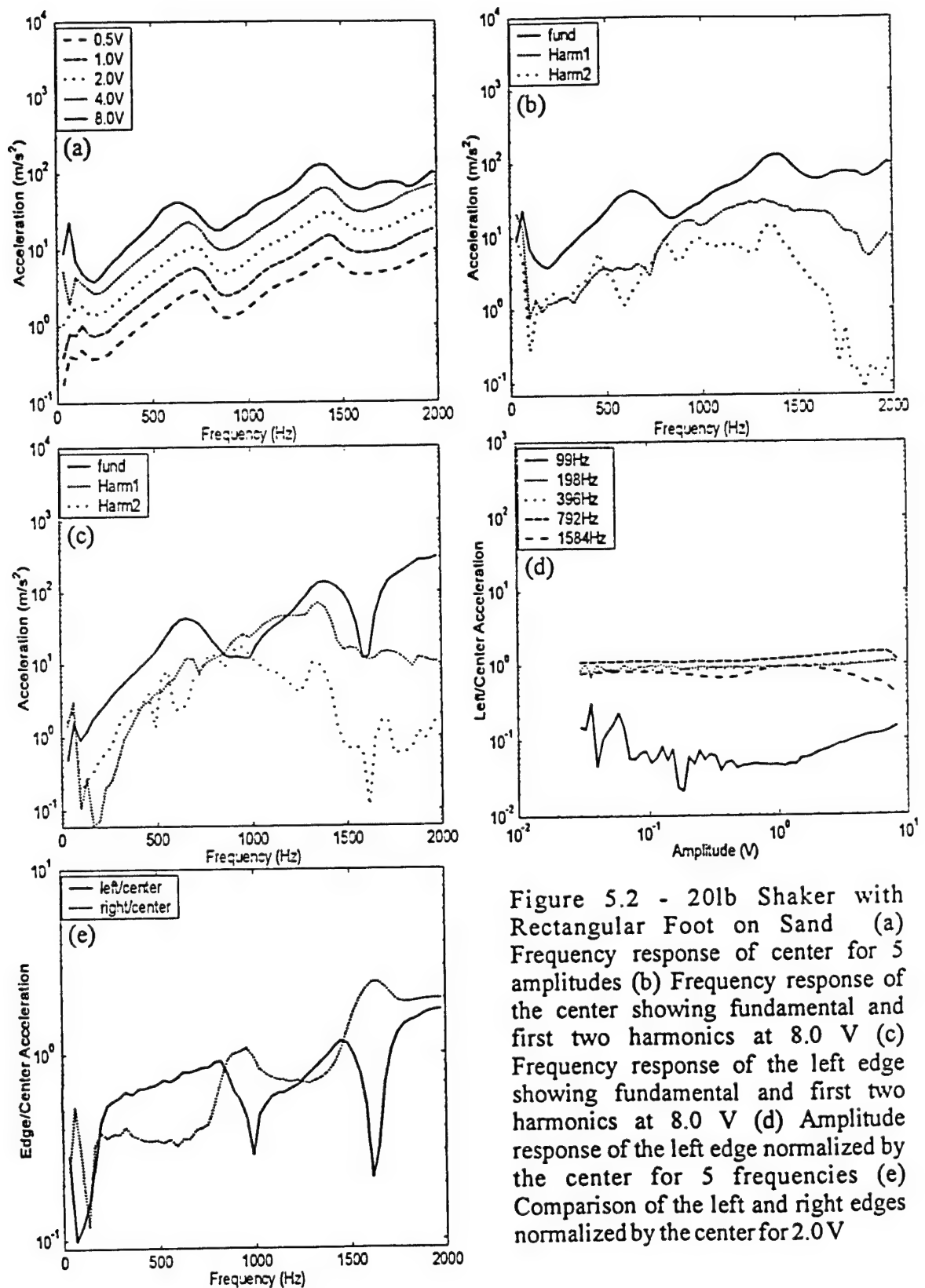
Figure 5.2 - 20lb Shaker with Rectangular Foot on Sand (a) Frequency response of center for 5 amplitudes (b) Frequency response of the center showing fundamental and first two harmonics at 8.0 V (c) Frequency response of the left edge showing fundamental and first two harmonics at 8.0 V (d) Amplitude response of the left edge normalized by the center for 5 frequencies (e) Comparison of the left and right edges normalized by the center for 2.0 V

35

Figure 5.3 - Amplitude Response for 20lb Shaker with Rectangular Foot (396 Hz)
Measured with Radar (origin is 26 cm from shaker foot) (a) Measured at x = 10 cm (b)
Measured at x = 40 cm

from a straight line at x = 40 cm than at x = 10 cm. This was expected since the nonlinearities of the sand would have more effect on the signal the further it propagated in the sandbox. Saturation was not seen on the high end of the amplitudes. Dynamic fluidization limited drive levels before signal saturation occurred.

To summarize, the small foot used in Experiment One had extremely complicated motion. It exhibited several resonances and harmonics were generated at the foot. It did not move up and down rigidly as assumed, but instead flexed in a nonsymmetrical way while also rocking back and forth. These factors combined to make the 20 pound shaker with small rectangular foot a poor choice for Experiment Two.

20lb Shaker (Circular Foot)

The four accelerometers were arranged in the following fashion for the test of this foot: three PCB 352B22 accelerometers were equally spaced on the bottom of the foot around the edge, and the PCB 352C67 accelerometer was placed on the bottom in the center. The same three tests done on the 20 lb shaker with small rectangular foot were again done for this foot.

The unloaded test produced results similar to those for the rectangular foot. Once again the 1584 Hz frequency did not increase as fast as other frequencies when the amplitude increased. Figure 5.4 shows the results of the unloaded, round foot tests. The frequency response at the center of the round foot is shown in (a). The frequency response measured by one of the edge accelerometers is shown in (b). It remains similar to the center frequency response up to about 1000 Hz at which point the behavior is very different. The measured resonances of 1225 Hz and 1575 Hz at the edge indicate that the

37
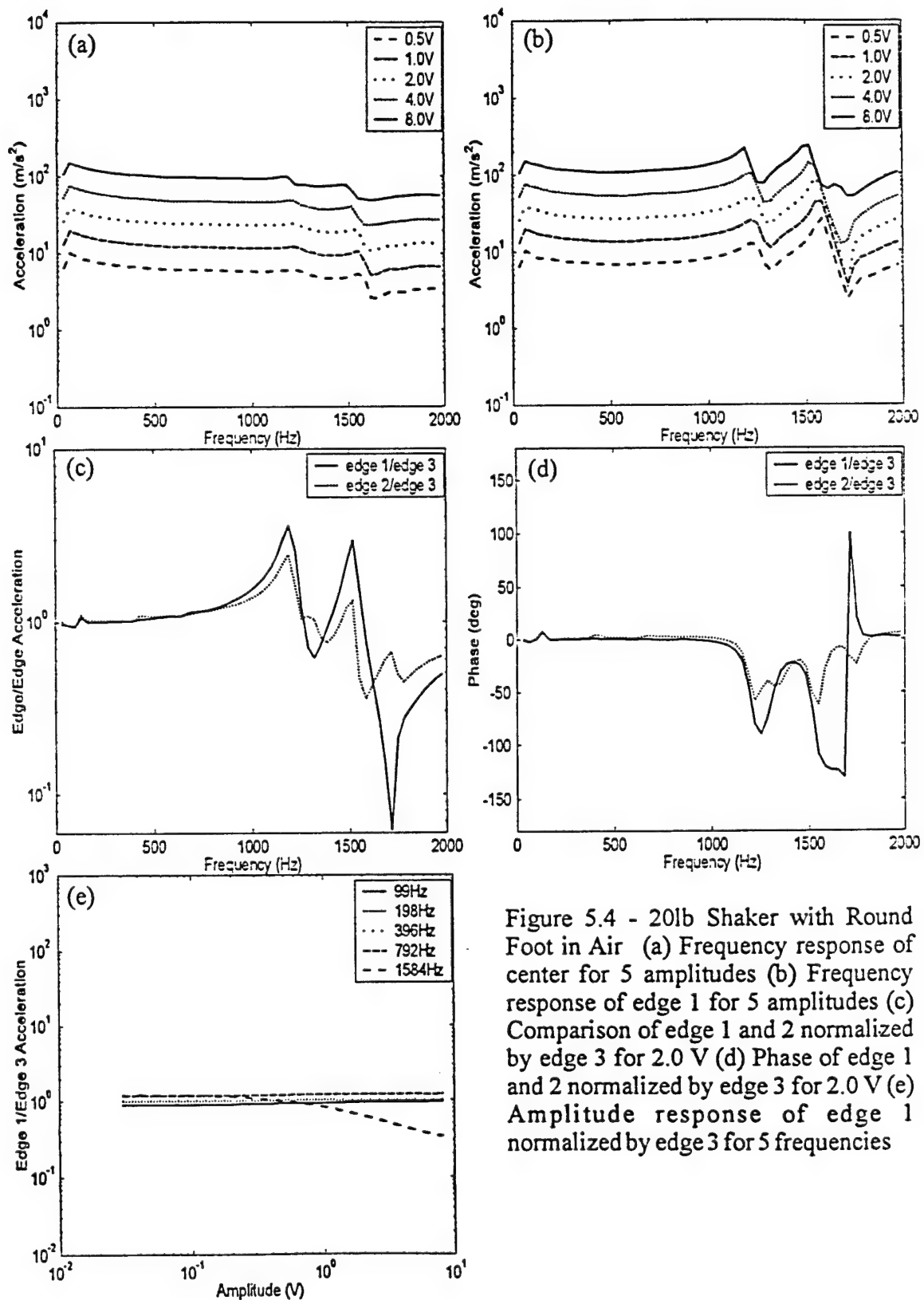
Figure 5.4 - 20lb Shaker with Round Foot in Air (a) Frequency response of center for 5 amplitudes (b) Frequency response of edge 1 for 5 amplitudes (c) Comparison of edge 1 and 2 normalized by edge 3 for 2.0 V (d) Phase of edge 1 and 2 normalized by edge 3 for 2.0 V (e) Amplitude response of edge 1 normalized by edge 3 for 5 frequencies

mode shape for these frequencies have anti-nodes at the edge. According to (c) and (d) the motion was not uniform around the foot. Two of the edge accelerometer responses normalized by the third edge are shown in (c). The curve remains close to one for frequencies less than 1000 Hz, which is also the range where the center motion was similar to the edge motion. Above 1000 Hz the edge motion is not uniform. The motion is complicated in that two edge accelerometer responses normalized by the same edge accelerometer yield very different results. There is edge motion occurring out of phase from the motion at another point on the edge as shown in (d). This appears to be a saddle-shaped mode, although three evenly spaced accelerometers on the edge did not confirm it. Finally, (e) shows that 1584 Hz does not increase, with an increase in amplitude, at the same rate around the edge.

The same tests were then performed on the round foot as it was sitting on the sand. Figure 5.5 shows the results of this test. The new frequency response of the center motion is seen in (a). Once again there are several resonances of this shaker – shaker foot configuration. The same two edges normalized by the third edge were checked again to see how the loaded conditions affected the complicated edge motion found in unloaded conditions. Once again the motion at one part of the edge is very different from motion at the other parts of the edge as indicated in (b) and (c). Not only is the foot bending, there are frequencies for which the bending is in phase and frequencies for which the bending is out of phase. The response of this foot as the amplitude increased was also examined by plotting an amplitude response of an edge normalized by an edge. This is shown in (d). Although the motion of the foot is very complicated due to the difference

39
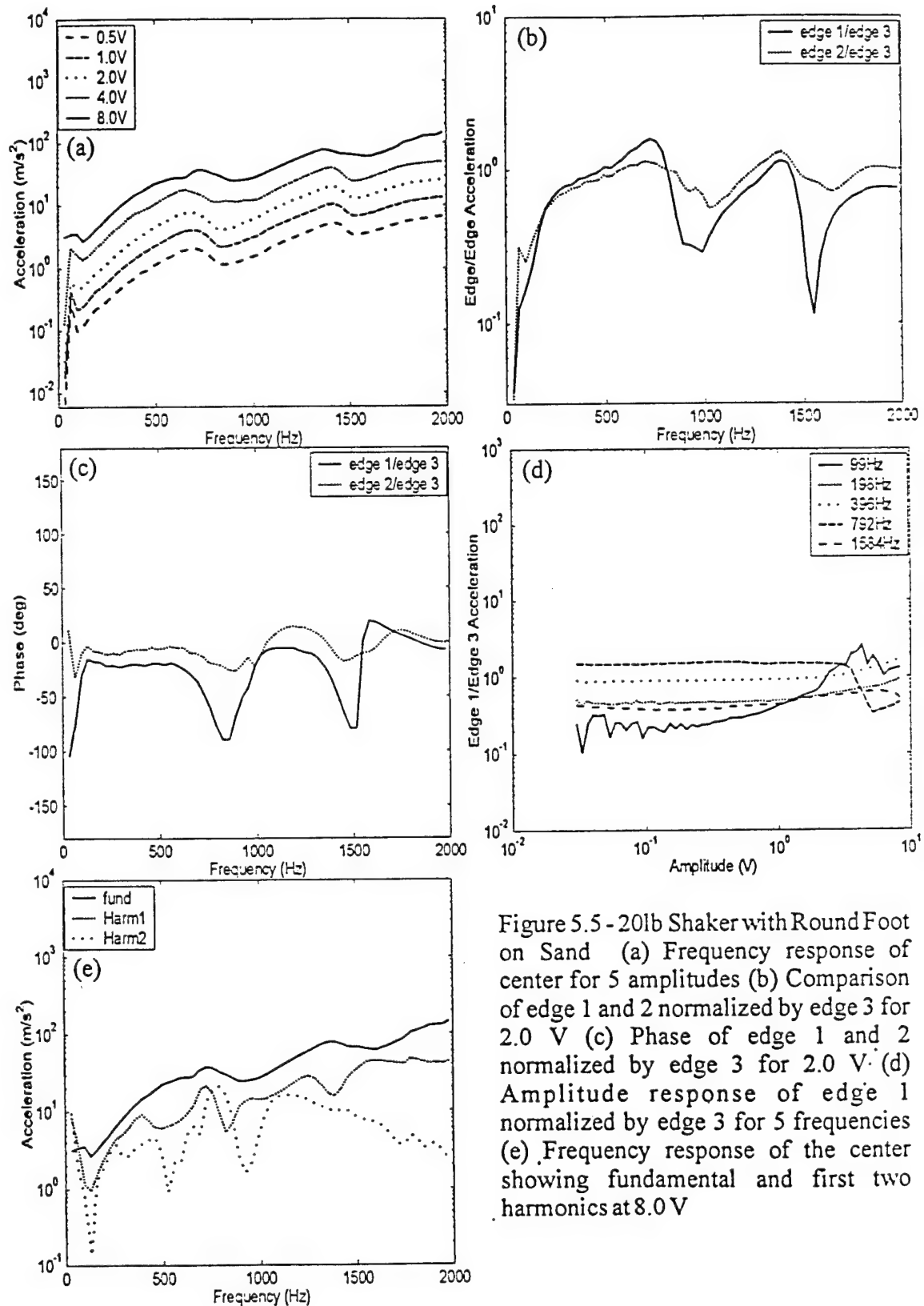
Figure 5.5 - 20lb Shaker with Round Foot on Sand (a) Frequency response of center for 5 amplitudes (b) Comparison of edge 1 and 2 normalized by edge 3 for 2.0 V (c) Phase of edge 1 and 2 normalized by edge 3 for 2.0 V (d) Amplitude response of edge 1 normalized by edge 3 for 5 frequencies (e) Frequency response of the center showing fundamental and first two harmonics at 8.0 V

in relative magnitudes around the edge, it is made even more complicated because this relativity changes with increasing amplitude. Finally, the harmonics being produced by the foot are shown in (e) for the center accelerometer response. There are a significant number of harmonics manifested above the noise floor throughout the range of frequencies. This indicates that the circular foot motion is nonlinear.

The round shaker foot was then used to check amplitude response for 396 Hz at x = 10 cm and x = 40 cm on the x axis of the sandbox. These curves are shown in Figure 5.6. The curves rise out of the noise floor once the amplitude reaches 0.1 volts. At x = 10 cm the saturation curve is rising linearly as expected. Instead of beginning to saturate however, the curve rises rapidly at 2.5 volts. The slope of this curve then decreases further up in amplitude. The curve at x = 40 cm is very nonlinear. It appears to reach saturation prior to one volt but then increases again. In both of the saturation measurements hysteresis is evident as the amplitudes sweep back down. This may be a result of front edge versus back edge arrivals but when the amplitudes come back down the curves become straighter which would indicate that some packing of the sand had occurred.

To summarize the results for the 20 pound shaker and round foot, the behavior was extremely complicated and nonlinear. Several resonances were present under loaded conditions. The foot began bending for frequencies above 1000 Hz. This bending was not symmetrical around the edges. It occurred with different magnitude and changed in and out of phase as the amplitude increased. The motion was too complicated for three accelerometers on the edge to accurately document the different mode shapes present.
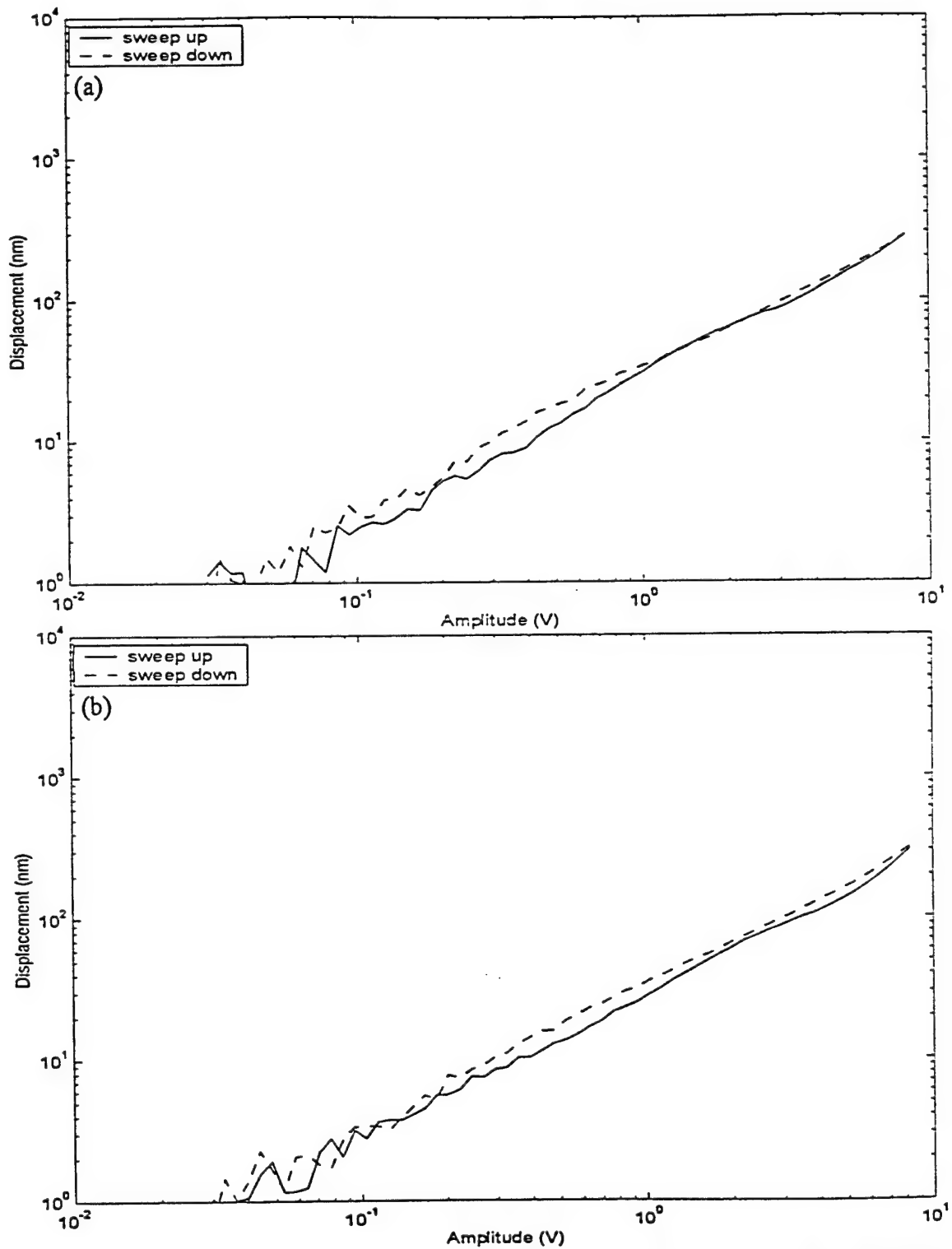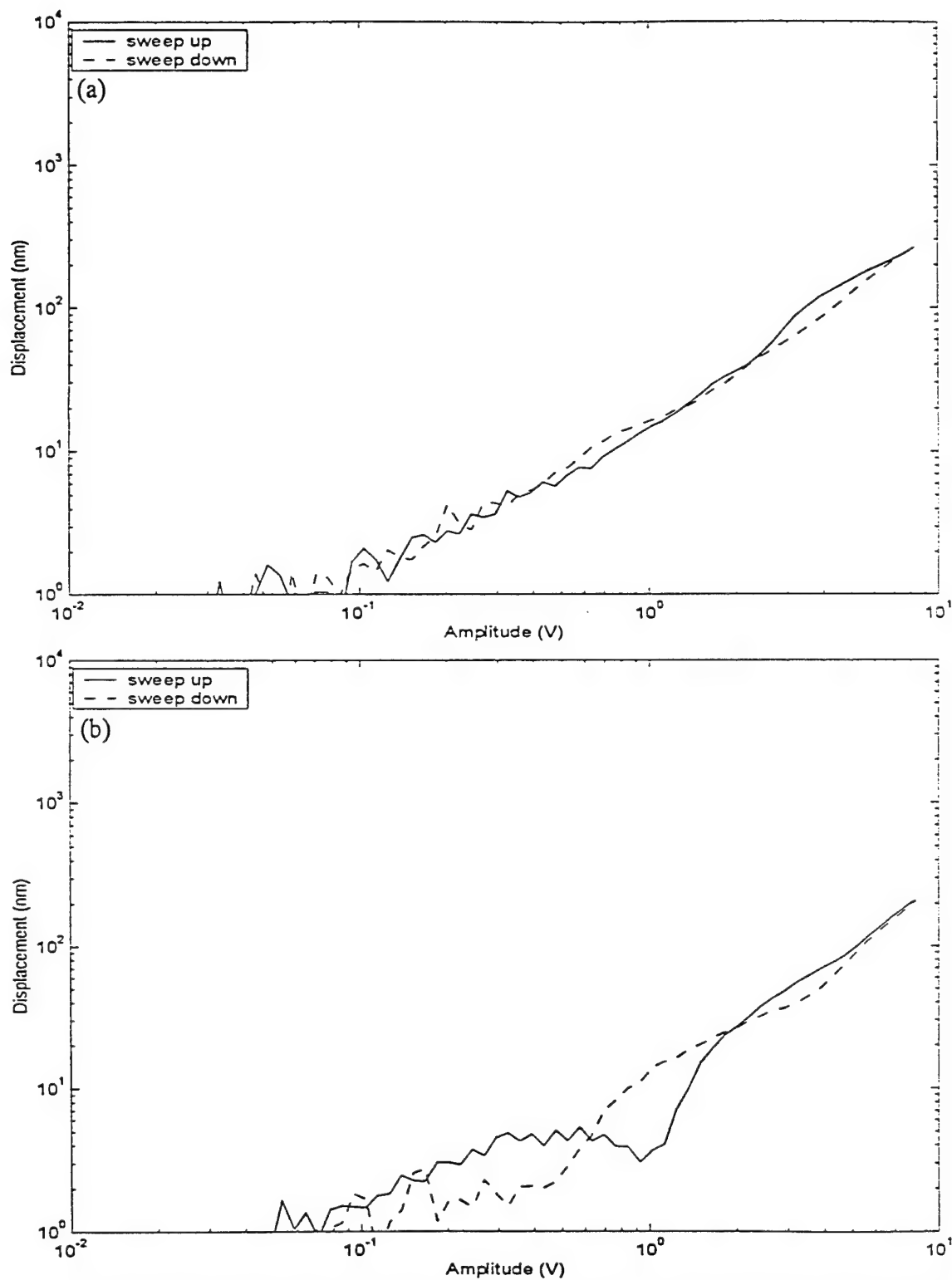
Figure 5.6 - Amplitude Response for 20lb Shaker with Round Foot (396 Hz) Measured with Radar (origin is 24 cm from shaker foot) (a) Measured at x = 10 cm (b) Measured at x = 40 cm

42

The one advantage that the round foot had over the rectangular foot was its increased

surface area which could facilitate longer measurements before experiencing dynamic

fluidization of the sand.

100lb Shaker (Rectangular Foot)

The four accelerometers were arranged in a similar manner for the test of this foot

as they were for the rectangular foot used on the 20 pound shaker (see Figure 3.3). The

three PCB 352B22 accelerometers were placed on the bottom of the foot at the left edge,

center, and right edge. Their sensitivities were 10.6 mV/g, 9.3 mV/g, and 10.1 mV/g

respectively. The PCB 352C67 was once again placed on the side of the foot, in the

center, to capture any horizontal motion.

The first test, which was done unloaded, yielded results similar to those for the 20

pound shaker with rectangular foot. Figure 5.7 shows these results. The frequency

response of the center accelerometer is shown in (a) and the amplitude response is shown

in (b). Just as in the 20 pound shaker test, this rectangular foot exhibited a null and one

resonance. Both of these occurred at lower frequencies than in the 20 pound shaker case

however. The null for the 100 pound shaker test in air is at 1250 Hz and the resonance is

centered around 1485 Hz. This resonance shows up in the 1584 Hz curve of (b). The left

edge normalized by the center amplitude response is shown in (c). A comparison of the

left and right edge acceleration normalized by the center is shown in (d). The motion is

very uniform across the shaker foot with the exception of a resonance around 1250 Hz

due to a dynamic vibration absorber effect. A 180 degree phase shift at this same
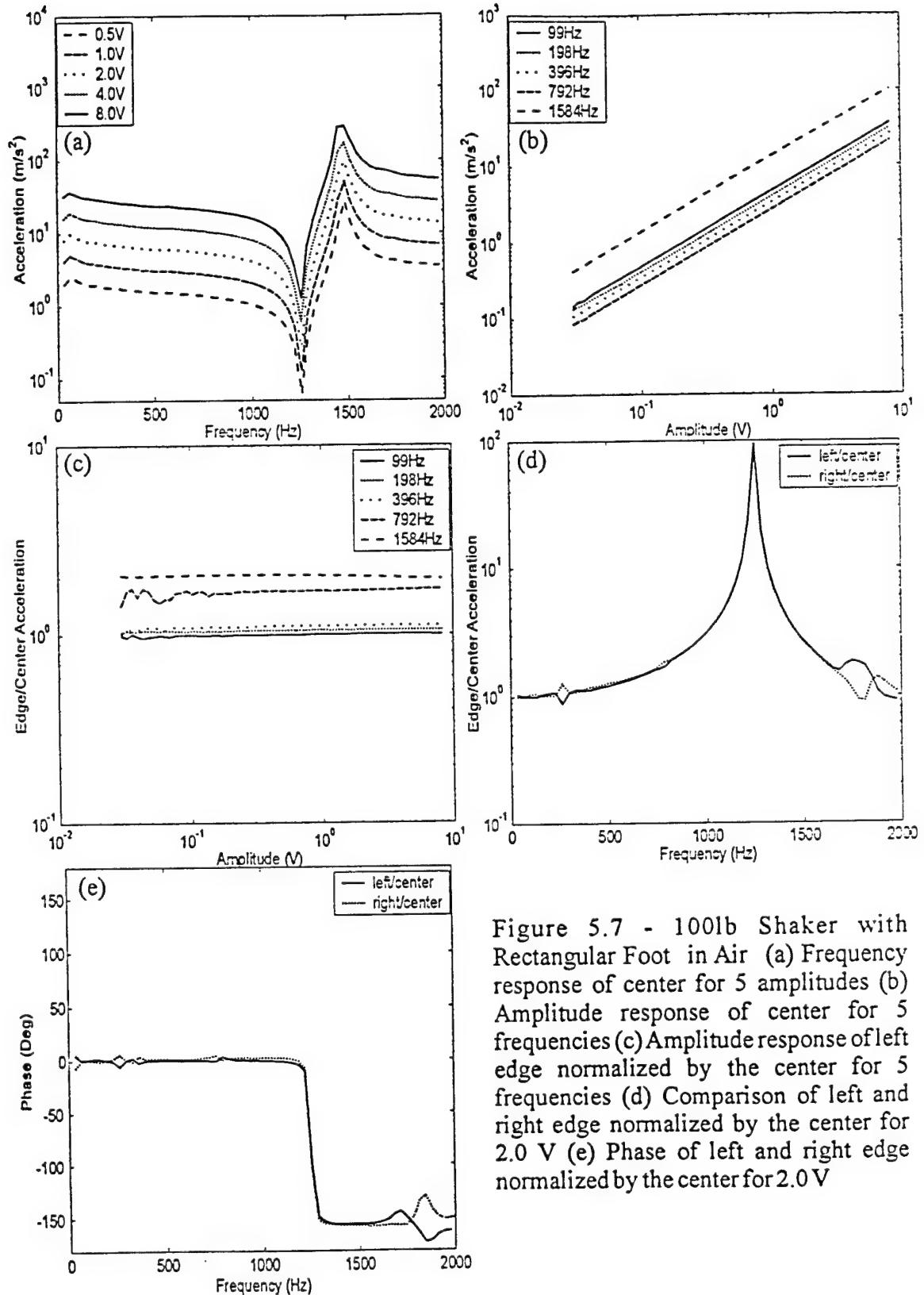
Figure 5.7 - 100lb Shaker with Rectangular Foot in Air (a) Frequency response of center for 5 amplitudes (b) Amplitude response of center for 5 frequencies (c) Amplitude response of left edge normalized by the center for 5 frequencies (d) Comparison of left and right edge normalized by the center for 2.0 V (e) Phase of left and right edge normalized by the center for 2.0 V

44

frequency is apparent in (e). According to (d) and (e) however, the motion of the two ends, while different than the center, is almost identical with respect to each other.

Figure 5.8 contains the results of the sand loaded test of the 100 pound shaker. When it was tested in the sand its frequency response exhibited fewer resonances than the 20 pound shaker with rectangular foot. The frequency response for the center motion is shown in (a). The frequency response showed a null around 100 Hz but this was not a repeatable result according to all of the measurements taken during Experiment Two. There was a resonance centered around 1585 Hz. The motion of this foot was nonlinear as indicated by the harmonics shown in (b). If these curves are compared with those for the small rectangular foot, one can see that the level of harmonics being produced in the 100 pound shaker arrangement is not as significant as for the 20 pound shaker arrangement. The relative motion of the ends is shown in (c) and (d). This indicates that although there is still some flexing of the left and right ends, it is symmetrical across the length of the foot. This motion was less complex than the motion of the 20 pound shaker with rectangular foot. Unlike the 20 pound shaker however, the 100 pound shaker exhibited significant motion in the horizontal direction. The center frequency response normalized by the horizontal response is shown in (e). Seventy percent of this frequency range contains magnitudes in the horizontal direction that are within 20 dB of the vertical magnitudes.

Finally, the amplitude response was measured at $x = 10$ cm and $x = 40$ cm with the radar. This is shown in Figure 5.9. In addition to producing larger displacements in the sand, this shaker – shaker foot combination produced a more linear amplitude
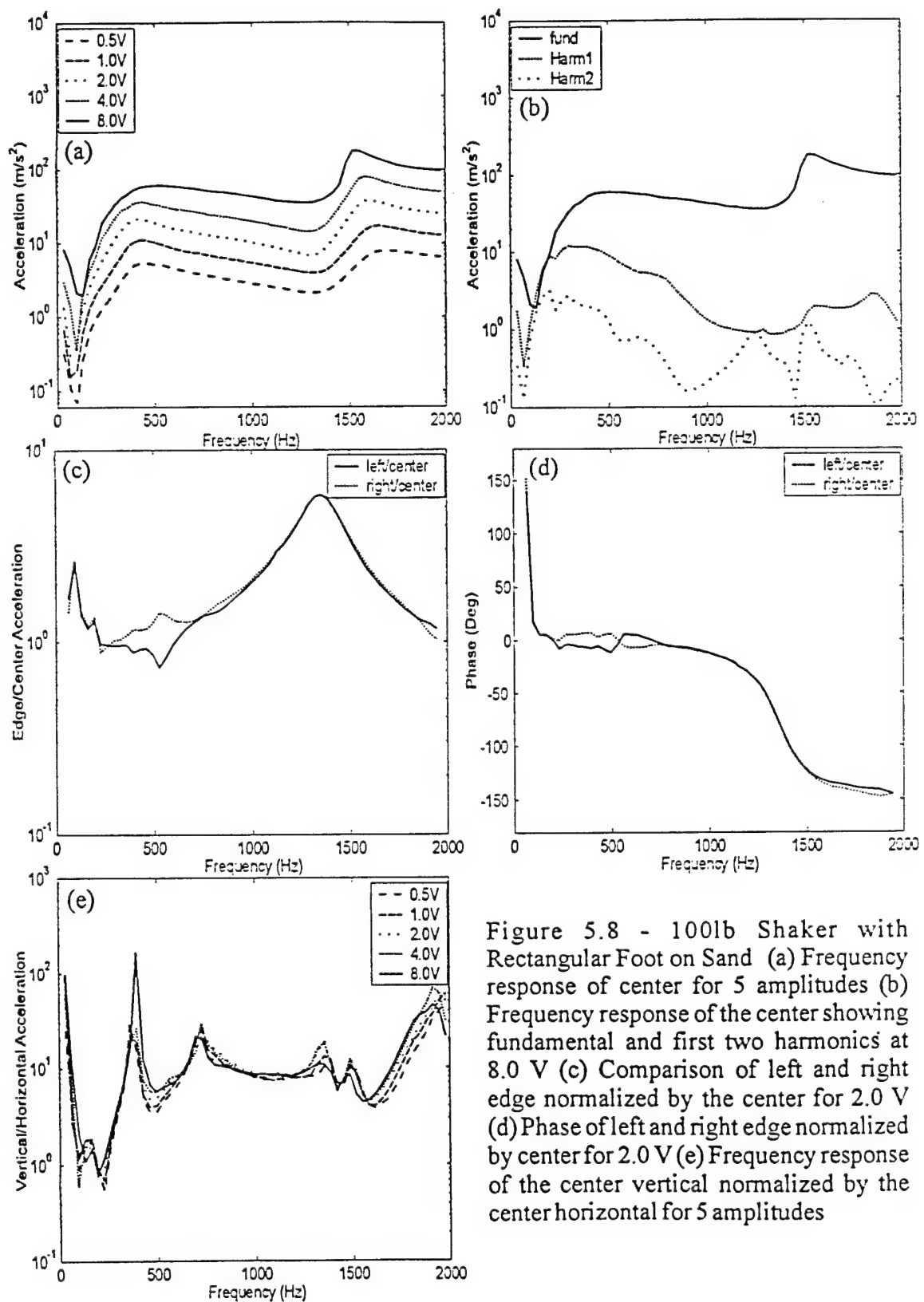
Figure 5.8 - 100lb Shaker with Rectangular Foot on Sand (a) Frequency response of center for 5 amplitudes (b) Frequency response of the center showing fundamental and first two harmonics at 8.0 V (c) Comparison of left and right edge normalized by the center for 2.0 V (d) Phase of left and right edge normalized by center for 2.0 V (e) Frequency response of the center vertical normalized by the center horizontal for 5 amplitudes

46
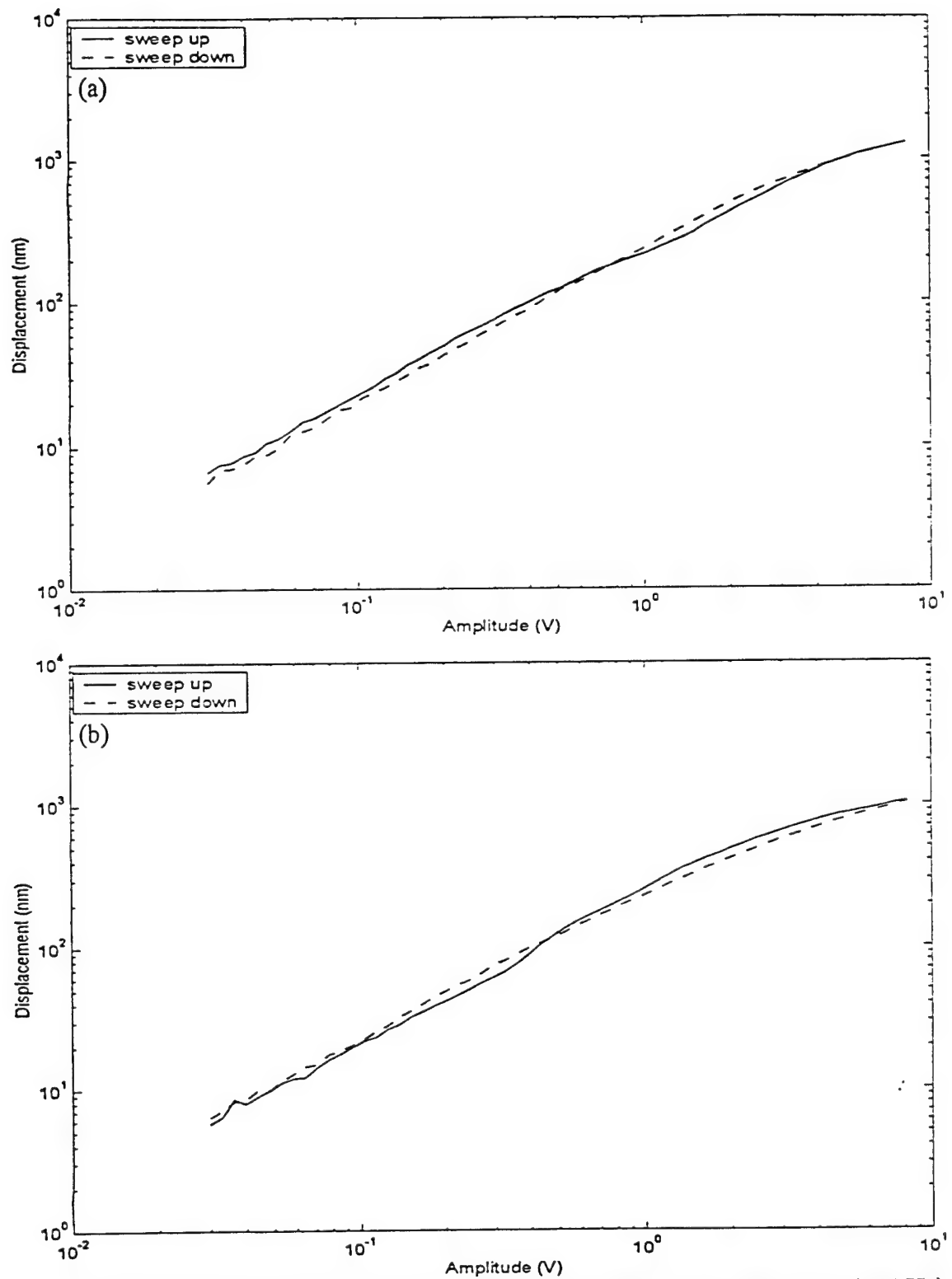
Figure 5.9 - Amplitude Response for 100lb Shaker with Rectangular Foot (396 Hz) Measured with Radar (origin is 26 cm from shaker foot) (a) Measured at x = 10 cm (b) Measured at x = 40 cm

response. The measurements for 396 Hz at x = 10 cm and x = 40 cm, as shown in (a) and (b) respectively, begin in an obvious linear region and progress to what appears to be the beginning of saturation. The curves also have less of a hysteresis effect than do the previous arrangements.

The 100 pound shaker with rectangular foot was chosen for Experiment Two. The reason for this decision was threefold. First, this arrangement produced the least amount of nonlinearities at the source. Fewer harmonics were produced in the foot, and the foot motion was more rigid than the other two arrangements tested. Second, the rectangular foot on the 100 pound shaker had sufficient surface area to support the shaker during extended experiments. This would allow for taking complete sets of data without moving the shaker or burying the shaker foot. Third, the 100 pound shaker and large rectangular foot had fewer resonances in the sand loaded condition. Ideally, a foot with no resonances would have been used but time did not permit designing and testing another foot.

CHAPTER VI

EXPERIMENT TWO

Procedures

This section includes two major topics. The first is how the experiments were designed. It describes what the techniques and methods for gathering data were and why they were chosen over others. The second major topic discusses the details of each individual test run in the laboratory. It documents the conditions that were unique to each test so that they may be considered during the evaluation of the data.

Design of Experiments

The objective of Experiment Two was to generate frequency and amplitude responses for the sand, correcting the mistakes from Experiment One. In particular, the input voltage was related to the shaker foot force, the data collection software was fixed to prevent leakage from influencing the noise floor, the range of amplitudes for the saturation curves were increased, and the tests were done without moving the shaker.

The first problem that needed to be fixed was the fact that the input voltages from Experiment One were meaningless without knowing what the power amplifier was doing. This was fixed by measuring the current between the power amplifier and the shaker with two different current probes to check accuracy. The force of the shaker foot was related to the current into the shaker by a 10 lbs/amp approximation given in the specification sheet for the 100lb shaker. A plot of the frequency response for shaker force per input

49

voltage is shown in Figure 6.1. The two current probes measured the same thing so Figure 6.1 shows the data from just one of them. Five different amplitudes were tested (0.5 V, 1.0 V, 2.0 V, 4.0 V, and 8.0 V) and each time the shaker force per input voltage curve was the same. All of the amplitude response tests and the first two frequency response tests of Experiment Two were done with the power amplifier on Gain Setting 1. The third and fourth frequency response tests of Experiment Two were done with the power amplifier on Gain Setting 2. Gain Setting 1 is approximately 7 dB greater than Gain Setting 2.

The second problem dealing with the data acquisition software was fixed by using buffers. In Experiment One a 4.096 second input was used, approximately three and a half seconds of which was a continuous wave signal and approximately half second of which was settling time. There were 65536 points recorded, so there were 16,384 points in 1.024 seconds of the signal. The first and last 16,384 points were windowed out to eliminate the ring-up and ring-down transients. The middle 32,768 points were used for the FFT. These points comprised exactly 2.048 seconds. When a 33 Hz signal was generated, 67.584 cycles of this waveform were contained in the middle 32,768 points saved. Neither the beginning nor the end coincided with the point between two cycles. This held true for frequencies other than 33 Hz also.

For Experiment Two the use of buffers guaranteed an integer number of cycles. The LabVIEW program created buffers containing 2048 points in each. This number always remained the same. When 11 Hz was generated there was one cycle of this waveform in each buffer (2048 pts/cycle). When 22 Hz was generated there were two
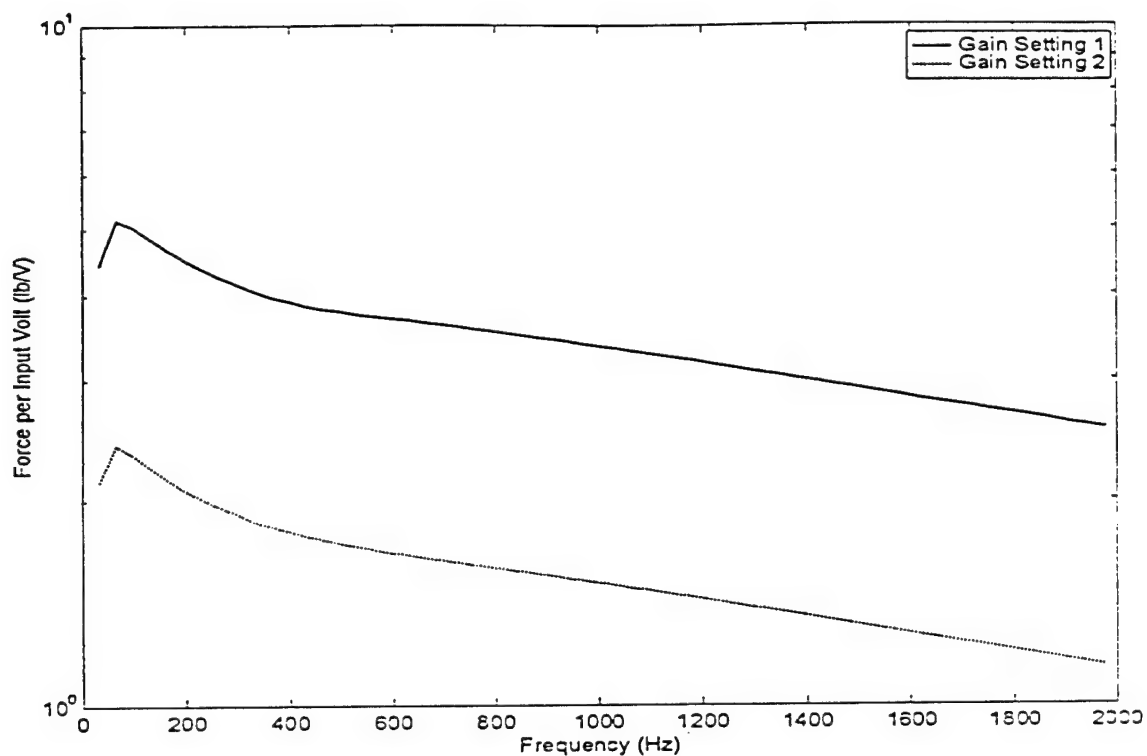
Figure 6.1 Shaker Foot Force to Input Voltage Relation
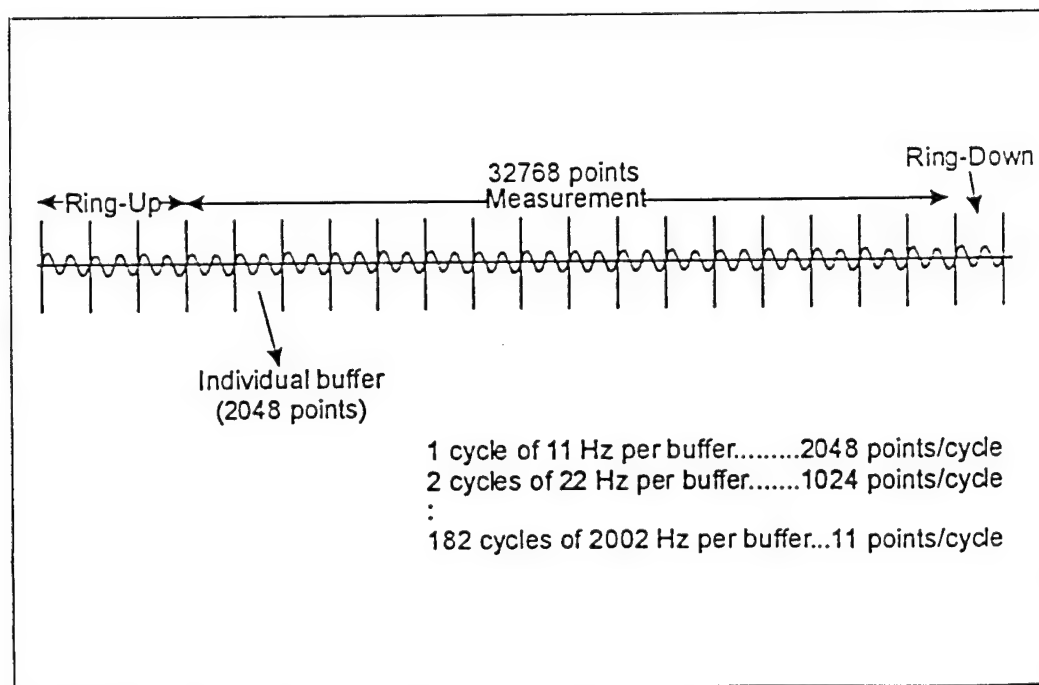
Figure 6.2 Buffer Technique of Taking Data
(22 Hz shown in figure)

51

cycles per buffer (1024 pts/cycle). There were three cycles per buffer for 33 Hz and so on so that there was always 2048 points per buffer and every buffer contained an integer number of cycles. The signal generation rate used was 22522.5234 pts/sec so each buffer was 0.09093 second long. This meant that the actual frequencies used did not match the requested frequencies exactly. For example, when 99 Hz, 198 Hz, 396 Hz, 792 Hz, and 1584 Hz were requested for the amplitude response tests, the actual frequencies used were 98.98 Hz, 197.95 Hz, 395.90 Hz, 791.81 Hz, and 1583.61 Hz. The rounded off frequencies are used throughout the discussion of the results.

Once LabVIEW generated one buffer based on the requested frequency, 19 more buffers were generated as shown in Figure 6.2. The first three buffers and the last buffer were windowed out to eliminate any ring-up and ring-down transient effects. The remaining 16 buffers were used to analyze the results. This ensured that the number of points used for the FFT was always a power of two (32,768 in this case) and the number of cycles was an integer value. The highest frequency requested was 2002 Hz. This frequency had 11 points per cycle which was enough to prevent aliasing.

The third problem from Experiment One that needed to be corrected was the range of amplitudes used to generate the amplitude response. Previously, the amplitudes were not low enough to ensure a beginning in the linear region of the curve. Experiment Two would take advantage of the widest range of amplitudes possible. The data acquisition card utilized would limit this. The maximum voltage that could be input from the LabVIEW program was 10 volts. Based on experience, the minimum input voltage that registered above the noise floor was somewhere around 0.025 volts. The starting

52

voltage was selected as 0.03 volts. The previous range of amplitudes for Experiment One was a difference of 24 dB from the low end to the high end. By starting at 0.03 volts, and increasing logarithmically, 60 measurements could be made covering about a 50 dB dynamic range. The highest voltage would be about 8.3 volts.

The fourth problem was selecting a gain setting on the power amplifier that would allow 8.3 volts to come in but the current sent to the shaker would not drive it at such a level that the foot buried into the sand. Several sample amplitude responses were generated in order to find this setting using the 0.03 to 8.3 volt range selected for the card. Once the setting on the amplifier was selected several things were checked. First, the beginning of the measurements had to be in the linear regime of the amplitude response. Second, the power amplifier setting had to be high enough so that 8.3 volts would result in the curve showing signs of saturation. Finally, the setting on the power amplifier had to be such that dynamic fluidization did not occur during a 24 hour test. The combination of voltages and the gain settings seen in Figure 6.1 allowed all of these criteria to be met.

When preparing for Experiment Two, lessons from Experiment One and from pre-experiment tests were applied to the design of the experiment. This resulted in four additional changes that were incorporated into Experiment Two. These changes were replacing the calibration runs (discussed in Appendix A – Experiment One Details) with a four-accelerometer test, the number of tests done at one time, how often the sand had to be reconditioned, and the duration of the incident signal.

In Experiment One a calibration scan was done between each measurement so that after the data was processed there was data taken at the same position, amplitude, and frequency for each measurement to compare to each other. It was realized during Experiment One however that the frequency responses and saturation curves being generated were actually repeatable as long as dynamic fluidization did not occur and the shaker was not lifted up and placed back down. Because of this, it was determined that the really important information was what kind of foot motion was being generated for that particular test due to that unique shaker foot to sand contact.

To answer this a test was run before every frequency response or amplitude response data group was taken. The test recorded the responses of four accelerometers placed in the same configuration described in Chapter V. Prior to the frequency response measurements, the four accelerometer test recorded 60 frequencies (33 Hz to 1980 Hz at 33 Hz increments) at five different amplitudes (0.5 V, 1.0 V, 2.0 V, 4.0 V, and 8.0 V). Prior to the amplitude response measurements, the four accelerometer test recorded 60 amplitudes (0.03 V to 8.3 V increasing logarithmically) at five different frequencies (99 Hz, 198 Hz, 396 Hz, 792 Hz, and 1584 Hz). In addition to this, two accelerometers were recorded at every point throughout both of the measurements. By doing this, for every piece of information collected, one could go back to see what the shaker foot was doing. It could then be determined how much of the results could be attributed to the motion of the shaker foot and how much could be attributed to the propagation path in the sand.

One of the specific things that the calibration tests of Experiment One were designed for was to check how much the sand drying affected the data being collected.

Now that a shaker, power amplifier setting, and input voltage had all been selected so that

dynamic fluidization did not occur, the method for checking drying effects was changed.

For Experiment Two, once a frequency response measurement was taken the procedure

was repeated. This allowed for a comparison of the results with nothing changing but the

moisture content in the sand. Every amplitude response set was also done twice without

moving anything. Another feature was also added to the amplitude response

measurements. Instead of sweeping up in amplitude and then going to the next

frequency, the test swept up in amplitude and then back down the same way. This

provided information for any hysteresis that might be present and pinpointed places

where the particular frequency, amplitude, and time had caused the shaker foot to sand

contact to change significantly.

Prior to Experiment One it was thought that ten hours was the maximum duration

that tests could be run before halting to rewet and repack the sand. After several weeks

of collecting data it was found that the conditions in the sandbox remained almost the

same for much longer. After wetting and packing the sand prior to a test the factors

affecting the wave propagation change the most during the first hour. It is during this

time that the moisture in the sand settles into some quasi-equilibrium state. After two

hours very little change occurs for the next 36 to 48 hours. The goal for Experiment Two

then was to be able to get two frequency response or two amplitude response

measurements done within 24 hours.

The last big change from Experiment One came after the buffers had been used to

run some sample experiments. Because the buffers fixed the leakage problem the noise

floor remained at a constant level. As the amplitudes were swept up an excellent signal to noise ratio was achieved. Because of this improved ratio many harmonics that were lost in noise previously were now seen. For example, at x = 10 cm (origin was 26 cm from the shaker foot) for 4.0 V, the first two harmonics were approximately 20 dB above the noise floor in the 100 – 600 Hz band. Depending on the frequency, amplitude, and position in the sandbox, up to a dozen harmonics could be discerned in the frequency spectrum. In Experiment One, two harmonics were saved, but for Experiment Two, five harmonics would be saved because five harmonics could often be seen above the noise floor. Another advantage of the improved signal to noise ratio was that the input signal did not have to be as long as it was for Experiment One. The signal was reduced in length from 3.6 seconds to 1.45 seconds and the same half second settling time was left at the end. When the accelerometer data was being taken the signal was reduced to 0.36 seconds. This saved a great deal of measurement time.

The final experimental design involved two major tests. One of the lessons learned from Experiment One was that for plotting frequency response, 24 amplitudes was much more detail than necessary. Similarly, for plotting amplitude response, 180 frequencies was far more than necessary. This prompted the use of two separate tests as opposed to the plan for Experiment One which was to take data dense in frequencies and dense in amplitudes and use the same set of data to plot either frequency or amplitude response. By breaking it into two separate tests the necessary information was captured while recording less than 30% of the information collected in Experiment One.

The first major test was to measure the frequency response. This test lasted approximately 25.5 hours. It began with the four accelerometer measurements already discussed. From there, two complete frequency response sets were taken. Each set began at 33 Hz, 0.5 V, and $x = 10$ cm. For all of the measurements mentioned here on, the origin ($x = 0$) was 26 cm from the shaker foot. The frequency then increased by 11 Hz increments up to 2002 Hz. The amplitude then increased to 1.0 V and the frequencies were swept through again. The amplitude was increased to 2.0 V, 4.0 V, and finally 8.0 V with 180 frequencies checked at each drive level. All of this was done at five different locations in the sandbox. These locations were $x = 10$ cm, 20 cm, 40 cm, 80 cm, and 160 cm. Throughout the entire process the response from two of the accelerometers was recorded in addition to the radar reading in the sandbox. This constituted one complete set of frequency response measurements. As soon as one was complete the entire procedure was repeated for a second set.

The second major test was to measure the amplitude response. This test lasted approximately 17.25 hours. It began with the four accelerometer measurements just as the frequency response data did. From there, two complete amplitude response sets were taken. Each set began at 0.03 V, 99 Hz, and $x = 10$ cm. The amplitude then increased by approximately 0.83 dB 60 times up to 8.3 V. The amplitudes then follow the same sequence coming back down. After this, the frequency increased to 198 Hz and the amplitudes were swept through again. The frequency continued to increase to 396 Hz, 792 Hz, and 1584 Hz as the 120 amplitudes were measured each time. All of this was done at five different locations in the sandbox. These locations were the same as for the

frequency response data sets. Once again the response from two of the accelerometers was recorded, in addition to the radar reading in the sandbox, throughout the entire process. This constituted one complete set of saturation curve measurements. As soon as one was complete the entire procedure was repeated for a second set.

Data Collection

A total of four frequency response tests (8 sets) and five amplitude response tests (10 sets) were conducted. The general procedure for any given test was the same. The sand was completely saturated with water. The actual water table remained 46 to 50 cm below the surface of the sandbox. After the sand was watered down it was packed with a hand tamper and allowed to sit for a minimum of two hours before the data was collected. Normally after about one hour the surface was given another light mist, repacked and left alone for another two to three hours. Once this was done the shaker was put on the sand and data collection commenced.

Several things were checked at the beginning of the measurements for a relative comparison of the conditions. These things included position of the radar waveguide and the radar power reading. Table 6.1 summarizes the pertinent data for all of the frequency response tests and Table 6.2 summarizes the pertinent data for the amplitude response tests. Each of the power readings at the origin found in Table 6.1 and 6.2 were +/- 0.01 dBm. The power reading for any given frequency response or amplitude response test remained within a 3 dB range throughout the entire test. Also, lower amplitudes were used for the fourth frequency response test. These amplitudes were 0.015625 V, 0.03125 V, 0.0625 V, 0.125 V, and 0.25 V.

Test	1	2	3	4
Date Started	26 Jan 00	7 Feb 00	11 Feb 00	13 Feb 00
Time Soaked and Packed	1030	1230	0840	0350
Time Misted and Repacked	1240	1300	1930	0550
Start Time	1453	1408	2123	0710
Accelerometer Placement	Center vertical & center horizontal	Center vertical & buried 3in. below foot	Center vertical & buried 5.5in. below foot	Center vertical & buried 5.5in. below foot
Gain Setting	1	1	2	2
Power Reading at Origin	10.17 dBm	12.12 dBm	8.24 dBm	9.17 dBm
Waveguide Distance from Sand (x=0)	2 cm	1.8 cm	1.5 cm	1.3 cm

Table 6.1 – Experimental Procedure Data for Frequency Response Tests

Test	1	2	3	4	5
Date Started	25 Jan 00	4 Feb 00	8 Feb 00	9 Feb 00	10 Feb 00
Time Soaked and Packed	0830	0630	1630	1400	1000
Time Misted and Repacked	1300	1030	1700	1515	1110
Start Time	1630	1239	1922	1643	1519
Accelerometer Placement	Center vertical & center horizontal	Center vertical & buried 3 in. below foot	Center vertical & buried 5.5 in. below foot	Center vertical & buried 5.5 in. below foot	Center vertical & buried 5.5 in. below foot
Gain Setting	1	1	1	1	1
Power Reading at Origin	10.04 dBm	11.65 dBm	9.95 dBm	10.45 dBm	9.55 dBm
Waveguide Distance from Sand (x=0)	2 cm	1.8 cm	1.8 cm	1.5 cm	1.5 cm

Table 6.2 – Experimental Procedure Data for Amplitude Response Tests

The two accelerometers that were recorded in conjunction with the radar measurements were of the following types and locations. The first frequency and amplitude response tests were done with two Kistler accelerometers mounted in the center of the foot. One was on top of the foot to measure vertical acceleration and the other was on the side to measure horizontal acceleration. The results, which will be discussed later, prompted the subsequent tests to be done with an accelerometer buried under the shaker foot. The second frequency and amplitude response tests were done with two PCB 352C67 accelerometers. One was attached to the bottom center of the foot to measure vertical acceleration and the other was buried in the sand three inches below the foot. The third amplitude response measurement was repeated with the buried accelerometer 5.5 inches below the shaker foot. The placement of the accelerometers for the third and fourth frequency response tests and the fourth and fifth amplitude response tests were done with the same accelerometers in the same place. They were PCB 352B22 accelerometers, one of which was mounted on the bottom center of the foot to measure vertical acceleration and the other was buried 5.5 inches below the shaker foot.

Results

Before the results of the frequency and amplitude response data are presented, one should note where the noise floor was for these experiments. Figure 6.3 shows the noise floor recorded for three different measurements. The first was recorded with Gain Setting 1 on the power amplifier and a drive amplitude of 8.0 V, the second was recorded with Gain Setting 2 on the power amplifier and a drive amplitude of 8.0 V, and the third was recorded with Gain Setting 2 on the power amplifier and a drive amplitude of 0.25 V.
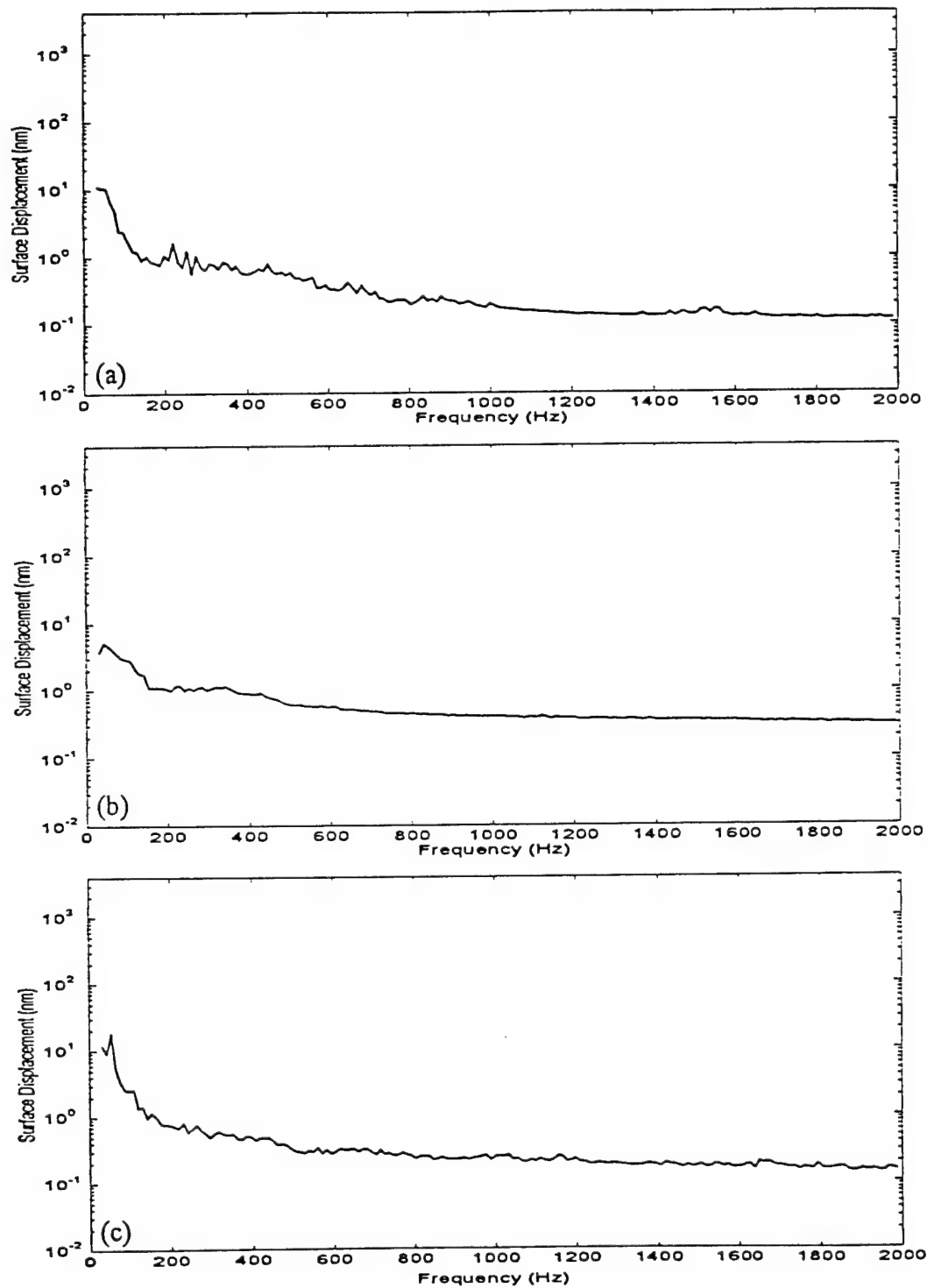
Figure 6.3 - Noise Floor Measured at First Position (x = 10 cm) for Fifth Amplitude
Tested During First Iteration (a) Test 2 - Gain Setting 1, Amplitude = 8.0 V (b) Test 3 -
Gain Setting 2, Amplitude = 8.0 V (c) Test 4 - Gain Setting 2, Amplitude = 0.25 V

61

These three graphs show that despite different drive levels, the noise floor did not change. This was expected and showed that the leakage problem from Experiment One was corrected. The noise floor remained as shown in Figure 6.3 for all of the measurements taken in Experiment Two.

Frequency Response Data

Four complete frequency response tests were taken. Each test consisted of two iterations. Each iteration included 180 frequencies taken at five drive levels at five different locations as previously described. Frequency Response Test 1 recorded data that indicated a coding error made the first drive level 0.05 V instead of the desired 0.5 V. For this reason, the first frequency response test is not used to describe the results.

Figure 6.4 shows the surface displacement as a function of frequency. The fundamental frequency is plotted for five drive amplitudes taken from Frequency Response Test 2 (first iteration). Graphs (a) though (e) are measurements taken at the five locations in the sandbox. Figure 6.5 shows the same data for Frequency Response Test 2 (second iteration). These iterations confirmed two things. First, the two sets of data were similar, as expected, because the shaker was not moved between the two iterations of this test. Second, the drying of sand did not significantly alter results throughout the 26 hours required to take all of the data shown in Figures 6.4 and 6.5. Therefore, repeatability of results may be achieved during a 26 hour period if the shaker is not moved.

There were certain characteristics common to the data shown in Figures 6.4 and 6.5. The waves attenuated as they propagated in the sandbox. This was shown by the
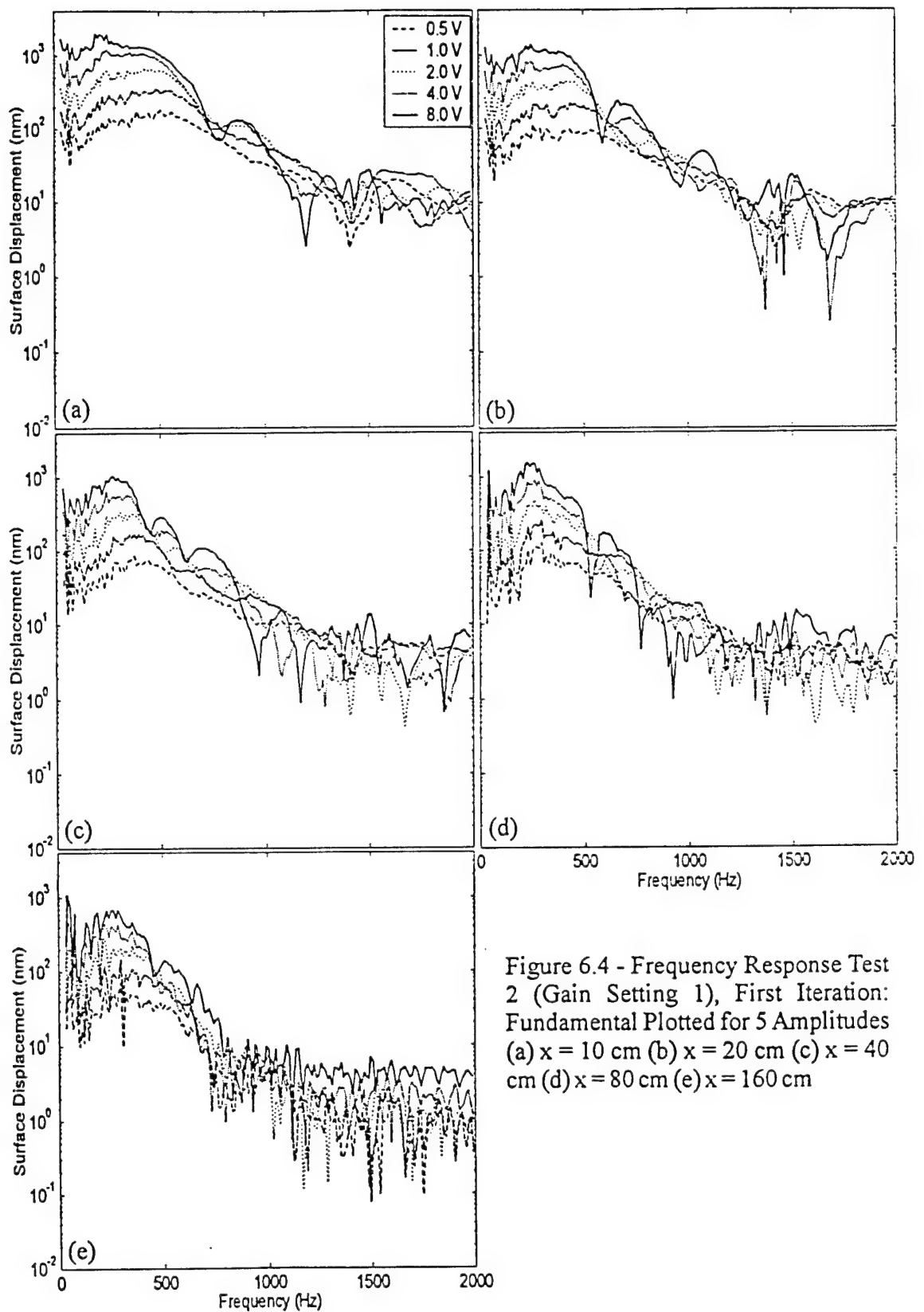
Figure 6.4 - Frequency Response Test 2 (Gain Setting 1), First Iteration: Fundamental Plotted for 5 Amplitudes (a) x = 10 cm (b) x = 20 cm (c) x = 40 cm (d) x = 80 cm (e) x = 160 cm

63
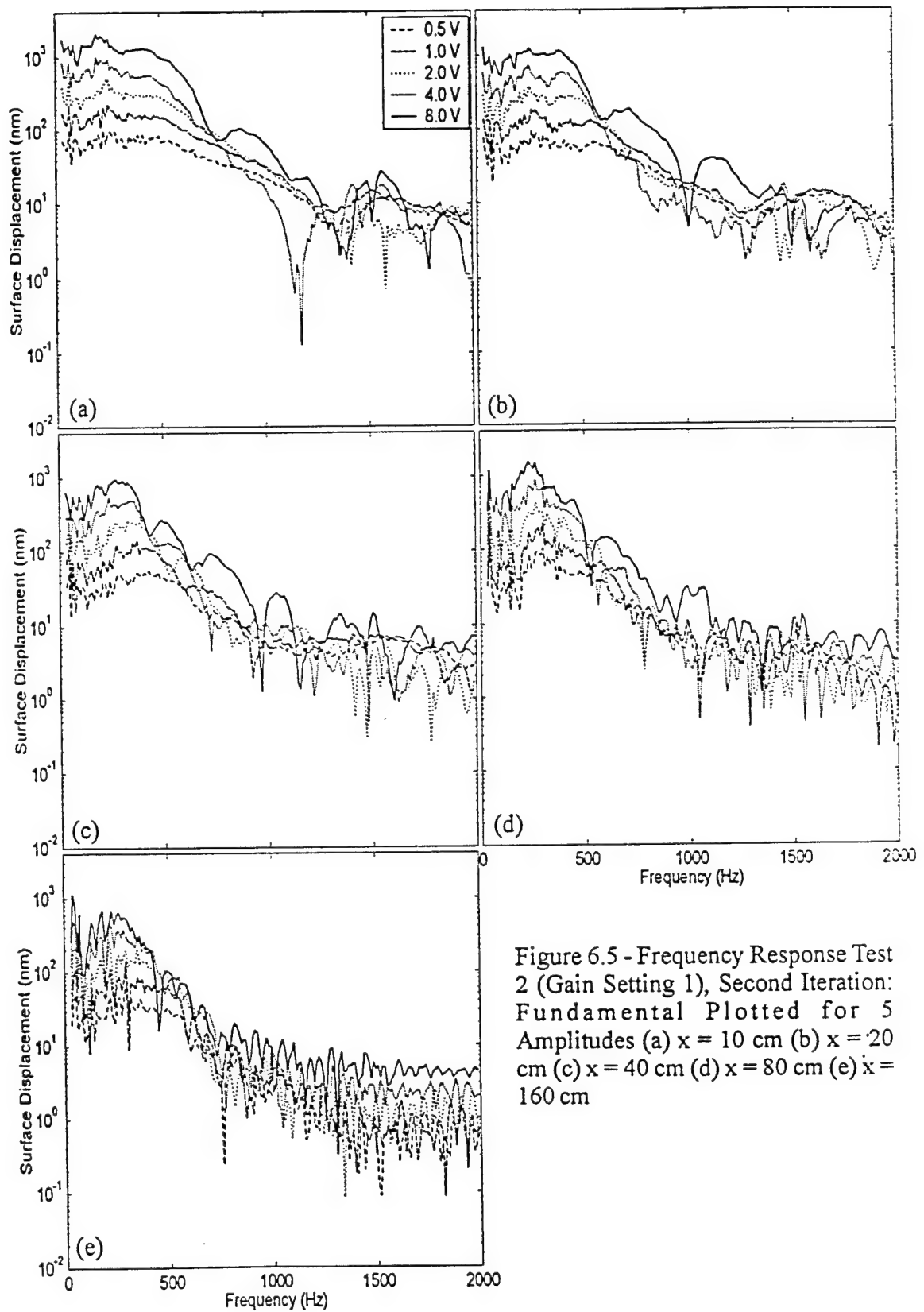
Figure 6.5 - Frequency Response Test 2 (Gain Setting 1), Second Iteration: Fundamental Plotted for 5 Amplitudes (a) x = 10 cm (b) x = 20 cm (c) x = 40 cm (d) x = 80 cm (e) x = 160 cm

decreasing surface displacements from x = 10 cm (a) to those at x = 160 cm (e). The amount of attenuation was frequency dependent however. In general, higher frequencies attenuated faster than lower frequencies. The largest surface displacements occurred in the 100 – 600 Hz band, but at x = 160 cm, the frequencies between 400 Hz and 600 Hz had attenuated more than those between 100 Hz and 400 Hz. Frequencies above 600 Hz did not propagate well as shown by the decreasing slope above 600 Hz.

These figures also show that the frequency response became more nonlinear with increasing drive amplitude as expected. By looking at the measurements taken at x = 10 cm, one can see that the surface displacement doubled as the drive amplitude doubled in the 100 – 600 Hz band. Above 600 Hz however, there was a point at which doubling the drive amplitude did not result in a doubling of the surface displacement. The amplitude where this occurred became lower and lower as the frequency increased.

Another common result seen in Figures 6.4 and 6.5 was that the frequency response varied more as the drive amplitude increased. This can best be seen by looking at the data recorded at x = 10 cm (a). The smaller amplitude curves are smoother for a wider range of frequencies. As the amplitude increased, nulls in the frequency response appeared. More nulls were present the higher the amplitude went. The amount of variability increased during propagation as seen by the increasing number of dips in the frequency response when comparing a given amplitude in (a) to those of (b), (c), (d), and (e).

Figure 6.6 shows the surface displacements versus frequency for Frequency Response Test 3 (first iteration). The fundamentals are plotted for five drive amplitudes
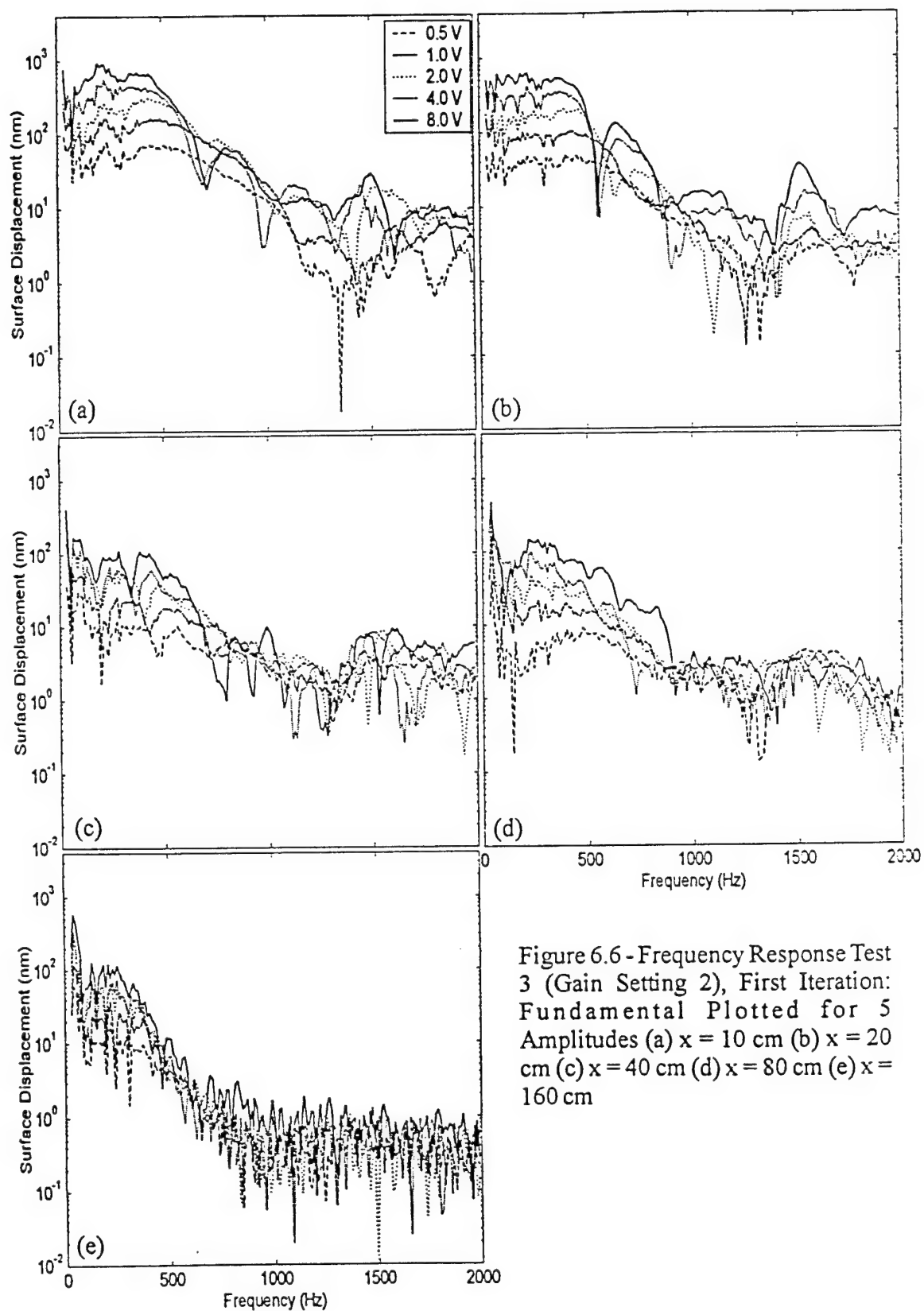
Figure 6.6 - Frequency Response Test 3 (Gain Setting 2), First Iteration: Fundamental Plotted for 5 Amplitudes (a) x = 10 cm (b) x = 20 cm (c) x = 40 cm (d) x = 80 cm (e) x = 160 cm

66

taken at five positions. This data was taken with the power amplifier on Gain Setting 2.

The data was consistent with Figures 6.4 and 6.5 in that surface displacements were

approximately 7 dB lower due to the gain setting, higher frequencies attenuated faster,

and lower amplitudes resulted in a more linear frequency response over a greater band of

frequencies. The frequencies between 800 – 2000 Hz have attenuated into the noise floor

at x = 160 cm for these drive amplitudes as shown by the flat frequency response in

Figure 6.6 (e).

Figure 6.7 shows the surface displacement versus frequency for Frequency

Response Test 4 (first iteration). This data was taken with the power amplifier on Gain

Setting 2. The fundamental, for five drive amplitudes at five locations, is shown in the

graphs of Figure 6.7. The data taken at x = 10 cm (a) showed that doubling the drive

amplitude doubled the surface displacement throughout the frequency band with the

exception of frequencies between 1200 Hz and 1300 Hz. The curves were relatively

smooth with the exception of this null and the lower frequencies that remained near the

noise floor for these drive amplitudes. As the waves propagated in the sandbox the same

increase in variability appeared in the higher frequencies. This variability was indicated

by the dips in the frequency response as seen in the other figures.

There were two results for Frequency Response Test 4 that differed from

Frequency Response Tests 2 and 3. First, the frequency band experiencing nonlinear

effects as the amplitude increased was different. As stated earlier, for Frequency

Response Test 2, 100 Hz – 600 Hz was the band that continued to double in surface

displacement as the amplitude doubled at x = 10 cm (Figure 6.4 (a)). At x = 160 cm the

Figure 6.7 - Frequency Response Test 4 (Gain Setting 2), First Iteration: Fundamental Plotted for 5 Amplitudes (a) x = 10 cm (b) x = 20 cm (c) x = 40 cm (d) x = 80 cm (e) x = 160 cm

68

frequencies between 400 Hz and 600 Hz had attenuated more and were more variable than those between 100 Hz and 400 Hz. For Frequency Response Test 4 however, the surface displacements doubled with doubling drive amplitude between 300 Hz and 1200 Hz at x = 10 cm (Figure 6.7 (a)). At x = 160 cm, with the exception of frequencies lower than 400 Hz which were in the noise floor, the surface displacements for frequencies through 1200 Hz still doubled as the drive amplitude doubled. The curves showed relatively smooth attenuation, without the increasing variability, for all five amplitudes.

The second difference in Frequency Response Test 4 was that surface displacement increased between x = 10 cm and x = 20 cm and between x = 20 cm and x = 40 cm. This was most likely due to a property of the sand at the time the measurements were taken. Because the increase in surface displacement was a broadband effect, it did not occur due to interference. This result was inconsistent with other data and inconsistent with the expected results. Properties of the sand that may have caused this include the water table height, a volume of sand that had a different density, or a volume of sand that retained a higher moisture content.

Figure 6.8 (a) shows the surface displacements versus frequency for Frequency Response Test 3 (first iteration) and Frequency Response Test 4 (first iteration). Both were measured at x = 10 cm. They were plotted on the same graph in order to see how the five lower amplitudes step up into the five higher amplitudes. It is important to note that the shaker had been moved, and the sand reconditioned, between the two tests so the same shaker foot to sand contact was not present for all ten amplitudes. This result can be observed by the nonlinear increase of the lower frequency range between 0.25 V and

69
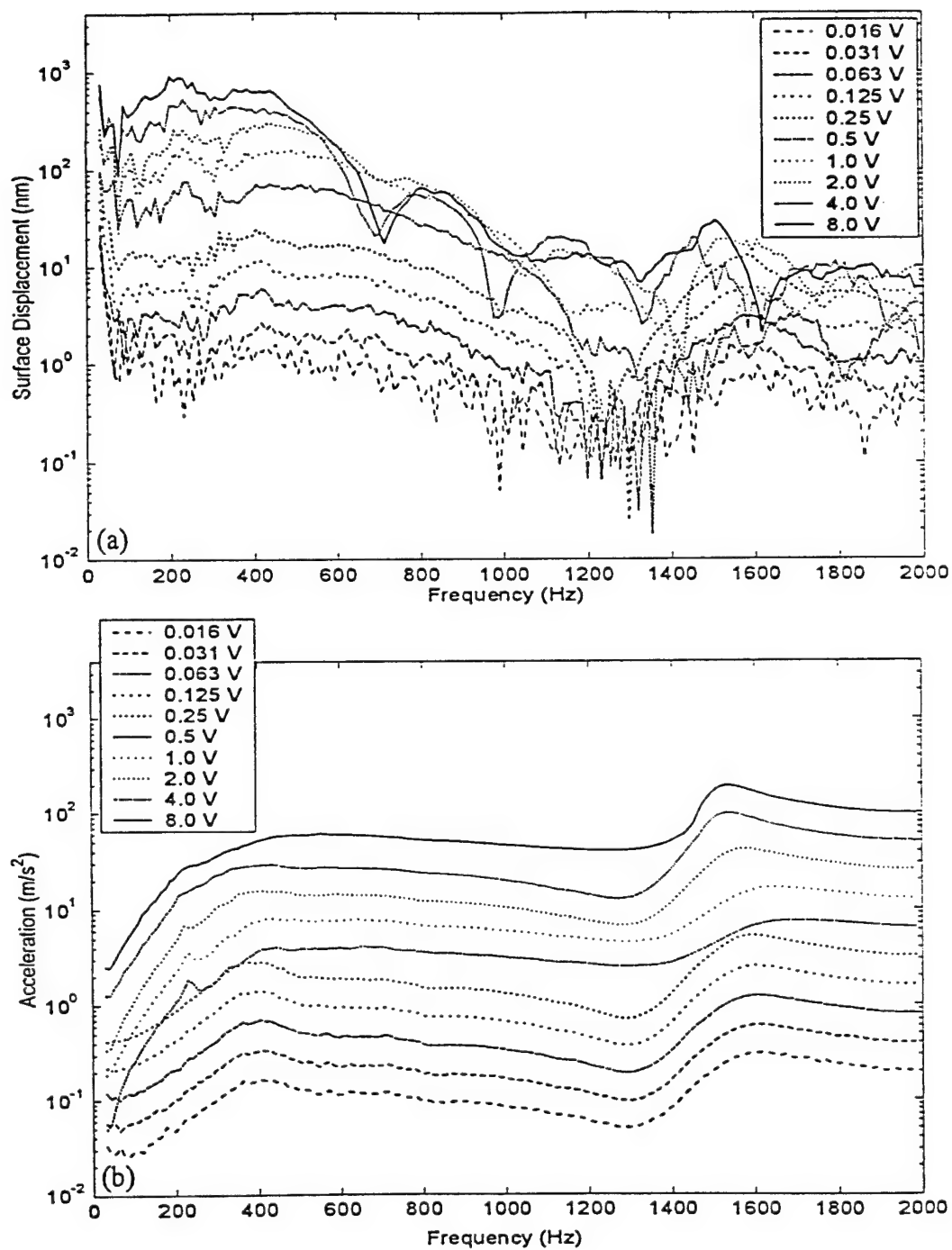
Figure 6.8 - Frequency Response Tests 3 and 4 (Gain Setting 2), First Iteration: Fundamental Plotted for 10 Amplitudes (a) Radar measurement at x = 10 cm (b) Accelerometer measurement of center taken while radar was at x = 10 cm

0.50 V. Figure 6.8 (b) shows the frequency response of the shaker foot, measured by the center accelerometer, for the same 10 measurements. The dependence of the frequency response on the shaker foot to sand contact was evident in this graph, particularly in the 0 – 400 Hz band.

In order to determine the degree of nonlinearities present, the harmonics produced were examined. Figure 6.9 compares the surface displacements for the fundamental and four harmonics at five locations ((a) – (e)) for a constant drive amplitude. The data is taken from Frequency Response Test 2 (first iteration) with an amplitude of 2.0 V. These results are nonlinear as shown by the harmonics generated. The fundamental and harmonics attenuated as they propagated through the sandbox. The higher harmonics attenuated the fastest, which showed once again that the higher frequencies did not propagate as well.

Figure 6.10 compares the surface displacements for the fundamental and four harmonics for five drive amplitudes ((a) – (e)) at one location. The data is taken from Frequency Response Test 2 (first iteration) at $x = 40$ cm. At the lowest amplitude (0.5 V), the first harmonic was above the noise floor for the 100 – 1000 Hz band and the second harmonic was discernable above the noise floor in the 100 – 700 Hz band. When the amplitude was 1.0 V, the first through fourth harmonics were generated in the 300 – 600 Hz band. At 4.0 V, at least one harmonic was generated throughout the frequency band of interest. These results showed that the wave propagation to 40 cm was nonlinear even at the lowest drive amplitude for Frequency Response Test 2. Appendix B contains a complete set of data for Frequency Response Test 2 (second iteration).
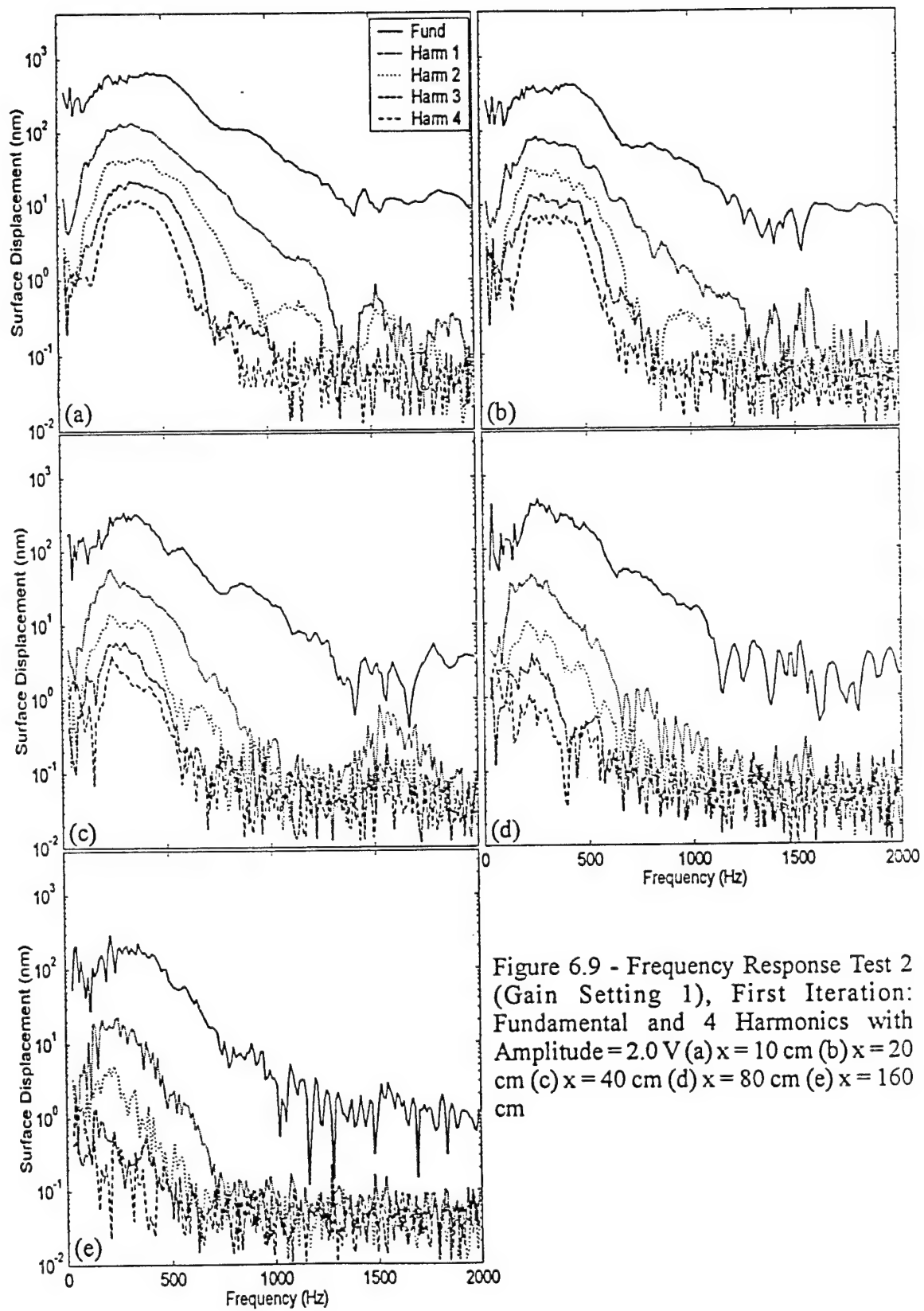
Figure 6.9 - Frequency Response Test 2 (Gain Setting 1), First Iteration: Fundamental and 4 Harmonics with Amplitude = 2.0 V (a) x = 10 cm (b) x = 20 cm (c) x = 40 cm (d) x = 80 cm (e) x = 160 cm
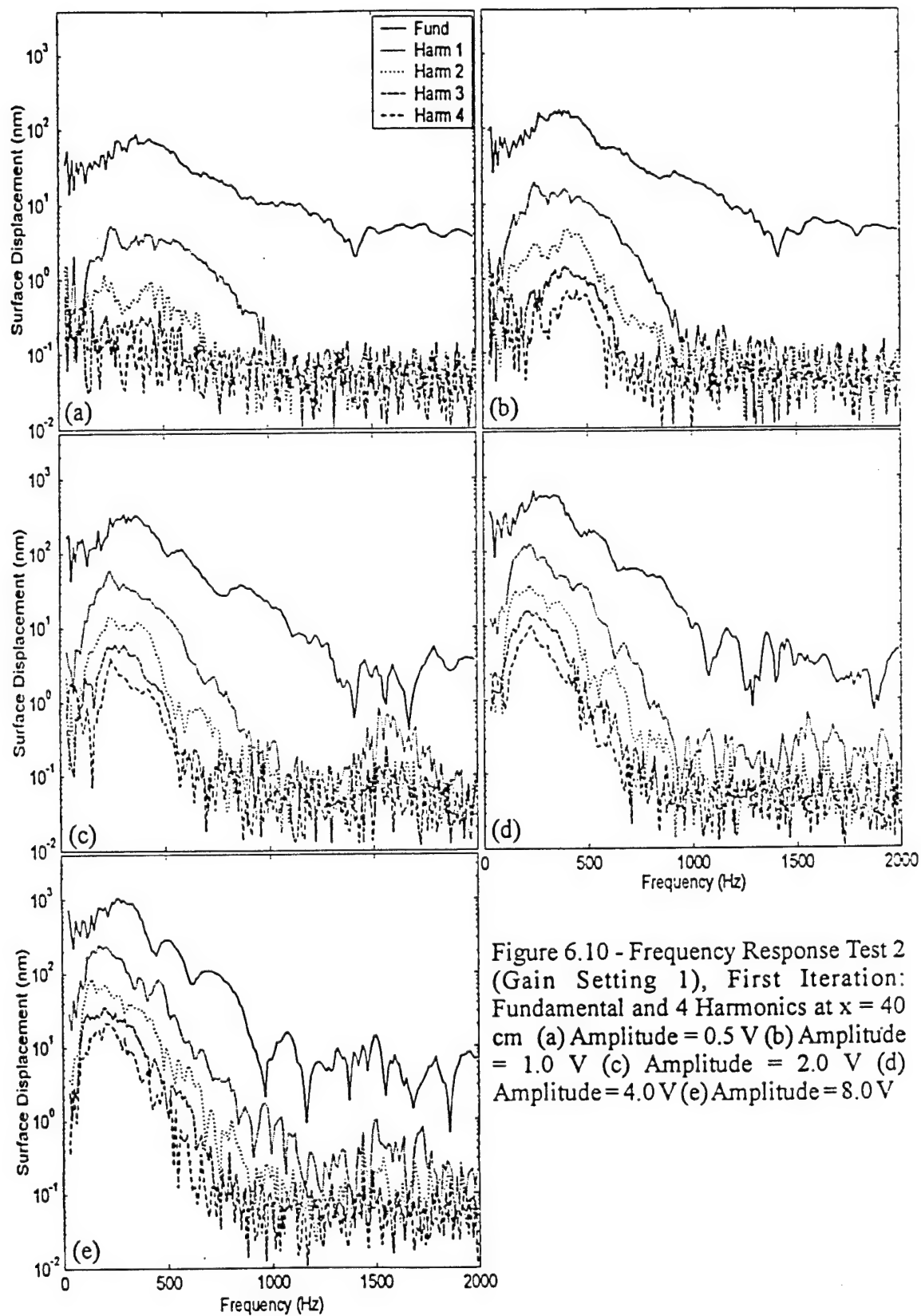
Figure 6.10 - Frequency Response Test 2 (Gain Setting 1), First Iteration: Fundamental and 4 Harmonics at x = 40 cm (a) Amplitude = 0.5 V (b) Amplitude = 1.0 V (c) Amplitude = 2.0 V (d) Amplitude = 4.0 V (e) Amplitude = 8.0 V

73

Amplitude Response Data

As with the frequency response data, the amplitude response data was taken with accelerometers mounted on the shaker foot so that any surface displacement read by the radar could be related to some foot motion. During Amplitude Response Test 1, the two accelerometers recorded throughout the measurements were Kistler accelerometers. They were both mounted on the center of the shaker foot, one for vertical acceleration and the other for horizontal acceleration. After processing the data, the curves of surface displacement versus amplitude for the vertical accelerometer were not repeating themselves between measurements of the same frequency. The last curve was rising at about one-third the rate of the first curve for 99 Hz. The amplitude response for higher frequencies repeated however.

This unexpected effect led to consultation with a geophysicist. It was hypothesized that propagation of lower frequencies was more dependent upon the solid matrix structure of the sand, and that propagation of higher frequencies was more dependent on the viscous forces of the water content in the sand [13]. It was thought that as the measurements were taken, the foot was packing the sand underneath it. If this occurred, the sand matrix structure was changing, thus changing the amplitude response of the shaker foot for low frequencies.

In order to confirm that the sand under the foot was being packed during the measurements, an accelerometer was buried three inches below the foot. Accelerations measured at this point should have changed over time as the volume of sand effectively coupled to the foot increased due to packing. Two PCB 352C67 accelerometers were

74

used to take the measurements. Besides the one buried, there was one mounted in the center of the shaker foot. Amplitude Response Test 2 was taken in this configuration but did not record results consistent with Amplitude Response Test 1. The accelerometer mounted on the foot did not have decreasing amplitude response curves at 99 Hz. Instead, the curves were consistent throughout the measurements as originally expected. The accelerations measured by the buried accelerometer did not change over time either.

This prompted an investigation of the accelerometers. The accelerometer measurements for Amplitude Response Test 1 were ruled invalid due to a particular Kistler accelerometer used to record vertical foot acceleration. For Amplitude Response Tests 3, 4, and 5, PCB 352B22 accelerometers were used. One was mounted on the center of the foot to measure vertical acceleration and one was buried 5.5 inches below the foot to see if the shaker foot was packing the sand. The hypothesis of lower frequencies being dependent on the sand matrix structure and higher frequencies being dependent on the viscous forces of the water was never confirmed nor denied. Neither did burying an accelerometer under the shaker foot confirm or deny that the sand under the foot was packed over time. Amplitude Response Tests 3, 4, and 5 (all taken on Gain Setting 1) are used to present the results.

Figure 6.11 shows surface displacement versus drive amplitude for Amplitude Response Test 3 (first iteration). The fundamental for five frequencies is plotted in each graph. Graphs (a) though (e) are the measurements taken at five different positions in the sandbox. The portion of the curves that is not smooth is data that was hidden in the noise
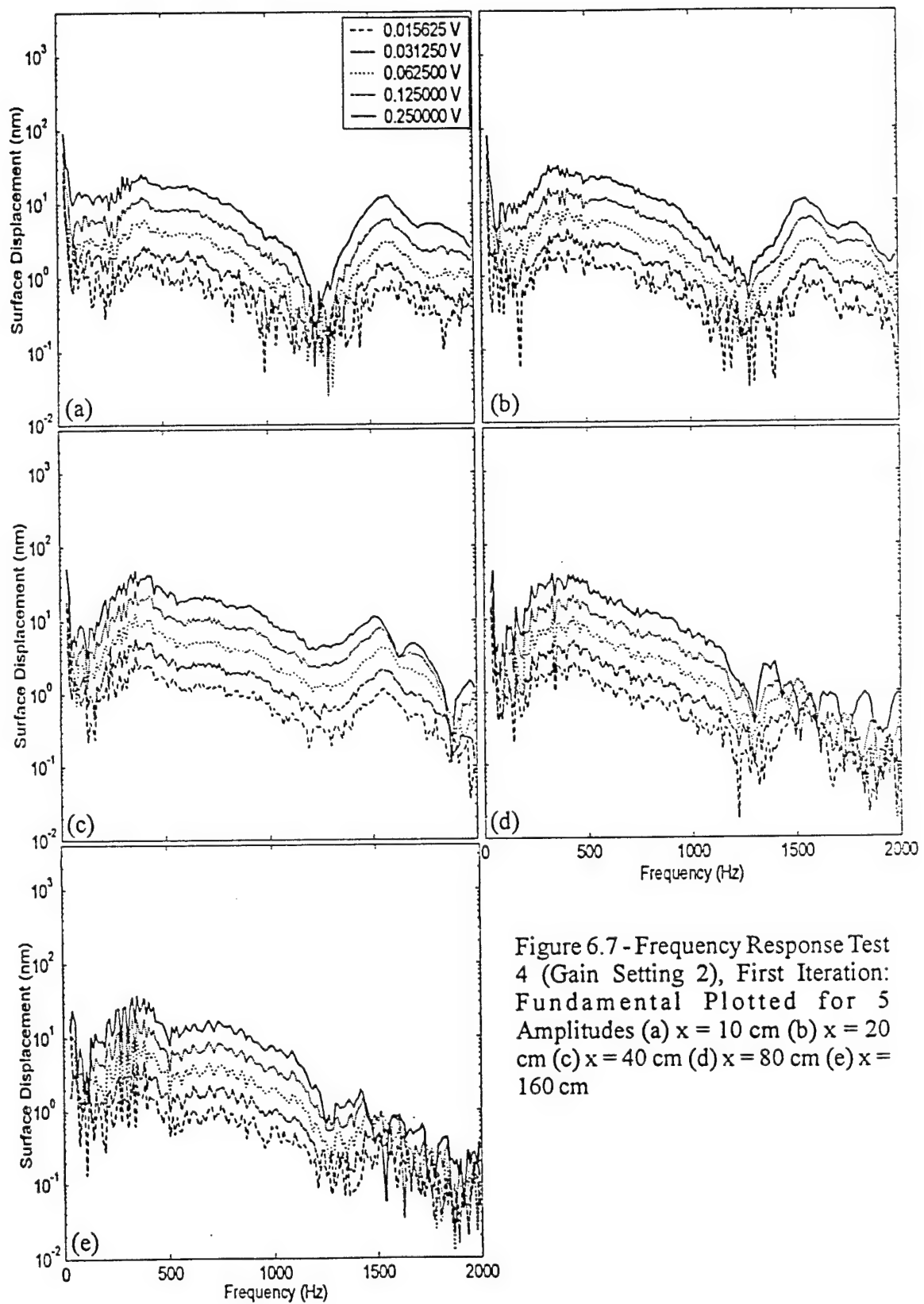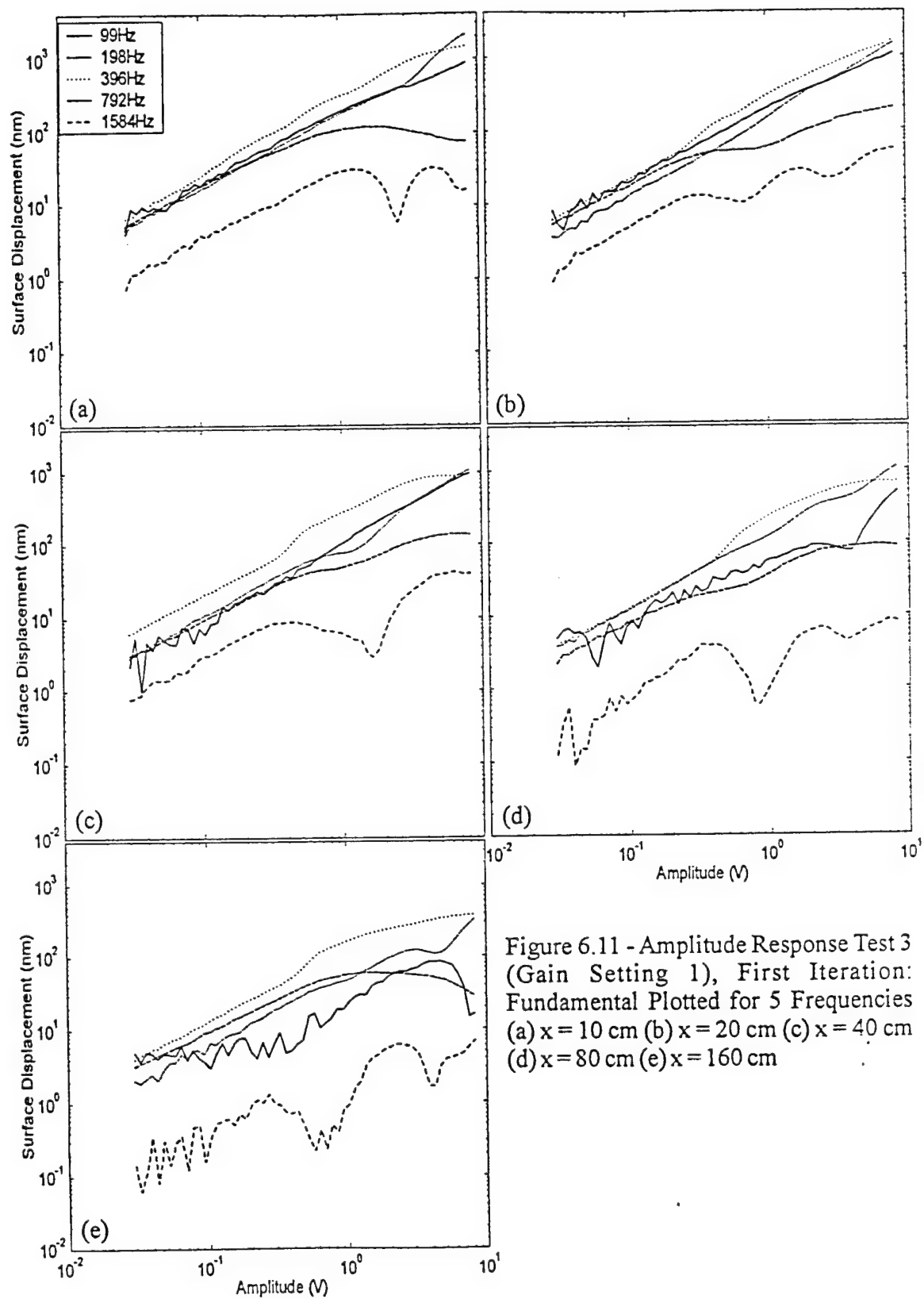
Figure 6.11 - Amplitude Response Test 3 (Gain Setting 1), First Iteration: Fundamental Plotted for 5 Frequencies (a) x = 10 cm (b) x = 20 cm (c) x = 40 cm (d) x = 80 cm (e) x = 160 cm

76

floor. For example, in (d), 99 Hz less than 10^0 and 1584 Hz less than 10^{-1} are in the noise.

Many of the observations made for the frequency response data were confirmed with this data. The waves attenuated as they propagated in the sandbox. This was seen by the surface displacement curves, for a given frequency, decreasing from one position to the next (from (a) to (e)). All of the curves began in a linear region. The curves entered a nonlinear region, as expected, when amplitude increased. The point at which these frequencies began to saturate was different for each of them, showing the frequency and amplitude dependence of saturation. The higher frequencies were less predictable than the lower frequencies. For Figure 6.11, 1584 Hz showed a particularly large amount of variability as it propagated through the sandbox. The largest surface displacements occurred for 396 Hz, which was also consistent with the frequency response tests.

Figure 6.12 shows the surface displacement versus drive amplitude for Amplitude Response Test 3 (second iteration). The fundamental of five frequencies was plotted for five locations just as it was in Figure 6.12. Approximately 8.5 hours elapsed between the beginning of the first iteration and the beginning of the second iteration. Because the shaker was not moved between these two iterations, the results were repeatable as seen in the figures. The degree of repeatability was frequency dependent however. 99 Hz, 198 Hz, and 396 Hz, at all five locations for the second iteration, were similar to those of the first iteration. 792 Hz was repeatable for x = 10 cm, 20 cm, and 40 cm. After 40 cm, the results were not repeatable in the nonlinear region. The variability
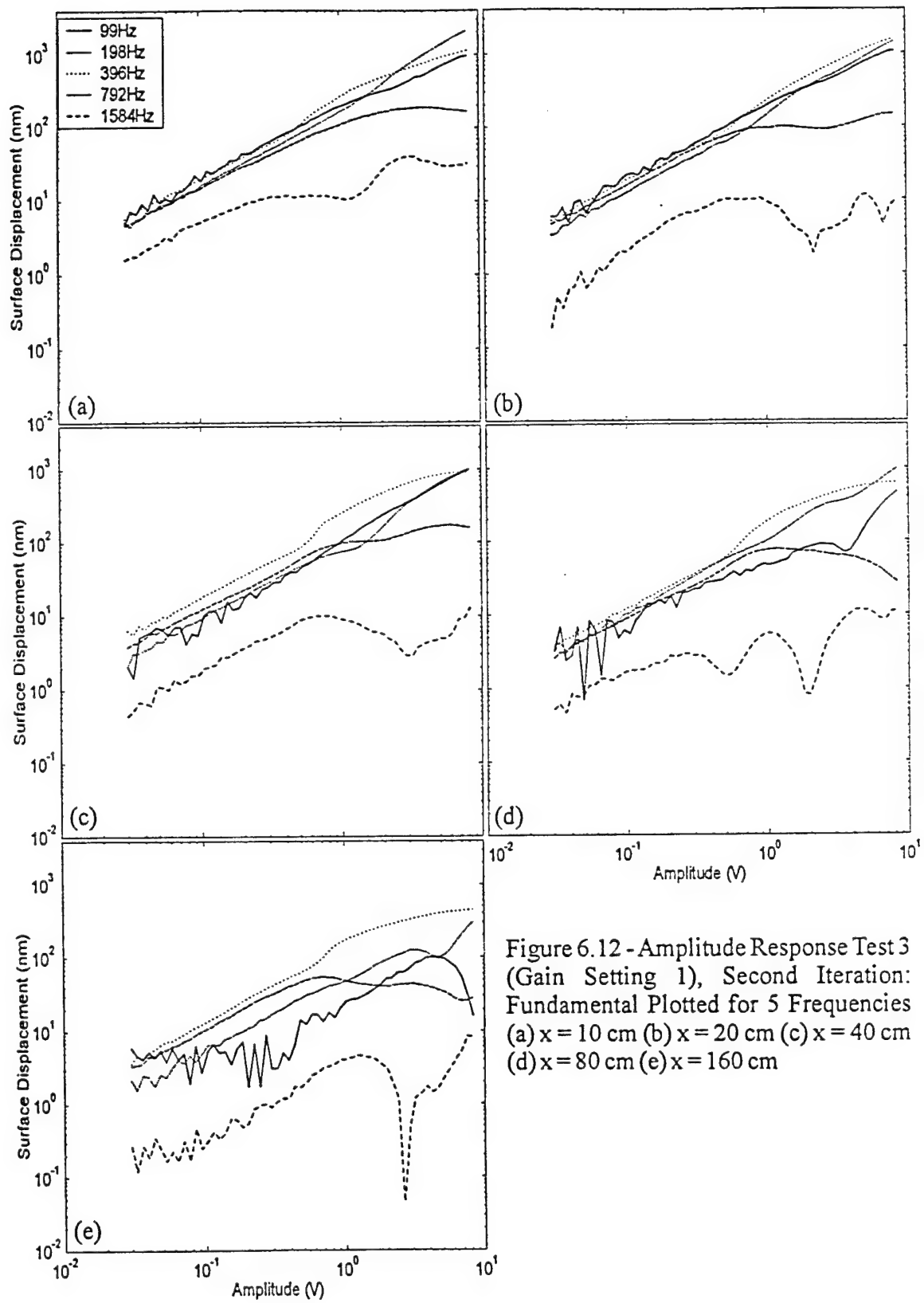
Figure 6.12 - Amplitude Response Test 3 (Gain Setting 1), Second Iteration: Fundamental Plotted for 5 Frequencies (a) x = 10 cm (b) x = 20 cm (c) x = 40 cm (d) x = 80 cm (e) x = 160 cm

78

of 1584 Hz was not reproducible in the second iteration. Although it still varied, the amplitude where the variation occurred and the extent of the variation was not repeatable.

Figure 6.13 shows surface displacement versus drive amplitude for Amplitude Response Test 4 (first iteration). The fundamental of five frequencies measured at five locations was plotted just as in the previous two figures. Although the relative magnitude of surface displacements shown in Figure 6.13 were similar to those of Amplitude Response Test 3, the shape of the curves was somewhat different due to the different shaker foot to sand contact that resulted from moving the shaker and reconditioning the sand. The differences are more apparent in the higher frequencies than in the lower frequencies.

Figure 6.14 shows surface displacement versus drive amplitude for Amplitude Response Test 5. The fundamental of five frequencies at five locations was once again plotted. A comparison of Figure 6.14 with either Figure 6.11 or Figure 6.13 confirms the results stated above. The results of Amplitude Test 5 were more similar to those of Amplitude Test 4 however. These two tests were done a day apart whereas Amplitude Test 5 and Amplitude Test 3 were done two days apart. The changed properties of the sand were more noticeable in the data that was taken two days apart.

As previously mentioned, data from two accelerometers was recorded throughout the amplitude response tests. Figure 6.15 is a side-by-side comparison of the surface displacement measured at some distance in the sandbox and the acceleration of the shaker foot for that measurement. This data was taken from Amplitude Response Test 5. Graph (a) shows the surface displacement versus drive amplitude for the fundamental of five
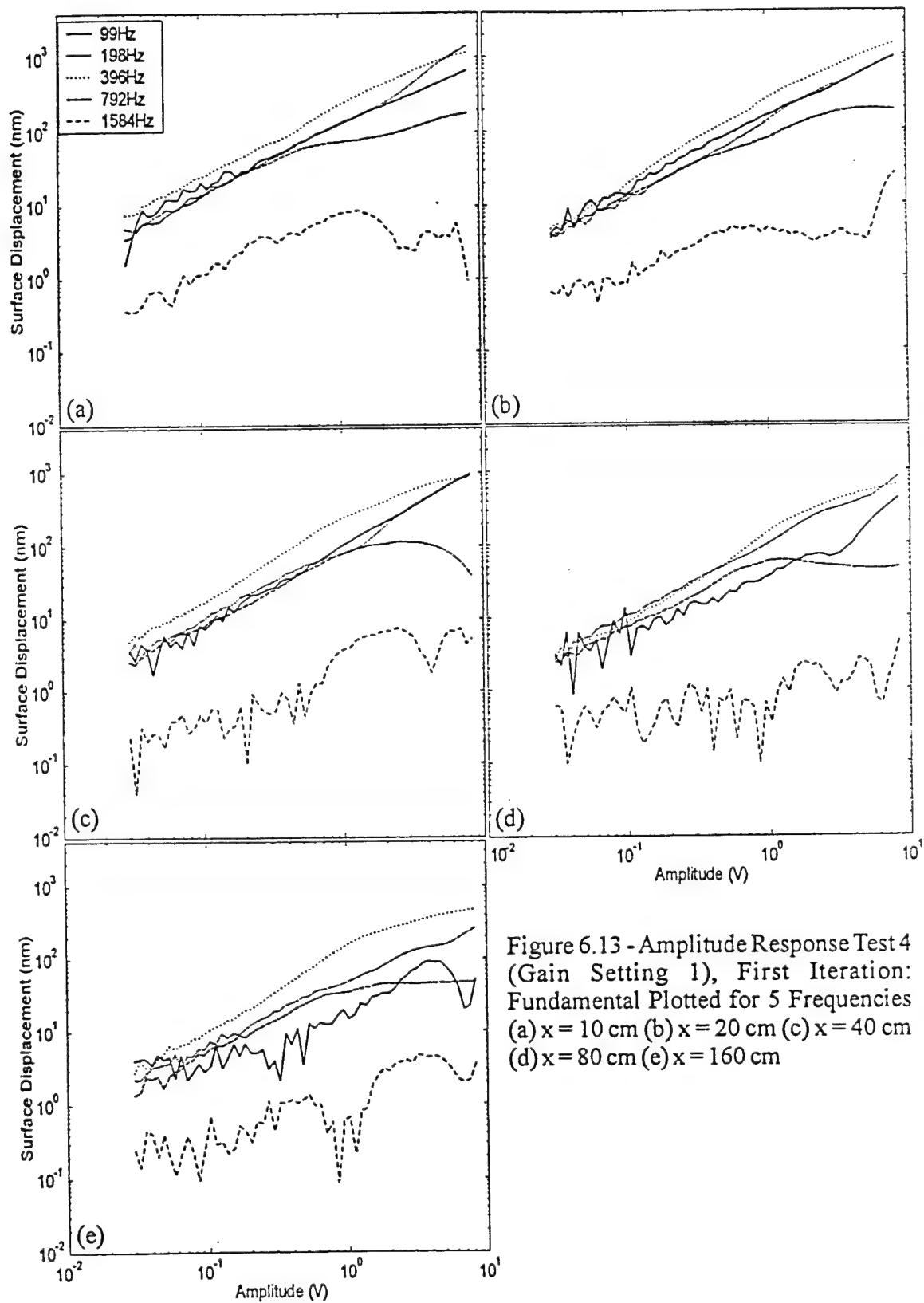
Figure 6.13 - Amplitude Response Test 4 (Gain Setting 1), First Iteration: Fundamental Plotted for 5 Frequencies (a) x = 10 cm (b) x = 20 cm (c) x = 40 cm (d) x = 80 cm (e) x = 160 cm

80
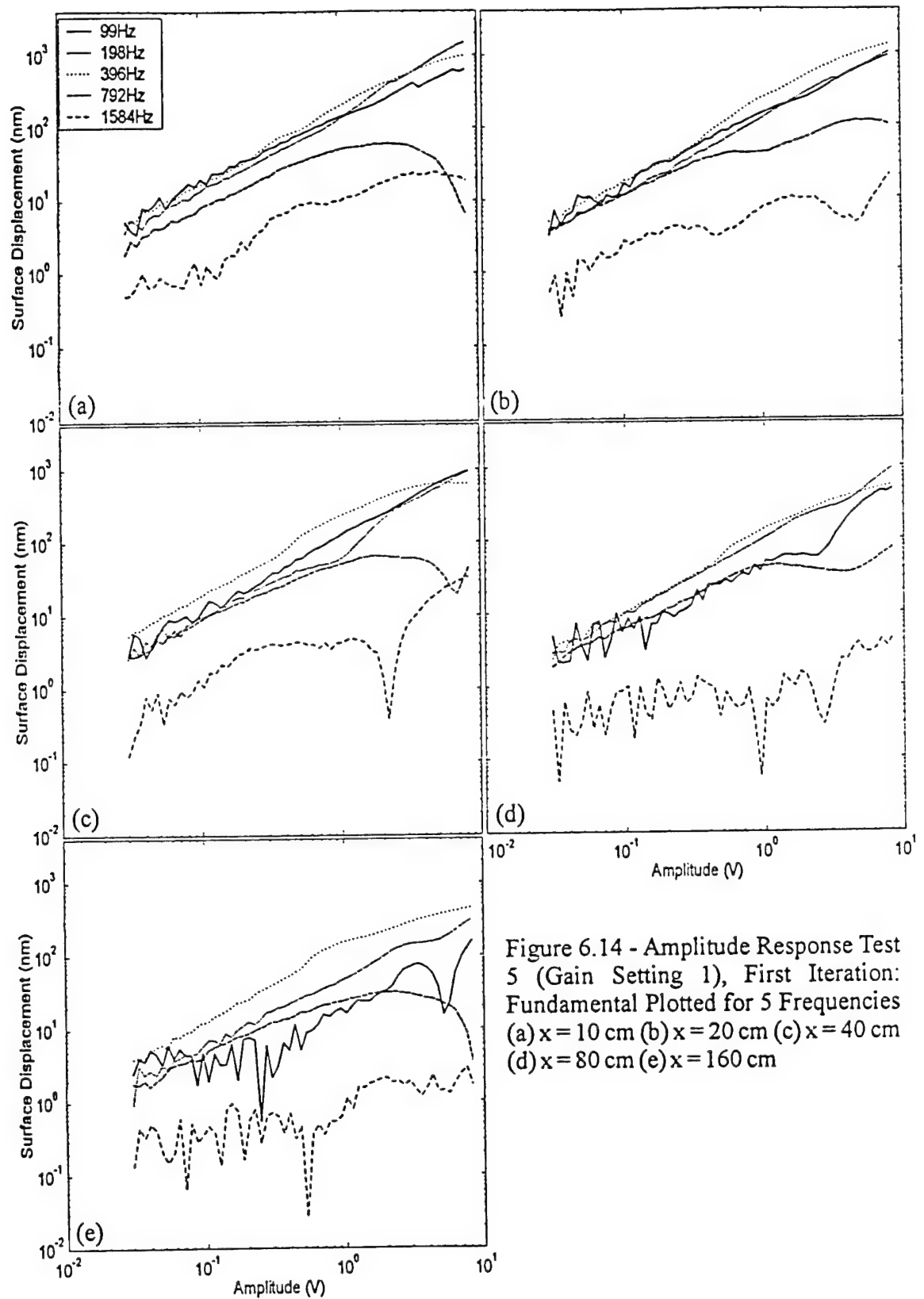
Figure 6.14 - Amplitude Response Test 5 (Gain Setting 1), First Iteration: Fundamental Plotted for 5 Frequencies (a) x = 10 cm (b) x = 20 cm (c) x = 40 cm (d) x = 80 cm (e) x = 160 cm

81
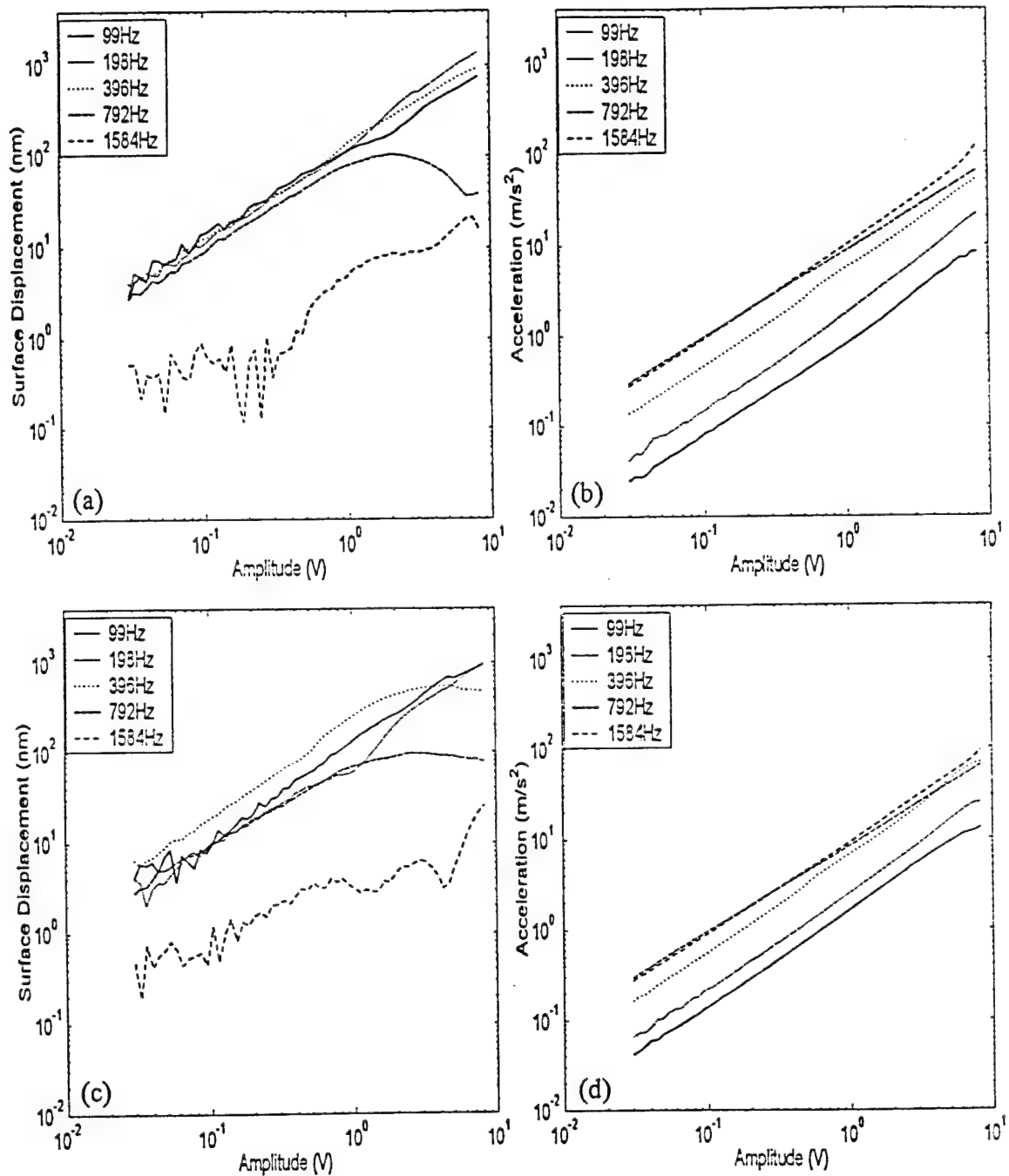
Figure 6.15 - Amplitude Response Test 5 (Gain Setting 1), Second Iteration: Comparison of Radar and Center Accelerometer Measurements for 5 Frequencies   (a) Surface displacement at x = 10 cm (b) Foot acceleration while radar was at x = 10 cm (c) Surface displacement at x = 40 cm (d) Foot acceleration while radar was at x = 40 cm

frequencies measured at x = 10 cm. Graph (b) was the amplitude response as measured in acceleration by the accelerometer mounted on the center of the shaker foot for the same five frequencies. Graph (c) showed the surface displacement versus amplitude measured at x = 40 cm and (d) was the corresponding amplitude response of the shaker foot. (b) and (d) showed that the amplitude response of the shaker foot was almost identical from measurement to measurement. They also showed that the shaker foot applied the most force at 792 Hz and 1584 Hz. By the time the wave propagated to x = 10 cm however, 792 Hz and 1584 Hz had attenuated to the point that 99 Hz, 198 Hz, and 396 Hz produced the largest surface displacements. This result emphasized how much more high frequencies attenuated than low frequencies.

Just as in the frequency response tests, the harmonics being produced were examined to determine the extent of nonlinearities present. Instead of showing the fundamental and its harmonics as seen for the frequency response tests however, this section of the results normalized the harmonics by the fundamental in order to show relative harmonic generation.

Figure 6.16 shows the first four harmonics of 396 Hz normalized by the amplitude response of the fundamental. The data is taken from Amplitude Response Test 5 (first iteration). Each graph ((a) – (e)) shows the amplitude response at a different location. At x = 10 cm, the first harmonic rose above the noise floor when the amplitude was 2e-1 V, the second harmonic rose above the noise floor when the amplitude was 6e-1 V, and the third harmonic rose above the noise floor when the amplitude was 1e0 V. The fourth

Figure 6.16 - Amplitude Response Test 5 (Gain Setting 1), First Iteration: 4 Harmonics Normalized by the Fundamental for 396 Hz at 5 Locations (a) x = 10 cm (b) x = 20 cm (c) x = 40 cm (d) x = 80 cm (e) x = 160 cm

harmonic just began to rise above the noise at an amplitude of 7e0 V. The harmonics

showed signs of saturation, but more harmonics were produced, as amplitude increased.

Graphs (b) and (c) showed that the harmonics attenuated with respect to the

fundamental as the wave propagated in the sandbox. This was expected because high

frequencies (harmonics of 396 Hz) attenuated faster than low frequencies (396 Hz). The

fourth harmonic rose above the noise floor at an amplitude of 3e0 V at $x = 20$ cm

however. This meant that at constant amplitude (3e0 V) and frequency (396 Hz), the

fourth harmonic was generated at 20 cm but not at 10 cm. This result showed that the

propagation path contributed to nonlinearity between $x = 10$ cm and $x = 20$ cm. From 40

cm to 160 cm this effect was not seen. The propagation was still nonlinear, but the

attenuation of the harmonic frequencies dominated the effect of nonlinear propagation.

Figure 6.17 shows four harmonics normalized by the fundamental versus

amplitude. The data came from Amplitude Response Test 5 (first iteration). All of the

graphs represent data measured at $x = 40$ cm. Each one was for a different frequency. 99

Hz, 198 Hz, and 396 Hz all produced significant harmonics at this point in the sand. The

frequency that had a harmonic rise above the noise floor first, as the amplitude increased,

was 396 Hz. The next frequency to generate a harmonic, as amplitude increased, was

198 Hz. This result was consistent with the frequency response tests showing the largest

surface displacements in the 100 Hz – 600 Hz band. The fist harmonic of 792 Hz rose

above the noise at 3e0 V and no harmonics were generated at 40 cm for 1584 Hz. Once

again this showed the effects of attenuation on the higher frequencies. Appendix C

contains a complete set of data for Amplitude Response Test 5 (second iteration).
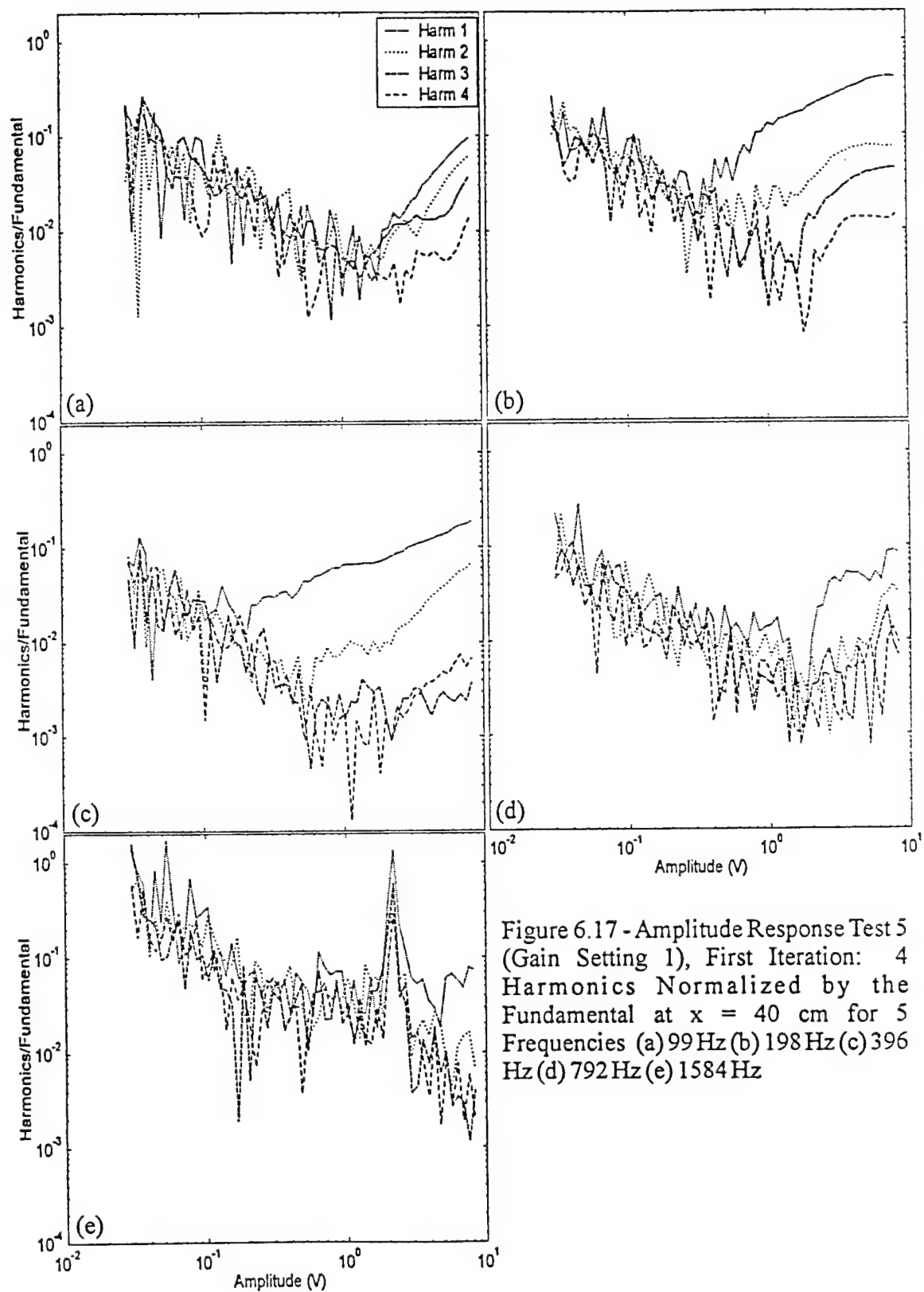
Figure 6.17 - Amplitude Response Test 5 (Gain Setting 1), First Iteration: 4 Harmonics Normalized by the Fundamental at x = 40 cm for 5 Frequencies (a) 99 Hz (b) 198 Hz (c) 396 Hz (d) 792 Hz (e) 1584 Hz

Nonlinearities at the Source

An important part of the results was what happened at the shaker for both the frequency response and amplitude response tests. It was shown that both variability and nonlinearity occur during propagation but the source also contributed to the overall effects seen in the data. Of the three shaker – shaker foot combinations tested, the 100 pound shaker with rectangular foot had the fewest modes of foot motion excited at the frequencies and amplitudes used, it had fewer resonances, and it produced fewer harmonics as recorded by the accelerometers. Despite this, there were still source considerations to take into account.

First, there was the matter of the shaker foot to sand contact. Every time the shaker foot was placed on the sand the foot-sand coupling was different. The data collected in Experiment Two showed that by leaving the shaker on the sand throughout the measurements, the results repeated well. The frequency response changed slightly whenever the shaker was moved and placed back on the sand.

This effect is more noticeable when viewed in the time-domain. Figure 6.18 (a) shows seven different waveforms from Experiment One (20lb shaker with rectangular foot) plotted on top of each other. They were all measured at x = 120 cm but the amplitudes increased linearly (increment = 0.04 V) from 0.14 V to 0.38 V. The first six amplitudes were recorded without moving the shaker. The waveforms were almost identical with the exception of the increased amplitude. Prior to the seventh measurement (drive amplitude = 0.38 V), the shaker was removed, the sand was watered and packed, and the shaker was placed back on the sand. The shape of this waveform
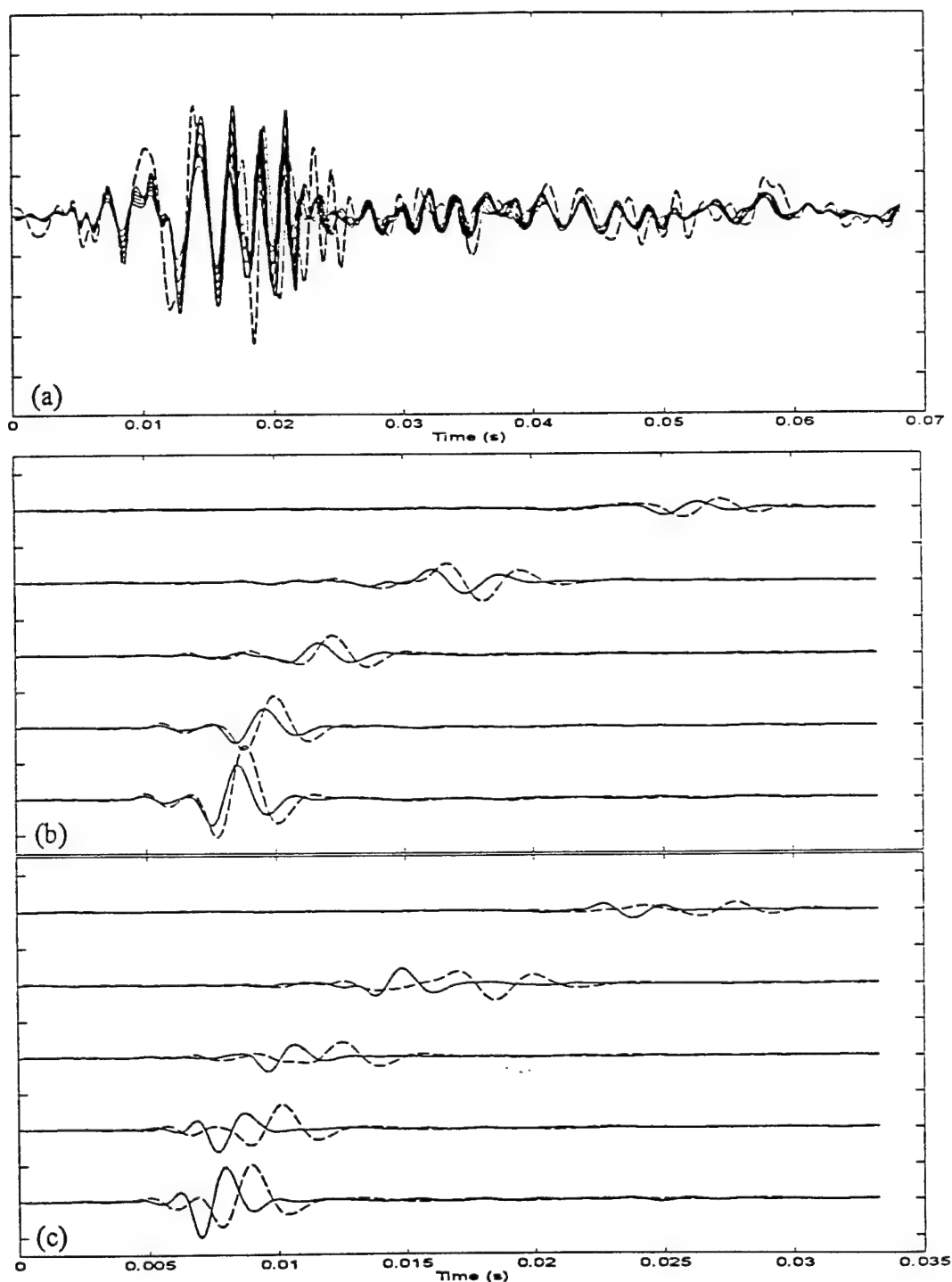
Figure 6.18 - (a) Waveform of 7 amplitudes (0.14 V - 0.38 V) from Experiment One, 20lb shaker with rectangular foot, shaker moved prior to recording 0.38 V (dotted line) (b) Waveform of 2.0 V and 4.0 V from Frequency Response Test 2 (first iteration) for 5 locations (c) Waveform of 0.5 V (scaled x4) and 8.0 V (scaled x0.5) from Frequency Response Test 2 (first iteration) for 5 locations

(dotted line) was significantly different due to the new shaker foot to sand contact. This showed that it was very important to understand whether or not the data being compared in Experiment Two was taken with or without moving the shaker.

Careful inspection of the waveforms plotted in Figure 6.18 (a) revealed another interesting feature. As the drive amplitude increased, the waveforms were recorded later in time at the same point in the sandbox. The cause of this was either a delay at the source, a decreased propagation speed, or a combination of both. Another possibility was that as the drive amplitude increased, the frequency content due to harmonic generation changed. When the frequency spectrum, which used a linear assumption, was convolved with the differentiated Gaussian and taken into the time-domain it may have filtered frequencies that resulted in a delay of the waveform.

Figure 6.18 (b) shows ten waveforms plotted for data recorded in Frequency Response Test 2 (first iteration). The two plotted at the bottom of the graph were recorded at x = 10 cm. The two above that were recorded at x = 20 cm, then x = 40 cm, x = 80 cm, and finally x = 160 cm is at the top of the graph. At each position there is a waveform that had a drive amplitude of 2.0 V (solid line) and one that had a drive amplitude of 4.0 V (dotted line). Using the highest peak as a reference, there was approximately 0.25 ms between the two waveforms at x = 10 cm. At x = 80 cm there was approximately 0.64 ms between the waveforms. This indicated that the waveform generated by the larger drive amplitude was propagating slower between these two points.

Figure 6.18 (c) shows ten waveforms plotted for data recorded in Frequency

Response Test 2 (first iteration). The two plotted at the bottom of the graph were

recorded at x = 10 cm. The two above that were recorded at x = 20 cm, then x = 40 cm, x

= 80 cm, and finally x = 160 cm is at the top of the graph. At each position there is a

waveform that had a drive amplitude of 0.5 V (solid line) and one that had a drive

amplitude of 8.0 V (dotted line). The waveform with the drive amplitude of 0.5 V was

scaled up by a factor of 4 and the waveform with the drive amplitude of 8.0 V was scaled

down by a factor of 2. This was done so that the two waveforms could be plotted on the

same graph for comparison. Using the highest peak as a reference, there was

approximately 1.0 ms between the two waveforms at x = 10 cm. At x = 80 cm there was

approximately 2.4 ms between the waveforms. This verified that the waveform with the

greater drive amplitude was propagating slower between these two points.

Figure 6.19 shows data recorded by the accelerometer mounted in the center of

the shaker foot for Amplitude Response Test 5 (first iteration). (a) through (e) are the

five frequencies (99 Hz, 198 Hz, 396 Hz, 792 Hz, and 1584 Hz respectively) measured

while the radar was at x = 10 cm. The graphs show four harmonics normalized by the

fundamental. This figure indicates that there was a significant contribution of harmonics
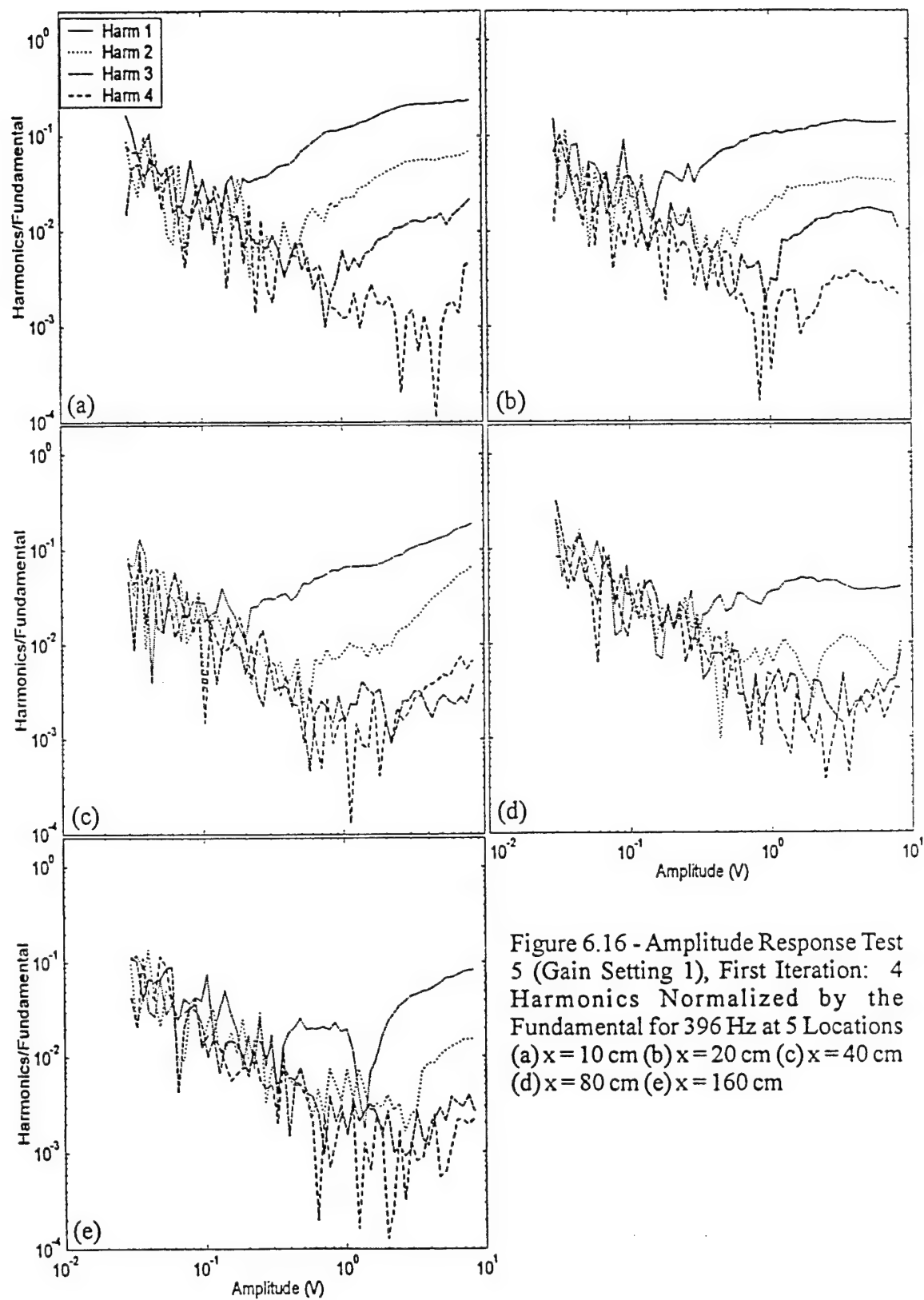
generated at the source in addition to that generated by the propagation path.
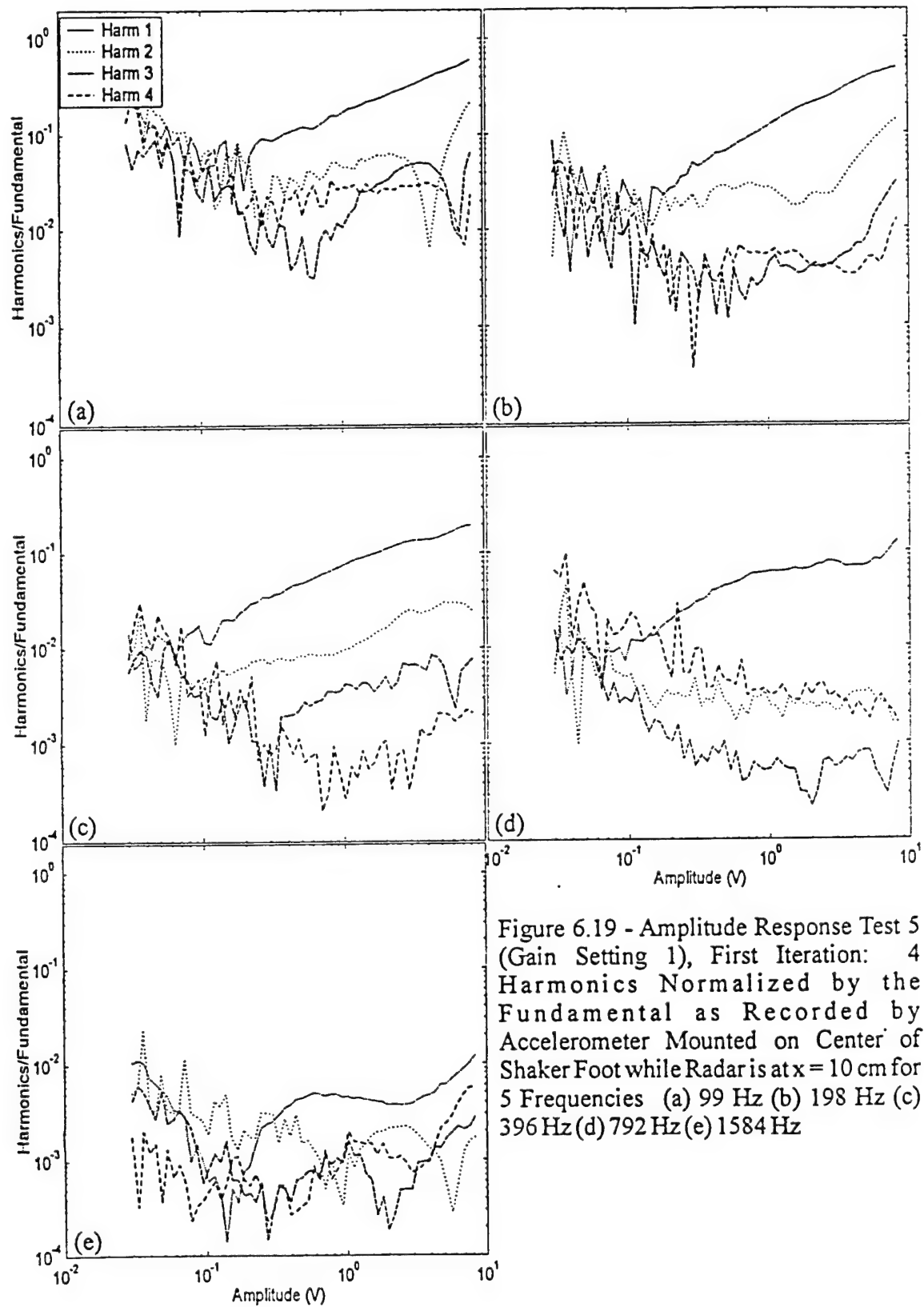
Figure 6.19 - Amplitude Response Test 5 (Gain Setting 1), First Iteration: 4 Harmonics Normalized by the Fundamental as Recorded by Accelerometer Mounted on Center of Shaker Foot while Radar is at x = 10 cm for 5 Frequencies (a) 99 Hz (b) 198 Hz (c) 396 Hz (d) 792 Hz (e) 1584 Hz

CHAPTER VII

CONCLUSIONS

The shaker foot and propagation path contributed to the nonlinearities of the investigated system. The source created nonlinearities as indicated by the harmonics recorded with accelerometers mounted on the shaker foot. The propagation path created nonlinearities due to a complex, three-dimensional crystalline matrix with pockets of varying amounts of water and air. This was seen by the number of generated harmonics increasing from one point to another in some of the data, despite attenuation being the dominant effect. The propagation path contributed to nonlinearities because of the changing solid particle wave paths and fluctuating viscous and cohesive properties.

The shaker foot to sand coupling was an important contributor to the results recorded. The results showed that once the shaker foot to sand contact was changed the results were not repeatable with the same degree of precision. When comparing sets of data taken before and after moving the shaker, it was seen that the different fundamentals and harmonics for the frequency responses behaved similarly with respect to each other, but changed slightly every time the shaker was moved. This difference was more pronounced in the time-domain. The surface displacements measured by the radar for higher frequencies, which were already variable, showed the biggest changes after changing the shaker foot to sand coupling.

When looking at the frequency response of the shaker foot, as measured by the accelerometers, the frequency band that was most susceptible to change due to the shaker foot to sand contact was 30 – 400 Hz. This was seen in Figure 6.8 (b) where two sets of data, with different shaker foot to sand contact, were plotted on the same graph. The frequency response of the 30 – 400 Hz band was significantly different. The changing frequency response in this band was consistent throughout the data. For example, Figure 5.8 (b) showed a null around 100 Hz that did not appear anywhere else in the data.

The degree to which the sources of nonlinearities affect the propagation of compressional, surface, and shear waves was dependent upon the type of shaker foot, the frequencies, and the amplitudes utilized. By carefully selecting these three things a wide variety of results were produced. These results ranged from near-linear responses to highly non-linear responses.

Different types of shakers and shaker feet affect the results. Of the combinations investigated a rectangular foot with a length to width ratio of approximately 10:1, and enough surface area to support the shaker without burying, produced the most linear results. The degree of nonlinearity was measured by the amount of harmonic generation recorded by the accelerometers mounted on the foot. Although the foot had a square cross section, the length to thickness ratio was still such that a bending-about-the-center mode of vibration was excited.

The circular foot produced amplitude responses which approached saturation and then began rising again. Because the amplitude at which this second rise began changed depending on where the measurement was taken, the result was affected by the

93

propagation path. This was not seen on the other two shaker feet. The likely cause of this was that the pressure wave and surface wave had different saturation thresholds. As the dominating wave saturated, the amplitude response had a decreased slope until the other wave, which was still increasing with drive amplitude, began to dominate. This would also account for some of the dips in the amplitude responses of the higher frequencies.

The difference between the round foot and the two rectangular feet was the surface area to frontal length ratio. If the surface wave was dependent on the frontal length while the compressional wave was dependent on the surface area, the saturation curves could behave as measured due to the dominating wave changing from compressional to surface during propagation. The other shaker feet would have a surface wave that dominated the curve from the beginning and therefore did not produce this two-rise effect. The foot motion must be well documented in order to accurately represent the source in the computer model. It is also important to ensure that the power amplifier and shaker are properly matched so that an impedance mismatch does not increase the nonlinearity of the source.

The range of frequencies used to generate the wave also impacted the results. Frequencies less than 600 Hz propagated well through the sand. Frequencies higher than 600 Hz were highly vulnerable to attenuation, particularly once the surface of the sand dried. A flatter frequency response, with less variability of the higher frequencies, was achieved with lower amplitudes as seen in Figure 6.8 (a). Doubling the amplitude doubled the surface displacement for the 100 – 1200 Hz frequency band. The 1300 –

94

2000 Hz frequency band also showed this behavior up to x = 20 cm where the 0.25 V amplitude began to exhibit the variability of the higher frequencies.

The 30 Hz – 2000 Hz frequency range used for the acousto-electromagnetic mine detection technique appears to be very well suited for this task. The generation of harmonics by the lower frequencies helps to increase the surface displacements of the higher frequency range. Anything above 2000 Hz however, would attenuate so quickly that no matter how much contribution from lower frequency harmonics was present there would not be enough energy in these frequencies to propagate an appreciable distance. The higher frequencies are also less useful in that the variability of their amplitude responses would produce nulls at unpredictable locations.

Increasing the drive amplitude caused system nonlinearities as expected. The threshold of linearity changed as a function of distance and frequency. Small amplitudes propagated well enough to be measured by the radar at the furthest point tested. These smaller amplitudes had a much flatter frequency response, although there was a null around 1250 Hz for the two smallest amplitudes tested. This null was due to the frequency response of the foot and what appeared to be some destructive interference. As the amplitude increased however, the surface displacements due to the lower frequencies rose faster than surface displacements due to the higher frequencies. This was important to note when trying to make the computer model match the actual experiments. Increasing the drive amplitude increased nonlinearity by first driving the shaker foot such that harmonics were generated and also caused the wave to propagate in a nonlinear way through the unconsolidated soil matrix.

The threshold of surface displacement for these experiments was approximately 3000 nm as measured at x = 10 cm. These displacements occurred in the 200 – 400 Hz frequency band, despite the accelerations measured on the shaker foot being greatest around 1500 Hz. Regardless of the amplitude or frequency used, the radar never measured any surface displacements greater than 3000 nm. The threshold did not change for different shakers and shaker feet combinations. The 20 pound shaker with small rectangular foot also saturated the sand at this point even though the surface area of the smaller shaker foot was almost 3.5 times less than that of the shaker foot used in Experiment Two. The larger shaker and shaker foot used more current without burying into the sand, but the additional current was used to drive the heavier foot and did not increase the magnitude of displacement in the sand.

CHAPTER VIII

RECOMMENDATIONS

There are many different shaker feet that could be used in the acousto-electromagnetic mine detection technique. A study of these possibilities should be conducted. The three possibilities examined as part of this research produced very different results that indicated that the many other possibilities could turn up a configuration much more suited for mine detection. Shaker feet could also be made that did not have resonances and had only one mode of vibration excited for the frequencies and drive amplitudes used. A shaker foot very similar to the one used in Experiment Two could be made with the same surface area but thicker cross section in order to achieve this.

If an investigation of shaker feet was conducted, it should focus on those with a large (> 10:1) length to width ratio. The amplitude response of the 20 pound shaker with circular foot showed that the small length to width ratio (1:1 in this case) resulted in a greater degree of nonlinearity. Making a large round foot for the 100 pound shaker would create the same nonlinearites.

The way that the shaker foot couples with the sand could also be changed. The only technique examined thus far was placing the foot on top of the sand surface and relying on the weight of the shaker to keep shaker foot to sand contact steady. Different foot – sand couplings should be investigated to determine if another technique is more

suited for the production of surface waves. One example would be something on the foot that penetrates the sand, such as nails, which is one configuration used by researchers at the University of Texas [4].

This research looked at what was happening only along the x-axis of the sandbox. At this point it would be beneficial to expand the research to looking in two dimensions. Very little is known about the directivity of the various shaker – shaker feet combinations. This directivity changes depending on which foot is used because of the unique shaker foot motions, sizes, and shapes. Since mine detection dwells in a limited three-dimensional space, which is very large on the surface, determining the directivity of these sources will become important.

The near-field radiation pattern of the shaker is very complicated. The reason for increasing surface displacements for the fundamental, between 10 cm and 40 cm, in Frequency Response Test 4, is still unknown. The low frequencies used and the size of the shaker foot resulted in a near-field of appreciable size. It could be worth the effort to try and characterize this near-field. If an array of sources is ever planned for implementation, determining what the behavior of frequencies in the near-field is will be even more important.

Some mine detection tests should be conducted with much lower drive amplitudes. Frequency Response Test 4 showed that lower drive levels produced a flatter frequency response. There was not as much variability in the form of frequency response nulls. The surface displacements due to higher frequencies were also greater with respect to the displacements of the lower frequencies than they were in the other frequency

response tests. It might be beneficial, for interrogation of very small objects, to lower the drive amplitude so that higher frequencies do not become variable as they do for higher amplitudes. If this were done, the incident signal duration would probably have to be lengthened to improve the signal to noise ratio. This would result in a trade-off of time to conduct a scan for better high frequency propagation.

Finally, two-dimensional scans for mines using an incident signal of reduced bandwidth should be tested in the event that time is more important than interrogation with frequencies greater than 1200 Hz. Because of the rapid attenuation of higher frequencies, it may not be worth using a chirp that contains frequencies between 1200 Hz and 2000 Hz. More than a second could be saved for each measurement by utilizing a 30 – 1200 Hz chirp. Under the current procedure for conducting two-dimensional scans, this would reduce the 9.5 hour scan by about 10 percent. This will become more and more important in the future as the research heads towards practical implementation. If neither time nor frequencies above 1200 Hz were critical, then the same length signal using a 30 Hz to 1200 Hz chirp could be used to improve the signal to noise ratio.

APPENDIX A

EXPERIMENT ONE DETAILS

Design of Experiments

In order to determine what type of experiments would be the most effective and efficient for this research, some initial tests were run on the sandbox. There were three specific factors that needed to be found. First, the maximum amplitude that the shaker could be driven without burying itself in the sand, and the minimum amplitude appearing above the noise floor needed to be found out. This would set the upper and lower limits of input voltages for the experiments. Second, the maximum duration a scan could be run, without experiencing nonlinearities due to the sand drying, was needed. This would determine how often the scans needed to be stopped in order to rewet and recompact the sand. Third, the minimum duration of the input signal, while still recording accurate data, needed to be found in order to minimize scan time.

Shaker Amplitude Range

Total amplitude in this experimental setup was produced by a combination of the DAC and an amplifier. In order to find the low end of the amplitude range the gain on the amplifier was turned all the way up. Lower and lower values of amplitude were then entered into the computer for the board until a value of 0.03 volts was found to be the smallest value that would still register above the noise floor. Harmonics were not seen, however, until the value entered in the computer was approximately 0.15 volts. The

lower end value of the amplitude range was then chosen as 0.06 volts entered in the computer and the amplifier set at maximum gain. This ensured that the data collected began in the linear region (no harmonics produced).

The goal for the experiment was to use approximately 24 different amplitudes at each point tested. About 10% of the amplitudes on the upper end of the range would cause the shaker foot to settle into the ground during a scan. A series of trials was run in order to determine where the amplitude would have to be set for the shaker foot to settle into the sand. It was determined that if the voltage entered into the computer was greater than 0.86 V, with the gain on the amplifier all the way up, this occurred. Therefore, 0.98 V was chosen as the upper end of the entered value of voltage.

Maximum Scan Duration

Drying Test Number 1 An experiment was conducted in order to determine how long the sand's propagation properties remained constant before drying effects became noticeable in the data. A program was written to conduct a 41 point scan (0 – 120 cm at 3 cm increment) along the x-axis every hour. A 3.5 second chirp from 30 Hz to 2000 Hz was used as the input signal. The sand was prepared for scanning and the program was executed. This data was recorded for a 72 hour period (73 scans).

The velocity of the surface wave remained at approximately 91 m/s during the entire 72 hour period. This velocity was calculated by measuring points on the waterfall graphs so a great deal of precision could not be achieved. The velocity most likely decreased at a rate that was too small to detect as the sand dried, however the surface wave velocity did remain somewhere in the 90.5 m/s – 92 m/s range.

Frequency propagation was also studied. During the first ten hours of drying there was no significant loss of frequency propagation. After ten hours however, frequencies greater than 900 Hz appeared to show a decrease in ability to propagate over the full 120 cm of the scan region. At the time, this was taken to mean that the sandbox would need to be rewetted and recompacted every eight to ten hours to ensure propagation of the higher frequencies.

The interpretation of the drying tests was not precisely correct due to the fact that a chirp was being used as the incident signal. This prevented a lot of energy being placed into any one frequency band and the signal to noise ratio was not as good as it should have been. Also, by the time Experiment Two was conducted, it was realized that the higher frequency's propagation ability actually drops off within the first couple of hours due to drying and the lower frequencies remain able to propagate regardless of moisture conditions.

Drying Test Number 2 It was determined through several sample data collections that drying effects might be affecting some of the frequencies when a sinusoidal input is used instead of the 30 – 2000 Hz chirp. A second drying test was conducted to examine this. The radar was positioned at point (40,0). Every 15 minutes a scan was taken from 100 – 2000 Hz, at 100 Hz increments, and amplitude equal to 0.5 V. Each frequency input was a 3.5 second sinusoid with a 0.5 second settling time. Only two seconds of the 3.5 available was used for data processing in order to minimize the impact of any start-up or shut-down transient signal.

Once this data had been collected, the effects of the sand drying were examined by looking at the frequency response of the surface displacements for the fundamental and harmonics. The changes were compared over time. The results were also examined for 200, 500, 800, 1100, 1400, and 1700 Hz by comparing surface displacements for the fundamentals as a function of time.

The results of the second drying test showed that certain frequencies were more susceptible to effects of drying than others. For example, the low range of frequencies (100 – 500 Hz) experience very little change from drying effects. In the mid-range of frequencies (600 – 1500 Hz), drying caused most of the frequency displacements to diminish. In the high range of frequencies (1600 – 2000 Hz), a variety of things took place. 1600 Hz remained about the same, 1700 and 1800 Hz increased as the sand dried, and 1900 and 2000 Hz decreased as the sand dried. The harmonics behaved similar to the fundamental frequencies but were less predictable.

The displacement of the frequencies remained relatively constant over a ten hour period. The largest changes occurred within the first hour after preparing the sand. With the exception of 500 Hz, the harmonics supported this observation. These results indicated that if the sand was reconditioned about every eight hours, the effects of drying would be minimized. Also, the sand would be allowed to reach a quasi-equilibrium by waiting one hour from the time of reconditioning before data collection would commence.

Minimum Input Signal Duration

A program was written to test 20 different frequencies (100-2000 Hz in 100 Hz increments), with amplitude equal to 0.5 V, at two different points (x = 40 cm and x = 120 cm). These tests were run three different times to determine if the signal duration had an effect on the output. The three time windows used were 4.096 seconds, 2.048 seconds, and 1.024 seconds. The time windows were composed of the signal followed by approximately 0.5 seconds of settling time. The settling time changed slightly depending on the frequency being tested so that the input sine wave ended after an integer number of periods each time.

The fundamental frequencies and some of the harmonics were seen using each one of these signal durations. However, the longer input signal yielded more harmonics registering outside of the noise level. It was suspected that the one second signal would yield the same results as the two and four second signal with slight differences in the signal to noise ratio. Because different signal lengths were producing a different number of harmonics, the data indicated that there might be a start-up and/or a shut-down transient present which was having less of an impact as it was averaged out over the longer signal duration.

The experiment was run again but this time the time-domain data was saved. This allowed the fast Fourier transform to be taken over different time windows. This was done two different ways. First, a one second time window, shifted a half second at a time, was used. Then a half second time window, shifted a half second at a time, was

104

used. In both cases the results were different for the first time window which verified the presence of a start-up transient.

As a result of this, the decision was made to use a 4.096 second time window. Approximately 3.5 seconds would be the signal and the remaining would be settling time. Only 2.048 seconds of the data collected would be used however, so that any start-up and shut-down transients could be eliminated before processing.

Data Collection

The data was collected in two different phases. The first phase was to get the data for the frequency and amplitude responses. The second phase gathered data in order to separate the pressure wave from the surface wave so that individual contributions could be studied. The third phase was gathering information for altered relative energy contents in the pressure and surface waves. Experiment One ended and planning for Experiment Two began before the third phase was completed.

Phase I

For this phase, a "scan" consisted of measuring 180 different frequencies at a certain amplitude and point. The frequencies ranged from 33 Hz to 2002 Hz by steps of 11 Hz. A scan was taken for 24 different amplitudes, at each of three different positions, for a total of 72 scans. The 24 amplitudes ranged from 0.06 volts to 0.96 volts on the board, in steps of 0.04 volts, with the gain on the amplifier all the way up.

The first 24 scans were taken with the radar at $x = 40$ cm, $y = 0$ cm, and $z = 0$ cm on the positioner. The distance from the lead edge of the shaker foot to the center of the waveguide was actually 71.2 cm. The actual distance from the surface of the sand to the

bottom edge of the waveguide was 2.0 cm. The power meter on the radar read −33 dBm (+/− 0.8 dBm) when it was raised to $z = 30$ cm on the positioner and microwave scattering foam was placed under the waveguide. The power meter read −1.55 dBm at the actual position where the data was taken.

The sand was watered down, compacted, and allowed to dry for one hour prior to beginning the data collection. The scans were done in order of increasing amplitude so as not to disturb the sand under the shaker foot. 15 scans were completed in 8.25 hours at which point a pause was taken to rewater and recompact the sand. Prior to starting again, the radar power was checked. It was −52 dBm (+/− 4 dBm) at $z = 30$ cm over the foam and −0.91 dBm at the measuring position. Five more scans were completed before the rewatering and recompacting procedure was once again performed. At this point the radar power meter read −32 dBm (+/− 1.5 dBm) at $z = 30$ cm over the foam and −0.94 dBm (+/− 1.5 dBm) at the measuring point. From this point on, the data collection had to be stopped after every scan in order to compact under the shaker foot because the amplitude was such that the shaker foot was burying itself in the sand. The power meter on the radar read −2.53 dBm, -2.59 dBm, and −2.74 dBm at the measuring position prior to the last three scans.

Throughout the entire process described above, calibration scans were taken before and after each data collection scan. These consisted of measuring 20 frequencies (100 Hz to 2000 Hz by 100 Hz increments) at the same amplitude (0.5 on the computer with the amplifier gain all the way up) and same position ($x = 40$ cm, $y = 0$ cm, and $z = 0$ cm on the positioner) each time. By measuring the exact same thing before and after

each scan, a comparison between the two could be made to see how much effect drying had during the scan. These calibration scans could be used to compare the condition of the sand during any scan regardless of when it was taken.

The second 24 scans were taken with the radar at $x = 80$ cm, $y = 0$ cm, and $z = 0$ cm on the positioner. The distance from the lead edge of the shaker foot to the center of the waveguide was actually 111.7 cm. The actual distance from the surface of the sand to the bottom edge of the waveguide was 2.1 cm. The power meter on the radar read -32.6 dBm ($+/-$ 0.4 dBm) when it was raised to $z = 30$ cm on the positioner and microwave scattering foam was placed under the waveguide. The power meter read -2.19 dBm ($+/-$ 0.01 dBm) at the actual position where the data was taken.

The sand was watered down, compacted, and allowed to dry for one hour prior to beginning the data collection just as it had been done for the scans at $x = 40$ cm. The scans were again done in order of increasing amplitude so as not to disturb the sand under the shaker foot. 15 scans were completed in 8.5 hours at which point the sand was rewatered and recompacted. Prior to starting again, the radar power was checked. It was -36.6 dBm ($+/-$ 0.5 dBm) at $z = 30$ cm over the foam and -3.00 dBm ($+/-$ 0.01 dBm) at the measuring position. Three more scans were completed before the rewatering and recompacting procedure was once again performed. At this point the radar power meter read -3.52 dBm ($+/-$ 0.01 dBm) at the measuring point. One scan was completed and the reconditioning procedure was repeated with the radar power meter reading -3.70 dBm ($+/-$ 0.01 dBm) at the measuring point. Two more scans were completed and then the data collection had to be stopped after every scan in order to compact under the shaker

foot because the amplitude was such that the shaker foot was burying itself in the sand. The power meter on the radar read –3.77 dBm, -3.80 dBm, and –3.86 dBm (+/- 0.01 dBm for each) at the measuring position prior to the last three scans.

Throughout the entire process described above, calibration scans were again taken before and after each data collection scan. The procedure for these calibration scans was exactly like the procedure described above for the point at x = 40 cm.

The final 24 scans were taken with the radar at x = 120 cm, y = 0 cm, and z = 0 cm on the positioner. The distance from the lead edge of the shaker foot to the center of the waveguide was actually 151.5 cm. The actual distance from the surface of the sand to the bottom edge of the waveguide was 1.5 cm. The power meter on the radar read –30.5 dBm (+/- 0.5 dBm) when it was raised to z = 30 cm on the positioner and microwave scattering foam was placed under the waveguide. The power meter read +0.69 dBm (+/- 0.01 dBm) at the actual position where the data was taken.

The sand was watered down, compacted, and allowed to dry for one hour and 20 minutes prior to beginning the data collection to once again allow it to reach a state of quasi-equilibrium. Beginning again with the lowest amplitude, 8 scans were completed in 4.5 hours at which point the sand was rewatered and recompacted. Prior to starting again, the radar power was checked. It was +0.85 dBm (+/- 0.01 dBm) at the measuring position. Ten more scans were completed in 5.75 hours before the sand had to be rewatered and recompacted. At this point the radar power meter read +2.90 dBm (+/- 0.01 dBm) at the measuring point. Three more scans were then completed before the data collection had to be stopped after every scan in order to compact under the shaker

foot to prevent it from burying itself in the sand. The power meter on the radar read +1.41 dBm, 0.93 dBm, and 0.79 dBm (+/- 0.01 dBm for each) at the measuring position prior to the last three scans.

Once again, calibration scans were taken before and after each data collection scan during the entire process described above. The procedure for these calibration scans was exactly like the procedure described above for the point at $x = 40$ cm.

Phase II

The data for this phase was collected in the same fashion as the data for the points at 40, 80, and 120 cm in Phase I. The only difference was the point at which the data was collected. During this part of the experiment, the point at $x = 190$ cm was used in order to allow the pressure wave and surface wave to separate in time. This point is at the far limit of the positioner in the experimental setup. By allowing the pressure wave and surface wave to separate, the contributions of each to the overall displacement were to be measured separately. The frequencies and amplitudes used were the same as those in Phase I of the data collection.

The distance from the lead edge of the shaker foot to the center of the waveguide was actually 220.7 cm. The actual distance from the surface of the sand to the bottom edge of the waveguide was 1.9 cm. The power meter on the radar read –29.9 dBm (+/- 0.4 dBm) when it was raised to $z = 30$ cm on the positioner and microwave scattering foam was placed under the waveguide. The power meter read +0.16 dBm at the actual position where the data was taken.

The sand was watered down, compacted, and allowed to dry for one hour and five minutes prior to beginning the data collection. 10 scans (amplitudes 0.30 – 0.66) were completed before pausing to rewater and recompact the sand. Prior to starting again, the radar power was checked. It was –28.15 dBm (+/- 0.1 dBm) at $z = 30$ cm over the foam and +2.29 dBm (+/- 0.01 dBm) at the measuring position. Five more scans (amplitudes 0.06 – 0.22) were completed before the rewatering and recompacting procedure was once again performed. At this point the radar power meter read –27.5 dBm (+/- 0.1 dBm) at $z = 30$ cm over the foam and –0.14 dBm (+/- 0.01 dBm) at the measuring point. This time four scans (amplitudes 0.26 and 0.70 – 0.78) were completed before reconditioning the sand. The radar power meter then read –25.15 dBm (+/- 0.1 dBm) at $Z = 30$ cm over the foam and +0.96 dBm at the measuring point. From this point on, the data collection had to be stopped after every scan (amplitudes 0.82 – 0.98) in order to compact under the shaker foot because the amplitude was such that the shaker foot was burying itself in the sand.

Throughout the entire process described above, calibration scans were taken before and after each data collection scan. These calibration scans were conducted in an identical manner to those described in Phase I of the data collection.

Results

As mentioned in Chapter IV, the reoccurring problems with the data were the increasing noise floor as amplitude increased, the erratic ends of the amplitude response curves as the shaker buried or was moved, and not enough amplitudes measured to

produce a smooth curve beginning in the linear region near the noise floor and increasing

to saturation.

APPENDIX B

ADDITIONAL FREQUENCY RESPONSE GRAPHS

This appendix contains a complete set of data for one of the frequency response measurements. The five figures come from the second iteration of the second frequency response test. This data was taken on Gain Setting 1. Figure B.1 shows the fundamental and four harmonics taken at $x = 10$ cm. The five graphs in this figure show the results for the following five amplitudes: 0.5 V, 1.0 V, 2.0 V, 4.0 V, and 8.0 V. Figures B.2 through B.5 show data taken at $x = 20$ cm, 40 cm, 80 cm, and 160 cm respectively. The same five amplitudes were used in each of these figures.
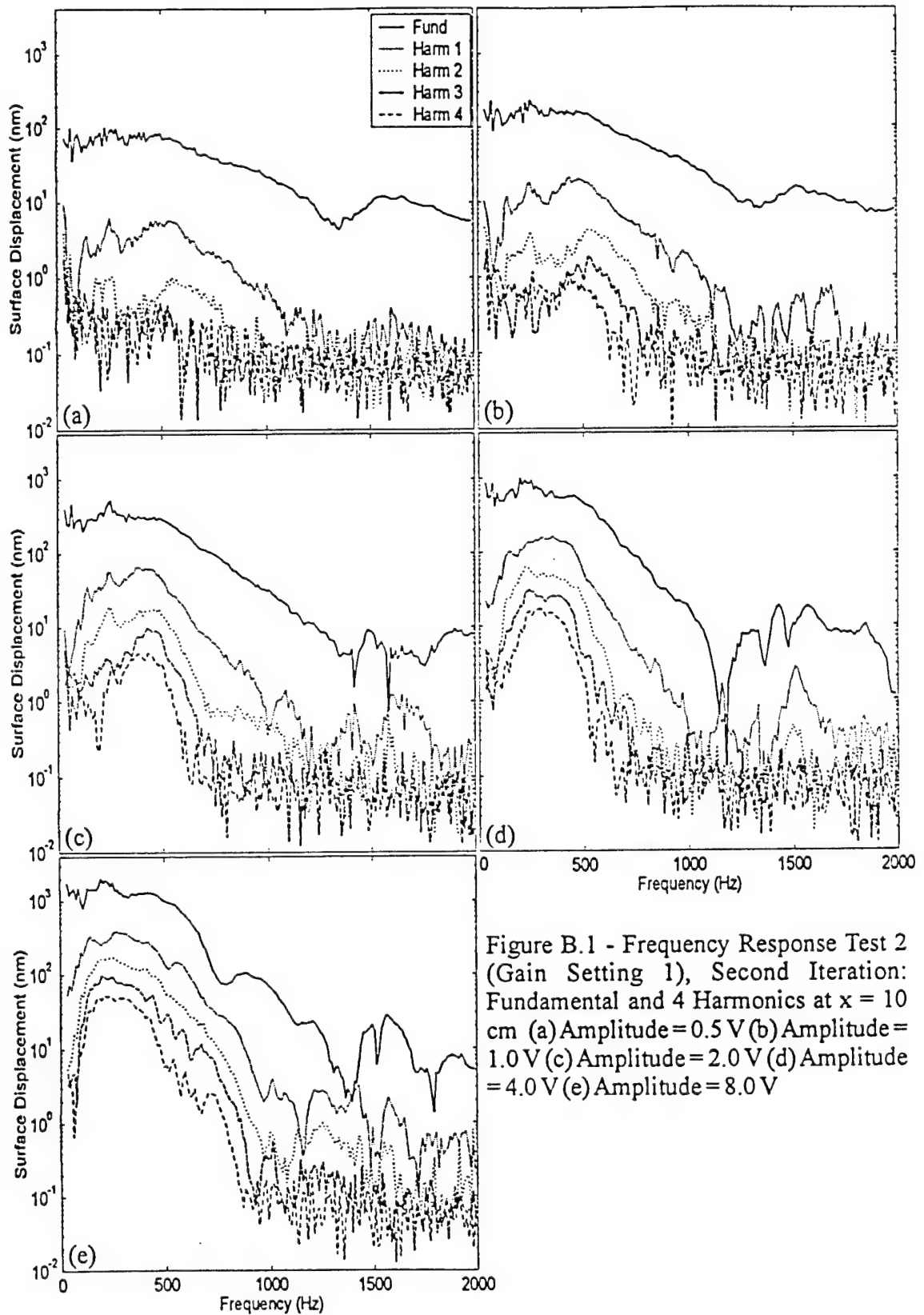
Figure B.1 - Frequency Response Test 2 (Gain Setting 1), Second Iteration: Fundamental and 4 Harmonics at x = 10 cm (a) Amplitude = 0.5 V (b) Amplitude = 1.0 V (c) Amplitude = 2.0 V (d) Amplitude = 4.0 V (e) Amplitude = 8.0 V
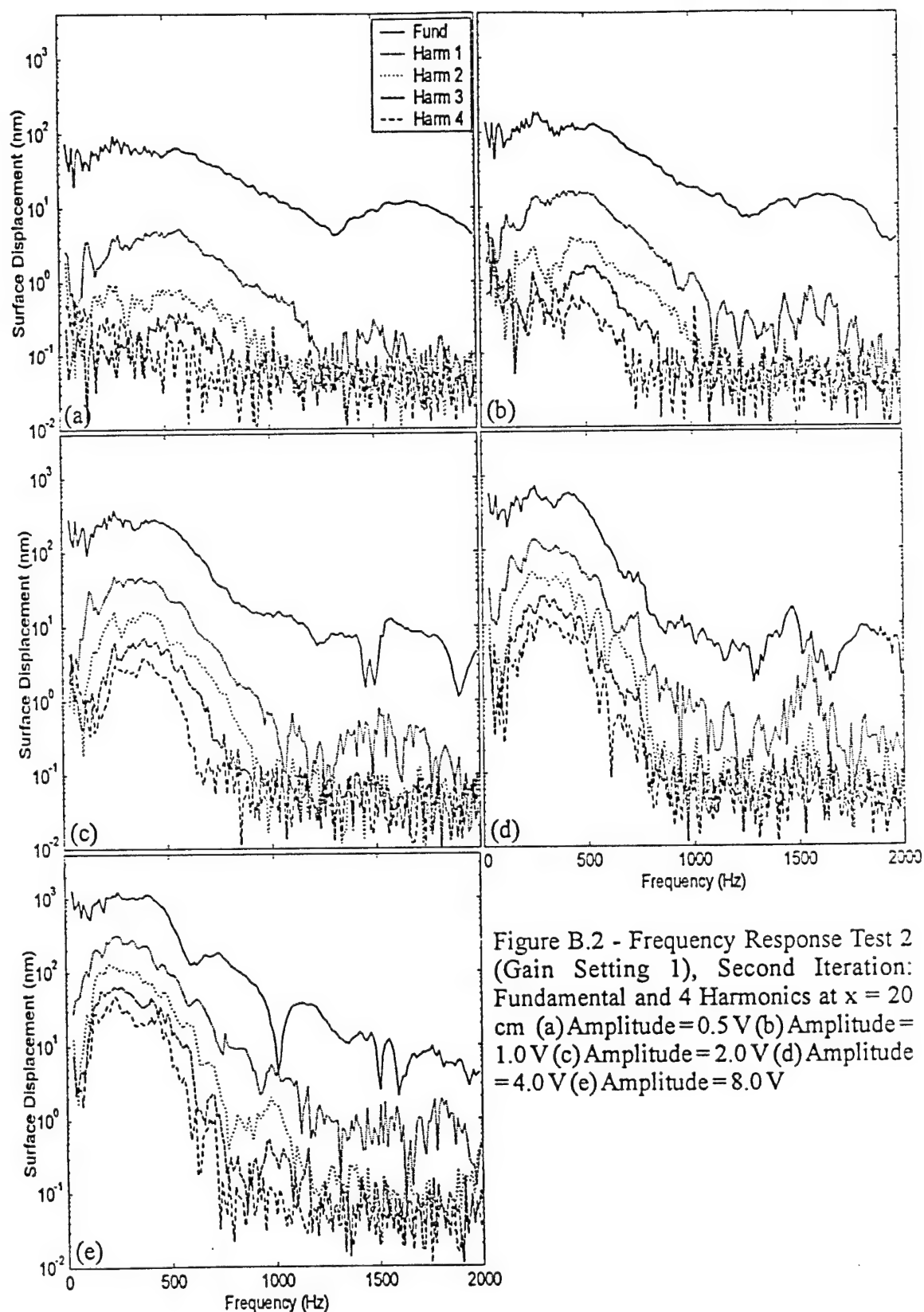
Figure B.2 - Frequency Response Test 2 (Gain Setting 1), Second Iteration: Fundamental and 4 Harmonics at x = 20 cm (a) Amplitude = 0.5 V (b) Amplitude = 1.0 V (c) Amplitude = 2.0 V (d) Amplitude = 4.0 V (e) Amplitude = 8.0 V

114
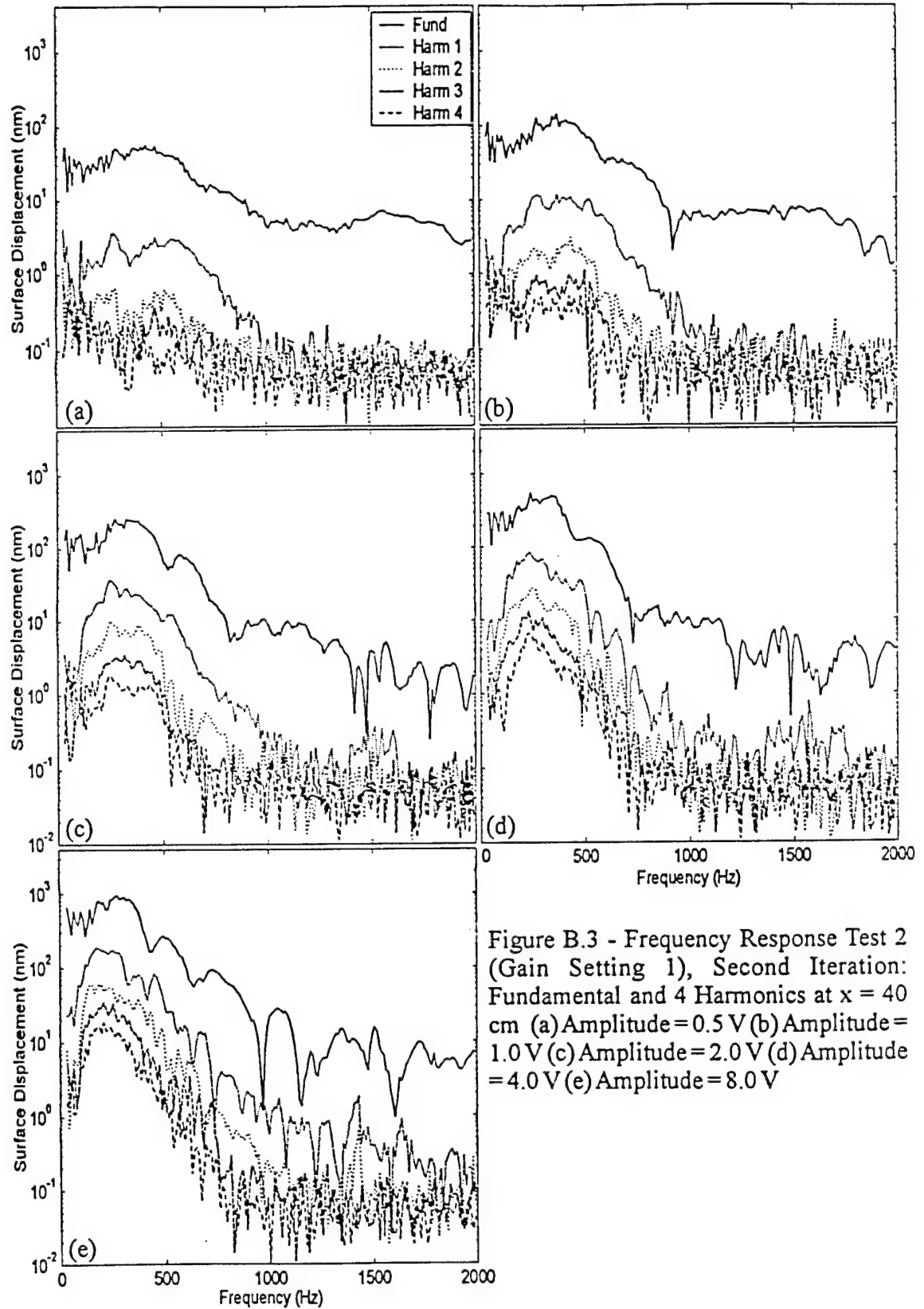
Figure B.3 - Frequency Response Test 2 (Gain Setting 1), Second Iteration: Fundamental and 4 Harmonics at x = 40 cm (a) Amplitude = 0.5 V (b) Amplitude = 1.0 V (c) Amplitude = 2.0 V (d) Amplitude = 4.0 V (e) Amplitude = 8.0 V

115
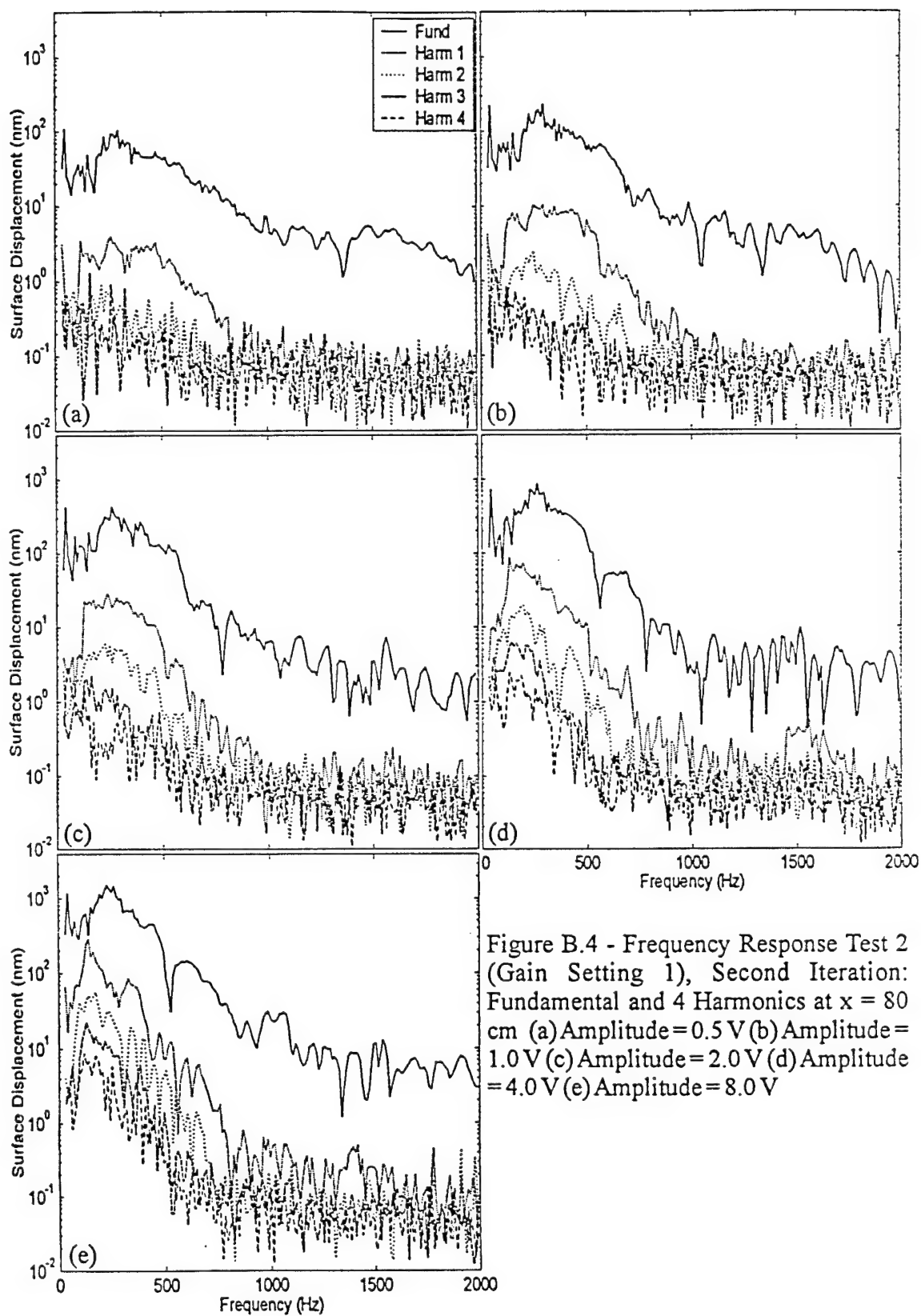
Figure B.4 - Frequency Response Test 2 (Gain Setting 1), Second Iteration: Fundamental and 4 Harmonics at x = 80 cm (a) Amplitude = 0.5 V (b) Amplitude = 1.0 V (c) Amplitude = 2.0 V (d) Amplitude = 4.0 V (e) Amplitude = 8.0 V
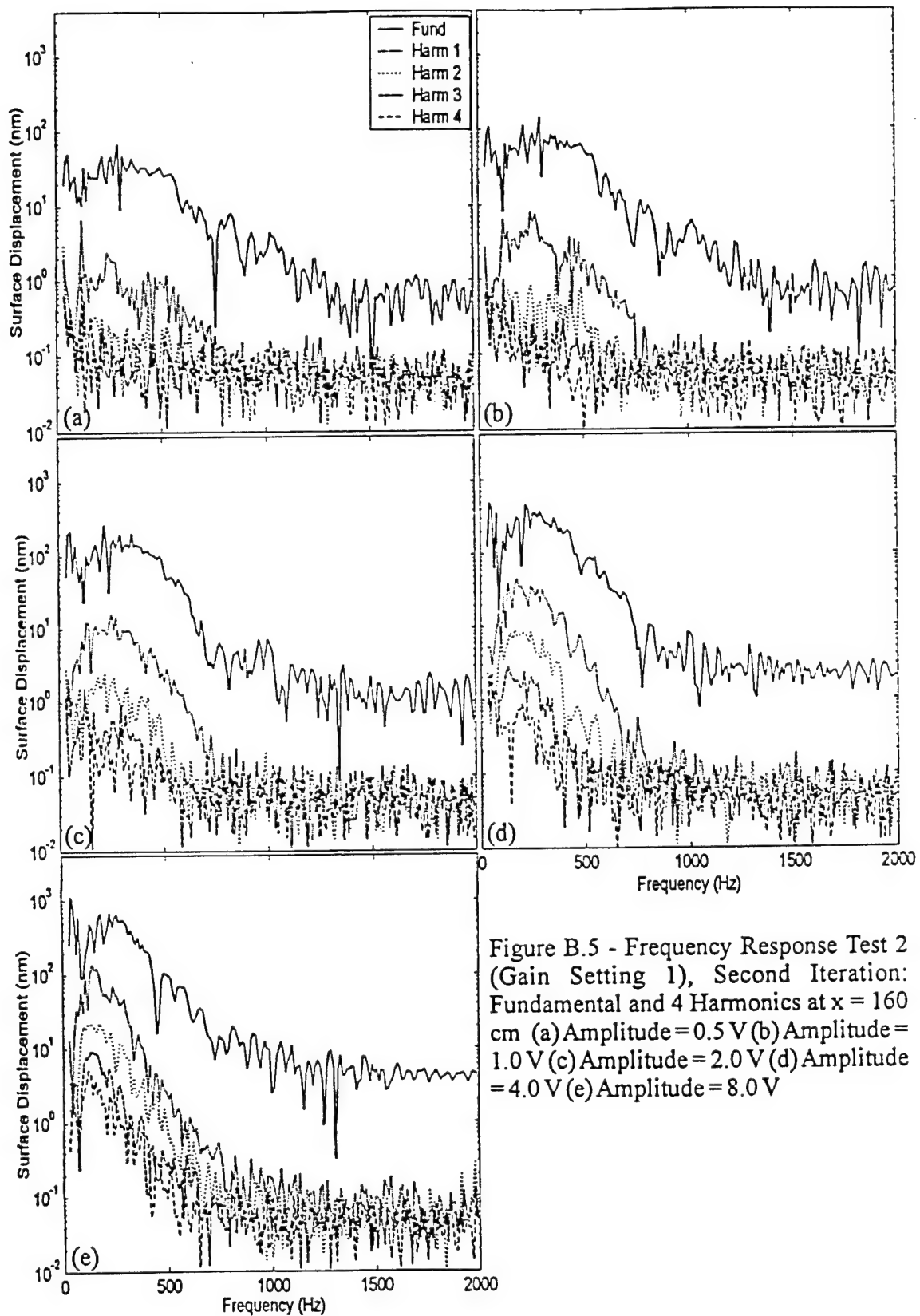
Figure B.5 - Frequency Response Test 2 (Gain Setting 1), Second Iteration: Fundamental and 4 Harmonics at x = 160 cm (a) Amplitude = 0.5 V (b) Amplitude = 1.0 V (c) Amplitude = 2.0 V (d) Amplitude = 4.0 V (e) Amplitude = 8.0 V

117

APPENDIX C

ADDITIONAL AMPLITUDE RESPONSE GRAPHS

This appendix contains a complete set of data for one of the amplitude response measurements. The five figures come from the second iteration of the fifth amplitude response test. This data was taken on Gain Setting 1. Figure C.1 shows four harmonics normalized by the fundamental at $x = 10$ cm. The five graphs ((a) – (e)) are the data taken for 99 Hz, 198 Hz, 396 Hz, 792 Hz, and 1584 Hz respectively. Figures C.2 through C.5 show the same information for $x = 20$ cm, 40 cm, 80 cm, and 160 cm respectively.
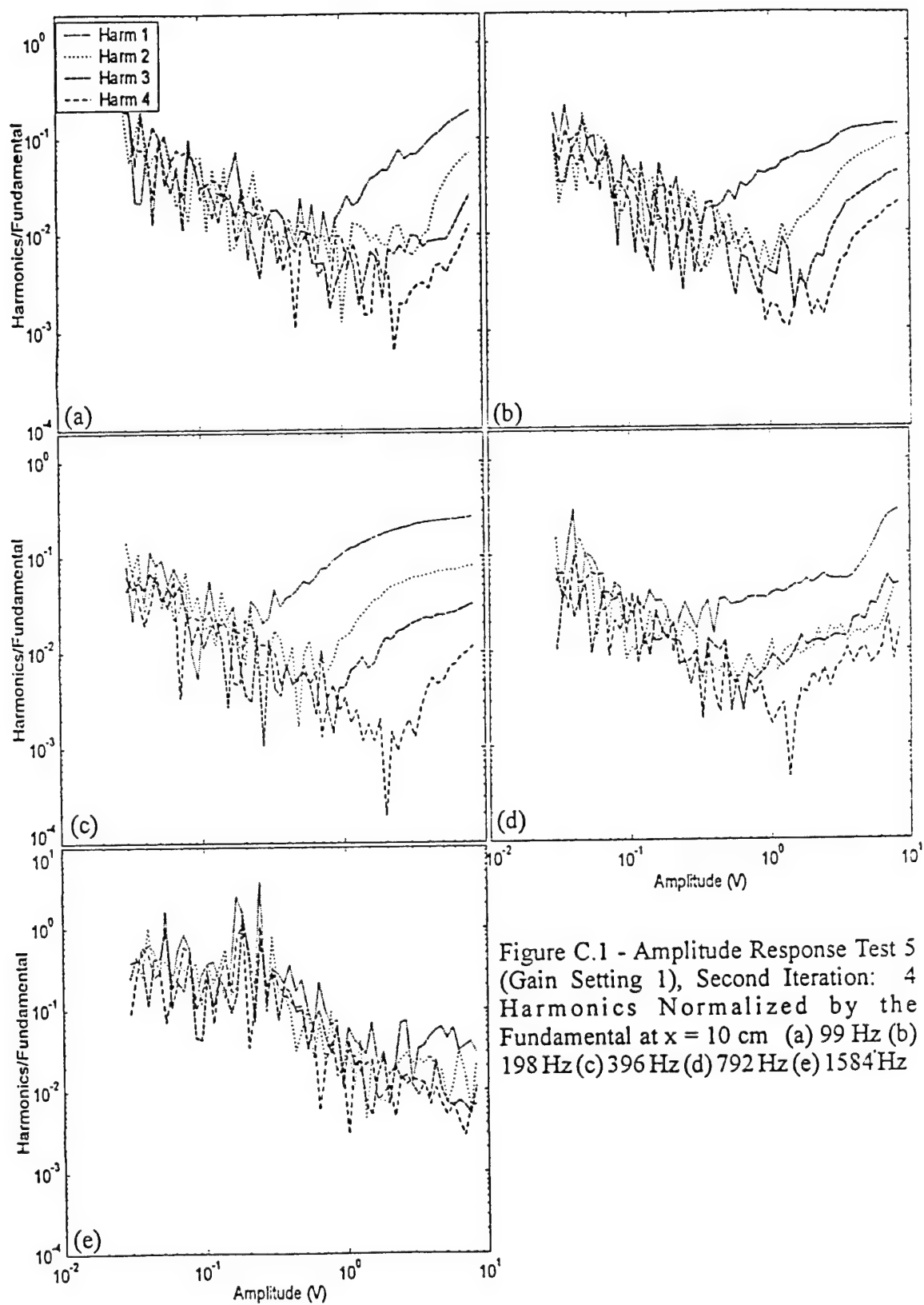
Figure C.1 - Amplitude Response Test 5 (Gain Setting 1), Second Iteration: 4 Harmonics Normalized by the Fundamental at x = 10 cm (a) 99 Hz (b) 198 Hz (c) 396 Hz (d) 792 Hz (e) 1584 Hz
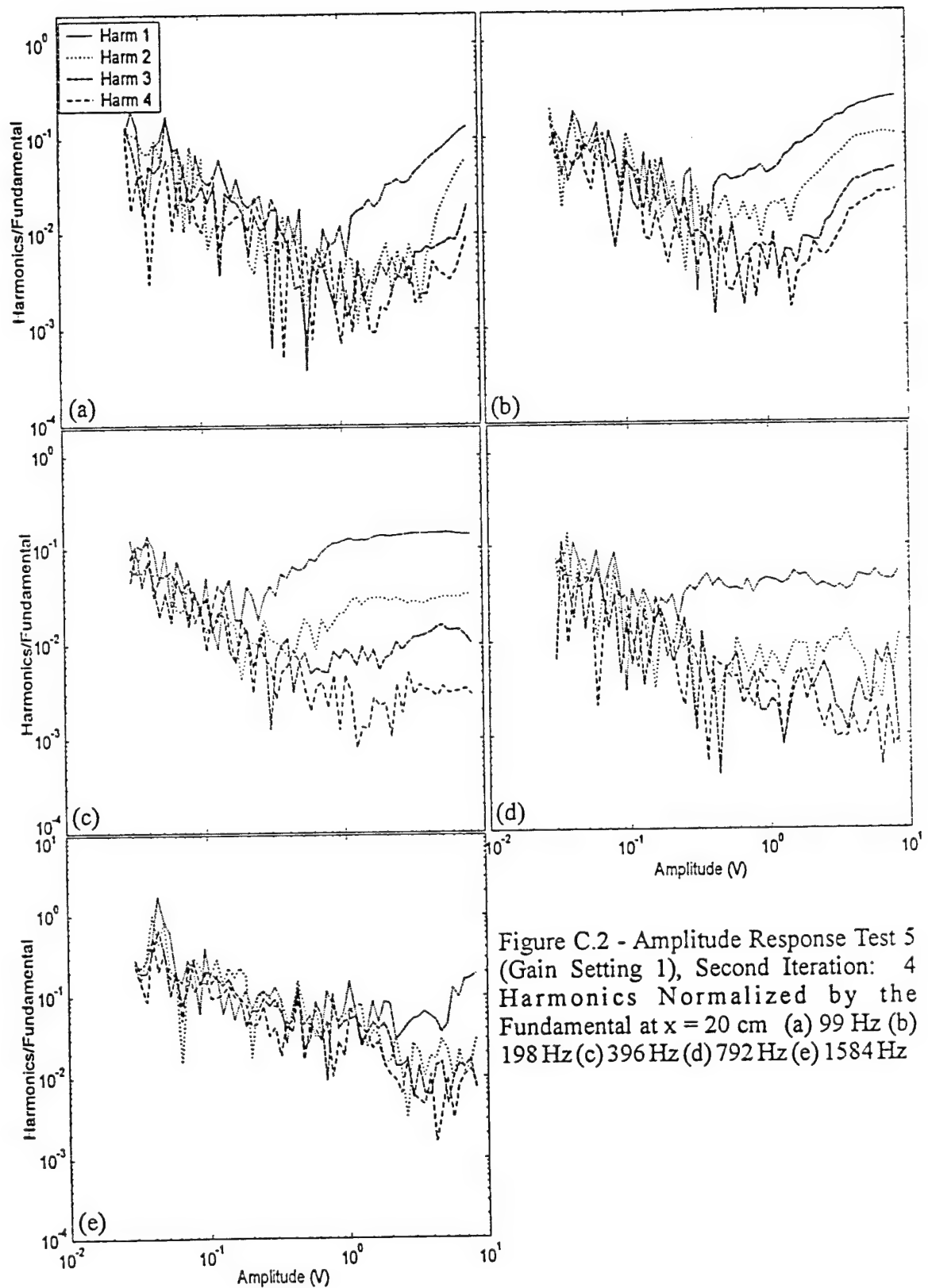
Figure C.2 - Amplitude Response Test 5 (Gain Setting 1), Second Iteration: 4 Harmonics Normalized by the Fundamental at x = 20 cm (a) 99 Hz (b) 198 Hz (c) 396 Hz (d) 792 Hz (e) 1584 Hz

Figure C.3 - Amplitude Response Test 5 (Gain Setting 1), Second Iteration: 4 Harmonics Normalized by the Fundamental at x = 40 cm (a) 99 Hz (b) 198 Hz (c) 396 Hz (d) 792 Hz (e) 1584 Hz
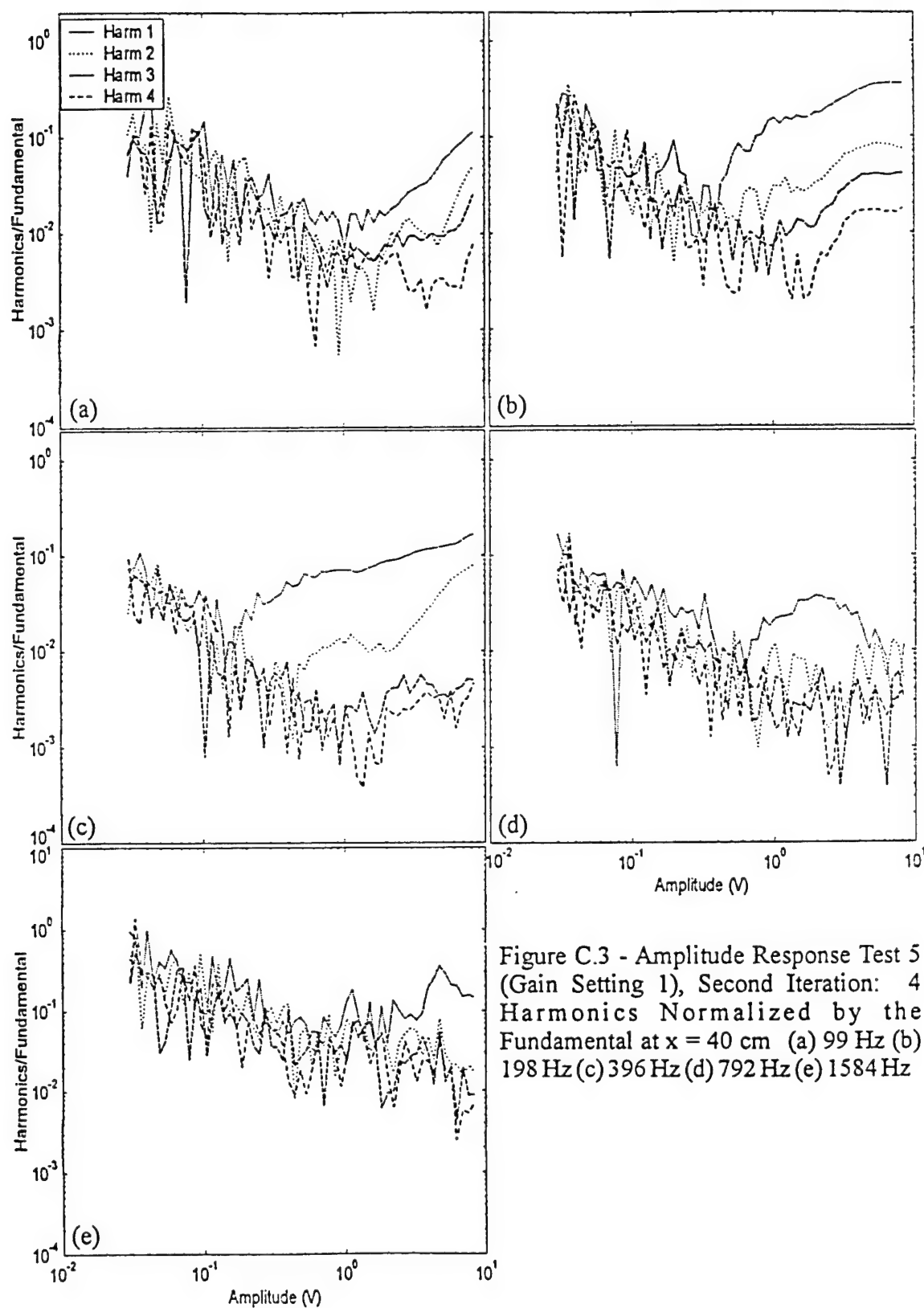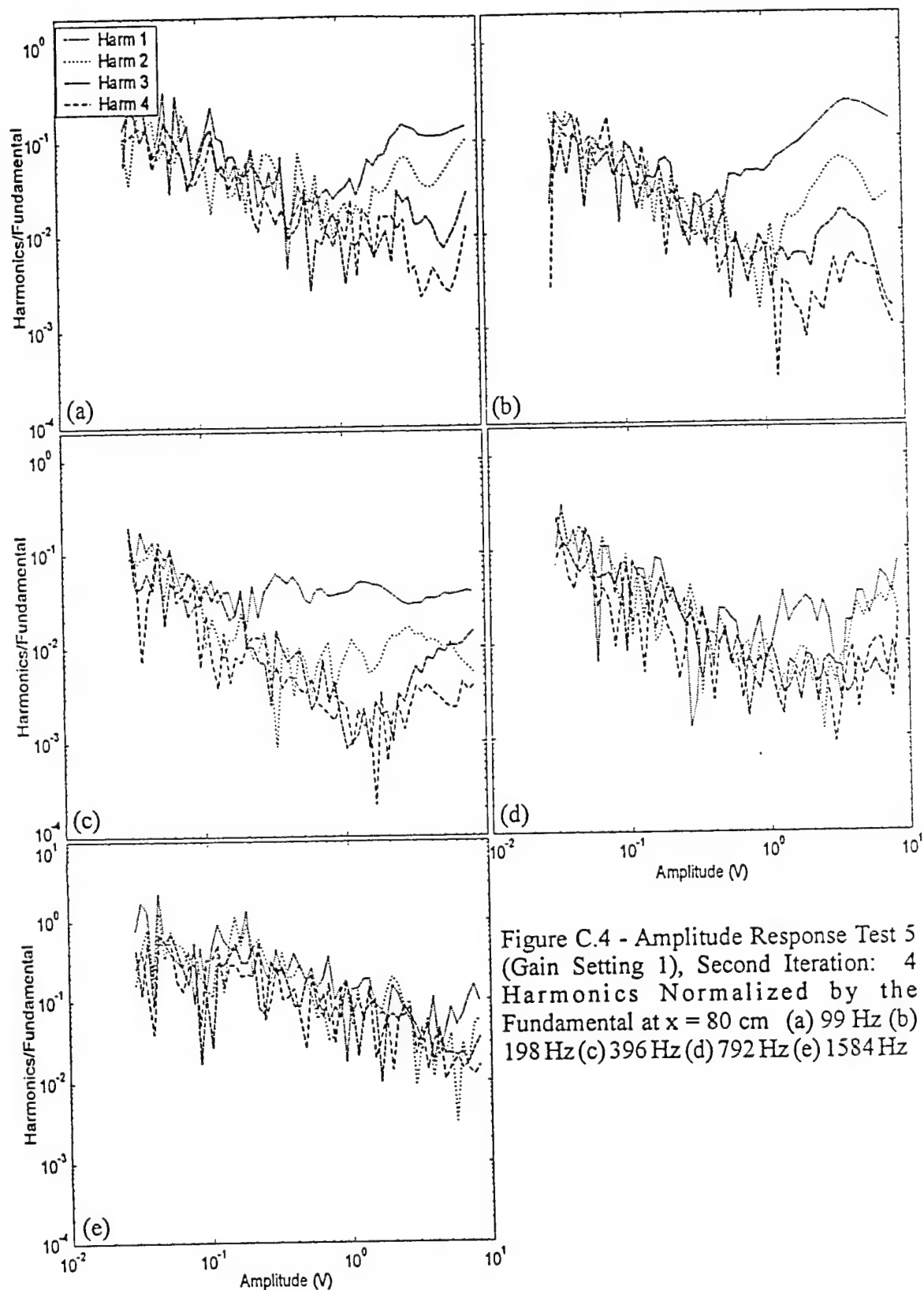
Figure C.4 - Amplitude Response Test 5 (Gain Setting 1), Second Iteration: 4 Harmonics Normalized by the Fundamental at x = 80 cm (a) 99 Hz (b) 198 Hz (c) 396 Hz (d) 792 Hz (e) 1584 Hz
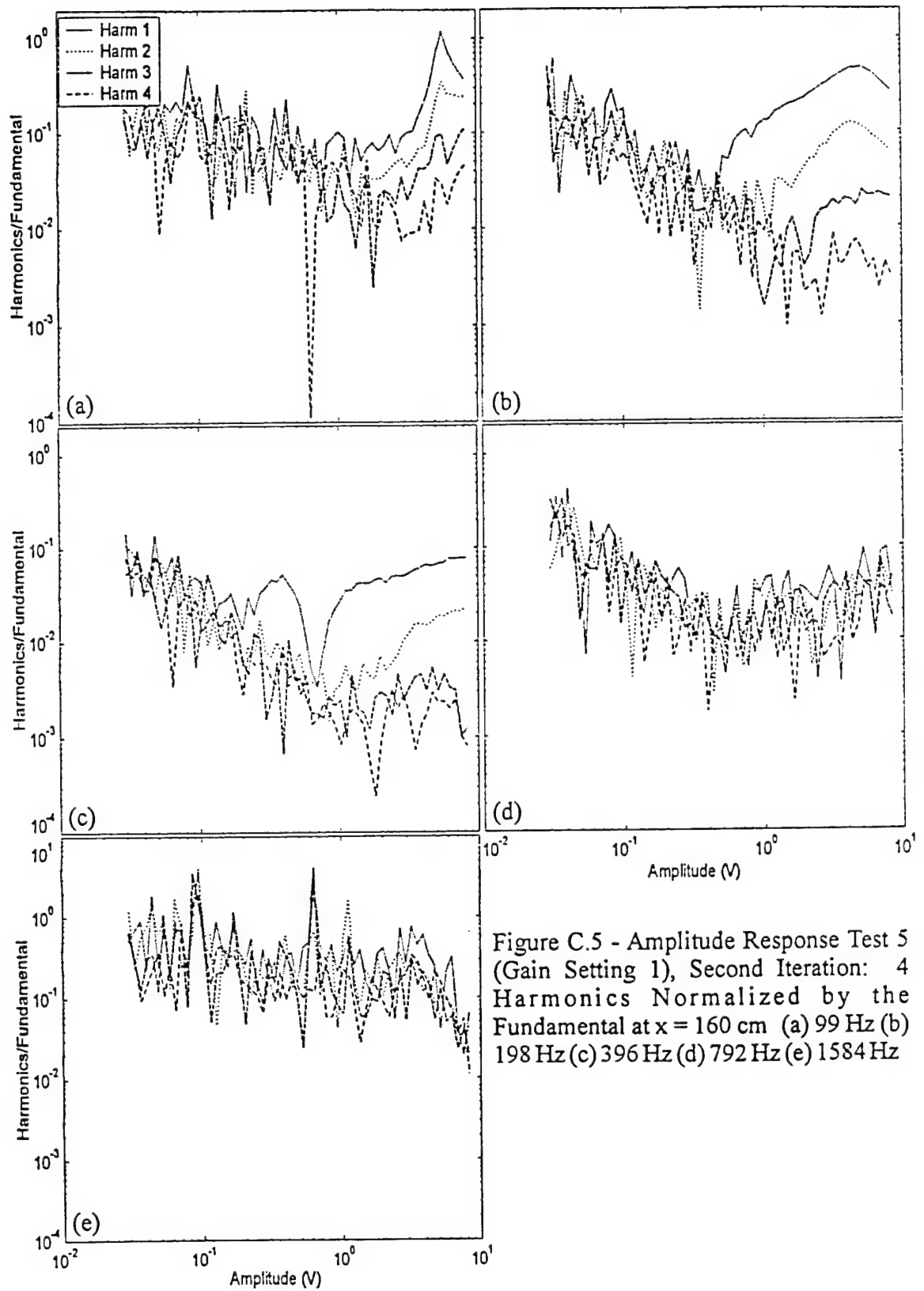
Figure C.5 - Amplitude Response Test 5 (Gain Setting 1), Second Iteration: 4 Harmonics Normalized by the Fundamental at x = 160 cm (a) 99 Hz (b) 198 Hz (c) 396 Hz (d) 792 Hz (e) 1584 Hz

APPENDIX D

MATLAB CODE

This appendix contains some of the MATLAB code used to process the data during Experiment Two. Program 1 is an example of how the LabVIEW files were read into MATLAB for the frequency response graphs and how they were broken into subgroups and saved as *.mat files. Program 2 is an example of how the saved *.mat files were used to plot five different positions on a graph of displacement versus frequency for a given amplitude. Program 3 is an example of how plots were generated of displacement versus frequency for the fundamental and five harmonics at a given position and amplitude.

In addition to the program examples contained in this appendix, programs were written to plot five different amplitudes on a graph of displacement versus frequency for a given position, plot the fundamental (with or without a comparison to a second experiment) at a given position and amplitude, plot the fundamental and harmonics normalized by the drive signal at a given position and amplitude, and plot the harmonics normalized by the fundamental at a given position and amplitude. The same types of programs were written to process the accelerometer data. All of these above mentioned programs were written for four different frequency response data sets. Similar programs were also written for the amplitude response data.

% This program takes a transfer function measurement and breaks all of the data into five
% matrices (amplitude groups) for the six .bin files saved.

% FIRST TRANSFUN MEASUREMENT

clear all

```
% Open and read files
pathname=strcat('c:\blace\datafiles\F20000126-145314\');
fileF=strcat(pathname,'parameters.bin');
fileG=strcat(pathname,'fund_harm.bin');
fileH=strcat(pathname,'noise.bin');
fileJ=strcat(pathname,'accel_A.bin');
fileK=strcat(pathname,'accel_B.bin');
fileL=strcat(pathname,'accel_noise.bin');
fidF=fopen(fileF,'r','ieee-be');
fidG=fopen(fileG,'r','ieee-be');
fidH=fopen(fileH,'r','ieee-be');
fidJ=fopen(fileJ,'r','ieee-be');
fidK=fopen(fileK,'r','ieee-be');
fidL=fopen(fileL,'r','ieee-be');
F=fread(fidF,'float32');
G=fread(fidG,'float32');
H=fread(fidH,'float32');
J=fread(fidJ,'float32');
K=fread(fidK,'float32');
L=fread(fidL,'float32');
```

```
% Initialize matrices
parameters0_5(1:5400,1)=0;
parameters1_0(1:5400,1)=0;
parameters2_0(1:5400,1)=0;
parameters4_0(1:5400,1)=0;
parameters8_0(1:5400,1)=0;
fund_harm0_5(1:21600,1)=0;
fund_harm1_0(1:21600,1)=0;
fund_harm2_0(1:21600,1)=0;
fund_harm4_0(1:21600,1)=0;
fund_harm8_0(1:21600,1)=0;
noise0_5(1:10800,1)=0;
noise1_0(1:10800,1)=0;
noise2_0(1:10800,1)=0;
noise4_0(1:10800,1)=0;
noise8_0(1:10800,1)=0;
accel_A0_5(1:10800,1)=0;
accel_A1_0(1:10800,1)=0;
accel_A2_0(1:10800,1)=0;
accel_A4_0(1:10800,1)=0;
accel_A8_0(1:10800,1)=0;
accel_B0_5(1:10800,1)=0;
accel_B1_0(1:10800,1)=0;
accel_B2_0(1:10800,1)=0;
accel_B4_0(1:10800,1)=0;
accel_B8_0(1:10800,1)=0;
accel_noise0_5(1:10800,1)=0;
accel_noise1_0(1:10800,1)=0;
accel_noise2_0(1:10800,1)=0;
accel_noise4_0(1:10800,1)=0;
accel_noise8_0(1:10800,1)=0;
```

```
% Load matrices by amplitude
parameters0_5(1:1080,1)=F(1:1080,1);            %x=10
parameters0_5(1081:2160,1)=F(5401:6480,1);      %x=20
```

125

```
parameters0_5(2161:3240,1)=F(10801:11880,1);        %x=40
parameters0_5(3241:4320,1)=F(16201:17280,1);        %x=80
parameters0_5(4321:5400,1)=F(21601:22680,1);        %x=160
parameters1_0(1:1080,1)=F(1081:2160,1);             %x=10
parameters1_0(1081:2160,1)=F(6481:7560,1);          %x=20
parameters1_0(2161:3240,1)=F(11881:12960,1);        %x=40
parameters1_0(3241:4320,1)=F(17281:18360,1);        %x=80
parameters1_0(4321:5400,1)=F(22681:23760,1);        %x=160
parameters2_0(1:1080,1)=F(2161:3240,1);             %x=10
parameters2_0(1081:2160,1)=F(7561:8640,1);          %x=20
parameters2_0(2161:3240,1)=F(12961:14040,1);        %x=40
parameters2_0(3241:4320,1)=F(18361:19440,1);        %x=80
parameters2_0(4321:5400,1)=F(23761:24840,1);        %x=160
parameters4_0(1:1080,1)=F(3241:4320,1);             %x=10
parameters4_0(1081:2160,1)=F(8641:9720,1);          %x=20
parameters4_0(2161:3240,1)=F(14041:15120,1);        %x=40
parameters4_0(3241:4320,1)=F(19441:20520,1);        %x=80
parameters4_0(4321:5400,1)=F(24841:25920,1);        %x=160
parameters8_0(1:1080,1)=F(4321:5400,1);             %x=10
parameters8_0(1081:2160,1)=F(9721:10800,1);         %x=20
parameters8_0(2161:3240,1)=F(15121:16200,1);        %x=40
parameters8_0(3241:4320,1)=F(20521:21600,1);        %x=80
parameters8_0(4321:5400,1)=F(25921:27000,1);        %x=160
fund_harm0_5(1:4320,1)=G(1:4320,1);                 %x=10
fund_harm0_5(4321:8640,1)=G(21601:25920,1);         %x=20
fund_harm0_5(8641:12960,1)=G(43201:47520,1);        %x=40
fund_harm0_5(12961:17280,1)=G(64801:69120,1);       %x=80
fund_harm0_5(17281:21600,1)=G(86401:90720,1);       %x=160
fund_harm1_0(1:4320,1)=G(4321:8640,1);              %x=10
fund_harm1_0(4321:8640,1)=G(25921:30240,1);         %x=20
fund_harm1_0(8641:12960,1)=G(47521:51840,1);        %x=40
fund_harm1_0(12961:17280,1)=G(69121:73440,1);       %x=80
fund_harm1_0(17281:21600,1)=G(90721:95040,1);       %x=160
fund_harm2_0(1:4320,1)=G(8641:12960,1);             %x=10
fund_harm2_0(4321:8640,1)=G(30241:34560,1);         %x=20
fund_harm2_0(8641:12960,1)=G(51841:56160,1);        %x=40
fund_harm2_0(12961:17280,1)=G(73441:77760,1);       %x=80
fund_harm2_0(17281:21600,1)=G(95041:99360,1);       %x=160
fund_harm4_0(1:4320,1)=G(12961:17280,1);            %x=10
fund_harm4_0(4321:8640,1)=G(34561:38880,1);         %x=20
fund_harm4_0(8641:12960,1)=G(56161:60480,1);        %x=40
fund_harm4_0(12961:17280,1)=G(77761:82080,1);       %x=80
fund_harm4_0(17281:21600,1)=G(99361:103680,1);      %x=160
fund_harm8_0(1:4320,1)=G(17281:21600,1);            %x=10
fund_harm8_0(4321:8640,1)=G(38881:43200,1);         %x=20
fund_harm8_0(8641:12960,1)=G(60481:64800,1);        %x=40
fund_harm8_0(12961:17280,1)=G(82081:86400,1);       %x=80
fund_harm8_0(17281:21600,1)=G(103681:108000,1);     %x=160
noise0_5(1:2160,1)=H(1:2160,1);                     %x=10
noise0_5(2161:4320,1)=H(10801:12960,1);             %x=20
noise0_5(4321:6480,1)=H(21601:23760,1);             %x=40
noise0_5(6481:8640,1)=H(32401:34560,1);             %x=80
noise0_5(8641:10800,1)=H(43201:45360,1);            %x=160
noise1_0(1:2160,1)=H(2161:4320,1);                  %x=10
noise1_0(2161:4320,1)=H(12961:15120,1);             %x=20
noise1_0(4321:6480,1)=H(23761:25920,1);             %x=40
noise1_0(6481:8640,1)=H(34561:36720,1);             %x=80
noise1_0(8641:10800,1)=H(45361:47520,1);            %x=160
noise2_0(1:2160,1)=H(4321:6480,1);                  %x=10
noise2_0(2161:4320,1)=H(15121:17280,1);             %x=20
noise2_0(4321:6480,1)=H(25921:28080,1);             %x=40
noise2_0(6481:8640,1)=H(36721:38880,1);             %x=80
noise2_0(8641:10800,1)=H(47521:49680,1);            %x=160
noise4_0(1:2160,1)=H(6481:8640,1);                  %x=10
noise4_0(2161:4320,1)=H(17281:19440,1);             %x=20
noise4_0(4321:6480,1)=H(28081:30240,1);             %x=40
```

126

```
noise4_0(6481:8640,1)=H(38881:41040,1);          %x=80
noise4_0(8641:10800,1)=H(49681:51840,1);         %x=160
noise8_0(1:2160,1)=H(8641:10800,1);              %x=10
noise8_0(2161:4320,1)=H(19441:21600,1);          %x=20
noise8_0(4321:6480,1)=H(30241:32400,1);          %x=40
noise8_0(6481:8640,1)=H(41041:43200,1);          %x=80
noise8_0(8641:10800,1)=H(51841:54000,1);         %x=160
accel_A0_5(1:2160,1)=J(1:2160,1);                %x=10
accel_A0_5(2161:4320,1)=J(10801:12960,1);        %x=20
accel_A0_5(4321:6480,1)=J(21601:23760,1);        %x=40
accel_A0_5(6481:8640,1)=J(32401:34560,1);        %x=80
accel_A0_5(8641:10800,1)=J(43201:45360,1);       %x=160
accel_A1_0(1:2160,1)=J(2161:4320,1);             %x=10
accel_A1_0(2161:4320,1)=J(12961:15120,1);        %x=20
accel_A1_0(4321:6480,1)=J(23761:25920,1);        %x=40
accel_A1_0(6481:8640,1)=J(34561:36720,1);        %x=80
accel_A1_0(8641:10800,1)=J(45361:47520,1);       %x=160
accel_A2_0(1:2160,1)=J(4321:6480,1);             %x=10
accel_A2_0(2161:4320,1)=J(15121:17280,1);        %x=20
accel_A2_0(4321:6480,1)=J(25921:28080,1);        %x=40
accel_A2_0(6481:8640,1)=J(36721:38880,1);        %x=80
accel_A2_0(8641:10800,1)=J(47521:49680,1);       %x=160
accel_A4_0(1:2160,1)=J(6481:8640,1);             %x=10
accel_A4_0(2161:4320,1)=J(17281:19440,1);        %x=20
accel_A4_0(4321:6480,1)=J(28081:30240,1);        %x=40
accel_A4_0(6481:8640,1)=J(38881:41040,1);        %x=80
accel_A4_0(8641:10800,1)=J(49681:51840,1);       %x=160
accel_A8_0(1:2160,1)=J(8641:10800,1);            %x=10
accel_A8_0(2161:4320,1)=J(19441:21600,1);        %x=20
accel_A8_0(4321:6480,1)=J(30241:32400,1);        %x=40
accel_A8_0(6481:8640,1)=J(41041:43200,1);        %x=80
accel_A8_0(8641:10800,1)=J(51841:54000,1);       %x=160
accel_B0_5(1:2160,1)=H(1:2160,1);                %x=10
accel_B0_5(2161:4320,1)=K(10801:12960,1);        %x=20
accel_B0_5(4321:6480,1)=K(21601:23760,1);        %x=40
accel_B0_5(6481:8640,1)=K(32401:34560,1);        %x=80
accel_B0_5(8641:10800,1)=K(43201:45360,1);       %x=160
accel_B1_0(1:2160,1)=K(2161:4320,1);             %x=10
accel_B1_0(2161:4320,1)=K(12961:15120,1);        %x=20
accel_B1_0(4321:6480,1)=K(23761:25920,1);        %x=40
accel_B1_0(6481:8640,1)=K(34561:36720,1);        %x=80
accel_B1_0(8641:10800,1)=K(45361:47520,1);       %x=160
accel_B2_0(1:2160,1)=K(4321:6480,1);             %x=10
accel_B2_0(2161:4320,1)=K(15121:17280,1);        %x=20
accel_B2_0(4321:6480,1)=K(25921:28080,1);        %x=40
accel_B2_0(6481:8640,1)=K(36721:38880,1);        %x=80
accel_B2_0(8641:10800,1)=K(47521:49680,1);       %x=160
accel_B4_0(1:2160,1)=K(6481:8640,1);             %x=10
accel_B4_0(2161:4320,1)=K(17281:19440,1);        %x=20
accel_B4_0(4321:6480,1)=K(28081:30240,1);        %x=40
accel_B4_0(6481:8640,1)=K(38881:41040,1);        %x=80
accel_B4_0(8641:10800,1)=K(49681:51840,1);       %x=160
accel_B8_0(1:2160,1)=K(8641:10800,1);            %x=10
accel_B8_0(2161:4320,1)=K(19441:21600,1);        %x=20
accel_B8_0(4321:6480,1)=K(30241:32400,1);        %x=40
accel_B8_0(6481:8640,1)=K(41041:43200,1);        %x=80
accel_B8_0(8641:10800,1)=K(51841:54000,1);       %x=160
accel_noise0_5(1:2160,1)=L(1:2160,1);            %x=10
accel_noise0_5(2161:4320,1)=L(10801:12960,1);    %x=20
accel_noise0_5(4321:6480,1)=L(21601:23760,1);    %x=40
accel_noise0_5(6481:8640,1)=L(32401:34560,1);    %x=80
accel_noise0_5(8641:10800,1)=L(43201:45360,1);   %x=160
accel_noise1_0(1:2160,1)=L(2161:4320,1);         %x=10
accel_noise1_0(2161:4320,1)=L(12961:15120,1);    %x=20
accel_noise1_0(4321:6480,1)=L(23761:25920,1);    %x=40
accel_noise1_0(6481:8640,1)=L(34561:36720,1);    %x=80
```

```
accel_noise1_0(8641:10800,1)=L(45361:47520,1);      %x=160
accel_noise2_0(1:2160,1)=L(4321:6480,1);            %x=10
accel_noise2_0(2161:4320,1)=L(15121:17280,1);       %x=20
accel_noise2_0(4321:6480,1)=L(25921:28080,1);       %x=40
accel_noise2_0(6481:8640,1)=L(36721:38880,1);       %x=80
accel_noise2_0(8641:10800,1)=L(47521:49680,1);      %x=160
accel_noise4_0(1:2160,1)=L(6481:8640,1);            %x=10
accel_noise4_0(2161:4320,1)=L(17281:19440,1);       %x=20
accel_noise4_0(4321:6480,1)=L(28081:30240,1);       %x=40
accel_noise4_0(6481:8640,1)=L(38881:41040,1);       %x=80
accel_noise4_0(8641:10800,1)=L(49681:51840,1);      %x=160
accel_noise8_0(1:2160,1)=L(8641:10800,1);           %x=10
accel_noise8_0(2161:4320,1)=L(19441:21600,1);       %x=20
accel_noise8_0(4321:6480,1)=L(30241:32400,1);       %x=40
accel_noise8_0(6481:8640,1)=L(41041:43200,1);       %x=80
accel_noise8_0(8641:10800,1)=L(51841:54000,1);      %x=160

% Save matrices as .mat files
save parameters0_51 parameters0_5;
save parameters1_01 parameters1_0;
save parameters2_01 parameters2_0;
save parameters4_01 parameters4_0;
save parameters8_01 parameters8_0;
save fund_harm0_51 fund_harm0_5;
save fund_harm1_01 fund_harm1_0;
save fund_harm2_01 fund_harm2_0;
save fund_harm4_01 fund_harm4_0;
save fund_harm8_01 fund_harm8_0;
save noise0_51 noise0_5;
save noise1_01 noise1_0;
save noise2_01 noise2_0;
save noise4_01 noise4_0;
save noise8_01 noise8_0;
save accel_A0_51 accel_A0_5;
save accel_A1_01 accel_A1_0;
save accel_A2_01 accel_A2_0;
save accel_A4_01 accel_A4_0;
save accel_A8_01 accel_A8_0;
save accel_B0_51 accel_B0_5;
save accel_B1_01 accel_B1_0;
save accel_B2_01 accel_B2_0;
save accel_B4_01 accel_B4_0;
save accel_B8_01 accel_B8_0;
save accel_noise0_51 accel_noise0_5;
save accel_noise1_01 accel_noise1_0;
save accel_noise2_01 accel_noise2_0;
save accel_noise4_01 accel_noise4_0;
save accel_noise8_01 accel_noise8_0;
```

```
% This program will ask for an amplitude and call up the appropriate transfer function data.
% It will then plot the five different positions for that amplitude on the same graph.

displ_freq10_fund(1:180,1)=0;
displ_freq20_fund(1:180,1)=0;
displ_freq40_fund(1:180,1)=0;
displ_freq80_fund(1:180,1)=0;
displ_freq160_fund(1:180,1)=0;
freq10(1:180,1)=0;
freq20(1:180,1)=0;
freq40(1:180,1)=0;
freq80(1:180,1)=0;
freq160(1:180,1)=0;

if exist('iteration')==0
  iteration=input('1st or 2d iteration (type "1" or "2"): ','s');
end;
if iteration=='1'
  if exist('amplitude')==0
    amplitude=input('Amplitude (enter 3 char): ','s');
  end;
  if amplitude=='0.5'
    load parameters0_51;
    load fund_harm0_51;
    load noise0_51;
    load accel_A0_51;
    load accel_B0_51;
    load accel_noise0_51;
    % Combine real and imaginary parts of displ_freq
    %FUNDAMENTAL
    for loop2=0:179
    displ_freq10_fund((1+loop2),1)=fund_harm0_5((13+loop2*24),1)-i*fund_harm0_5((14+loop2*24),1);
    displ_freq20_fund((1+loop2),1)=fund_harm0_5((4333+loop2*24),1)-i*fund_harm0_5((4334+loop2*24),1);
    displ_freq40_fund((1+loop2),1)=fund_harm0_5((8653+loop2*24),1)-i*fund_harm0_5((8654+loop2*24),1);
    displ_freq80_fund((1+loop2),1)=fund_harm0_5((12973+loop2*24),1)-i*fund_harm0_5((12974+loop2*24),1);
    displ_freq160_fund((1+loop2),1)=fund_harm0_5((17293+loop2*24),1)-i*fund_harm0_5((17294+loop2*24),1);
    end
    % Write out frequencies recorded
    freq10(1:180,1)=parameters0_5((3:6:1080),1);
    freq20(1:180,1)=parameters0_5((1083:6:2160),1);
    freq40(1:180,1)=parameters0_5((2163:6:3240),1);
    freq80(1:180,1)=parameters0_5((3243:6:4320),1);
    freq160(1:180,1)=parameters0_5((4323:6:5400),1);
  elseif amplitude=='1.0'
    load parameters1_01;
    load fund_harm1_01;
    load noise1_01;
    load accel_A1_01;
    load accel_B1_01;
    load accel_noise1_01;
    % Combine real and imaginary parts of displ_freq
    %FUNDAMENTAL
    for loop2=0:179
    displ_freq10_fund((1+loop2),1)=fund_harm1_0((13+loop2*24),1)+i*fund_harm1_0((14+loop2*24),1);
    displ_freq20_fund((1+loop2),1)=fund_harm1_0((4333+loop2*24),1)+i*fund_harm1_0((4334+loop2*24),1);
    displ_freq40_fund((1+loop2),1)=fund_harm1_0((8653+loop2*24),1)+i*fund_harm1_0((8654+loop2*24),1);
    displ_freq80_fund((1+loop2),1)=fund_harm1_0((12973+loop2*24),1)+i*fund_harm1_0((12974+loop2*24),1);
    displ_freq160_fund((1+loop2),1)=fund_harm1_0((17293+loop2*24),1)+i*fund_harm1_0((17294+loop2*24),1);
    end
    % Write out amplitudes recorded
    freq10(1:180,1)=parameters1_0((3:6:1080),1);
    freq20(1:180,1)=parameters1_0((1083:6:2160),1);
    freq40(1:180,1)=parameters1_0((2163:6:3240),1);
    freq80(1:180,1)=parameters1_0((3243:6:4320),1);
    freq160(1:180,1)=parameters1_0((4323:6:5400),1);
  elseif amplitude=='2.0'
    load parameters2_01;
```

```
        load fund_harm2_01;
        load noise2_01;
        load accel_A2_01;
        load accel_B2_01;
        load accel_noise2_01;
        % Combine real and imaginary parts of displ_freq
        %FUNDAMENTAL
        for loop2=0:179
        displ_freq10_fund((1+loop2),1)=fund_harm2_0((13+loop2*24),1)+i*fund_harm2_0((14+loop2*24),1);
        displ_freq20_fund((1+loop2),1)=fund_harm2_0((4333+loop2*24),1)+i*fund_harm2_0((4334+loop2*24),1);
        displ_freq40_fund((1+loop2),1)=fund_harm2_0((8653+loop2*24),1)+i*fund_harm2_0((8654+loop2*24),1);
        displ_freq80_fund((1+loop2),1)=fund_harm2_0((12973+loop2*24),1)+i*fund_harm2_0((12974+loop2*24),1);
        displ_freq160_fund((1+loop2),1)=fund_harm2_0((17293+loop2*24),1)+i*fund_harm2_0((17294+loop2*24),1);
        end
        % Write out amplitudes recorded
        freq10(1:180,1)=parameters2_0((3:6:1080),1);
        freq20(1:180,1)=parameters2_0((1083:6:2160),1);
        freq40(1:180,1)=parameters2_0((2163:6:3240),1);
        freq80(1:180,1)=parameters2_0((3243:6:4320),1);
        freq160(1:180,1)=parameters2_0((4323:6:5400),1);
elseif amplitude=='4.0'
        load parameters4_01;
        load fund_harm4_01;
        load noise4_01;
        load accel_A4_01;
        load accel_B4_01;
        load accel_noise4_01;
        % Combine real and imaginary parts of displ_freq
        %FUNDAMENTAL
        for loop2=0:179
        displ_freq10_fund((1+loop2),1)=fund_harm4_0((13+loop2*24),1)+i*fund_harm4_0((14+loop2*24),1);
        displ_freq20_fund((1+loop2),1)=fund_harm4_0((4333+loop2*24),1)+i*fund_harm4_0((4334+loop2*24),1);
        displ_freq40_fund((1+loop2),1)=fund_harm4_0((8653+loop2*24),1)+i*fund_harm4_0((8654+loop2*24),1);
        displ_freq80_fund((1+loop2),1)=fund_harm4_0((12973+loop2*24),1)+i*fund_harm4_0((12974+loop2*24),1);
        displ_freq160_fund((1+loop2),1)=fund_harm4_0((17293+loop2*24),1)+i*fund_harm4_0((17294+loop2*24),1);
        end
        % Write out amplitudes recorded
        freq10(1:180,1)=parameters4_0((3:6:1080),1);
        freq20(1:180,1)=parameters4_0((1083:6:2160),1);
        freq40(1:180,1)=parameters4_0((2163:6:3240),1);
        freq80(1:180,1)=parameters4_0((3243:6:4320),1);
        freq160(1:180,1)=parameters4_0((4323:6:5400),1);
    elseif amplitude=='8.0'
        load parameters8_01;
        load fund_harm8_01;
        load noise8_01;
        load accel_A8_01;
        load accel_B8_01;
        load accel_noise8_01;
        % Combine real and imaginary parts of displ_freq
        %FUNDAMENTAL
        for loop2=0:179
        displ_freq10_fund((1+loop2),1)=fund_harm8_0((13+loop2*24),1)+i*fund_harm8_0((14+loop2*24),1);
        displ_freq20_fund((1+loop2),1)=fund_harm8_0((4333+loop2*24),1)+i*fund_harm8_0((4334+loop2*24),1);
        displ_freq40_fund((1+loop2),1)=fund_harm8_0((8653+loop2*24),1)+i*fund_harm8_0((8654+loop2*24),1);
        displ_freq80_fund((1+loop2),1)=fund_harm8_0((12973+loop2*24),1)+i*fund_harm8_0((12974+loop2*24),1);
        displ_freq160_fund((1+loop2),1)=fund_harm8_0((17293+loop2*24),1)+i*fund_harm8_0((17294+loop2*24),1);
        end
        % Write out amplitudes recorded
        freq10(1:180,1)=parameters8_0((3:6:1080),1);
        freq20(1:180,1)=parameters8_0((1083:6:2160),1);
        freq40(1:180,1)=parameters8_0((2163:6:3240),1);
        freq80(1:180,1)=parameters8_0((3243:6:4320),1);
        freq160(1:180,1)=parameters8_0((4323:6:5400),1);
    end;

elseif iteration=='2'
        if exist('amplitude')==0
            amplitude=input('Amplitude (enter 3 char): ','s');
        end;
```

130

```matlab
    if amplitude=='0.5'
    load parameters0_52;
    load fund_harm0_52;
    load noise0_52;
    load accel_A0_52;
    load accel_B0_52;
    load accel_noise0_52;
    % Combine real and imaginary parts of displ_freq
    %FUNDAMENTAL
    for loop2=0:179
    displ_freq10_fund((1+loop2),1)=fund_harm0_5((13+loop2*24),1)+i*fund_harm0_5((14+loop2*24),1);
    displ_freq20_fund((1+loop2),1)=fund_harm0_5((4333+loop2*24),1)+i*fund_harm0_5((4334+loop2*24),1);
    displ_freq40_fund((1+loop2),1)=fund_harm0_5((8653+loop2*24),1)+i*fund_harm0_5((8654+loop2*24),1);
    displ_freq80_fund((1+loop2),1)=fund_harm0_5((12973+loop2*24),1)+i*fund_harm0_5((12974+loop2*24),1);
    displ_freq160_fund((1+loop2),1)=fund_harm0_5((17293+loop2*24),1)+i*fund_harm0_5((17294+loop2*24),1);
    end
    % Write out frequencies recorded
    freq10(1:180,1)=parameters0_5((3:6:1080),1);
    freq20(1:180,1)=parameters0_5((1083:6:2160),1);
    freq40(1:180,1)=parameters0_5((2163:6:3240),1);
    freq80(1:180,1)=parameters0_5((3243:6:4320),1);
    freq160(1:180,1)=parameters0_5((4323:6:5400),1);
elseif amplitude=='1.0'
    load parameters1_02;
    load fund_harm1_02;
    load noise1_02;
    load accel_A1_02;
    load accel_B1_02;
    load accel_noise1_02;
    % Combine real and imaginary parts of displ_freq
    %FUNDAMENTAL
    for loop2=0:179
    displ_freq10_fund((1+loop2),1)=fund_harm1_0((13+loop2*24),1)+i*fund_harm1_0((14+loop2*24),1);
    displ_freq20_fund((1+loop2),1)=fund_harm1_0((4333+loop2*24),1)-i*fund_harm1_0((4334+loop2*24),1);
    displ_freq40_fund((1+loop2),1)=fund_harm1_0((8653+loop2*24),1)+i*fund_harm1_0((8654+loop2*24),1);
    displ_freq80_fund((1+loop2),1)=fund_harm1_0((12973+loop2*24),1)+i*fund_harm1_0((12974-loop2*24),1);
    displ_freq160_fund((1+loop2),1)=fund_harm1_0((17293-loop2*24),1)-i*fund_harm1_0((17294+loop2*24),1);
    end
    % Write out amplitudes recorded
    freq10(1:180,1)=parameters1_0((3:6:1080),1);
    freq20(1:180,1)=parameters1_0((1083:6:2160),1);
    freq40(1:180,1)=parameters1_0((2163:6:3240),1);
    freq80(1:180,1)=parameters1_0((3243:6:4320),1);
    freq160(1:180,1)=parameters1_0((4323:6:5400),1);
elseif amplitude=='2.0'
    load parameters2_02;
    load fund_harm2_02;
    load noise2_02;
    load accel_A2_02;
    load accel_B2_02;
    load accel_noise2_02;
    % Combine real and imaginary parts of displ_freq
    %FUNDAMENTAL
    for loop2=0:179
    displ_freq10_fund((1+loop2),1)=fund_harm2_0((13+loop2*24),1)+i*fund_harm2_0((14+loop2*24),1);
    displ_freq20_fund((1+loop2),1)=fund_harm2_0((4333+loop2*24),1)+i*fund_harm2_0((4334+loop2*24),1);
    displ_freq40_fund((1+loop2),1)=fund_harm2_0((8653+loop2*24),1)+i*fund_harm2_0((8654+loop2*24),1);
    displ_freq80_fund((1+loop2),1)=fund_harm2_0((12973+loop2*24),1)+i*fund_harm2_0((12974+loop2*24),1);
    displ_freq160_fund((1+loop2),1)=fund_harm2_0((17293+loop2*24),1)+i*fund_harm2_0((17294+loop2*24),1);
    end
    % Write out amplitudes recorded
    freq10(1:180,1)=parameters2_0((3:6:1080),1);
    freq20(1:180,1)=parameters2_0((1083:6:2160),1);
    freq40(1:180,1)=parameters2_0((2163:6:3240),1);
    freq80(1:180,1)=parameters2_0((3243:6:4320),1);
    freq160(1:180,1)=parameters2_0((4323:6:5400),1);
elseif amplitude=='4.0'
    load parameters4_02;
    load fund_harm4_02;
    load noise4_02;
```

```matlab
    load accel_A4_02;
    load accel_B4_02;
    load accel_noise4_02;
    % Combine real and imaginary parts of displ_freq
    %FUNDAMENTAL
    for loop2=0:179
    displ_freq10_fund((1+loop2),1)=fund_harm4_0((13+loop2*24),1)+i*fund_harm4_0((14+loop2*24),1);
    displ_freq20_fund((1+loop2),1)=fund_harm4_0((4333+loop2*24),1)+i*fund_harm4_0((4334+loop2*24),1);
    displ_freq40_fund((1+loop2),1)=fund_harm4_0((8653+loop2*24),1)+i*fund_harm4_0((8654+loop2*24),1);
    displ_freq80_fund((1+loop2),1)=fund_harm4_0((12973+loop2*24),1)+i*fund_harm4_0((12974+loop2*24),1);
    displ_freq160_fund((1+loop2),1)=fund_harm4_0((17293+loop2*24),1)+i*fund_harm4_0((17294+loop2*24),1);
    end
    % Write out amplitudes recorded
    freq10(1:180,1)=parameters4_0((3:6:1080),1);
    freq20(1:180,1)=parameters4_0((1083:6:2160),1);
    freq40(1:180,1)=parameters4_0((2163:6:3240),1);
    freq80(1:180,1)=parameters4_0((3243:6:4320),1);
    freq160(1:180,1)=parameters4_0((4323:6:5400),1);
elseif amplitude=='8.0'
    load parameters8_02;
    load fund_harm8_02;
    load noise8_02;
    load accel_A8_02;
    load accel_B8_02;
    load accel_noise8_02;
    % Combine real and imaginary parts of displ_freq
    %FUNDAMENTAL
    for loop2=0:179
    displ_freq10_fund((1+loop2),1)=fund_harm8_0((13+loop2*24),1)+i*fund_harm8_0((14+loop2*24),1);
    displ_freq20_fund((1+loop2),1)=fund_harm8_0((4333+loop2*24),1)+i*fund_harm8_0((4334+loop2*24),1);
    displ_freq40_fund((1+loop2),1)=fund_harm8_0((8653+loop2*24),1)+i*fund_harm8_0((8654+loop2*24),1);
    displ_freq80_fund((1+loop2),1)=fund_harm8_0((12973+loop2*24),1)+i*fund_harm8_0((12974+loop2*24),1);
    displ_freq160_fund((1+loop2),1)=fund_harm8_0((17293+loop2*24),1)+i*fund_harm8_0((17294+loop2*24),1);
    end
    % Write out amplitudes recorded
    freq10(1:180,1)=parameters8_0((3:6:1080),1);
    freq20(1:180,1)=parameters8_0((1083:6:2160),1);
    freq40(1:180,1)=parameters8_0((2163:6:3240),1);
    freq80(1:180,1)=parameters8_0((3243:6:4320),1);
    freq160(1:180,1)=parameters8_0((4323:6:5400),1);
  end;
end;

% Plot results
figure(1)
semilogy(freq10,abs(displ_freq10_fund),'-')
hold on
semilogy(freq20,abs(displ_freq20_fund),'--')
semilogy(freq40,abs(displ_freq40_fund),'-.')
semilogy(freq80,abs(displ_freq80_fund),':')
semilogy(freq160,abs(displ_freq160_fund),'-')
title1='Displacement vs Frequency';
title2=' Amplitude = ';
title2=strcat(title2,amplitude,'Volts');
title3=' Iteration = ';
title3=strcat(title3,iteration);
title_data=char({title1,title2,title3});
title(title_data);
ylabel('Displacement')
xlabel('Frequency (Hz)')
legend('10 cm','20 cm','40 cm','80 cm','160 cm')
hold off
orient landscape

figure(2)
plot(freq10,abs(displ_freq10_fund),'-')
hold on
plot(freq20,abs(displ_freq20_fund),'--')
plot(freq40,abs(displ_freq40_fund),'-.')
plot(freq80,abs(displ_freq80_fund),':')
```

```
plot(freq160,abs(displ_freq160_fund),'-')
title1='Displacement vs Frequency';
title2=' Amplitude = ';
title2=strcat(title2,amplitude,'Volts');
title3=' Iteration = ';
title3=strcat(title3,iteration);
title_data=char({title1,title2,title3});
title(title_data);
ylabel('Displacement')
xlabel('Frequency (Hz)')
legend('10 cm','20 cm','40 cm','80 cm','160 cm')
hold off
orient landscape

figure(3)
loglog(freq10,abs(displ_freq10_fund),'-')
hold on
loglog (freq20,abs(displ_freq20_fund),'--')
loglog (freq40,abs(displ_freq40_fund),'-.')
loglog (freq80,abs(displ_freq80_fund),':')
loglog (freq160,abs(displ_freq160_fund),'-')
title1='Displacement vs Frequency';
title2=' Amplitude = ';
title2=strcat(title2,amplitude,'Volts');
title3=' Iteration = ';
title3=strcat(title3,iteration);
title_data=char({title1,title2,title3});
title(title_data);
ylabel('Displacement')
xlabel('Frequency (Hz)')
legend('10 cm','20 cm','40 cm','80 cm','160 cm')
hold off
orient landscape
```

133

```
% This program will ask for an amplitude and a position and call up the appropriate
% transfer function data. It will then plot the transfer function for that location
% and amplitude showing the fundamental and five harmonics on the same graph.

% Initialize matrices
displ_freq10_fund(1:180,1)=0;
displ_freq20_fund(1:180,1)=0;
displ_freq40_fund(1:180,1)=0;
displ_freq80_fund(1:180,1)=0;
displ_freq160_fund(1:180,1)=0;
displ_freq10_harm1(1:180,1)=0;
displ_freq20_harm1(1:180,1)=0;
displ_freq40_harm1(1:180,1)=0;
displ_freq80_harm1(1:180,1)=0;
displ_freq160_harm1(1:180,1)=0;
displ_freq10_harm2(1:180,1)=0;
displ_freq20_harm2(1:180,1)=0;
displ_freq40_harm2(1:180,1)=0;
displ_freq80_harm2(1:180,1)=0;
displ_freq160_harm2(1:180,1)=0;
displ_freq10_harm3(1:180,1)=0;
displ_freq20_harm3(1:180,1)=0;
displ_freq40_harm3(1:180,1)=0;
displ_freq80_harm3(1:180,1)=0;
displ_freq160_harm3(1:180,1)=0;
displ_freq10_harm4(1:180,1)=0;
displ_freq20_harm4(1:180,1)=0;
displ_freq40_harm4(1:180,1)=0;
displ_freq80_harm4(1:180,1)=0;
displ_freq160_harm4(1:180,1)=0;
displ_freq10_harm5(1:180,1)=0;
displ_freq20_harm5(1:180,1)=0;
displ_freq40_harm5(1:180,1)=0;
displ_freq80_harm5(1:180,1)=0;
displ_freq160_harm5(1:180,1)=0;
freq10(1:180,1)=0;
freq20(1:180,1)=0;
freq40(1:180,1)=0;
freq80(1:180,1)=0;
freq160(1:180,1)=0;

if exist('iteration')==0
  iteration=input('1st or 2d iteration (type "1" or "2"): ','s');
end;
if iteration=='1'
  if exist('amplitude')==0
      amplitude=input('Amplitude (enter 3 char): ','s');
  end;
  if amplitude=='0.5'
      load parameters0_51;
      load fund_harm0_51;
      load noise0_51;
      load accel_A0_51;
      load accel_B0_51;
      load accel_noise0_51;
      % Combine real and imaginary parts of displ_freq
      %FUNDAMENTAL
      for loop2=0:179
      displ_freq10_fund((1+loop2),1)=fund_harm0_5((13+loop2*24),1)+i*fund_harm0_5((14+loop2*24),1);
      displ_freq20_fund((1+loop2),1)=fund_harm0_5((4333+loop2*24),1)+i*fund_harm0_5((4334+loop2*24),1);
      displ_freq40_fund((1+loop2),1)=fund_harm0_5((8653+loop2*24),1)+i*fund_harm0_5((8654+loop2*24),1);
      displ_freq80_fund((1+loop2),1)=fund_harm0_5((12973+loop2*24),1)+i*fund_harm0_5((12974+loop2*24),1);
      displ_freq160_fund((1+loop2),1)=fund_harm0_5((17293+loop2*24),1)+i*fund_harm0_5((17294+loop2*24),1);
```

134

```matlab
end
%HARMONIC 1
for loop2=0:179
displ_freq10_harm1((1+loop2),1)=fund_harm0_5((15+loop2*24),1)+i*fund_harm0_5((16+loop2*24),1);
displ_freq20_harm1((1+loop2),1)=fund_harm0_5((4335+loop2*24),1)+i*fund_harm0_5((4336+loop2*24),1);
displ_freq40_harm1((1+loop2),1)=fund_harm0_5((8655+loop2*24),1)+i*fund_harm0_5((8656+loop2*24),1);
displ_freq80_harm1((1+loop2),1)=fund_harm0_5((12975+loop2*24),1)+i*fund_harm0_5((12976+loop2*24),1);
displ_freq160_harm1((1+loop2),1)=fund_harm0_5((17295+loop2*24),1)+i*fund_harm0_5((17296+loop2*24),1);
end
%HARMONIC 2
for loop2=0:179
displ_freq10_harm2((1+loop2),1)=fund_harm0_5((17+loop2*24),1)+i*fund_harm0_5((18+loop2*24),1);
displ_freq20_harm2((1+loop2),1)=fund_harm0_5((4337+loop2*24),1)+i*fund_harm0_5((4338+loop2*24),1);
displ_freq40_harm2((1+loop2),1)=fund_harm0_5((8657+loop2*24),1)+i*fund_harm0_5((8658+loop2*24),1);
displ_freq80_harm2((1+loop2),1)=fund_harm0_5((12977+loop2*24),1)+i*fund_harm0_5((12978+loop2*24),1);
displ_freq160_harm2((1+loop2),1)=fund_harm0_5((17297+loop2*24),1)+i*fund_harm0_5((17298+loop2*24),1);
end
%HARMONIC 3
for loop2=0:179
displ_freq10_harm3((1+loop2),1)=fund_harm0_5((19+loop2*24),1)+i*fund_harm0_5((20+loop2*24),1);
displ_freq20_harm3((1+loop2),1)=fund_harm0_5((4339+loop2*24),1)+i*fund_harm0_5((4340+loop2*24),1);
displ_freq40_harm3((1+loop2),1)=fund_harm0_5((8659+loop2*24),1)+i*fund_harm0_5((8660+loop2*24),1);
displ_freq80_harm3((1+loop2),1)=fund_harm0_5((12979+loop2*24),1)+i*fund_harm0_5((12980+loop2*24),1);
displ_freq160_harm3((1+loop2),1)=fund_harm0_5((17299+loop2*24),1)+i*fund_harm0_5((17300+loop2*24),1);
end
%HARMONIC 4
for loop2=0:179
displ_freq10_harm4((1+loop2),1)=fund_harm0_5((21+loop2*24),1)+i*fund_harm0_5((22+loop2*24),1);
displ_freq20_harm4((1+loop2),1)=fund_harm0_5((4341+loop2*24),1)+i*fund_harm0_5((4342+loop2*24),1);
displ_freq40_harm4((1+loop2),1)=fund_harm0_5((8661+loop2*24),1)+i*fund_harm0_5((8662+loop2*24),1);
displ_freq80_harm4((1+loop2),1)=fund_harm0_5((12981+loop2*24),1)+i*fund_harm0_5((12982+loop2*24),1);
displ_freq160_harm4((1+loop2),1)=fund_harm0_5((17301+loop2*24),1)+i*fund_harm0_5((17302+loop2*24),1);
end
%HARMONIC 5
for loop2=0:179
displ_freq10_harm5((1+loop2),1)=fund_harm0_5((23+loop2*24),1)+i*fund_harm0_5((24+loop2*24),1);
displ_freq20_harm5((1+loop2),1)=fund_harm0_5((4343+loop2*24),1)+i*fund_harm0_5((4344+loop2*24),1);
displ_freq40_harm5((1+loop2),1)=fund_harm0_5((8663+loop2*24),1)+i*fund_harm0_5((8664+loop2*24),1);
displ_freq80_harm5((1+loop2),1)=fund_harm0_5((12983+loop2*24),1)+i*fund_harm0_5((12984+loop2*24),1);
displ_freq160_harm5((1+loop2),1)=fund_harm0_5((17303+loop2*24),1)+i*fund_harm0_5((17304+loop2*24),1);
end
% Write out frequencies recorded
freq10(1:180,1)=parameters0_5((3:6:1080),1);
freq20(1:180,1)=parameters0_5((1083:6:2160),1);
freq40(1:180,1)=parameters0_5((2163:6:3240),1);
freq80(1:180,1)=parameters0_5((3243:6:4320),1);
freq160(1:180,1)=parameters0_5((4323:6:5400),1);
elseif amplitude=='1.0'
load parameters1_01;
load fund_harm1_01;
load noise1_01;
load accel_A1_01;
load accel_B1_01;
load accel_noise1_01;
% Combine real and imaginary parts of displ_freq
%FUNDAMENTAL
for loop2=0:179
displ_freq10_fund((1+loop2),1)=fund_harm1_0((13+loop2*24),1)+i*fund_harm1_0((14+loop2*24),1);
displ_freq20_fund((1+loop2),1)=fund_harm1_0((4333+loop2*24),1)+i*fund_harm1_0((4334+loop2*24),1);
displ_freq40_fund((1+loop2),1)=fund_harm1_0((8653+loop2*24),1)+i*fund_harm1_0((8654+loop2*24),1);
displ_freq80_fund((1+loop2),1)=fund_harm1_0((12973+loop2*24),1)+i*fund_harm1_0((12974+loop2*24),1);
displ_freq160_fund((1+loop2),1)=fund_harm1_0((17293+loop2*24),1)+i*fund_harm1_0((17294+loop2*24),1);
end
%HARMONIC 1
for loop2=0:179
displ_freq10_harm1((1+loop2),1)=fund_harm1_0((15+loop2*24),1)+i*fund_harm1_0((16+loop2*24),1);
```

135

```matlab
displ_freq20_harm1((1+loop2),1)=fund_harm1_0((4335+loop2*24),1)+i*fund_harm1_0((4336+loop2*24),1);
displ_freq40_harm1((1+loop2),1)=fund_harm1_0((8655+loop2*24),1)+i*fund_harm1_0((8656+loop2*24),1);
displ_freq80_harm1((1+loop2),1)=fund_harm1_0((12975+loop2*24),1)+i*fund_harm1_0((12976+loop2*24),1);
displ_freq160_harm1((1+loop2),1)=fund_harm1_0((17295+loop2*24),1)+i*fund_harm1_0((17296+loop2*24),1);
end
%HARMONIC 2
for loop2=0:179
displ_freq10_harm2((1+loop2),1)=fund_harm1_0((17+loop2*24),1)+i*fund_harm1_0((18+loop2*24),1);
displ_freq20_harm2((1+loop2),1)=fund_harm1_0((4337+loop2*24),1)+i*fund_harm1_0((4338+loop2*24),1);
displ_freq40_harm2((1+loop2),1)=fund_harm1_0((8657+loop2*24),1)+i*fund_harm1_0((8658+loop2*24),1);
displ_freq80_harm2((1+loop2),1)=fund_harm1_0((12977+loop2*24),1)+i*fund_harm1_0((12978+loop2*24),1);
displ_freq160_harm2((1+loop2),1)=fund_harm1_0((17297+loop2*24),1)+i*fund_harm1_0((17298+loop2*24),1);
end
%HARMONIC 3
for loop2=0:179
displ_freq10_harm3((1+loop2),1)=fund_harm1_0((19+loop2*24),1)+i*fund_harm1_0((20+loop2*24),1);
displ_freq20_harm3((1+loop2),1)=fund_harm1_0((4339+loop2*24),1)+i*fund_harm1_0((4340+loop2*24),1);
displ_freq40_harm3((1+loop2),1)=fund_harm1_0((8659+loop2*24),1)+i*fund_harm1_0((8660+loop2*24),1);
displ_freq80_harm3((1+loop2),1)=fund_harm1_0((12979+loop2*24),1)+i*fund_harm1_0((12980+loop2*24),1);
displ_freq160_harm3((1+loop2),1)=fund_harm1_0((17299+loop2*24),1)+i*fund_harm1_0((17300+loop2*24),1);
end
%HARMONIC 4
for loop2=0:179
displ_freq10_harm4((1+loop2),1)=fund_harm1_0((21+loop2*24),1)+i*fund_harm1_0((22+loop2*24),1);
displ_freq20_harm4((1+loop2),1)=fund_harm1_0((4341+loop2*24),1)+i*fund_harm1_0((4342+loop2*24),1);
displ_freq40_harm4((1+loop2),1)=fund_harm1_0((8661+loop2*24),1)+i*fund_harm1_0((8662+loop2*24),1);
displ_freq80_harm4((1+loop2),1)=fund_harm1_0((12981+loop2*24),1)+i*fund_harm1_0((12982+loop2*24),1);
displ_freq160_harm4((1+loop2),1)=fund_harm1_0((17301+loop2*24),1)+i*fund_harm1_0((17302+loop2*24),1);
end
%HARMONIC 5
for loop2=0:179
displ_freq10_harm5((1+loop2),1)=fund_harm1_0((23+loop2*24),1)+i*fund_harm1_0((24+loop2*24),1);
displ_freq20_harm5((1+loop2),1)=fund_harm1_0((4343+loop2*24),1)+i*fund_harm1_0((4344+loop2*24),1);
displ_freq40_harm5((1+loop2),1)=fund_harm1_0((8663+loop2*24),1)+i*fund_harm1_0((8664+loop2*24),1);
displ_freq80_harm5((1+loop2),1)=fund_harm1_0((12983+loop2*24),1)+i*fund_harm1_0((12984+loop2*24),1);
displ_freq160_harm5((1+loop2),1)=fund_harm1_0((17303+loop2*24),1)+i*fund_harm1_0((17304+loop2*24),1);
end
% Write out frequencies recorded
freq10(1:180,1)=parameters1_0((3:6:1080),1);
freq20(1:180,1)=parameters1_0((1083:6:2160),1);
freq40(1:180,1)=parameters1_0((2163:6:3240),1);
freq80(1:180,1)=parameters1_0((3243:6:4320),1);
freq160(1:180,1)=parameters1_0((4323:6:5400),1);
elseif amplitude=='2.0'
    load parameters2_01;
    load fund_harm2_01;
    load noise2_01;
    load accel_A2_01;
    load accel_B2_01;
    load accel_noise2_01;
    % Combine real and imaginary parts of displ_freq
    %FUNDAMENTAL
    for loop2=0:179
    displ_freq10_fund((1+loop2),1)=fund_harm2_0((13+loop2*24),1)+i*fund_harm2_0((14+loop2*24),1);
    displ_freq20_fund((1+loop2),1)=fund_harm2_0((4333+loop2*24),1)+i*fund_harm2_0((4334+loop2*24),1);
    displ_freq40_fund((1+loop2),1)=fund_harm2_0((8653+loop2*24),1)+i*fund_harm2_0((8654+loop2*24),1);
    displ_freq80_fund((1+loop2),1)=fund_harm2_0((12973+loop2*24),1)+i*fund_harm2_0((12974+loop2*24),1);
    displ_freq160_fund((1+loop2),1)=fund_harm2_0((17293+loop2*24),1)+i*fund_harm2_0((17294+loop2*24),1);
    end
    %HARMONIC 1
    for loop2=0:179
    displ_freq10_harm1((1+loop2),1)=fund_harm2_0((15+loop2*24),1)+i*fund_harm2_0((16+loop2*24),1);
    displ_freq20_harm1((1+loop2),1)=fund_harm2_0((4335+loop2*24),1)+i*fund_harm2_0((4336+loop2*24),1);
    displ_freq40_harm1((1+loop2),1)=fund_harm2_0((8655+loop2*24),1)+i*fund_harm2_0((8656+loop2*24),1);
    displ_freq80_harm1((1+loop2),1)=fund_harm2_0((12975+loop2*24),1)+i*fund_harm2_0((12976+loop2*24),1);
    displ_freq160_harm1((1+loop2),1)=fund_harm2_0((17295+loop2*24),1)+i*fund_harm2_0((17296+loop2*24),1);
```

```
end
%HARMONIC 2
for loop2=0:179
displ_freq10_harm2((1+loop2),1)=fund_harm2_0((17+loop2*24),1)+i*fund_harm2_0((18+loop2*24),1);
displ_freq20_harm2((1+loop2),1)=fund_harm2_0((4337+loop2*24),1)+i*fund_harm2_0((4338+loop2*24),1);
displ_freq40_harm2((1+loop2),1)=fund_harm2_0((8657+loop2*24),1)+i*fund_harm2_0((8658+loop2*24),1);
displ_freq80_harm2((1+loop2),1)=fund_harm2_0((12977+loop2*24),1)+i*fund_harm2_0((12978+loop2*24),1);
displ_freq160_harm2((1+loop2),1)=fund_harm2_0((17297+loop2*24),1)+i*fund_harm2_0((17298+loop2*24),1);
end
%HARMONIC 3
for loop2=0:179
displ_freq10_harm3((1+loop2),1)=fund_harm2_0((19+loop2*24),1)+i*fund_harm2_0((20+loop2*24),1);
displ_freq20_harm3((1+loop2),1)=fund_harm2_0((4339+loop2*24),1)+i*fund_harm2_0((4340+loop2*24),1);
displ_freq40_harm3((1+loop2),1)=fund_harm2_0((8659+loop2*24),1)+i*fund_harm2_0((8660+loop2*24),1);
displ_freq80_harm3((1+loop2),1)=fund_harm2_0((12979+loop2*24),1)+i*fund_harm2_0((12980+loop2*24),1);
displ_freq160_harm3((1+loop2),1)=fund_harm2_0((17299+loop2*24),1)+i*fund_harm2_0((17300+loop2*24),1);
end
%HARMONIC 4
for loop2=0:179
displ_freq10_harm4((1+loop2),1)=fund_harm2_0((21+loop2*24),1)+i*fund_harm2_0((22+loop2*24),1);
displ_freq20_harm4((1+loop2),1)=fund_harm2_0((4341+loop2*24),1)+i*fund_harm2_0((4342+loop2*24),1);
displ_freq40_harm4((1+loop2),1)=fund_harm2_0((8661+loop2*24),1)+i*fund_harm2_0((8662+loop2*24),1);
displ_freq80_harm4((1+loop2),1)=fund_harm2_0((12981+loop2*24),1)+i*fund_harm2_0((12982+loop2*24),1);
displ_freq160_harm4((1+loop2),1)=fund_harm2_0((17301+loop2*24),1)+i*fund_harm2_0((17302+loop2*24),1);
end
%HARMONIC 5
for loop2=0:179
displ_freq10_harm5((1+loop2),1)=fund_harm2_0((23+loop2*24),1)+i*fund_harm2_0((24+loop2*24),1);
displ_freq20_harm5((1+loop2),1)=fund_harm2_0((4343+loop2*24),1)+i*fund_harm2_0((4344+loop2*24),1);
displ_freq40_harm5((1+loop2),1)=fund_harm2_0((8663+loop2*24),1)+i*fund_harm2_0((8664+loop2*24),1);
displ_freq80_harm5((1+loop2),1)=fund_harm2_0((12983+loop2*24),1)+i*fund_harm2_0((12984+loop2*24),1);
displ_freq160_harm5((1+loop2),1)=fund_harm2_0((17303+loop2*24),1)+i*fund_harm2_0((17304+loop2*24),1);
end
% Write out frequencies recorded
freq10(1:180,1)=parameters2_0((3:6:1080),1);
freq20(1:180,1)=parameters2_0((1083:6:2160),1);
freq40(1:180,1)=parameters2_0((2163:6:3240),1);
freq80(1:180,1)=parameters2_0((3243:6:4320),1);
freq160(1:180,1)=parameters2_0((4323:6:5400),1);
elseif amplitude=='4.0'
    load parameters4_01;
    load fund_harm4_01;
    load noise4_01;
    load accel_A4_01;
    load accel_B4_01;
    load accel_noise4_01;
    % Combine real and imaginary parts of displ_freq
    %FUNDAMENTAL
    for loop2=0:179
    displ_freq10_fund((1+loop2),1)=fund_harm4_0((13+loop2*24),1)+i*fund_harm4_0((14+loop2*24),1);
    displ_freq20_fund((1+loop2),1)=fund_harm4_0((4333+loop2*24),1)+i*fund_harm4_0((4334+loop2*24),1);
    displ_freq40_fund((1+loop2),1)=fund_harm4_0((8653+loop2*24),1)+i*fund_harm4_0((8654+loop2*24),1);
    displ_freq80_fund((1+loop2),1)=fund_harm4_0((12973+loop2*24),1)+i*fund_harm4_0((12974+loop2*24),1);
    displ_freq160_fund((1+loop2),1)=fund_harm4_0((17293+loop2*24),1)+i*fund_harm4_0((17294+loop2*24),1);
    end
    %HARMONIC 1
    for loop2=0:179
    displ_freq10_harm1((1+loop2),1)=fund_harm4_0((15+loop2*24),1)+i*fund_harm4_0((16+loop2*24),1);
    displ_freq20_harm1((1+loop2),1)=fund_harm4_0((4335+loop2*24),1)+i*fund_harm4_0((4336+loop2*24),1);
    displ_freq40_harm1((1+loop2),1)=fund_harm4_0((8655+loop2*24),1)+i*fund_harm4_0((8656+loop2*24),1);
    displ_freq80_harm1((1+loop2),1)=fund_harm4_0((12975+loop2*24),1)+i*fund_harm4_0((12976+loop2*24),1);
    displ_freq160_harm1((1+loop2),1)=fund_harm4_0((17295+loop2*24),1)+i*fund_harm4_0((17296+loop2*24),1);
    end
    %HARMONIC 2
    for loop2=0:179
    displ_freq10_harm2((1+loop2),1)=fund_harm4_0((17+loop2*24),1)+i*fund_harm4_0((18+loop2*24),1);
```

```matlab
        displ_freq20_harm2((1+loop2),1)=fund_harm4_0((4337+loop2*24),1)+i*fund_harm4_0((4338+loop2*24),1);
        displ_freq40_harm2((1+loop2),1)=fund_harm4_0((8657+loop2*24),1)+i*fund_harm4_0((8658+loop2*24),1);
        displ_freq80_harm2((1+loop2),1)=fund_harm4_0((12977+loop2*24),1)+i*fund_harm4_0((12978+loop2*24),1);
        displ_freq160_harm2((1+loop2),1)=fund_harm4_0((17297+loop2*24),1)+i*fund_harm4_0((17298+loop2*24),1);
    end
    %HARMONIC 3
    for loop2=0:179
        displ_freq10_harm3((1+loop2),1)=fund_harm4_0((19+loop2*24),1)+i*fund_harm4_0((20+loop2*24),1);
        displ_freq20_harm3((1+loop2),1)=fund_harm4_0((4339+loop2*24),1)+i*fund_harm4_0((4340+loop2*24),1);
        displ_freq40_harm3((1+loop2),1)=fund_harm4_0((8659+loop2*24),1)+i*fund_harm4_0((8660+loop2*24),1);
        displ_freq80_harm3((1+loop2),1)=fund_harm4_0((12979+loop2*24),1)+i*fund_harm4_0((12980+loop2*24),1);
        displ_freq160_harm3((1+loop2),1)=fund_harm4_0((17299+loop2*24),1)+i*fund_harm4_0((17300+loop2*24),1);
    end
    %HARMONIC 4
    for loop2=0:179
        displ_freq10_harm4((1+loop2),1)=fund_harm4_0((21+loop2*24),1)+i*fund_harm4_0((22+loop2*24),1);
        displ_freq20_harm4((1+loop2),1)=fund_harm4_0((4341+loop2*24),1)+i*fund_harm4_0((4342+loop2*24),1);
        displ_freq40_harm4((1+loop2),1)=fund_harm4_0((8661+loop2*24),1)+i*fund_harm4_0((8662+loop2*24),1);
        displ_freq80_harm4((1+loop2),1)=fund_harm4_0((12981+loop2*24),1)+i*fund_harm4_0((12982+loop2*24),1);
        displ_freq160_harm4((1+loop2),1)=fund_harm4_0((17301+loop2*24),1)+i*fund_harm4_0((17302+loop2*24),1);
    end
    %HARMONIC 5
    for loop2=0:179
        displ_freq10_harm5((1+loop2),1)=fund_harm4_0((23+loop2*24),1)+i*fund_harm4_0((24+loop2*24),1);
        displ_freq20_harm5((1+loop2),1)=fund_harm4_0((4343+loop2*24),1)+i*fund_harm4_0((4344+loop2*24),1);
        displ_freq40_harm5((1+loop2),1)=fund_harm4_0((8663+loop2*24),1)+i*fund_harm4_0((8664+loop2*24),1);
        displ_freq80_harm5((1+loop2),1)=fund_harm4_0((12983+loop2*24),1)+i*fund_harm4_0((12984+loop2*24),1);
        displ_freq160_harm5((1+loop2),1)=fund_harm4_0((17303+loop2*24),1)+i*fund_harm4_0((17304+loop2*24),1);
    end
    % Write out frequencies recorded
    freq10(1:180,1)=parameters4_0((3:6:1080),1);
    freq20(1:180,1)=parameters4_0((1083:6:2160),1);
    freq40(1:180,1)=parameters4_0((2163:6:3240),1);
    freq80(1:180,1)=parameters4_0((3243:6:4320),1);
    freq160(1:180,1)=parameters4_0((4323:6:5400),1);
elseif amplitude=='8.0'
    load parameters8_01;
    load fund_harm8_01;
    load noise8_01;
    load accel_A8_01;
    load accel_B8_01;
    load accel_noise8_01;
    % Combine real and imaginary parts of displ_freq
    %FUNDAMENTAL
    for loop2=0:179
        displ_freq10_fund((1+loop2),1)=fund_harm8_0((13+loop2*24),1)+i*fund_harm8_0((14+loop2*24),1);
        displ_freq20_fund((1+loop2),1)=fund_harm8_0((4333+loop2*24),1)+i*fund_harm8_0((4334+loop2*24),1);
        displ_freq40_fund((1+loop2),1)=fund_harm8_0((8653+loop2*24),1)+i*fund_harm8_0((8654+loop2*24),1);
        displ_freq80_fund((1+loop2),1)=fund_harm8_0((12973+loop2*24),1)+i*fund_harm8_0((12974+loop2*24),1);
        displ_freq160_fund((1+loop2),1)=fund_harm8_0((17293+loop2*24),1)+i*fund_harm8_0((17294+loop2*24),1);
    end
    %HARMONIC 1
    for loop2=0:179
        displ_freq10_harm1((1+loop2),1)=fund_harm8_0((15+loop2*24),1)+i*fund_harm8_0((16+loop2*24),1);
        displ_freq20_harm1((1+loop2),1)=fund_harm8_0((4335+loop2*24),1)+i*fund_harm8_0((4336+loop2*24),1);
        displ_freq40_harm1((1+loop2),1)=fund_harm8_0((8655+loop2*24),1)+i*fund_harm8_0((8656+loop2*24),1);
        displ_freq80_harm1((1+loop2),1)=fund_harm8_0((12975+loop2*24),1)+i*fund_harm8_0((12976+loop2*24),1);
        displ_freq160_harm1((1+loop2),1)=fund_harm8_0((17295+loop2*24),1)+i*fund_harm8_0((17296+loop2*24),1);
    end
    %HARMONIC 2
    for loop2=0:179
        displ_freq10_harm2((1+loop2),1)=fund_harm8_0((17+loop2*24),1)+i*fund_harm8_0((18+loop2*24),1);
        displ_freq20_harm2((1+loop2),1)=fund_harm8_0((4337+loop2*24),1)+i*fund_harm8_0((4338+loop2*24),1);
        displ_freq40_harm2((1+loop2),1)=fund_harm8_0((8657+loop2*24),1)+i*fund_harm8_0((8658+loop2*24),1);
        displ_freq80_harm2((1+loop2),1)=fund_harm8_0((12977+loop2*24),1)+i*fund_harm8_0((12978+loop2*24),1);
        displ_freq160_harm2((1+loop2),1)=fund_harm8_0((17297+loop2*24),1)+i*fund_harm8_0((17298+loop2*24),1);
```

```
    end
    %HARMONIC 3
    for loop2=0:179
    displ_freq10_harm3((1+loop2),1)=fund_harm8_0((19+loop2*24),1)+i*fund_harm8_0((20+loop2*24),1);
    displ_freq20_harm3((1+loop2),1)=fund_harm8_0((4339+loop2*24),1)+i*fund_harm8_0((4340+loop2*24),1);
    displ_freq40_harm3((1+loop2),1)=fund_harm8_0((8659+loop2*24),1)+i*fund_harm8_0((8660+loop2*24),1);
    displ_freq80_harm3((1+loop2),1)=fund_harm8_0((12979+loop2*24),1)+i*fund_harm8_0((12980+loop2*24),1);
    displ_freq160_harm3((1+loop2),1)=fund_harm8_0((17299+loop2*24),1)+i*fund_harm8_0((17300+loop2*24),1);
    end
    %HARMONIC 4
    for loop2=0:179
    displ_freq10_harm4((1+loop2),1)=fund_harm8_0((21+loop2*24),1)+i*fund_harm8_0((22+loop2*24),1);
    displ_freq20_harm4((1+loop2),1)=fund_harm8_0((4341+loop2*24),1)+i*fund_harm8_0((4342+loop2*24),1);
    displ_freq40_harm4((1+loop2),1)=fund_harm8_0((8661+loop2*24),1)+i*fund_harm8_0((8662+loop2*24),1);
    displ_freq80_harm4((1+loop2),1)=fund_harm8_0((12981+loop2*24),1)+i*fund_harm8_0((12982+loop2*24),1);
    displ_freq160_harm4((1+loop2),1)=fund_harm8_0((17301+loop2*24),1)+i*fund_harm8_0((17302+loop2*24),1);
    end
    %HARMONIC 5
    for loop2=0:179
    displ_freq10_harm5((1+loop2),1)=fund_harm8_0((23+loop2*24),1)+i*fund_harm8_0((24+loop2*24),1);
    displ_freq20_harm5((1+loop2),1)=fund_harm8_0((4343+loop2*24),1)-i*fund_harm8_0((4344-loop2*24),1);
    displ_freq40_harm5((1+loop2),1)=fund_harm8_0((8663+loop2*24),1)+i*fund_harm8_0((8664+loop2*24),1);
    displ_freq80_harm5((1+loop2),1)=fund_harm8_0((12983+loop2*24),1)+i*fund_harm8_0((12984-loop2*24),1);
    displ_freq160_harm5((1+loop2),1)=fund_harm8_0((17303+loop2*24),1)-i*fund_harm8_0((17304+loop2*24),1);
    end
    % Write out frequencies recorded
    freq10(1:180,1)=parameters8_0((3:6:1080),1);
    freq20(1:180,1)=parameters8_0((1083:6:2160),1);
    freq40(1:180,1)=parameters8_0((2163:6:3240),1);
    freq80(1:180,1)=parameters8_0((3243:6:4320),1);
    freq160(1:180,1)=parameters8_0((4323:6:5400),1);
  end;

elseif iteration=='2'
      if exist('amplitude')==0
      amplitude=input('Amplitude (enter 3 char): ','s');
      end;
    if amplitude=='0.5'
      load parameters0_52;
      load fund_harm0_52;
      load noise0_52;
      load accel_A0_52;
      load accel_B0_52;
      load accel_noise0_52;
      % Combine real and imaginary parts of displ_freq
      %FUNDAMENTAL
      for loop2=0:179
      displ_freq10_fund((1+loop2),1)=fund_harm0_5((13+loop2*24),1)+i*fund_harm0_5((14+loop2*24),1);
      displ_freq20_fund((1+loop2),1)=fund_harm0_5((4333+loop2*24),1)+i*fund_harm0_5((4334+loop2*24),1);
      displ_freq40_fund((1+loop2),1)=fund_harm0_5((8653+loop2*24),1)+i*fund_harm0_5((8654+loop2*24),1);
      displ_freq80_fund((1+loop2),1)=fund_harm0_5((12973+loop2*24),1)+i*fund_harm0_5((12974+loop2*24),1);
      displ_freq160_fund((1+loop2),1)=fund_harm0_5((17293+loop2*24),1)+i*fund_harm0_5((17294+loop2*24),1);
      end
      %HARMONIC 1
      for loop2=0:179
      displ_freq10_harm1((1+loop2),1)=fund_harm0_5((15+loop2*24),1)+i*fund_harm0_5((16+loop2*24),1);
      displ_freq20_harm1((1+loop2),1)=fund_harm0_5((4335+loop2*24),1)+i*fund_harm0_5((4336+loop2*24),1);
      displ_freq40_harm1((1+loop2),1)=fund_harm0_5((8655+loop2*24),1)+i*fund_harm0_5((8656+loop2*24),1);
      displ_freq80_harm1((1+loop2),1)=fund_harm0_5((12975+loop2*24),1)+i*fund_harm0_5((12976+loop2*24),1);
      displ_freq160_harm1((1+loop2),1)=fund_harm0_5((17295+loop2*24),1)+i*fund_harm0_5((17296+loop2*24),1);
      end
      %HARMONIC 2
      for loop2=0:179
      displ_freq10_harm2((1+loop2),1)=fund_harm0_5((17+loop2*24),1)+i*fund_harm0_5((18+loop2*24),1);
      displ_freq20_harm2((1+loop2),1)=fund_harm0_5((4337+loop2*24),1)+i*fund_harm0_5((4338+loop2*24),1);
      displ_freq40_harm2((1+loop2),1)=fund_harm0_5((8657+loop2*24),1)+i*fund_harm0_5((8658+loop2*24),1);
```

```
displ_freq80_harm2((1+loop2),1)=fund_harm0_5((12977+loop2*24),1)+i*fund_harm0_5((12978+loop2*24),1);
displ_freq160_harm2((1+loop2),1)=fund_harm0_5((17297+loop2*24),1)+i*fund_harm0_5((17298+loop2*24),1);
end
%HARMONIC 3
for loop2=0:179
displ_freq10_harm3((1+loop2),1)=fund_harm0_5((19+loop2*24),1)+i*fund_harm0_5((20+loop2*24),1);
displ_freq20_harm3((1+loop2),1)=fund_harm0_5((4339+loop2*24),1)+i*fund_harm0_5((4340+loop2*24),1);
displ_freq40_harm3((1+loop2),1)=fund_harm0_5((8659+loop2*24),1)+i*fund_harm0_5((8660+loop2*24),1);
displ_freq80_harm3((1+loop2),1)=fund_harm0_5((12979+loop2*24),1)+i*fund_harm0_5((12980+loop2*24),1);
displ_freq160_harm3((1+loop2),1)=fund_harm0_5((17299+loop2*24),1)+i*fund_harm0_5((17300+loop2*24),1);
end
%HARMONIC 4
for loop2=0:179
displ_freq10_harm4((1+loop2),1)=fund_harm0_5((21+loop2*24),1)+i*fund_harm0_5((22+loop2*24),1);
displ_freq20_harm4((1+loop2),1)=fund_harm0_5((4341+loop2*24),1)+i*fund_harm0_5((4342+loop2*24),1);
displ_freq40_harm4((1+loop2),1)=fund_harm0_5((8661+loop2*24),1)+i*fund_harm0_5((8662+loop2*24),1);
displ_freq80_harm4((1+loop2),1)=fund_harm0_5((12981+loop2*24),1)+i*fund_harm0_5((12982+loop2*24),1);
displ_freq160_harm4((1+loop2),1)=fund_harm0_5((17301+loop2*24),1)+i*fund_harm0_5((17302+loop2*24),1);
end
%HARMONIC 5
for loop2=0:179
displ_freq10_harm5((1+loop2),1)=fund_harm0_5((23+loop2*24),1)+i*fund_harm0_5((24+loop2*24),1);
displ_freq20_harm5((1+loop2),1)=fund_harm0_5((4343+loop2*24),1)+i*fund_harm0_5((4344+loop2*24),1);
displ_freq40_harm5((1+loop2),1)=fund_harm0_5((8663+loop2*24),1)+i*fund_harm0_5((8664+loop2*24),1);
displ_freq80_harm5((1+loop2),1)=fund_harm0_5((12983+loop2*24),1)+i*fund_harm0_5((12984+loop2*24),1);
displ_freq160_harm5((1+loop2),1)=fund_harm0_5((17303+loop2*24),1)+i*fund_harm0_5((17304+loop2*24),1);
end
% Write out frequencies recorded
freq10(1:180,1)=parameters0_5((3:6:1080),1);
freq20(1:180,1)=parameters0_5((1083:6:2160),1);
freq40(1:180,1)=parameters0_5((2163:6:3240),1);
freq80(1:180,1)=parameters0_5((3243:6:4320),1);
freq160(1:180,1)=parameters0_5((4323:6:5400),1);
elseif amplitude=='1.0'
    load parameters1_02;
    load fund_harm1_02;
    load noise1_02;
    load accel_A1_02;
    load accel_B1_02;
    load accel_noise1_02;
    % Combine real and imaginary parts of displ_freq
    %FUNDAMENTAL
    for loop2=0:179
    displ_freq10_fund((1+loop2),1)=fund_harm1_0((13+loop2*24),1)+i*fund_harm1_0((14+loop2*24),1);
    displ_freq20_fund((1+loop2),1)=fund_harm1_0((4333+loop2*24),1)+i*fund_harm1_0((4334+loop2*24),1);
    displ_freq40_fund((1+loop2),1)=fund_harm1_0((8653+loop2*24),1)+i*fund_harm1_0((8654+loop2*24),1);
    displ_freq80_fund((1+loop2),1)=fund_harm1_0((12973+loop2*24),1)+i*fund_harm1_0((12974+loop2*24),1);
    displ_freq160_fund((1+loop2),1)=fund_harm1_0((17293+loop2*24),1)+i*fund_harm1_0((17294+loop2*24),1);
    end
    %HARMONIC 1
    for loop2=0:179
    displ_freq10_harm1((1+loop2),1)=fund_harm1_0((15+loop2*24),1)+i*fund_harm1_0((16+loop2*24),1);
    displ_freq20_harm1((1+loop2),1)=fund_harm1_0((4335+loop2*24),1)+i*fund_harm1_0((4336+loop2*24),1);
    displ_freq40_harm1((1+loop2),1)=fund_harm1_0((8655+loop2*24),1)+i*fund_harm1_0((8656+loop2*24),1);
    displ_freq80_harm1((1+loop2),1)=fund_harm1_0((12975+loop2*24),1)+i*fund_harm1_0((12976+loop2*24),1);
    displ_freq160_harm1((1+loop2),1)=fund_harm1_0((17295+loop2*24),1)+i*fund_harm1_0((17296+loop2*24),1);
    end
    %HARMONIC 2
    for loop2=0:179
    displ_freq10_harm2((1+loop2),1)=fund_harm1_0((17+loop2*24),1)+i*fund_harm1_0((18+loop2*24),1);
    displ_freq20_harm2((1+loop2),1)=fund_harm1_0((4337+loop2*24),1)+i*fund_harm1_0((4338+loop2*24),1);
    displ_freq40_harm2((1+loop2),1)=fund_harm1_0((8657+loop2*24),1)+i*fund_harm1_0((8658+loop2*24),1);
    displ_freq80_harm2((1+loop2),1)=fund_harm1_0((12977+loop2*24),1)+i*fund_harm1_0((12978+loop2*24),1);
    displ_freq160_harm2((1+loop2),1)=fund_harm1_0((17297+loop2*24),1)+i*fund_harm1_0((17298+loop2*24),1);
    end
    %HARMONIC 3
```

```
for loop2=0:179
    displ_freq10_harm3((1+loop2),1)=fund_harm1_0((19+loop2*24),1)+i*fund_harm1_0((20+loop2*24),1);
    displ_freq20_harm3((1+loop2),1)=fund_harm1_0((4339+loop2*24),1)+i*fund_harm1_0((4340+loop2*24),1);
    displ_freq40_harm3((1+loop2),1)=fund_harm1_0((8659+loop2*24),1)+i*fund_harm1_0((8660+loop2*24),1);
    displ_freq80_harm3((1+loop2),1)=fund_harm1_0((12979+loop2*24),1)+i*fund_harm1_0((12980+loop2*24),1);
    displ_freq160_harm3((1+loop2),1)=fund_harm1_0((17299+loop2*24),1)+i*fund_harm1_0((17300+loop2*24),1);
end
%HARMONIC 4
for loop2=0:179
    displ_freq10_harm4((1+loop2),1)=fund_harm1_0((21+loop2*24),1)+i*fund_harm1_0((22+loop2*24),1);
    displ_freq20_harm4((1+loop2),1)=fund_harm1_0((4341+loop2*24),1)+i*fund_harm1_0((4342+loop2*24),1);
    displ_freq40_harm4((1+loop2),1)=fund_harm1_0((8661+loop2*24),1)+i*fund_harm1_0((8662+loop2*24),1);
    displ_freq80_harm4((1+loop2),1)=fund_harm1_0((12981+loop2*24),1)+i*fund_harm1_0((12982+loop2*24),1);
    displ_freq160_harm4((1+loop2),1)=fund_harm1_0((17301+loop2*24),1)+i*fund_harm1_0((17302+loop2*24),1);
end
%HARMONIC 5
for loop2=0:179
    displ_freq10_harm5((1+loop2),1)=fund_harm1_0((23+loop2*24),1)+i*fund_harm1_0((24+loop2*24),1);
    displ_freq20_harm5((1+loop2),1)=fund_harm1_0((4343+loop2*24),1)+i*fund_harm1_0((4344+loop2*24),1);
    displ_freq40_harm5((1+loop2),1)=fund_harm1_0((8663+loop2*24),1)+i*fund_harm1_0((8664+loop2*24),1);
    displ_freq80_harm5((1+loop2),1)=fund_harm1_0((12983+loop2*24),1)-i*fund_harm1_0((12984-loop2*24),1);
    displ_freq160_harm5((1+loop2),1)=fund_harm1_0((17303+loop2*24),1)-i*fund_harm1_0((17304+loop2*24),1);
end
% Write out frequencies recorded
freq10(1:180,1)=parameters1_0((3:6:1080),1);
freq20(1:180,1)=parameters1_0((1083:6:2160),1);
freq40(1:180,1)=parameters1_0((2163:6:3240),1);
freq80(1:180,1)=parameters1_0((3243:6:4320),1);
freq160(1:180,1)=parameters1_0((4323:6:5400),1);
elseif amplitude=='2.0'
    load parameters2_02;
    load fund_harm2_02;
    load noise2_02;
    load accel_A2_02;
    load accel_B2_02;
    load accel_noise2_02;
    % Combine real and imaginary parts of displ_freq
    %FUNDAMENTAL
    for loop2=0:179
        displ_freq10_fund((1+loop2),1)=fund_harm2_0((13+loop2*24),1)+i*fund_harm2_0((14+loop2*24),1);
        displ_freq20_fund((1+loop2),1)=fund_harm2_0((4333+loop2*24),1)+i*fund_harm2_0((4334+loop2*24),1);
        displ_freq40_fund((1+loop2),1)=fund_harm2_0((8653+loop2*24),1)+i*fund_harm2_0((8654+loop2*24),1);
        displ_freq80_fund((1+loop2),1)=fund_harm2_0((12973+loop2*24),1)+i*fund_harm2_0((12974+loop2*24),1);
        displ_freq160_fund((1+loop2),1)=fund_harm2_0((17293+loop2*24),1)+i*fund_harm2_0((17294+loop2*24),1);
    end
    %HARMONIC 1
    for loop2=0:179
        displ_freq10_harm1((1+loop2),1)=fund_harm2_0((15+loop2*24),1)+i*fund_harm2_0((16+loop2*24),1);
        displ_freq20_harm1((1+loop2),1)=fund_harm2_0((4335+loop2*24),1)+i*fund_harm2_0((4336+loop2*24),1);
        displ_freq40_harm1((1+loop2),1)=fund_harm2_0((8655+loop2*24),1)+i*fund_harm2_0((8656+loop2*24),1);
        displ_freq80_harm1((1+loop2),1)=fund_harm2_0((12975+loop2*24),1)+i*fund_harm2_0((12976+loop2*24),1);
        displ_freq160_harm1((1+loop2),1)=fund_harm2_0((17295+loop2*24),1)+i*fund_harm2_0((17296+loop2*24),1);
    end
    %HARMONIC 2
    for loop2=0:179
        displ_freq10_harm2((1+loop2),1)=fund_harm2_0((17+loop2*24),1)+i*fund_harm2_0((18+loop2*24),1);
        displ_freq20_harm2((1+loop2),1)=fund_harm2_0((4337+loop2*24),1)+i*fund_harm2_0((4338+loop2*24),1);
        displ_freq40_harm2((1+loop2),1)=fund_harm2_0((8657+loop2*24),1)+i*fund_harm2_0((8658+loop2*24),1);
        displ_freq80_harm2((1+loop2),1)=fund_harm2_0((12977+loop2*24),1)+i*fund_harm2_0((12978+loop2*24),1);
        displ_freq160_harm2((1+loop2),1)=fund_harm2_0((17297+loop2*24),1)+i*fund_harm2_0((17298+loop2*24),1);
    end
    %HARMONIC 3
    for loop2=0:179
        displ_freq10_harm3((1+loop2),1)=fund_harm2_0((19+loop2*24),1)+i*fund_harm2_0((20+loop2*24),1);
        displ_freq20_harm3((1+loop2),1)=fund_harm2_0((4339+loop2*24),1)+i*fund_harm2_0((4340+loop2*24),1);
        displ_freq40_harm3((1+loop2),1)=fund_harm2_0((8659+loop2*24),1)+i*fund_harm2_0((8660+loop2*24),1);
```

```matlab
displ_freq80_harm3((1+loop2),1)=fund_harm2_0((12979+loop2*24),1)+i*fund_harm2_0((12980+loop2*24),1);
displ_freq160_harm3((1+loop2),1)=fund_harm2_0((17299+loop2*24),1)+i*fund_harm2_0((17300+loop2*24),1);
end
%HARMONIC 4
for loop2=0:179
displ_freq10_harm4((1+loop2),1)=fund_harm2_0((21+loop2*24),1)+i*fund_harm2_0((22+loop2*24),1);
displ_freq20_harm4((1+loop2),1)=fund_harm2_0((4341+loop2*24),1)+i*fund_harm2_0((4342+loop2*24),1);
displ_freq40_harm4((1+loop2),1)=fund_harm2_0((8661+loop2*24),1)+i*fund_harm2_0((8662+loop2*24),1);
displ_freq80_harm4((1+loop2),1)=fund_harm2_0((12981+loop2*24),1)+i*fund_harm2_0((12982+loop2*24),1);
displ_freq160_harm4((1+loop2),1)=fund_harm2_0((17301+loop2*24),1)+i*fund_harm2_0((17302+loop2*24),1);
end
%HARMONIC 5
for loop2=0:179
displ_freq10_harm5((1+loop2),1)=fund_harm2_0((23+loop2*24),1)+i*fund_harm2_0((24+loop2*24),1);
displ_freq20_harm5((1+loop2),1)=fund_harm2_0((4343+loop2*24),1)+i*fund_harm2_0((4344+loop2*24),1);
displ_freq40_harm5((1+loop2),1)=fund_harm2_0((8663+loop2*24),1)+i*fund_harm2_0((8664+loop2*24),1);
displ_freq80_harm5((1+loop2),1)=fund_harm2_0((12983+loop2*24),1)+i*fund_harm2_0((12984+loop2*24),1);
displ_freq160_harm5((1+loop2),1)=fund_harm2_0((17303+loop2*24),1)+i*fund_harm2_0((17304+loop2*24),1);
end
% Write out frequencies recorded
freq10(1:180,1)=parameters2_0((3:6:1080),1);
freq20(1:180,1)=parameters2_0((1083:6:2160),1);
freq40(1:180,1)=parameters2_0((2163:6:3240),1);
freq80(1:180,1)=parameters2_0((3243:6:4320),1);
freq160(1:180,1)=parameters2_0((4323:6:5400),1);
elseif amplitude=='4.0'
    load parameters4_02;
    load fund_harm4_02;
    load noise4_02;
    load accel_A4_02;
    load accel_B4_02;
    load accel_noise4_02;
    % Combine real and imaginary parts of displ_freq
    %FUNDAMENTAL
    for loop2=0:179
    displ_freq10_fund((1+loop2),1)=fund_harm4_0((13+loop2*24),1)+i*fund_harm4_0((14+loop2*24),1);
    displ_freq20_fund((1+loop2),1)=fund_harm4_0((4333+loop2*24),1)+i*fund_harm4_0((4334+loop2*24),1);
    displ_freq40_fund((1+loop2),1)=fund_harm4_0((8653+loop2*24),1)+i*fund_harm4_0((8654+loop2*24),1);
    displ_freq80_fund((1+loop2),1)=fund_harm4_0((12973+loop2*24),1)+i*fund_harm4_0((12974+loop2*24),1);
    displ_freq160_fund((1+loop2),1)=fund_harm4_0((17293+loop2*24),1)+i*fund_harm4_0((17294+loop2*24),1);
    end
    %HARMONIC 1
    for loop2=0:179
    displ_freq10_harm1((1+loop2),1)=fund_harm4_0((15+loop2*24),1)+i*fund_harm4_0((16+loop2*24),1);
    displ_freq20_harm1((1+loop2),1)=fund_harm4_0((4335+loop2*24),1)+i*fund_harm4_0((4336+loop2*24),1);
    displ_freq40_harm1((1+loop2),1)=fund_harm4_0((8655+loop2*24),1)+i*fund_harm4_0((8656+loop2*24),1);
    displ_freq80_harm1((1+loop2),1)=fund_harm4_0((12975+loop2*24),1)+i*fund_harm4_0((12976+loop2*24),1);
    displ_freq160_harm1((1+loop2),1)=fund_harm4_0((17295+loop2*24),1)+i*fund_harm4_0((17296+loop2*24),1);
    end
    %HARMONIC 2
    for loop2=0:179
    displ_freq10_harm2((1+loop2),1)=fund_harm4_0((17+loop2*24),1)+i*fund_harm4_0((18+loop2*24),1);
    displ_freq20_harm2((1+loop2),1)=fund_harm4_0((4337+loop2*24),1)+i*fund_harm4_0((4338+loop2*24),1);
    displ_freq40_harm2((1+loop2),1)=fund_harm4_0((8657+loop2*24),1)+i*fund_harm4_0((8658+loop2*24),1);
    displ_freq80_harm2((1+loop2),1)=fund_harm4_0((12977+loop2*24),1)+i*fund_harm4_0((12978+loop2*24),1);
    displ_freq160_harm2((1+loop2),1)=fund_harm4_0((17297+loop2*24),1)+i*fund_harm4_0((17298+loop2*24),1);
    end
    %HARMONIC 3
    for loop2=0:179
    displ_freq10_harm3((1+loop2),1)=fund_harm4_0((19+loop2*24),1)+i*fund_harm4_0((20+loop2*24),1);
    displ_freq20_harm3((1+loop2),1)=fund_harm4_0((4339+loop2*24),1)+i*fund_harm4_0((4340+loop2*24),1);
    displ_freq40_harm3((1+loop2),1)=fund_harm4_0((8659+loop2*24),1)+i*fund_harm4_0((8660+loop2*24),1);
    displ_freq80_harm3((1+loop2),1)=fund_harm4_0((12979+loop2*24),1)+i*fund_harm4_0((12980+loop2*24),1);
    displ_freq160_harm3((1+loop2),1)=fund_harm4_0((17299+loop2*24),1)+i*fund_harm4_0((17300+loop2*24),1);
    end
    %HARMONIC 4
```

```matlab
for loop2=0:179
    displ_freq10_harm4((1+loop2),1)=fund_harm4_0((21+loop2*24),1)+i*fund_harm4_0((22+loop2*24),1);
    displ_freq20_harm4((1+loop2),1)=fund_harm4_0((4341+loop2*24),1)+i*fund_harm4_0((4342+loop2*24),1);
    displ_freq40_harm4((1+loop2),1)=fund_harm4_0((8661+loop2*24),1)+i*fund_harm4_0((8662+loop2*24),1);
    displ_freq80_harm4((1+loop2),1)=fund_harm4_0((12981+loop2*24),1)+i*fund_harm4_0((12982+loop2*24),1);
    displ_freq160_harm4((1+loop2),1)=fund_harm4_0((17301+loop2*24),1)+i*fund_harm4_0((17302+loop2*24),1);
end
%HARMONIC 5
for loop2=0:179
    displ_freq10_harm5((1+loop2),1)=fund_harm4_0((23+loop2*24),1)+i*fund_harm4_0((24+loop2*24),1);
    displ_freq20_harm5((1+loop2),1)=fund_harm4_0((4343+loop2*24),1)+i*fund_harm4_0((4344+loop2*24),1);
    displ_freq40_harm5((1+loop2),1)=fund_harm4_0((8663+loop2*24),1)+i*fund_harm4_0((8664+loop2*24),1);
    displ_freq80_harm5((1+loop2),1)=fund_harm4_0((12983+loop2*24),1)+i*fund_harm4_0((12984+loop2*24),1);
    displ_freq160_harm5((1+loop2),1)=fund_harm4_0((17303+loop2*24),1)+i*fund_harm4_0((17304+loop2*24),1);
end
% Write out frequencies recorded
freq10(1:180,1)=parameters4_0((3:6:1080),1);
freq20(1:180,1)=parameters4_0((1083:6:2160),1);
freq40(1:180,1)=parameters4_0((2163:6:3240),1);
freq80(1:180,1)=parameters4_0((3243:6:4320),1);
freq160(1:180,1)=parameters4_0((4323:6:5400),1);
elseif amplitude=='8.0'
    load parameters8_02;
    load fund_harm8_02;
    load noise8_02;
    load accel_A8_02;
    load accel_B8_02;
    load accel_noise8_02;
    % Combine real and imaginary parts of displ_freq
    %FUNDAMENTAL
    for loop2=0:179
        displ_freq10_fund((1+loop2),1)=fund_harm8_0((13+loop2*24),1)+i*fund_harm8_0((14+loop2*24),1);
        displ_freq20_fund((1+loop2),1)=fund_harm8_0((4333+loop2*24),1)+i*fund_harm8_0((4334+loop2*24),1);
        displ_freq40_fund((1+loop2),1)=fund_harm8_0((8653+loop2*24),1)+i*fund_harm8_0((8654+loop2*24),1);
        displ_freq80_fund((1+loop2),1)=fund_harm8_0((12973+loop2*24),1)+i*fund_harm8_0((12974+loop2*24),1);
        displ_freq160_fund((1+loop2),1)=fund_harm8_0((17293+loop2*24),1)+i*fund_harm8_0((17294+loop2*24),1);
    end
    %HARMONIC 1
    for loop2=0:179
        displ_freq10_harm1((1+loop2),1)=fund_harm8_0((15+loop2*24),1)+i*fund_harm8_0((16+loop2*24),1);
        displ_freq20_harm1((1+loop2),1)=fund_harm8_0((4335+loop2*24),1)+i*fund_harm8_0((4336+loop2*24),1);
        displ_freq40_harm1((1+loop2),1)=fund_harm8_0((8655+loop2*24),1)+i*fund_harm8_0((8656+loop2*24),1);
        displ_freq80_harm1((1+loop2),1)=fund_harm8_0((12975+loop2*24),1)+i*fund_harm8_0((12976+loop2*24),1);
        displ_freq160_harm1((1+loop2),1)=fund_harm8_0((17295+loop2*24),1)+i*fund_harm8_0((17296+loop2*24),1);
    end
    %HARMONIC 2
    for loop2=0:179
        displ_freq10_harm2((1+loop2),1)=fund_harm8_0((17+loop2*24),1)+i*fund_harm8_0((18+loop2*24),1);
        displ_freq20_harm2((1+loop2),1)=fund_harm8_0((4337+loop2*24),1)+i*fund_harm8_0((4338+loop2*24),1);
        displ_freq40_harm2((1+loop2),1)=fund_harm8_0((8657+loop2*24),1)+i*fund_harm8_0((8658+loop2*24),1);
        displ_freq80_harm2((1+loop2),1)=fund_harm8_0((12977+loop2*24),1)+i*fund_harm8_0((12978+loop2*24),1);
        displ_freq160_harm2((1+loop2),1)=fund_harm8_0((17297+loop2*24),1)+i*fund_harm8_0((17298+loop2*24),1);
    end
    %HARMONIC 3
    for loop2=0:179
        displ_freq10_harm3((1+loop2),1)=fund_harm8_0((19+loop2*24),1)+i*fund_harm8_0((20+loop2*24),1);
        displ_freq20_harm3((1+loop2),1)=fund_harm8_0((4339+loop2*24),1)+i*fund_harm8_0((4340+loop2*24),1);
        displ_freq40_harm3((1+loop2),1)=fund_harm8_0((8659+loop2*24),1)+i*fund_harm8_0((8660+loop2*24),1);
        displ_freq80_harm3((1+loop2),1)=fund_harm8_0((12979+loop2*24),1)+i*fund_harm8_0((12980+loop2*24),1);
        displ_freq160_harm3((1+loop2),1)=fund_harm8_0((17299+loop2*24),1)+i*fund_harm8_0((17300+loop2*24),1);
    end
    %HARMONIC 4
    for loop2=0:179
        displ_freq10_harm4((1+loop2),1)=fund_harm8_0((21+loop2*24),1)+i*fund_harm8_0((22+loop2*24),1);
        displ_freq20_harm4((1+loop2),1)=fund_harm8_0((4341+loop2*24),1)+i*fund_harm8_0((4342+loop2*24),1);
        displ_freq40_harm4((1+loop2),1)=fund_harm8_0((8661+loop2*24),1)+i*fund_harm8_0((8662+loop2*24),1);
```

```
        displ_freq80_harm4((1+loop2),1)=fund_harm8_0((12981+loop2*24),1)+i*fund_harm8_0((12982+loop2*24),1);
        displ_freq160_harm4((1+loop2),1)=fund_harm8_0((17301+loop2*24),1)+i*fund_harm8_0((17302+loop2*24),1);
        end
        %HARMONIC 5
        for loop2=0:179
        displ_freq10_harm5((1+loop2),1)=fund_harm8_0((23+loop2*24),1)+i*fund_harm8_0((24+loop2*24),1);
        displ_freq20_harm5((1+loop2),1)=fund_harm8_0((4343+loop2*24),1)+i*fund_harm8_0((4344+loop2*24),1);
        displ_freq40_harm5((1+loop2),1)=fund_harm8_0((8663+loop2*24),1)+i*fund_harm8_0((8664+loop2*24),1);
        displ_freq80_harm5((1+loop2),1)=fund_harm8_0((12983+loop2*24),1)+i*fund_harm8_0((12984+loop2*24),1);
        displ_freq160_harm5((1+loop2),1)=fund_harm8_0((17303+loop2*24),1)+i*fund_harm8_0((17304+loop2*24),1);
        end
        % Write out frequencies recorded
        freq10(1:180,1)=parameters8_0((3:6:1080),1);
        freq20(1:180,1)=parameters8_0((1083:6:2160),1);
        freq40(1:180,1)=parameters8_0((2163:6:3240),1);
        freq80(1:180,1)=parameters8_0((3243:6:4320),1);
        freq160(1:180,1)=parameters8_0((4323:6:5400),1);
    end;
end;

% Plot results
if exist('position')==0
    position=input('Position in cm (enter 5 char): ','s');
end;
if position=='10.00'
        figure(1)
        semilogy(freq10,abs(displ_freq10_fund),'-')
        hold on
        semilogy(freq10,abs(displ_freq10_harm1),'--')
        semilogy(freq10,abs(displ_freq10_harm2),'-.')
        semilogy(freq10,abs(displ_freq10_harm3),':')
        semilogy(freq10,abs(displ_freq10_harm4),'-')
        semilogy(freq10,abs(displ_freq10_harm5),'--')
        title1='Displacement vs Frequency';
        title2='   Amplitude = ';
        title3='   Position = ';
        title2=strcat(title2,amplitude,'Volts');
        title3=strcat(title3,position,'cm');
        title4='   Iteration = ';
        title4=strcat(title4,iteration);
        title_data=char({title1,title2,title3,title4});
        title(title_data);
        ylabel('Displacement')
        xlabel('Frequency (Hz)')
        legend('Fund','Harm 1','Harm 2','Harm 3','Harm 4','Harm 5')
        hold off
        orient landscape
        figure(2)
        plot(freq10,abs(displ_freq10_fund),'-')
        hold on
        plot(freq10,abs(displ_freq10_harm1),'--')
        plot(freq10,abs(displ_freq10_harm2),'-.')
        plot(freq10,abs(displ_freq10_harm3),':')
        plot(freq10,abs(displ_freq10_harm4),'-')
        plot(freq10,abs(displ_freq10_harm5),'--')
        title1='Displacement vs Frequency';
        title2='   Amplitude = ';
        title3='   Position = ';
        title2=strcat(title2,amplitude,'Volts');
        title3=strcat(title3,position,'cm');
        title4='   Iteration = ';
        title4=strcat(title4,iteration);
        title_data=char({title1,title2,title3,title4});
        title(title_data);
        ylabel('Displacement')
        xlabel('Frequency (Hz)')
```

144

```matlab
        legend('Fund','Harm 1','Harm 2','Harm 3','Harm 4','Harm 5')
        hold off
        orient landscape
elseif position=='20.00'
        figure(1)
        semilogy(freq20,abs(displ_freq20_fund),'-')
        hold on
        semilogy(freq20,abs(displ_freq20_harm1),'--')
        semilogy(freq20,abs(displ_freq20_harm2),'-.')
        semilogy(freq20,abs(displ_freq20_harm3),':')
        semilogy(freq20,abs(displ_freq20_harm4),'-')
        semilogy(freq20,abs(displ_freq20_harm5),'--')
        title1='Displacement vs Frequency';
        title2='  Amplitude = ';
        title3='  Position = ';
        title2=strcat(title2,amplitude,'Volts');
        title3=strcat(title3,position,'cm');
        title4='  Iteration = ';
        title4=strcat(title4,iteration);
        title_data=char({title1,title2,title3,title4});
        title(title_data);
        ylabel('Displacement')
        xlabel('Frequency (Hz)')
        legend('Fund','Harm 1','Harm 2','Harm 3','Harm 4','Harm 5')
        hold off
        orient landscape
        figure(2)
        plot(freq20,abs(displ_freq20_fund),'-')
        hold on
        plot(freq20,abs(displ_freq20_harm1),'--')
        plot(freq20,abs(displ_freq20_harm2),'-.')
        plot(freq20,abs(displ_freq20_harm3),':')
        plot(freq20,abs(displ_freq20_harm4),'-')
        plot(freq20,abs(displ_freq20_harm5),'--')
        title1='Displacement vs Frequency';
        title2='  Amplitude = ';
        title3='  Position = ';
        title2=strcat(title2,amplitude,'Volts');
        title3=strcat(title3,position,'cm');
        title4='  Iteration = ';
        title4=strcat(title4,iteration);
        title_data=char({title1,title2,title3,title4});
        title(title_data);
        ylabel('Displacement')
        xlabel('Frequency (Hz)')
        legend('Fund','Harm 1','Harm 2','Harm 3','Harm 4','Harm 5')
        hold off
        orient landscape
elseif position=='40.00'
        figure(1)
        semilogy(freq40,abs(displ_freq40_fund),'-')
        hold on
        semilogy(freq40,abs(displ_freq40_harm1),'--')
        semilogy(freq40,abs(displ_freq40_harm2),'-.')
        semilogy(freq40,abs(displ_freq40_harm3),':')
        semilogy(freq40,abs(displ_freq40_harm4),'-')
        semilogy(freq40,abs(displ_freq40_harm5),'--')
        title1='Displacement vs Frequency';
        title2='  Amplitude = ';
        title3='  Position = ';
        title2=strcat(title2,amplitude,'Volts');
        title3=strcat(title3,position,'cm');
        title4='  Iteration = ';
        title4=strcat(title4,iteration);
        title_data=char({title1,title2,title3,title4});
        title(title_data);
```

145

```matlab
        ylabel('Displacement')
        xlabel('Frequency (Hz)')
        legend('Fund','Harm 1','Harm 2','Harm 3','Harm 4','Harm 5')
        hold off
        orient landscape
        figure(2)        .
        plot(freq40,abs(displ_freq40_fund),'-')
        hold on
        plot(freq40,abs(displ_freq40_harm1),'--')
        plot(freq40,abs(displ_freq40_harm2),'-.')
        plot(freq40,abs(displ_freq40_harm3),':')
        plot(freq40,abs(displ_freq40_harm4),'-')
        plot(freq40,abs(displ_freq40_harm5),'--')
        title1='Displacement vs Frequency';
        title2=' Amplitude = ';
        title3=' Position = ';
        title2=strcat(title2,amplitude,'Volts');
        title3=strcat(title3,position,'cm');
        title4=' Iteration = ';
        title4=strcat(title4,iteration);
        title_data=char({title1,title2,title3,title4});
        title(title_data);
        ylabel('Displacement')
        xlabel('Frequency (Hz)')
        legend('Fund','Harm 1','Harm 2','Harm 3','Harm 4','Harm 5')
        hold off
        orient landscape
elseif position=='80.00'
        figure(1)
        semilogy(freq80,abs(displ_freq80_fund),'-')
        hold on
        semilogy(freq80,abs(displ_freq80_harm1),'--')
        semilogy(freq80,abs(displ_freq80_harm2),'-.')
        semilogy(freq80,abs(displ_freq80_harm3),':')
        semilogy(freq80,abs(displ_freq80_harm4),'-')
        semilogy(freq80,abs(displ_freq80_harm5),'--')
        title1='Displacement vs Frequency';
        title2=' Amplitude = ';
        title3=' Position = ';
        title2=strcat(title2,amplitude,'Volts');
        title3=strcat(title3,position,'cm');
        title4=' Iteration = ';
        title4=strcat(title4,iteration);
        title_data=char({title1,title2,title3,title4});
        title(title_data);
        ylabel('Displacement')
        xlabel('Frequency (Hz)')
        legend('Fund','Harm 1','Harm 2','Harm 3','Harm 4','Harm 5')        .   .
        hold off
        orient landscape
        figure(2)
        plot(freq80,abs(displ_freq80_fund),'-')
        hold on
        plot(freq80,abs(displ_freq80_harm1),'--')
        plot(freq80,abs(displ_freq80_harm2),'-.')
        plot(freq80,abs(displ_freq80_harm3),':')
        plot(freq80,abs(displ_freq80_harm4),'-')
        plot(freq80,abs(displ_freq80_harm5),'--')
        title1='Displacement vs Frequency';
        title2=' Amplitude = ';
        title3=' Position = ';
        title2=strcat(title2,amplitude,'Volts');
        title3=strcat(title3,position,'cm');
        title4=' Iteration = ';
        title4=strcat(title4,iteration);
        title_data=char({title1,title2,title3,title4});
```

146

```
        title(title_data);
        ylabel('Displacement')
        xlabel('Frequency (Hz)')
        legend('Fund','Harm 1','Harm 2','Harm 3','Harm 4','Harm 5')
        hold off
        orient landscape
elseif position=='160.0'
        figure(1)
        semilogy(freq160,abs(displ_freq160_fund),'-')
        hold on
        semilogy(freq160,abs(displ_freq160_harm1),'--')
        semilogy(freq160,abs(displ_freq160_harm2),'-.')
        semilogy(freq160,abs(displ_freq160_harm3),':')
        semilogy(freq160,abs(displ_freq160_harm4),'-')
        semilogy(freq160,abs(displ_freq160_harm5),'--')
        title1='Displacement vs Frequency';
        title2=' Amplitude = ';
        title3=' Position = ';
        title2=strcat(title2,amplitude,'Volts');
        title3=strcat(title3,position,'cm');
        title4=' Iteration = ';
        title4=strcat(title4,iteration);
        title_data=char({title1,title2,title3,title4});
        title(title_data);
        ylabel('Displacement')
        xlabel('Frequency (Hz)')
        legend('Fund','Harm 1','Harm 2','Harm 3','Harm 4','Harm 5')
        hold off
        orient landscape
        figure(2)
        plot(freq160,abs(displ_freq160_fund),'-')
        hold on
        plot(freq160,abs(displ_freq160_harm1),'--')
        plot(freq160,abs(displ_freq160_harm2),'-.')
        plot(freq160,abs(displ_freq160_harm3),':')
        plot(freq160,abs(displ_freq160_harm4),'-')
        plot(freq160,abs(displ_freq160_harm5),'--')
        title1='Displacement vs Frequency';
        title2=' Amplitude = ';
        title3=' Position = ';
        title2=strcat(title2,amplitude,'Volts');
        title3=strcat(title3,position,'cm');
        title4=' Iteration = ';
        title4=strcat(title4,iteration);
        title_data=char({title1,title2,title3,title4});
        title(title_data);
        ylabel('Displacement')
        xlabel('Frequency (Hz)')
        legend('Fund','Harm 1','Harm 2','Harm 3','Harm 4','Harm 5')
        hold off
        orient landscape
    end
```

147

APPENDIX E

LABVIEW CODE

LabVIEW programming was done by Dr. Gregg D. Larson, a research engineer assigned to the investigation of acousto-electromagnetic mine detection at the Georgia Institute of Technology. The software evolved from existing code and continued to evolve over the year that data was collected for this thesis. This appendix includes only a couple of the numerous subroutines utilized for taking data in Experiment 2.

The program found on pages 149 and 150 was the major program collecting the radar data. This code drove several subroutines and was driven itself by other programs. The overall controlling code is found in the second program (page 151). From this code, all of the data for Experiment 2 was collected. This included the four-accelerometer measurements and the alternating two-accelerometer/radar measurements for both the frequency response tests and the saturation curve tests.

151
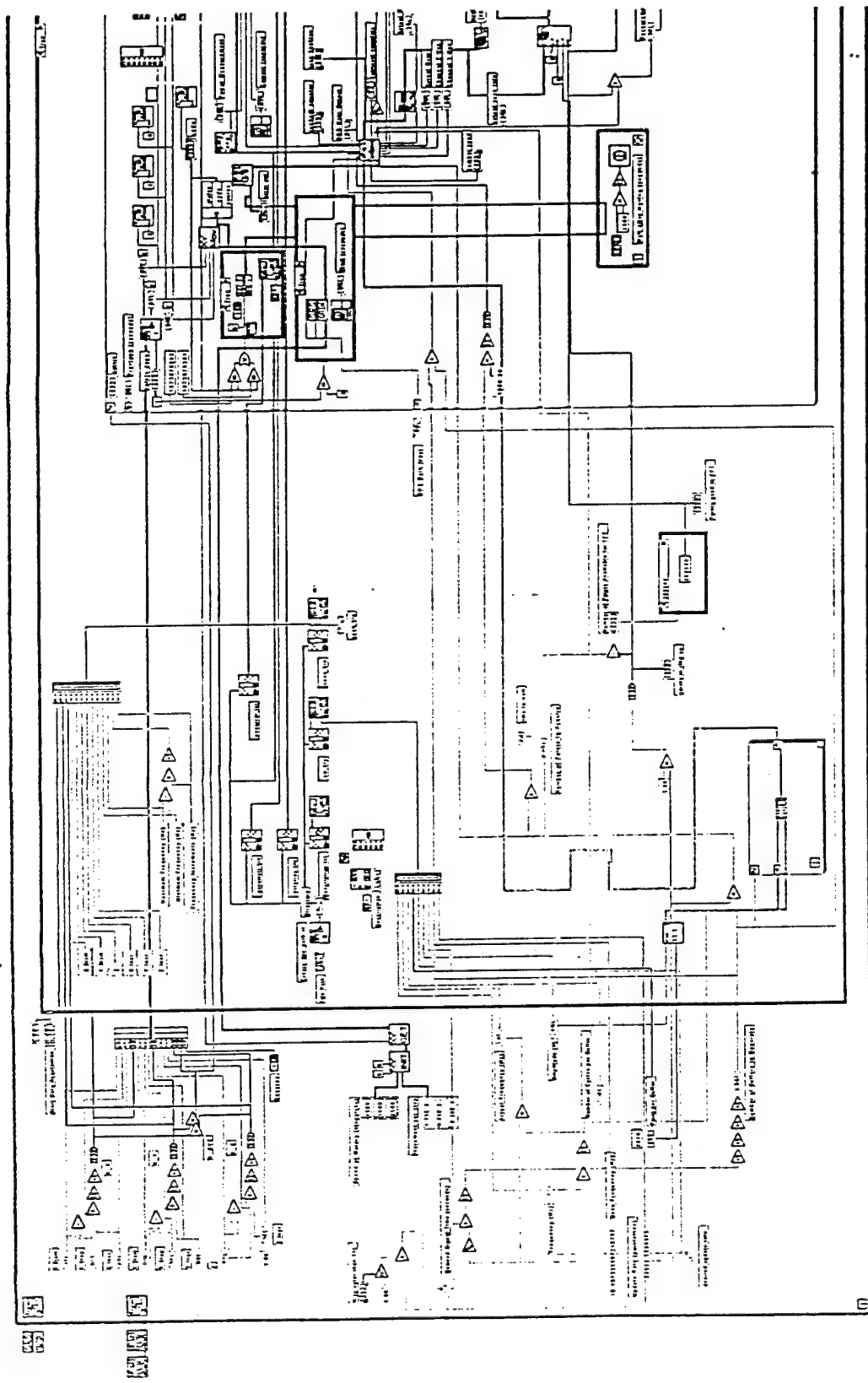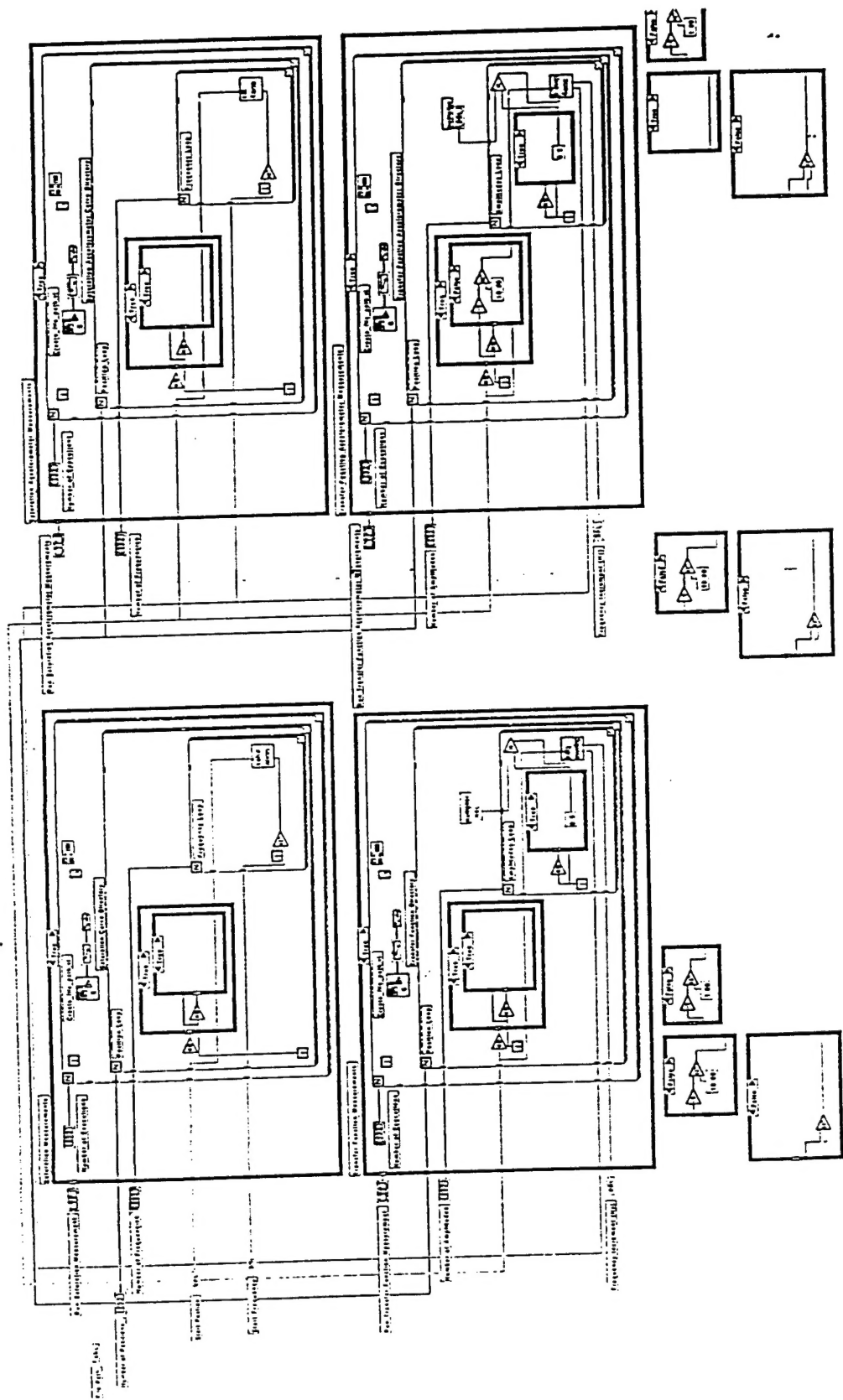
REFERENCES

[1]   Ashley, Steven, "Searching for Land Mines," Mechanical Engineering, April 1996.

[2]   Scott, Waymond R. and James S. Martin, "Experimental Investigation for the Acousto-Electromagnetic Sensor for Locating Land Mines," Georgia Institute of Technology, 1999.

[3]   Prakash, Shamsher, Soil Dynamics, McGraw-Hill Book Company, New York, NY, 1981.

[4]   Smith, Eric, Preston S. Wilson, Fred W. Bacon, et. al., "Measurement and Localization of Interface Wave Reflections from a Buried Target," University of Texas at Austin, August 1997.

[5]   Ganji, Vahid, Nenad Gucunski, and Ali Maher, "Detection of Underground Obstacles by SASW Method – Numerical Aspects," Journal of Geotechnical and Geoenvironmental Engineering, March 1997.

[6]   Donskly, Dimitri, "Nonlinear Vibro-Acoustic Technique for Landmine Detection," Stevens Institute of Technology.

[7]   Don, C.G. and D.E. Lawrence, "Detecting Buried Objects, Such as Land Mines, Using Acoustic Impulses," Echoes, Winter 1998.

[8]   Schroeder, Christoph and Waymond R. Scott, "Finite-Difference Time-Domain Model for Elastic Waves in the Ground," Georgia Institute of Technology, 1999.

[9]   Richart, F.E., J.R. Hall, Jr., and R.D. Woods, Vibrations of Soils and Foundations, Prentice-Hall, Inc., Englewood Cliffs, NJ, 1970.

[10]   Roh, Heui-Sol, W. Arnott, James M. Sabatier, et. al., "Measurement and Calculation of Acoustic Propagation Constants in Arrays of Small Air-filled Rectangular Tubes," Journal of Acoustical Society of America, June 1991.

[11]   Attenborough, Keith, James M. Sabatier, Henry E. Bass, et. al., "The Acoustic Transfer Function at the Surface of a Layered Poroelastic Soil," Journal of Acoustical Society of America, May 1986.

[12]   Gilbert, Kenneth E. and James M. Sabatier, "Buried Object Detection – Final Report," National Center for Physical Acoustics, January 1987.

[13]   Santamarina, J. Carlos, Civil and Environmental Engineering Department, Georgia Institute of Technology, private communication.

REPORT DOCUMENTATION PAGE

Form Approved
OMB No. 0704-0188

1. REPORT DATE (DD-MM-YYYY)	2. REPORT DATE	3. DATES COVERED (From - To)
11-07-20000	Performance: Year 1	Jul 1999 - July 2000

4. TITLE AND SUBTITLE

Investigation of the Interaction of Elastic Waves with Buried Mines

5a. CONTRACT NUMBER
N00014-99-1-0995

5b. GRANT NUMBER

5c. PROGRAM ELEMENT NUMBER

6. AUTHOR(S)

Scott, Waymond, R., Jr.,
Rogers, Peter, H., and
Martin, James, S.

5d. PROJECT NUMBER

5e. TASK NUMBER

5f. WORK UNIT NUMBER

7. PERFORMING ORGANIZATION NAME(S) AND ADDRESS(ES)
Georgia Tech Research Corporation/ Georgia Institute of Technology
Centennail Research Building
400 Tenth Street
Atlanta, GA 30332-0420

8. PERFORMING ORGANIZATION REPORT NUMBER

9. SPONSORING/MONITORING AGENCY NAME(S) AND ADDRESS(ES)

Office of Naval Research
Ballston Center Tower One
800 North Quincy Street
Arlington, VA 22217-5660

10. SPONSOR/MONITOR'S ACRONYM(S)
ONR

11. SPONSORING/MONITORING AGENCY REPORT NUMBER

12. DISTRIBUTION AVAILABILITY STATEMENT

Approved for Public Release; distribution is Unlimited

13. SUPPLEMENTARY NOTES

14. ABSTRACT
The objective of this research is to support ongoing development of the seismic mine detection technique. Specifically this involves the creation of a reliable three-dimensional theoretical (numerical) model for the propagation of elastic waves in the earth. The model will be used to investigate the interaction of elastic waves with buried objects. The model model will provide both a predictive capability for system performance and a technique for the design of future field experiments. As a part of this modeling, an experimental effort to measure the relevant physical properties of soils and mines has also been undertaken.

15. SUBJECT TERMS

Land mine detection, elastic waves, seismic waves, finite-difference time-domain model. FDTD model, finite difference model

16. SECURITY CLASSIFICATION OF:			17. LIMITATION OF ABSTRACT	18. NUMBER OF PAGES	19a. NAME OF RESPONSIBLE PERSON
a. REPORT	b. ABSTRACT	c. THIS PAGE	SAR	200	Waymond Scott
U	U	U			19b. TELEPONE NUMBER (Include area code) 404-894-3048

Standard Form 298 (Rev. 8-98)
Prescribed by ANSI-Std Z39-18